

Electronic Thesis and Dissertation Repository

---

12-7-2018 9:30 AM

## Performance of Single and Groups of Hollow Bar Micropiles in Sand

Maged Abdlrahem, *The University of Western Ontario*

Supervisor: M Hesham El Naggar, *The University of Western Ontario*

A thesis submitted in partial fulfillment of the requirements for the Doctor of Philosophy degree in Civil and Environmental Engineering

© Maged Abdlrahem 2018

Follow this and additional works at: <https://ir.lib.uwo.ca/etd>



Part of the [Civil and Environmental Engineering Commons](#)

---

### Recommended Citation

Abdlrahem, Maged, "Performance of Single and Groups of Hollow Bar Micropiles in Sand" (2018). *Electronic Thesis and Dissertation Repository*. 5869.  
<https://ir.lib.uwo.ca/etd/5869>

This Dissertation/Thesis is brought to you for free and open access by Scholarship@Western. It has been accepted for inclusion in Electronic Thesis and Dissertation Repository by an authorized administrator of Scholarship@Western. For more information, please contact [wlsadmin@uwo.ca](mailto:wlsadmin@uwo.ca).

## ABSTRACT

Hollow bar micropiles (HBMP) have gained wide acceptance due to their efficient load transfer mechanism, which facilitates carrying considerable relative load in compression and tension, and small installation equipment, which allows installation in sites with limited access. The HBMP is commonly constructed using a drill bit/ hollow bar diameter ratio ( $D_b/D_h$ ) of around 2, and they are typically designed as type B micropiles as classified by the Federal Highway Administration (FHWA), even though they are constructed differently. Thus, this thesis presents the results of laboratory and field testing programs as well as three-dimensional nonlinear finite element analyses that were conducted to investigate the performance of single and groups of HBMP. The study investigated the effects of increasing the  $D_b/D_h$  ratio from 2.25, which represents the current practice, to 3 and the micropiles spacing. Twenty two full- scale HBMP's were installed in cohesionless soil, six of which were single micropiles and the remainder were divided into four micropile groups. Each group comprised four micropiles arranged in a square configuration. Two single micropiles and two groups were constructed with a drill bit of  $D_b = 115$  mm, and four single micropiles and two groups were constructed with a drill bit of  $D_b = 152$  mm. One group of each set had a spacing to micropile diameter ratio ( $s/D_b$ ) = 3, and the other group had  $s/D_b = 5$ . The single micropiles were subjected to compression, tension, and then lateral load tests while the micropile groups were subjected to axial centric monotonic compressive loading.

The results demonstrated that increasing  $D_b/D_h$  to 3 improved the micropiles performance and increased their compression and uplift capacities. The axial stiffness of single micropiles increased by 38% and 32% in compression and uplift, while their capacity increased by 17% and 22.5%, respectively. The obtained results from the lateral load tests indicated that increasing  $D_b/D_h$  to 3 improved the lateral capacity by about 32% and the piles were substantially stiffer. As expected, micropile groups constructed with the large diameter drill bits displayed higher stiffness and load carrying capacity than the groups constructed with small diameter bits, which confirms the effectiveness of using a larger drill bit. The axial group stiffness increased by 41% and 59% as the  $D_b/D_h$  increases from

2.25 to 3 for groups constructed at  $s/D = 3$  and 5, respectively. In addition, the group efficiency ratio values at both the working load and ultimate capacity were found to be close to unity for all groups. Finite element simulations investigated the effect of micropile installation in cohesionless soils. In addition, the model was used to extend the load – settlement curves to the failure load when it was not possible to load the micropiles to failure during field testing because of equipment limitation. The numerical model results confirmed that the micropile group efficiency is equal to unity for micropiles in a 2x2 and 3x3 arrangement.

**Keywords:** Single micropiles, field tests, finite element, micropile groups, group efficiency factor, group settlement ratio

## **CO-AUTHORSHIP STATEMENT**

This thesis is prepared in accordance with the regulation for an Integrated-Article format thesis stipulated by the school of graduate and post graduate studies at Western University. The work was carried out by the author under supervision of Dr. M. H. El Naggar. The work includes field tests, laboratory tests, numerical modeling, data analysis, results interpretation, and thesis writing. The thesis contains eight chapters that includes the introduction, literature review, and conclusion. The results of the work will be used in journals and conferences publications, which will be co-authored with Dr. M. H. El Naggar.

## **ACKNOWLEDGMENTS**

In the name of Allah, the most compassionate the most merciful. I would like to thank Allah for his guidance and help, without him this work would not see the light.

The author would like to express his sincere gratitude to Dr. M. H. El Naggar for his supervision, guidance, and never-ending support.

I would like to thank my family: my father, my mother, my wife, and my children for their support, help, encouragement and prayers. Words would not be enough to thank you all, you are always there for me.

Also, I would like to show appreciation for HC MATCON for providing the site, equipment, and helping in the testing program.

I would also like to show appreciation to my brothers, sisters, and friends, and specially to Dr. Wenbing Wu from China University of Geosciences for his help during the field testing program.

# TABLE OF CONTENTS

ABSTRACT.....	i
CO-AUTHORSHIP STATEMENT .....	iii
ACKNOWLEDGMENTS .....	iv
TABLE OF CONTENTS.....	v
LIST OF TABLES .....	xi
LIST OF FIGURES .....	xiii
CHAPTER 1 .....	1
1 Introduction.....	1
1.1 Overview.....	1
1.2 Research objectives.....	3
1.3 Methodology.....	4
1.4 Thesis outline .....	5
1.5 References.....	8
CHAPTER 2 .....	10
2 Literature Review.....	10
2.1 Introduction.....	10
2.2 Micropiles .....	10
2.2.1 Classification of micropiles .....	11
2.2.2 Hollow bar micropiles.....	15
2.3 Design of micropiles.....	17
2.3.1 Structural capacity of micropiles .....	17
2.3.2 Geotechnical capacity of micropiles.....	18

2.3.3	Geotechnical Capacity of Micropile Group .....	19
2.4	Axial Monotonic Behaviour of Micropiles .....	21
2.4.1	Single Micropiles .....	21
2.4.2	Micropile Groups .....	24
2.5	Lateral Performance of Micropiles .....	26
2.6	Summary .....	27
2.7	References .....	29
CHAPTER 3	.....	32
3	Evaluation of Axial Performance of Hollow Bar Micropiles Constructed with Different Drill Bit to Hollow Bar Diameter Ratio .....	32
3.1	Introduction .....	32
3.2	Geotechnical Site Characterization .....	39
3.3	Micropile installation .....	44
3.4	Test Setup, Instrumentation and Procedures .....	49
3.4.1	Loading setup .....	49
3.4.2	Pile instrumentation .....	50
3.4.3	Load test procedure .....	51
3.4.4	Loading sequence .....	53
3.5	Test Results and Analysis .....	54
3.5.1	Monotonic compression tests .....	54
3.5.2	Ultimate compressive capacity .....	54
3.5.3	Distribution of axial forces in micropiles .....	59
3.5.4	Toe resistance of micropiles .....	63
3.5.5	Unit skin friction of micropiles .....	65
3.5.6	Cyclic compression tests .....	66
3.5.7	Monotonic tension tests .....	69

3.5.8	Uplift capacity.....	72
3.5.9	Cyclic Tension Tests.....	73
3.6	Discussions and Conclusions.....	78
3.7	References.....	80
CHAPTER 4	.....	85
4	Axial Performance of Micropile Groups in Cohesionless Soil from Full Scale Tests.....	85
4.1	Introduction.....	85
4.2	Geotechnical Site Characterization.....	89
4.3	Installation of Micropiles.....	95
4.4	Micropiles Installation Procedure.....	95
4.5	Test Setup, Instrumentation and Procedures.....	96
4.5.1	Loading Equipment and Micropile Instrumentation.....	98
4.5.2	Load Test Procedure.....	99
4.6	Test Results and Analysis.....	100
4.6.1	Load – settlement curves.....	100
4.6.2	Unit skin friction and toe resistance of individual micropiles.....	108
4.7	Numerical Modelling.....	116
4.7.1	3D Mesh Geometry.....	116
4.7.2	Material Models.....	117
4.7.3	Model Calibration and Verification.....	119
4.8	Settlement Ratio.....	124
4.9	Conclusions.....	127
4.10	References.....	130
CHAPTER 5	.....	135



5	Lateral Performance of Single and Groups of Hollow Bar Micropiles in Cohesionless Soil. ....	135
5.1	Introduction.....	135
5.2	Geotechnical Site Characterization.....	138
5.3	Installation of Micropiles .....	142
5.4	Test Setup, Instrumentation and Loading Procedures .....	145
5.5	Test Results and Analysis .....	148
5.5.1	Monotonic Load – Deflection Curves for Single Micropiles .....	148
5.5.2	Monotonic Load – Deflection Curve for Micropile Group. ....	151
5.5.3	Cyclic Load-Deflection Curves for Single Micropiles. ....	152
5.5.4	Pure Bending Tests .....	159
5.6	Numerical Modeling .....	162
5.7	Conclusions.....	168
5.8	References.....	170
	CHAPTER 6 .....	174
6	Improving the Mechanical Properties of Grout for Micropile Application .....	174
6.1	Introduction.....	174
6.2	Objective and Scope of Work.....	175
6.3	Mechanical Properties of Fiber-Reinforced Grout .....	176
6.3.1	Mechanical Properties of Tested Fiber-Reinforced Grouts .....	178
6.4	Pure Bending Tests .....	183
6.4.1	Results of Pure Bending Tests .....	185
6.5	Numerical Modeling .....	187
6.5.1	Results of Numerical Modeling .....	188
6.6	Full-Scale Test .....	191
6.6.1	Site Exploration .....	192

6.6.2	Loading setup and Pile Instrumentation .....	193
6.6.3	Results of Full-Scale Lateral Test.....	195
6.7	Summary and Conclusions .....	196
6.8	References.....	198
CHAPTER 7	.....	201
7	Numerical Modelling of Hollow Bar Micropiles in Cohesionless Soils.....	201
7.1	Introduction.....	201
7.2	Installation of Micropiles .....	204
7.3	Load Test Results.....	206
7.4	Numerical Modeling .....	207
7.4.1	Material Models .....	208
7.4.2	3D Mesh Geometry.....	210
7.4.3	Increasing $K_o$ Method .....	212
7.4.4	Cavity Expansion Method.....	212
7.5	Numerical Analysis Procedure .....	213
7.5.1	Model Calibration and Verification .....	213
7.5.2	Single Micropiles .....	214
7.5.3	Micropile Groups .....	219
7.6	Parametric Study.....	228
7.6.1	Soil Strength Parameters.....	228
7.6.2	Slenderness ratio .....	232
7.6.3	Interface Reduction Factor ( $R_{inter}$ ) .....	233
7.6.4	Number of Micropiles in the Group.....	235
7.6.5	Spacing to Diameter Ratio of Micropile in the Group.....	237
7.6.6	Effect of Relative Density on Performance of Micropile Group .....	238

7.6.7	Settlement Ratio of Micropile Group .....	239
7.6.8	Interaction Factor between Two-Micropiles Group .....	242
7.7	Summery and Main Findings.....	245
7.8	References.....	248
CHAPTER 8	.....	251
8	Summary, Conclusions and Recommendations.....	251
8.1	Summary.....	251
8.2	Conclusions.....	253
8.2.1	Single Micropiles .....	253
8.2.2	Micropiles Group.....	256
8.3	Recommendations for Future Research .....	257
Curriculum Vitae	.....	258

## LIST OF TABLES

Table 2-1 Typical values of Grout-to-Ground Bond for micropile design.....	20
Table 3-1 Testing stages and loading sequences .....	53
Table 3-2 Interpreted failure load methods and plunging failure .....	58
Table 3-3 Ultimate skin friction for MP2 and MP3.....	66
Table 3-4 Interpreted failure load methods and plunging failure for tension tests.....	73
Table 4-1 Summary of SPT N values for BH1 and BH2.....	91
Table 4-2 Interpreted failure load for single micropiles .....	101
Table 4-3 Micropile groups stiffness .....	104
Table 4-4 Interpreted failure load methods for micropile groups.....	107
Table 4-5 Summary of group efficiency .....	107
Table 4-6 Ultimate skin friction of instrumented micropiles in the groups.....	110
Table 4-7 Comparison between transferred load at different depths .....	115
Table 4-8 Geotechnical parameters used in FEM.....	120
Table 4-9 Comparison between empirical formulas for $R_s$ with the measured values ..	127
Table 5-1 Boreholes logs and N values .....	139
Table 5-2 Testing stages and loading sequences .....	147
Table 5-3 Interpreted ultimate lateral capacity of micropiles.....	150
Table 5-4 Material properties used in LPile .....	164
Table 6-1 Properties of fibers used in this study.....	178

Table 6-2 Correlated relative density from SPT and CPT .....	193
Table 7-1 Soil parameters from the site investigation .....	206
Table 7-2 Geotechnical parameters used in FEM.....	210
Table 7-3 Soil Parameters used in the parametric study.....	229
Table 7-4 Comparison between ultimate bond strength values from FE and FHWA ....	231
Table 7-5 Summary of the effect of slenderness ratio on the failure load.....	233
Table 7-6 Micropile group stiffness with different s/D .....	239
Table 7-7 Comparison between Rs with different s/D ratio .....	242

## LIST OF FIGURES

Figure 2-1 CASE 1 micropiles (after FHWA, 2005).....	12
Figure 2-2 CASE 2 micropiles (after FHWA, 2005).....	13
Figure 2-3 Micropile classification based on the method of grouting (after FHWA, 2005) .....	14
Figure 2-4 HBMP installation procedure.....	16
Figure 3-1 BH1 and BH2 log with SPT N values and water content .....	40
Figure 3-2(a) CPT1 (b) CPT2 sounding with SBT .....	41
Figure 3-3 Properties of soil at test site: a) relative density; b) angle of internal friction; c) grain size distribution.....	43
Figure 3-4 Plan view of single micropiles location .....	44
Figure 3-5 Load-slip curves obtained from pull-out tests.....	48
Figure 3-6 Load transfer mechanism for HBMP .....	48
Figure 3-7 Load test setup: a) compression; and b) tension .....	50
Figure 3-8 Micropile head instruments for compression test .....	52
Figure 3-9 Load- settlement curves for compression tests .....	56
Figure 3-10 Exhumed micropiles MP3 and diameter measurement along the depth.....	60
Figure 3-11 Stress-strain relationship for MP2 and MP3 from SG1 .....	61
Figure 3-12 Distribution of axial forces with depth for MP2 and MP3.....	62
Figure 3-13 Total applied load versus toe resistance for MP2 and MP3.....	63

Figure 3-14 Toe resistance versus toe settlement for MP2 and MP3 .....	64
Figure 3-15 Distribution of unit skin friction for MP2 and MP3 .....	66
Figure 3-16 Cyclic compression loading for MP1 .....	67
Figure 3-17 Micropile (MP1) head movement versus number of cycles. ....	67
Figure 3-18 Axial stiffness of MP1 with number of cycles.....	69
Figure 3-19 Load- settlement curves for tension tests .....	71
Figure 3-20 Load – settlement curve for MP1 .....	74
Figure 3-21 Load settlement curve for MP6.....	74
Figure 3-22 Head micropile settlement vs number of cycles for MP1 .....	75
Figure 3-23 Head micropile settlement vs number of cycles for MP6.....	76
Figure 3-24 MP1 axial micropile head stiffness vs number of cycles .....	77
Figure 3-25 MP6 axial micropile head stiffness vs number of cycles .....	77
Figure 4-1 Plan view of micropiles groups locations, BHs and CPTs (Dimensions in meters and Not to scale).....	89
Figure 4-2 CPT soundings with SBT: a) CPT1; b) CPT2 .....	93
Figure 4-3 Direct shear test results: a) horizontal settlement vs. vertical settlement; b) measured angle of internal friction .....	94
Figure 4-4 a) Compression test setup; b) head instruments of micropile groups. ....	98
Figure 4-5 Compression load – settlement curves for single micropiles.....	102
Figure 4-6 Effect of increasing $D_b/D_h$ on group behaviour for groups with: a) $s/D_b = 3$ ; b) $s/D_b = 5$ .....	104

Figure 4-7 Structural failure of loading bar for MPG1 .....	105
Figure 4-8 Effect of spacing to diameter ratio on group behaviour for groups with: a) $D_b/D_h = 2.25$ ; and b) $D_b/D_h=3.0$ .....	106
Figure 4-9 Distribution of unit shaft resistance for micropile groups .....	111
Figure 4-10 Total applied load versus toe resistance of instrumented micropiles.....	112
Figure 4-11 Load distribution along the micropile depth; single and groups: a) $D_b/D_h = 2.25$ ; and b) $D_b/D_h=3.0$ .....	115
Figure 4-12 Finite element model geometry.....	117
Figure 4-13 (a) FE model calibration for micropiles with $D_b/D_h=3$ ; and (b) model verification for micropiles with $D_b/D_h=2.25$ .....	122
Figure 4-14 Comparison between Load-settlement curves for MPG1 and MPG2 field and FE model.....	123
Figure 4-15 Comparison between Load-settlement curves for MPG1 and MPG2 field and FE model.....	124
Figure 4-16 Settlement ratio versus micropile group settlement .....	125
Figure 4-17 Mean and COV of $R_s$ of micropile groups with applied loads.....	126
Figure 5-1 CPT soundings with SBT: a) CPT1; b) CPT2 .....	141
Figure 5-2 Grain size distribution of soil at test site.....	142
Figure 5-3 Plan view of micropiles locations along with boreholes and CPT soundings locations. ....	143
Figure 5-4 Load test setup: a) Single micropiles; and b) Micropiles group .....	146
Figure 5-5 Load – deflection curves; a) $D_b/D_h=3$ and b) $D_b/D_h=2.25$ .....	149



Figure 5-6 Load – deflection curves: a) Micropile groups MPG4 and b) Comparison with single micropile.....	152
Figure 5-7 Load – deflection curves for lateral monotonic and cycle tests.....	154
Figure 5-8 Local failure mechanism due to cyclic loading.....	155
Figure 5-9 . Normalized micropile head stiffness versus number of cycles for micropiles with $D_b/D_h=3$ .....	158
Figure 5-10 Degradation parameter at different stress levels for micropiles with $D_b/D_h=3$ and 2.25.....	159
Figure 5-11 Exhumed micropile MP3 and diameter measurement along the depth.....	160
Figure 5-12 Pure bending test on the exhumed micropile MP3 .....	161
Figure 5-13 Moment-Curvature curve for the exhumed micropile MP3.....	162
Figure 5-14 Comparison between load -deflection curves for micropiles MP3 and MP4 with LPile results .....	163
Figure 5-15 Moment-Curvature curves for the exhumed micropile MP3 and Lpile model .....	165
Figure 5-16 (a) Calibration and (b) validation of LPile model.....	166
Figure 5-17 Deflection and bending moment versus depth (LPile model); a) $D_b/D_h=2.25$ and b) $D_b/D_h=3$ .....	168
Figure 6-1 Four different type of fibers .....	178
Figure 6-2 (a) compressive strength; (b) tensile strength for four types of fibers with different dosages .....	180
Figure 6-3 (a) Modulus of elasticity; (b) Flexural strength for four types of fibers with different dosages .....	183

Figure 6-4 Load test setup.....	185
Figure 6-5 Moment-curvature curves obtained from pure moment tests .....	186
Figure 6-6 Post cracking behaviour of fiber reinforced and non-reinforced grouted micropiles.....	187
Figure 6-7 Load-deflection curves using Reese model for the three micropiles; NF, MSF1% and SF1% .....	189
Figure 6-8 Bending moment along the depth of the three micropiles using Reese model .....	190
Figure 6-9 Maximum bending moment versus maximum head deflection curves for three micropiles.....	191
Figure 6-10 Lateral load test setup.....	194
Figure 6-11 Load vs deflection curves for MP6 with MSF 1% and MP1, MP2 and MP5 with No fibers .....	195
Figure 7-1 Plan view of micropiles locations, SPTs and CPTs (Dimensions in meters and Not to scale) .....	205
Figure 7-2 FE model calibration and verification using increasing $K_o$ method: a) $D_b/D_h = 3$ ; and b) $D_b/D_h=2.25$ .....	215
Figure 7-3 FE model calibration and verification using Cavity Expansion method: a) $D_b/D_h = 3$ ; and b) $D_b/D_h=2.25$ .....	216
Figure 7-4 Radial stress vs depth at the interface using cavity expansion (CE) and $K_o$ pressure method .....	217
Figure 7-5 Stresses at 3m and 5 m depth using cavity expansion .....	218
Figure 7-6 Shear stress vs depth using Cavity Expansion (CE) .....	219

Figure 7-7 Comparison between Load-settlement curves for MPG3 and MPG4 from field tests and Increasing $K_0$ Method.....	220
Figure 7-8 Comparison between Load-settlement curves for MPG1 and MPG2 from field tests and Increasing $K_0$ method.....	221
Figure 7-9 Load vs settlement curves for different soil parameters .....	230
Figure 7-10 Effect of Lateral earth pressure coefficient on micropile performance .....	232
Figure 7-11 Effect of the interface reduction factor on micropile performance.....	234
Figure 7-12 Effect of the interface reduction factor on the failure load of micropiles ...	234
Figure 7-13 Full 3D model with deformed mesh.....	235
Figure 7-14 Load vs settlement of 3* 3 micropiles group .....	236
Figure 7-15 Load vs settlement for different spacing between micropile groups .....	237
Figure 7-16 Effect of relative density on the load - settlement curves of micropile group with different s/D ratios. ....	238
Figure 7-17 Settlement ratio $R_s$ for different relative densities and s/D ratios .....	241
Figure 7-18 Interaction factor for different slenderness ratio .....	245

## LIST OF ABBREVIATIONS

<i>AASHTO</i>	The American Association of State Highway and Transportation Officials
<i>ASTM</i>	The American Society for Testing and Materials
<i>BH</i>	Borehole
<i>CPT<sub>u</sub></i>	Piezocone penetration test
<i>FE</i>	Finite element
<i>FHWA</i>	The Federal Highway Administration
<i>FOREVER</i>	The French National Project on Micropiles
<i>FS</i>	Factor of safety
<i>ID</i>	Inner diameter of hollow bar
<i>LVDT</i>	Linear Variable Differential Transducer
<i>MP</i>	Micropile
<i>OD</i>	Outer diameter of hollow bar

## LIST OF SYMBOLS

$A$	Pile cross-sectional area
$A_{bar}$	Cross sectional area of steel bar
$A_{casing}$	Cross sectional area of steel casing
$A_g$	Area of the grout
$A_s$	Area of steel
$C$	Effective cohesion
$C_u$	Undrained shear strength
$D$	Diameter of micropile
$D_b$	Drill bit diameter
$D_h$	Hollow bar diameter
$E$	Young's Modulus
$E_g$	Modulus of elasticity of grout
$E_p$	Modulus of elasticity of micropile
$E_s$	Modulus of elasticity of hollow bar
$E_{50}^{ref}$	Triaxial loading stiffness
$E_{oed}^{ref}$	Oedometer loading stiffness
$E_{ur}^{ref}$	Triaxial unloading stiffness
$f'_c$	Compression strength of the grout

$f_s$	Unit skin friction resistance
$f_y$	Yield strength of hollow bar
$K$	Micropile head stiffness
$L$	Pile length
$L_p$	Bond length
$L/d$	Slenderness ratio
$N$	Measured SPT number
$n$	Number of micropiles in group
$N_{1,60}$	Standard penetration number corrected to an average energy ratio of 60% and overburden pressure
$P_p$	Applied load to the micropile head
$P_{C-allowable}$	Allowable structural axial compression load
$P_{T-allowable}$	Allowable structural axial tension load
$Q_g$	Ultimate group capacity
$R_{int}$	Interface reduction factor
$\alpha_{bond}$	Unit Value of Grout-to-Ground Bond
$\varphi'$	Effective friction angle
$\psi$	Dilation angle
$\eta$	Group efficiency factor
$\gamma'$	Effective unit weight of soil

$\gamma_{dry}$	Dry unit weight of soil
$\gamma_{sat}$	Saturated unit weight of soil
$\nu$	Poisson's ratio

## CHAPTER 1

# 1 Introduction

---

## 1.1 Overview

A micropile is a small diameter (less than 300mm) drilled and grouted pile as described by the Federal Highway Association (FHWA, 2005). Micropiles can carry considerable axial compression and tension loads due to large grout/ground shear resistance, which facilitates load transfer by friction. Micropiles are used for retrofitting existing foundations and to support new construction, especially when the use of larger diameter piles is not feasible. Micropiles were first conceived in Italy by Dr. Fernando Lizzi as a solution for retrofitting historical buildings that were damaged during World War II. The application of micropiles in foundation engineering in North America grew in the 1970's, especially in the east coast of the United State (Bruce and Nicholson 1989). Joe and Gray (2007) reported that micropiles were first introduced in Canada in the mid 1970's. In Japan, the first application of micropiles was for the protection of a lookout tower foundation in 1980, and since then was used widely in several applications (Tsukada and Ichimura, 1997). In China, simulating the underpinning of Hu-Qui Tower through a laboratory model in 1980 was the first trial of introducing micropiles (Han and Ye, 2006). Bruce and Yeung (1983) reported an early case study in Hong Kong that after consideration, micropiles were selected as a solution for limited access and minimal disturbance during construction conditions.

There are two main studies presented in the literature performed by FHWA in North America and the FOREVER project in Europe, which focused mainly on types and



behaviour of micropiles. FHWA (2005) has classified the micropiles into four categories as follows. Type A: the grout is placed under gravity and no pressure is required. Type B: the grout is typically applied under a pressure range from 0.5 to 1 MPa as the temporary casing is withdrawn. Type C: the grout is placed in two-step process; first, the grout is poured under gravity only, and before it hardens, similar grout is pressured at  $> 1$  MPa without the use of packer. Type D: it is also a two – step process, where the grout is placed first under gravity as in Type A or pressurized as in Type B; after the initial grout hardens, additional grout is pressurized between 2 to 9 MPa through sleeved pipe by using packers, as many times as needed. However, the construction method of hollow bar micropiles (HBMP) is different than these types, and consequently their behavior is expected to be different. Even though the construction technique of HBMP is different from Type B micropiles, FHWA considers HBMP as Type B micropiles based on the applied pressure. On the other hand, recent studies suggested that HBMP should be classified as Type E (Timothy et al., 2012; Abdelaziz and El Naggar, 2014). However, there are no specific design guidelines for hollow bar micropiles yet. In addition, there is a gap in literature related to the effects of several factors on the performance of HBMP, such as the effect of increasing the drill bit/ hollow bar ( $D_b/D_h$ ) ratio, the grouting pressure and group behaviour.

The current study investigates the beneficial effects of increasing  $D_b/D_h$  from 2.25 to 3 on micropile performance and capacity, while offering a competitive cost. In current design practice, the diameter of the micropile is evaluated based on FHWA design guidelines then the value is divided by two to establish the diameter of the hollow bar required to achieve the design capacity. For example, if the target diameter of the micropile is 152 mm, a hollow bar diameter of 76 mm would be selected. Considering the shearing resistances of

interfaces reinforcing bar-grout and grout-ground, it may be possible to increase  $D_b/D_h$  to 3. Correspondingly, the diameter of the hollow bar would be 51 mm instead of 76 mm, which means the quantity of steel can be reduced by 50%. Additionally, the performance of single and groups of hollow bar micropiles installed in cohesionless soil was investigated and reported. It is anticipated that the results of this study will help researchers and practitioners to design foundations comprising of hollow bar micropiles installed in cohesionless soil.

## 1.2 Research objectives

The main objectives of this work are to investigate the axial and lateral performance of HBMP installed in cohesionless soil. The study focuses on the effects of drill bit/ hollow bar ( $D_b/D_h$ ) ratio, grouting pressure spacing to diameter ratio on the behavior of HBMP foundations. The detailed objectives of this research are to:

- Investigate the axial monotonic performance of single hollow bar micropiles installed in cohesionless soil with two different drill bit/ hollow bar ratios, ( $D_b/D_h$ ) = 2.25 and 3.
- Study the load transfer mechanism of HBMP under axial monotonic loading.
- Investigate the axial monotonic performance of hollow bar micropile groups installed in cohesionless soil with two different drill bit/ hollow bar ratios, ( $D_b/D_h$ ) = 2.25 and 3.
- Evaluate the effect of the commonly used spacing to micropile diameter ratio (i.e.,  $s/D_b = 3$  and 5) on the performance of micropile groups.

- Recommend a group efficiency factor considering different spacing to micropile diameter ratios.
- Evaluate the actual micropile diameter considering different size drill bit based on exhumed test micropiles.
- Examine the behaviour of micropiles under monotonic and cyclic lateral loading.
- Study the possibility of improving the lateral performance of micropiles by using fibers-reinforced grout mix.
- Develop a calibrated and verified 3D finite element model to simulate the performance of single and groups of micropiles for further investigation.

### 1.3 Methodology

In order to achieve the objectives of this study, a comprehensive investigation program was planned and performed in four consecutive stages:

- **Site investigation:** An extensive site investigation including a site survey, boreholes, SPT tests, CPTu tests, and collecting samples, which were used for laboratory investigation.
- **Field testing:** Six single micropiles were installed and tested in cohesionless soil. Two micropiles were instrumented with three vibrating wire strain gauges. Four single micropiles were installed with  $D_b/D_h$  ratios of 3 and two single micropiles were installed with  $D_b/D_h$  ratios of 2.25. Four groups of micropiles were also installed and tested with different  $D_b/D_h$  ratios, 2.25 and 3, and two different common micropiles spacings,  $s = 3D_b$  and  $5D_b$ . Each group has at least one instrumented micropile with three vibrating wire strain gauges. The load settlement

curves were used to evaluate the micropiles stiffness and capacity, while the load distribution obtained from stain gauge readings were used to evaluate the load transfer mechanism.

- **Laboratory testing:** Performing laboratory tests to determine the mechanical properties of neat grout and reinforced grout. The optimum dosage will be selected and used for further investigation. Also, pure bending moment tests were carried out on model micropiles.
- **Numerical analysis:** Three-dimensional finite element models were developed using the commercial software PLAXIS 3D. The models were calibrated and verified using the field test results. A parametric study was performed to investigate the effect of several factors on the performance of micropiles including geometry, different soil properties, and soil-micropile interface reduction factor

## 1.4 Thesis outline

The presented thesis has been organized in an Integrated Article format and comprises eight chapters as follows:

**Chapter 1** Includes an introduction and general overview that provide the historical background on micropiles and the need for execution of research is explained. Research objectives are highlighted and the methodology to achieve the research objectives is described.

**Chapter 2** Provides an extensive literature review of the current state of practice related to micropiles. It also describes the design classifications of micropiles including philosophy of behaviour and method of grouting. It also presents the installation procedure of hollow

bar micropiles. Lastly, it explains the structural and geotechnical design methods for single and groups of micropiles.

**Chapter 3** reports the performance of single micropiles under monotonic and cyclic axial loading. The effect of increasing the drill bit/ hollow bar ( $D_b/D_h$ ) ratio from 2.25 (the commonly used range in practice is typically 2 -2.5) to 3 was evaluated. The increase in micropile diameter due to the installation procedure is presented along with the benefits of increasing the  $D_b/D_h$  ratio from 2.25 to 3. The values of the ultimate bond resistance for HBMP installed in dense sand are compared to FHWA Type B micropiles and a new range is suggested.

**Chapter 4** presents the results of full-scale loading tests on four groups of micropiles and investigates the performance of micropile groups with different drill bit/ hollow bar diameter ratios of 2.25 and 3. Additionally, two different common spacing between the micropiles in groups are tested,  $s = 3D_b$  and  $5D_b$ . A finite element analysis was conducted to complement the experimental results and further evaluate the micropile groups axial capacity when the ultimate load was not reached.

**Chapter 5** addresses the performance of HBMPs under monotonic and cyclic lateral loading conditions from full-scale tests results. The effects of increasing the drill bit/hollow bar diameter ratio from 2.25 to 3 are discussed in terms of lateral stiffness and deflection. Also, the results of cyclic loading are presented in terms of its degradation parameter. Lastly, the results of the developed numerical models are discussed.

**Chapter 6** presents the results of laboratory tests, which include the mechanical properties of neat grout and reinforced grout. The results of pure bending tests for model micropiles are also presented and discussed.

**Chapter 7** reports the results of the numerical analysis of single and groups of micropiles installed in sand. Two different approaches for micropile modelling are compared and discussed. Parametric study is performed to analyze some parameters that were not feasible to examine as part of the testing program.

**Chapter 8** summarizes the main conclusions drawn from this project and recommendations for future research are suggested.

## 1.5 References

- Abd Elaziz, A. Y., & El Naggar, M. H. (2014). Geotechnical Capacity of Hollow-Bar Micropiles in Cohesive Soils. *Canadian Geotechnical Journal*, 51(10), 1123-1138.
- Bruce, D.A., & Nicholson, P.J. (1989). The Practice and Application of Pin Pilling. *ASCE Foundation Engineering Conference.*, Evanston, IL, p. 19.
- Bruce, D. A., Dimillio, A. F., & Juran, I. (1997). Micropiles: The State of Practice Part1: Characteristics, Definitions and Classifications. *In Proceeding of ICE - Ground Improvement 1997* 1:1. p. 25-35.
- Bruce, D.A., and Yeung, C.K. (1983). Minipilling at the Hong Kong Country Club. *Hong Kong Contractor* 1983, Hong Kong, p. 13-18.
- FHWA. (2005). *Micropiles Design and Construction*. Federal Highway Administration (FHWA), U.S. Department of Transportation, Washington, D.C. Publication No. FHWA-NHI-05-039.
- Li, J., and Kast, G. (2007). 30 years of GEWI-Pile Application in Canada. *In Proceedings of 8<sup>th</sup> International Workshop on Micropiles*. Toronto, Canada.
- Han, J., & Ye, S.L. (2006a). A Field Study on the Behavior of Micropiles in Clay under Compression or Tension. *Canadian Geotechnical Journal*, 43(1), 19-29.
- Timothy, M. J., Bean, J. J. & Bolton, M. K. (2012). MiniJET: A New Type of Micropile. *In Proceedings Grouting and Deep Mixing*. American Society of Civil Engineers (ASCE), New Orleans, Louisiana, 1095-1104.

Tsukada, Y. & Ichimura, Y. (1997). Micropiles in Japan: Present Status and Future Prospects. *In Proceedings on 5<sup>th</sup> International Workshop on Micropiles*. Seattle, p, 265- 278.



## CHAPTER 2

# 2 Literature Review

---

## 2.1 Introduction

This chapter a brief review of relevant literature on single and groups of micropiles since Dr. Lizzi introduced this new piling system to retrofit old monuments and historical buildings damaged during the World War II in Italy. Classification and different design philosophy of micropiles will be discussed in details and the main features of hollow bar micropile and its differences from other types of micropiles in terms of construction technique and performance characteristics will be highlighted.

## 2.2 Micropiles

Micropiles were first introduced as small piles elements to provide axial and lateral support to structures, inspired by roots of trees that can sustain the axial and lateral loads; hence, they were named as root piles. The term micropile was later standardized in North America by Federal Highway Administration (FHWA, 2005). Micropiles are now widely used for retrofitting of existing structures and for supporting new construction, especially when the use of larger diameter piles is not feasible.

Micropile is a small diameter (less than 300mm) drilled and grouted pile. Micropiles can carry a considerable amount of axial compression and tension loads due to the large grout/ground shear strength (bond) values and mainly transfer the loads by shaft friction. Juran et al. (1999) suggested that micropiles can sustain up to 5000 kN with typical load

values of 300 - 1000 kN. With the advent of more powerful drilling equipment, the micropiles diameter increased from around 100 mm to 300 mm in the current practice (Juran et al., 1999). Micropiles are a favorable option where the subsurface conditions are difficult, site with limited access, or noise and vibration need to be kept minimal as well as for minimizing structural settlement (Bruce et al., 2005).

## **2.2.1 Classification of micropiles**

Micropiles are classified based on two main criteria: philosophy of behavior and method of grouting (FHWA, 2005). The following section discusses both criteria.

### **2.2.1.1 Philosophy of Behavior (Design)**

Micropiles can be classified into two main categories depending on design philosophy, namely: CASE 1 and CASE 2. In CASE 1, micropiles are loaded directly and the reinforcement is the major source of resisting the applied loads as shown in Figure 2.1. In this case, micropiles are used to transfer the structural loads to deeper strata, mainly by the side (shaft) resistance as the competent grout transfers the applied loads to the surrounding soil. CASE 2 micropiles are used to reinforce the soil as reticulated network to resist the applied loads as shown in Figure 2.2. In this case, the structural load is applied to the whole reinforced soil mass; thus, micropiles provide stability and support to the soil, and are lightly reinforced. The vast majority of the micropiles applications around the world involves CASE 1 micropiles (FHWA, 2005).

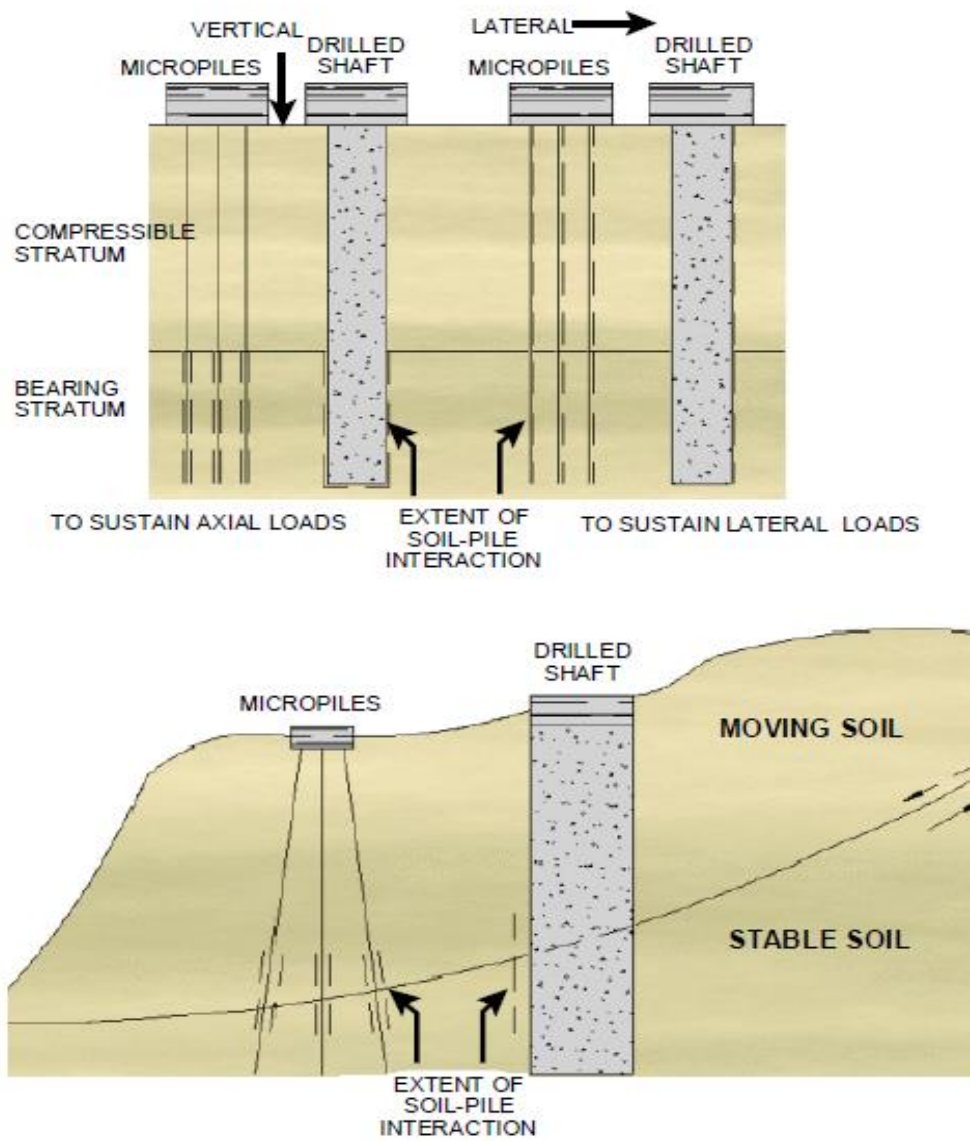
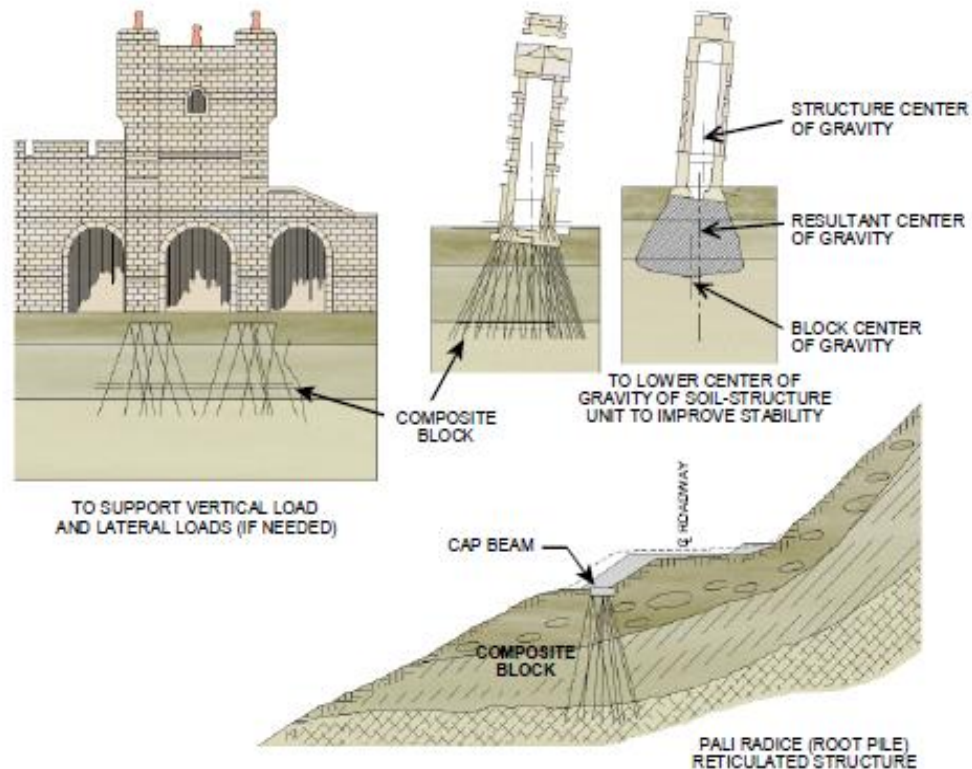


Figure 2-1 CASE 1 micropiles (after FHWA, 2005)

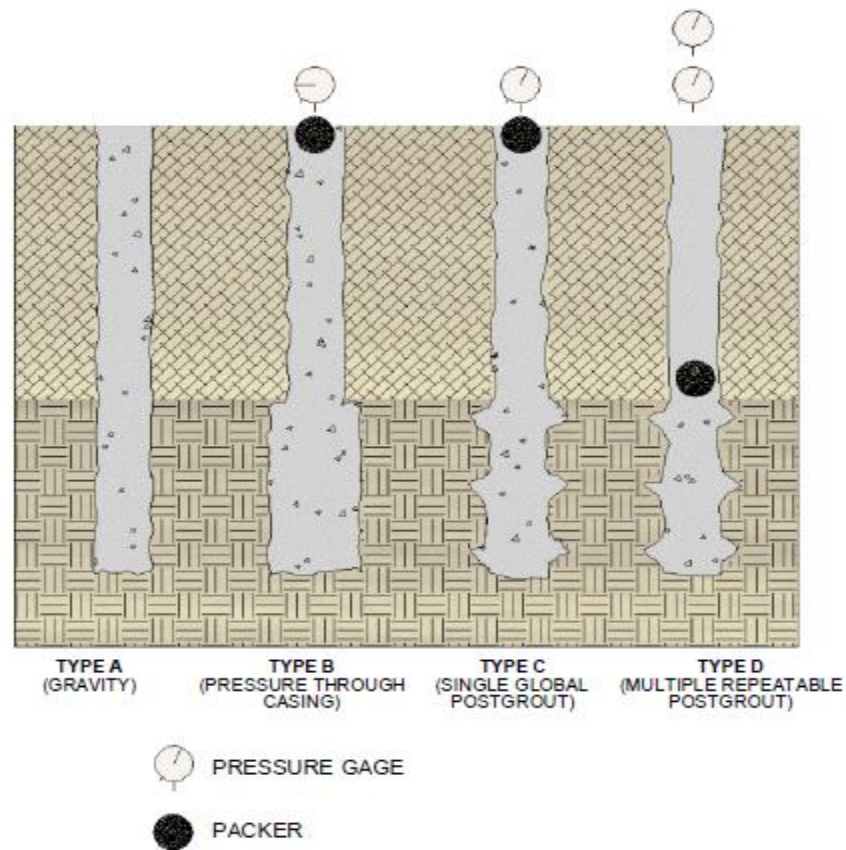


**Figure 2-2 CASE 2 micropiles (after FHWA, 2005)**

### 2.2.1.2 Method of grouting

The micropiles are classified based on their method of construction, i.e, the method of drilling and placing the grout. In particular, the method of grouting has a major influence on the grout – ground bond strength. Accordingly, FHWA (2005) has classified the micropiles into four categories as follows. Type A: the grout is placed under gravity and no pressure is required. Type B: the grout is typically applied under a pressure range from 0.5 to 1 MPa as the temporary casing is withdrawn. Type C: the grout is placed in two-step process; first, the grout is poured under gravity only, and before it hardens, similar grout is

pressured at  $> 1$  MPa without the use of packer. Type D: it is also a two – step process, where the grout is placed first under gravity as in Type A or pressurized as in Type B; after the initial grout hardens, additional grout is pressurized between 2 to 9 MPa through sleeved pipe by using packers, as many times as needed. According to this classification, hollow bar micropile is usually designated as Type B. However, the construction technique is completely different than that of Type B. Figure 2.3 shows the FHWA classification schematically.



**Figure 2-3 Micropile classification based on the method of grouting (after FHWA, 2005)**

### **2.2.2 Hollow bar micropiles**

According to FHWA classification of micropiles, hollow bar micropiles (HBMP) are designated as Type B micropiles. However, the construction technique is completely different from Type B. The construction method of hollow bar micropiles involves two main stages, which can be performed in a one-step process: advancing the drilling bit attached to a threaded hollow bar to the required depth and pressurizing the grout through nozzles in the drill bit. Therefore, it was suggested to designate hollow bar micropiles as Type E to supplement the current four types of micropiles (Timothy et al., 2012; Abd Elaziz and El Naggar, 2014). The American Association of State Highway and Transportation Official (AASHTO 2012) classified the HBMP as Type E based on the method of installation where the initial grout has a high water/cement ratio to stabilize the ground and then replaced by structural grout. The method of installation of HBMP provides a high grout-to-soil bond strength, which results in greater capacity compared to conventionally cased or uncased micropiles. Figure 2.4 shows the installation procedure for hollow bar micropiles, from setting the location of micropiles to pressurizing the competent grout.



(a) Setting micropiles location



(b) Attaching the hollow bar to the driller



(c) Drilling



(d) Attaching the 2<sup>nd</sup> segment



(e) Finish drilling



(f) Pressurizing the competent grout

**Figure 2-4 HBMP installation procedure**

## 2.3 Design of micropiles

The design philosophy of micropile differs slightly from the conventional drilled shaft. Drilled shafts typically have a large cross-sectional area resulting in a high stiffness and structural capacity, and therefore the geotechnical capacity controls the design. However, due to the small diameter of micropiles by definition, both structural and geotechnical capacities can control the design, and both need to be calculated and compared.

### 2.3.1 Structural capacity of micropiles

FHWA (2010) and AASHTO (2012) adopted the allowable stress design method (ASD) for the design of micropiles. The allowable compression load for a cased length is given by:

$$P_{c-allowable} = [0.4 f'_{c-grout} A_{grout} + 0.47 F_{y-steel} (A_{bar} + A_{casing})] \quad (1.1)$$

where:

$P_{c-allowable}$  = allowable compression load;

$f'_{c-grout}$  = unconfined compressive strength of grout;

$A_{grout}$  = area of grout in the micropile cross-section;

$F_{y-steel}$  = yield stress of steel;

$A_{bar}$  = cross-sectional area of the steel reinforcing bar;

$A_{casing}$  = cross-sectional area of the steel casing.



The allowable compressive strength is limited to the minimum for any individual micropile component. Therefore, the yield stress of steel used in Equation 1.1 is the minimum of: (1) yield stress of casing; (2) yield stress of the central steel bar; and (3) maximum stress of cased grout failure. For hollow bar micropiles where no casing is used, the allowable compression load is given as:

$$P_{c-allowable} = [0.4 f'_{c-grout} A_{grout} + 0.47 F_{y-steel} A_{bar}] \quad (1.2)$$

The allowable tension load of cased micropiles can be obtained as:

$$P_{t-allowable} = [0.55 F_{y-steel} (A_{bar} + A_{casing})] \quad (1.3)$$

While the allowable tension load of hollow bar micropiles can be calculated as:

$$P_{t-allowable} = [0.55 F_{y-steel} A_{bar}] \quad (1.4)$$

### 2.3.2 Geotechnical capacity of micropiles

The applied compression and tension loads to the micropile head is resisted mainly through the bond length. The bond length (or sometime called bond zone) is formed around the central bar because of the grout being pressurized into the surrounding soil. Due to the relatively small cross-sectional area of micropiles, FHWA (2005) ignores the contribution of end bearing to the total capacity of micropiles and considers only the shaft resistance as the main source for micropile capacity. For hollow bar micropiles, the embedded length of micropiles is equal to the bond length as no casing is required for hollow bar micropile installation. FHWA (2005) provides an equation that can be used to calculate the allowable geotechnical capacity of micropiles;

$$P_{G-allowable} = \frac{\alpha_{bond}}{FS} * \pi * D_b * L_p \quad (1.5)$$

where:

$\alpha_{bond}$  = grout to ground ultimate bond strength;

$FS$  = factor of safety applied to the ultimate bond strength;

$D_b$  = diameter of drill bit hole;

$L_p$  = bond length.

Table 2.1 presents the FHWA (2005) guidance for selecting the grout-to-ground ultimate bond strength based on the type of soil and the type of micropiles: Type A, B, C and D. FHWA (2005) recommends using an overall factor of safety of 2 after meeting two requirements. Firstly, performing at least one ultimate or verification test before micropile installation and one additional ultimate or verification test for each different ground conditions encountered during construction; and secondly conducting proof testing for 5% of the total number of installed micropiles. For difficult ground conditions such as creeping soils, high plasticity soils, weak rock, or when previous experience on similar ground is limited, a factor of safety of 2.5 should be used to estimate the bond length.

### 2.3.3 Geotechnical Capacity of Micropile Group

Micropiles are typically installed in groups rather than as single micropiles to resist compression, tension, and lateral loads. For cohesive soils, the efficiency of a micropile group is a function of the micropiles spacing and the contact between the micropile cap and the underlying soil. Accordingly, the group capacity can be given by:

$$Q_g = (\alpha_{bond} * \pi * D_b * L_b) * \text{no of micropiles in group} * \eta \quad (1.6)$$

Where  $Q_g$  = the ultimate group capacity; and  $\eta$  = efficiency factor.

FHWA (2005) recommends some values for the efficiency factor if the micropile cap is not in firm contact with the underlying soft soil (undrained shear strength of the soil is less than 95 kPa): between 0.65 for a spacing  $2.5D_b$  and 1.0 when the spacing is equal to  $6D_b$ .

The values in between can be interpolated.

**Table 2-1 Typical values of Grout-to-Ground Bond for micropile design**

Soil/Rock Description	Grout-to-Ground Bond Ultimate Strengths, kPa			
	Type A	Type B	Type C	Type D
<b>Silt &amp; Clay</b> (some sand) (Soft, medium plastic)	35 – 70	35-96	50-120	50-145
<b>Silt &amp; Clay</b> (some sand) (stiff, dense to very dense)	50 – 120	70-190	95-190	95-190
<b>Sand</b> (some silt) (fine, loose-medium dense)	70 – 145	70-190	95-190	95-240
<b>Sand</b> (some silt, gravel) (fine-coarse, med.-very dense)	95 – 215	120-360	145-360	145-385
<b>Gravel</b> (some sand) (medium-very dense)	95 – 265	120-360	145-360	145-385
<b>Glacial Till</b> (silt, sand, gravel) (medium-very dense, cemented)	95 – 190	95-310	120-310	120-335
<b>Soft Shales</b> (fresh-moderate fracturing, little to no weathering)	205 - 550	N/A	N/A	N/A
<b>Slates and Hard Shales</b> (fresh-moderate fracturing, little to no weathering)	515 - 1,380	N/A	N/A	N/A

<b>Limestone</b> (fresh-moderate fracturing, little to no weathering)	1,035 - 2,070	N/A	N/A	N/A
<b>Sandstone</b> (fresh-moderate fracturing, little to no weathering)	520 - 1,725	N/A	N/A	N/A
<b>Granite and Basalt</b> (fresh-moderate fracturing, little to no weathering)	1,380 – 4,200	N/A	N/A	N/A

For micropiles installed in cohesionless soil, FHWA (2005) recommends calculating the capacity of the micropile groups as the sum of the capacity of individual micropiles as long as the micropiles are installed with a center-to-center distance equal to  $3D_b$  or greater.

## 2.4 Axial Monotonic Behaviour of Micropiles

### 2.4.1 Single Micropiles

Bruce et al. (1993) performed laboratory and field tests on micropiles considering three different micropiles configurations. The field test was performed on Type A micropiles embedded on rock and Type B micropiles in soil. The tests were conducted with and without internal steel cages. The elastic Ratio concept was introduced based on the data obtained from these tests. The Elastic ratio is defined as the ratio between the elastic settlement of the pile and the applied load. Based on the elastic ratio concept, the elastic settlement can be used to evaluate the length of the stressed micropile. The stressed length can be used to evaluate the load distribution to the surrounding ground.

Jeon and Kulhawy (2001) reviewed the results of twenty-one full-scale compression tests on micropiles with varying diameter from 150 mm to 190 mm and embedded lengths between 9 m and 30 m. Three different types of micropiles were included: Type B, C and D. They concluded that the load-carrying capacity of micropiles is different than drilled shafts because of the method of micropile installation which utilizes pressurized grout. They indicated that the capacity of micropiles installed in sand is larger than drilled shafts by 1.5 to 2.5 times, whereas for clay soil the capacity of micropiles can be greater than 1.5 times the capacity of drilled shafts.

Han and Ye (2006 a & b) carried out a field test on micropiles installed in native Shanghai clay. The applied loads simulated the case of adding stories to an existing building. Two monotonic compressions and two monotonic tension tests were carried out on single micropiles. Additionally, one group of four piles was tested. They concluded that the mobilized ultimate skin friction was 0.9 to 1.2 times the soil undrained shear strength. Thomson et al. (2007) presented the results of axial compression, uplift and lateral load tests on micropiles installed in mainly sandy soil that were used to upgrade pier foundations. Based on the load test results, they concluded that the ultimate bond resistances values of grouted micropiles provided by FHWA (2000) seem to be reasonable. Similarly, Wolosick (2009) reported the ultimate bond strength for micropiles Type A, B and D installed in clays and sands. He evaluated bond strength values from load tests and reported excellent agreement between measured grout-to-ground bond and nominal bond strength values proposed by FHWA (2005).

Meanwhile, Stuedlein et al. (2008) reported the results of compression and tension tests for micropiles installed in medium dense to dense, gravelly sand. The micropiles had a cased

length of 3.05 m and a 5.20 m bond zone length. The casing diameter was 140 mm with a 13 mm wall thickness. The load–settlement curves indicated a stiffer response of micropiles when subjected to compression loading compared to response under uplift loading. They noted that ignoring the contribution of end bearing resistance seems to be conservative.

The hollow bar micropile (HBMP) utilizes a threaded hollow steel bar as the main reinforcing element, which also serves as the drilling and grouting conduit. HBMPs have been known with different names such as Self Drilling Micropiles and Injection Bore Micropiles. The construction procedure of HBMP involves two main stages that are performed in one-step process: advancing the drilling bit attached to a threaded hollow bar to the required depth; and injecting the grout through the nozzles of the drill bit. The grout is injected under pressure which mostly transformed to velocity at the nozzles to scour and transport the soil, and that grout penetration in to open graded formations. Pressurizing the grout can also densify the surrounding soil and increase the effective micropile diameter. The method of installation of HBMP provides a high grout to soil bond strength, which results in greater capacity compared with conventional cased or uncased micropiles.

Abd Elaziz and El Naggar (2012) conducted a field study on single hollow core micropiles in stiff silty clay. Ten axial load tests were conducted on four micropiles which included three monotonic compression, two monotonic tension, four cyclic compression, and one cyclic tension axial tests. It was reported that the bond strength values suggested by FHWA (2005) for silty clay deposit may be underestimated when considering the micropiles as type B. No degradation in stiffness was reported after 15 cycles of loading. Additionally, Drbe and El Naggar (2014) conducted full-scale load tests on eight micropiles installed in

cohesive soil to evaluate the suitability of FHWA design guidelines. It was concluded that the values of grout – ground bond strength reported by FHWA for type B micropile underestimated the bond strength for cohesive soils.

### **2.4.2 Micropile Groups**

Based on the pile cap contact condition with the underlying soil, two different types of pile groups may be identified, free standing groups and piled foundations. In free standing groups, the pile cap is not in contact with the soil beneath it, whereas in the case of piled foundations the pile cap is resting on the underlying soil. In both cases, the efficiency factor is considered as the ratio of the ultimate load capacity of the pile group to the sum of the load capacity of single piles.

Cooke (1974) discussed the effect of pile spacing on group efficiency. He defined the efficiency as the ratio of the average load per pile in a group when failure occurs to the ultimate bearing capacity of a comparable single pile. The settlement ratio was defined as the settlement of the pile group divided by the settlement of a single pile when they carry the same proportion of their ultimate load.

O'Neill (1983) conducted full-scale tests on 3×3 pile groups in stiff clay. He stated that the pile group capacity can be estimated with reasonable accuracy as the sum of individual piles (i.e., group efficiency is 1.0).

Fleming et al. (1992) suggested efficiency factors based on the pile slenderness ratio, pile stiffness ratio, pile spacing ratio, soil homogeneity, and Poisson's ratio. Fleming et al. (2009) claimed that the concept of efficiency for pile groups is more relevant with respect

to the stiffness of a foundation rather than its capacity. Correspondingly, Randolph (1994) showed that using less central piles can be more efficient in reducing the settlement beneath a piled raft when compared with a grid configuration.

The French National Research Project on Micropiles “FOREVER” is one of the major research projects on micropiles. Based on the results of 54 loading tests (full-scale and scaled models) on micropile groups, only groups with a large number of micropiles provided an efficiency factor greater than one whereas the majority of groups had an efficiency factor less than or close to one (Frank and Schlosser, 2009).

Rose et al. (2013) carried out a centrifuge model and numerical analysis on a perimeter pile group in clay. The main objective was to establish the relative effectiveness of pile groups with no inner pile when compared to a grid configuration. It was demonstrated that the common grid group is less efficient than a perimeter group; a group efficiency of more than one was reported. They suggested that block group failure of perimeter pile groups can occur when the spacing is less than 2 d. They also suggested that the capacity of linear groups is not affected by interaction when pile-to-pile spacing is between 1.25 and 3 d. However, they claimed that the test conditions and procedures are not analogous and are not necessarily applicable to all pile groups in clay.

Abd Elaziz and El Naggar (2014) conducted full-scale load tests on pairs of hollow bar micropiles installed in soft soil. The test results were used to calibrate a three-dimensional finite element model. A parametric study was then performed based on the calibrated model. A group efficiency factor of one was suggested for hollow bar micropile groups installed in cohesive soil.



## 2.5 Lateral Performance of Micropiles

The lateral performance of micropiles is generally dependent on the flexural rigidity ( $EI$ ) of the micropile and the surrounding soil strength and stiffness. In other words, it is a soil-structure interaction issue and both pile and soil have an influence on each other and the overall pile-soil system response. One of the main limitations of micropiles is the ability to support large lateral loads due to their high slenderness ratio and small flexural rigidity. To overcome this issue, a steel casing must be installed in the top part of the micropile to increase its flexural rigidity.

Poulos and Davis (1980) introduced an elastic continuum model that allows variation of Young's modulus with depth. It also takes into account the non-linearity of the soil around the piles. Teerawut (2002) performed lateral load tests on micropiles installed in sand with several relative densities and back figured the  $p$ - $y$  curves. He concluded that the stiffness of  $p$ - $y$  curves increases with increase in micropile diameter. However, a marginal increase for stiffness in dense sand was reported.

Richards and Rothbauer (2004) compared the results of lateral load tests performed on micropiles installed as part of eight different projects to the predictions of the methods recommended by NAVFAC and CLM as well as predictions from LPILE analyses. They concluded that the predictions of LPILE, which is based on the  $p$ - $y$  curve approach, compared well with the measured responses. Meanwhile, the deflections obtained from CLM or NAVFAC methods were significantly less than the measured values.

Long et al. (2004) summarized the results of ten lateral load tests on micropiles. Micropiles were installed in clay overlying sand with a total length of 15.20 m. Casings with 13.8 mm thickness and 224 mm outer diameter were installed for the upper 9 m portion of the piles. The results obtained from the tests were compared with conventional  $p$ - $y$  curves using the LPILE program. There was a good agreement between the two results.

Abd Elaziz and El Naggar (2015) studied the performance of hollow bar micropiles under monotonic and cyclic lateral loads installed in stiff silty clay. The load test results were used to calibrate a numerical model, which was then used to perform a parametric study. They concluded that the properties of soil along a depth of 10 times the micropile diameter governed the load - settlement curve. They demonstrated the ability of hollow bar micropiles to carry moderate lateral loads with the appropriate reinforcement configuration and pile head fixity.

## **2.6 Summary**

In this chapter, a brief review of relevant literature was conducted focusing on micropile performance under axial and lateral loads. The review demonstrated the scarcity of available data on the performance of hollow bar micropiles installed in cohesionless soil and subjected to axial and lateral loads. Furthermore, the effect of several factors on the behaviour of single HBMP and groups, such as the effect of increasing the drill bit/ hollow bar ( $D_b/D_h$ ) ratio and grouting pressure, as well as micropiles spacing need to be addressed. To fully exploit the constructional advantages of micropiles in different applications, this research effort attempts to evaluate the performance of single HBMP and groups installed

in sand and establish some guideline for their design considering the micropile spacing to diameter ratios that are most commonly used in practice: 3 and 5.

## 2.7 References

- AASHTO. (2012). *AASHTO LRFD Bridge Design Specification*, Customary U.S. Units. The American Association of State Highway and Transportation Officials (AASHTO). Section 10.
- Abd Elaziz, A. Y., & El Naggar, M. H. (2012). Axial Behaviour of Hollow Core Micropiles Under Monotonic and Cyclic Loadings. *Geotechnical Testing Journal*, 35(2), 249-260.
- Abd Elaziz, A. Y., & El Naggar, M. H. (2014). Geotechnical Capacity of Hollow-Bar Micropiles in Cohesive Soils. *Canadian Geotechnical Journal*, 51(10), 1123-1138.
- Abd Elaziz, A.Y., & El Naggar, M.H. (2015). Performance of Hollow Bar Micropiles under Monotonic and Cyclic Lateral Loads. *Journal of Geotech. GeoEnvironmental Eng.* 141 (5): 04015010.
- Broms, B. B. (1964a). Lateral Resistance of Piles in Cohesionless Soils. *Journal of the Soil Mechanics and Foundations Division*, 90(3): 123-158.
- Broms, B. B. (1964b). Lateral Resistance of Piles in Cohesive Soils. *Journal of the Soil Mechanics and Foundations*, 90(2): 27-64.
- Bruce, D. A. (1993). Micropiles: The State of Practice Part 1. *ASCE Geotechnical Special Publication*, 1-26.
- Bruce, D. A., Cadden, A. W., & Sabatini, P. J. (2005). Practical advice for foundation design – micropile for structural support. *Conf. GeoFrontiers 2005. Contemporary Issues in Foundation Engineering*: pp. 1-25.
- Cooke, R. W. (1974). *Piled foundations: A Survey of Research at the Building Research Station*. Building Research Establishment.

- Drbe, O. E., & EL Naggat M. H. (2014). Axial Monotonic and Cyclic Compression Behaviour of Hollow Bar Micropiles. *Canadian Geotechnical Journal*. 52: 426-441.
- FHWA. (2005). *Micropiles Design and Construction*. Federal Highway Administration (FHWA), U.S. Department of Transportation, Washington, D.C. Publication No. FHWA-NHI-05-039.
- Fleming, W. G. K, Weltman, A. J., Randolph, M. F. & Elson, W. K. (2009). *Piling Engineering*. Abingdon: Taylor and Francis.
- Frank, R. & Schlosser, F. (2009). Some Lessons Learnt from the 'FOREVER' French National Research Project on Micropiles. *In Proceedings of 9<sup>th</sup> International Society of Micropiles Workshop*, London, UK.
- Han, J., & Ye, S.L. (2006a). A Field Study on the Behavior of Micropiles in Clay under Compression or Tension. *Canadian Geotechnical Journal*, 43(1), 19-29.
- Jeon, S. S. & Kulhawy, F. H. (2001). Evaluation of Axial Compression Behaviour of Micropiles. *In Proceedings of a specialty conference: Foundations and Ground Improvement (GSP 113)* (pp. 460-471). Blacksburg, Virginia: ASCE.
- Juran, I., Bruce, D. A., Dimillio, A. & Benslimane, A. (1999). Micropiles: The State of Practice. Part II: Design of Single Micropiles and Groups and Networks of Micropiles. *Ground Improvement*, 3, 89-110.
- Long, J., Maniaci, M., Menezes, G. & Ball, R. (2004). Results of Lateral Load Tests on Micropiles. *In Proceedings of sessions of the GeoSupport Conference: Innovation and Cooperation in the Geo-Industry*, Orlando, Florida: Geo-Institute of the American Society of Civil Engineers, pp. 122-133.
- O'Neill, M. W. (1983). Group Action in Offshore Piles. *Geotechnical Engineering in Offshore Practice*. Houston: ASCE.

- Poulos, H. G. & Davis, E. H. (1980). *Pile Foundation Analysis and Design*. New York: Wiley.
- Randolph, M. F. (1994). Design Methods for Pile groups and Piled Rafts. *Soil Mechanics and Foundation*, Vol. 4, pp. 718-742.
- Richards, T. D. & Rothbauer, M. J. (2004). Lateral Loads on Pin Piles (Micropiles). In *Proceedings of the GeoSupport Conference: Drilled Shafts, Micropiling, Deep Mixing, Remedial Methods and Specialty Foundation Systems*, Orlando Florida, United States: American Society of Civil Engineers, pp. 158-174.
- Rose, A.V., Taylor, R. N. & El Naggar, M. (2013). Numerical Modelling of Perimeter Pile Groups in Clay. *Canadian Geotechnical Journal*, 50(3): 250-258.
- Stuedlein, A. W., Gibson, M. D., & Horvits, G. E. (2008). Tension and Compression Micropile Load Test in Gravelly Sand. In *proceedings of 6th International conference on case histories in geotechnical engineering*, Arlington, VA.
- Teerawut, J. (2002). *Effect of Diameter on the Behaviour of Laterally Loaded Piles in Weakly Cemented Sand*. Ph.D. Dissertation, University of California, San Diego, California.
- Thomson, P., Leew, B., Zakeri, A., Becker, D., Bunce, C. & Dittrich, P. (2007). Axial Compression, Axial Tension and Lateral Load Response of Pre-Production Micropiles for the CPR Mile 62.4 Nipigon Subdivision Bridge. In *Proceedings of the 8th International Workshop on Micropiles (IWM)*. Toronto, ON, Canada.
- Timothy, M. J., Bean, J. J. & Bolton, M. K. (2012). MiniJET: A New Type of Micropile. In *Proceedings Grouting and Deep Mixing*. American Society of Civil Engineers (ASCE), New Orleans, Louisiana, 1095-1104.
- Wolosick, J. (2009). Ultimate micropile bond stresses observed during load testing in clays and sands. In *Proceedings Selected Papers of the 2009 Int. Foundation Congress and Equipment Expo*. ASCE, New York, 12-22.

## CHAPTER 3

### **3 Evaluation of Axial Performance of Hollow Bar Micropiles Constructed with Different Drill Bit to Hollow Bar Diameter Ratio**

---

#### **3.1 Introduction**

A micropile is a small diameter drilled and grouted pile as described by FHWA (2005). Micropiles can carry considerable axial compression and tension loads due to the large grout/ground shear resistance, which facilitates load transfer by friction. Micropiles have been used for retrofitting existing foundations, and to support new construction, especially when the use of larger diameter piles is not feasible. There has been a rapid growth in using micropiles over the last few decades (Bruce and Nicholson 1989; Pearlman and Wolosick 1992, Li and Kast 2007; Kershaw 2014). A comprehensive study on micropiles behaviour was commissioned by Federal Highway Association (FHWA) in 1993 and was performed in parallel to a similar study in France in 1992, including centrifuge and full-scale field testing (Bruce et al. 1997). These studies helped understand the behaviour of micropiles and expand their use in foundation design.

As the method of grouting has major influence on the grout – ground bond strength, FHWA (2005) has classified the micropiles into four categories. Type A: the grout is placed under gravity and no pressure is required. Type B: The grout is typically pressurized under a pressure range from 0.5 to 1 MPa as the temporary casing is withdrawn. Type C: the grout is placed in two-step process. First, the grout is poured under gravity only as in Type A. Before the hardening of the grout, similar grout is pressured of at least 1MPa without the

use of packer. Type D: Like Type C, it is a two – step process, the grout is placed under gravity as in Type A and sometimes pressurized as in Type B. After hardening of the initial grout, additional grout is applied at pressure between 2 to 9 MPa through sleeved pipe by using packers, as many times as needed.

Stuedlein et al. (2008) reported compression and tension tests of Type B micropiles installed in medium dense to dense, gravelly sand. The load– settlement curves indicated that micropiles subjected to compression loading exhibited a stiffer response than those subjected to uplift loading. They noted that ignoring the contribution of end bearing resistance seems to be conservative for micropiles resting on gravelly sand. Wolosick (2009) reported the ultimate skin friction for micropiles Type A, B and D installed in clays and sands. He evaluated the ultimate skin friction values from load tests and reported excellent agreement between measured ultimate skin friction and nominal bond strength values proposed by FHWA (2005). Han and Ye (2006) conducted full-scale load tests on four Type B single micropiles installed in soft clay soil and subjected to compression and or tension loading. They reported the load-settlement responses, elastic moduli, load transfer distribution, toe resistance and skin friction. It was found that for a micropile under compression loads, the average ultimate skin friction was about 0.90 – 1.20 times the undrained shear strength of the native soil. While under tension loads, it was about 0.68 – 0.73 times the undrained shear strength of the native soil. The measured values of ultimate skin friction were less than the lower value suggested by FHWA for Type B.

The hollow bar micropile (HBMP) utilizes a threaded hollow steel bar as the main reinforcing element, which also serves as the drilling and grouting conduit. HBMPs have been known with different names such as Self Drilling Micropiles and Injection Bore



Micropiles. The construction procedure of HBMP involves two main stages that are performed in one-step process: advancing the drilling bit attached to a threaded hollow bar to the required depth; and injection the flashing grout through the nozzles of the drill bit till the required level is achieved, a structural grout is injected. The grout is injected under pressure, which increases grout velocity at the nozzles to scour and transport the soil. This allows grout penetration into formed openings, hence increasing the effective micropile diameter. Pressurizing the grout can also densify the surrounding soil.

HBMP is typically designed as a Type B as per the classification of FHWA (2005). However, the construction technique is completely different than a type B micropile. It was suggested recently to denote hollow bar micropiles as Type E micropile (Timothy et al., 2012; Abd Elaziz and El Naggar, 2014). The American Association of State Highway and Transportation Officials (AASHTO 2012) classified the HBMP as Type E based on the method of installations where the initial grout has high water/cement ratio to stabilize the ground and then replaced by structural grout. The method of installation of HBMP provides a high grout to soil bond strength, which results in greater capacity compared with conventional cased or uncased micropiles.

Gomez et al. (2008) reported a case study in which HBMPs were employed for retrofitting of foundations for two bridges. In total, 260 micropiles were installed; 180 in sand and 80 in stiff silty clay. Proof test up to 150% of the design load was performed on all micropiles. In addition, four micropiles were tested to at least two and a half times the design load or to failure. It was concluded that HBMP provides a significant bond capacity for granular soil, generally greater than Type B micropile as suggested by FHWA (2005). Meanwhile, for HBMP constructed in stiff silty clay the ultimate skin friction values were in good

agreement with Type B micropile. Furthermore, Timothy et al. (2012) suggested that the grout injected at a moderate pressure for Type E micropiles results in a marginal increase in diameter in excess of the drill bit diameter. However, they concluded that the combination of jet grouting with threaded hollow bar can create a larger diameter micropile.

Abd Elaziz and El Nagggar (2012 & 2014) conducted full-scale field tests to investigate the axial behaviour of HBMP under monotonic and cyclic loading in cohesive soils. Ten monotonic and cyclic axial loading tests were performed on four HBMP. The results showed that the ultimate skin friction values suggested by FHWA Type B installed in silty clay soil underestimated the capacity of HBMP. In addition, they reported there is no sign of full debonding at the pile-soil interface after 15 cycles with load amplitude of 33%. The vertical settlement of the micropiles increased with increasing the number of cyclic loading. Although, the micropile head stiffness remained constant. Abd Elaziz and El Nagggar (2014) developed a finite element model for the HBMP and calibrated it using the field test results and employed it to conduct a parametric study. Based on the results obtained from the numerical model, they proposed an equation to evaluate the axial capacity of HBMP installed in cohesive soil. Drbe and El Nagggar (2014) conducted full-scale load tests on eight micropiles installed in cohesive soil to evaluate the suitability of FHWA design guidelines. It was concluded that the values of grout – ground bond strength reported by FHWA for type B micropile underestimated the ultimate skin friction in case of cohesive soil by about 19% in case of micropiles with drill bit of 178 mm. They reported that the micropiles performed well during the cyclic loading.

Micropiles subjected to tension loads, transfer the applied loads to the adjacent soil by friction at the micropile-soil interface. The load transferred to the surrounding soil results in increased shear stresses and strains in the soil. As the shear stresses approach soil strength, failure occurs and the micropile experiences large settlement with a small increase in the applied load. This failure load, also defined as ultimate pile capacity, is determined most reliably from pile load tests.

Chan and Hanna (1980) performed cyclic pullout load tests on model piles installed in sand in lab environment. They reported that for small cyclic tensile load between 15 to 20% of the ultimate load, small settlement occurred, and the settlement rate decreased with the number of cycles. While for large cyclic loads between 30 to 70%, the pile experienced large settlements and failed with the increase of number of load cycles. Turner and Kulhawy (1990) performed laboratory experimental study on the effects of repeatable loads on uplift capacity of drilled shafts in granular soils. They reported that the cyclic loading significantly affected the capacity of drilled shafts in sand. Cavey et al. (2000) installed grouted micropiles in loose to medium dense sand and silt and tested them under cyclic loading conditions. Their results demonstrated that a considerable reduction occurred in the micropile capacity after a small number of cycles. The ultimate capacity reduced by 60% after just two cycles.

Yacyshyn (2009) reported results of two-way cyclic tests on drilled and grouted GEWI-Piles installed in dense, medium to fine sands. The tested micropiles were classified as Type "D" in accordance with the U.S. Federal Highway Administration (FHWA). The permanent settlement under tension cyclic loading ranged from 4.5 to 8.2 mm.

The total settlement of micropile is a combination of its elastic deformation and that of the surrounding soil. Sulaiman and Coyle (1976) proposed a load transfer method (T-Z) to evaluate response of piles installed in cohesionless soil and subjected to tension loading. Randolph and Worth (1978) proposed a method based on elastic continuum approach for estimating the load- settlement behaviour of pile under compression loads. In this method, the total settlement is given by the sum of the settlement due to the deformation below the pile toe and the surrounding soils.

The cyclic nature of loading affects its settlement behaviour and should be accounted for in the analysis. Poulos (1988) suggested the concept of cyclic stability diagram in which the stability can be identified by three states: (i) stable region, where cyclic loading has no effect on pile capacity; (ii) metastable region in which the cyclic loading affects the pile capacity but does not cause failure; and (iii) unstable region, in which the cyclic loading causes failure at a specific number of load cycles. Jardine (1991) proposed a similar concept to cyclic stability diagram by Poulos known as cyclic interaction diagram. Instead of the applied load in axis coordinate in the cyclic stability diagram, the cyclic interaction diagram uses the shear stresses on the pile surface. Juran and Weinstein (2009) presented a new short-term testing procedure and interpretation model to predict the strain-rate dependent under static and cyclic loading. The model was validated experimentally in controlled laboratory environment.

Most of the available methods for evaluation of cyclic loading effects on piles are based on observations for conventional piles (i.e. driven piles or drilled shafts). However, the method of construction of hollow bar micropiles is expected to have a significant impact

on their cyclic performance. Hence, there is a need to evaluate the cyclic performance of HBMP subjected to cyclic loading and to develop analytical tools suitable for HBMP.

Therefore, the geotechnical performance of hollow bar micropiles under tensile and compression cyclic loading is reported in this study.

In all above-mentioned studies on the performance of hollow bar micropiles, the drill bit/hollow bar ( $D_b/D_h$ ) ratio was less than 2.5. In addition, no design guidelines for HBMP are established yet due to gap in knowledge of the effect of several factors on their behaviour. In particular, the effects of drill bit/hollow bar ( $D_b/D_h$ ) ratio and grouting pressure on the performance and capacity of HBMP have not been studied.

The objective of this work is to investigate the performance of HBMP installed in sand under monotonic and cyclic loading and to evaluate the effect of increasing the drill bit/hollow bar ( $D_b/D_h$ ) ratio from 2.25 (commonly used range in practice 2 -2.5) to 3. It should be noted that ( $D_b/D_h$ ) is influenced by two factors: the limitation of available pressure that needs to be maintained in order to take advantage of the efficient load transfer mechanism of HBMP; and the structural integrity of the grout-steel interface. The results of the full-scale load tests are presented and discussed in terms of load – settlement curves, axial force distribution, axial head stiffness, tip resistance and skin friction for both compression and tension loading conditions. The results should be of value for both practitioners and researchers.

### 3.2 Geotechnical Site Characterization

The site is located near Ayr, Ontario. Extensive site exploration was performed for this project, which included both in-situ and laboratory tests. Three boreholes were drilled to various depths using hollow stem augers of 130mm, followed by standard penetration test (SPT). Soil samples were extracted from the borings using split spoon sampling method and transported to the laboratory for further testing. Figure 3.1 shows the SPT results for the closest boreholes to the test micropiles location (BH1 and BH2). The first 200 mm consisted of granular base fill with some gravel and recycled asphalt overlaying a layer of brown very dense sand up to 11m depth. Seams of silt and silty clay were encountered at different levels. The ground water table was observed between 9.5 to 10.5m from the ground surface. In addition, four piezocone penetration tests (CPTu) were performed across the site, two of them were in the vicinity of the test locations (CPTu1 and CPTu2). The soundings for CPTu1 and CPTu2 are shown in Figure 3.2 with the soil behaviour type (SBT) along the depth according to the classification chart proposed by Robertson (1990). The average cone resistance corrected for the pore water pressure ( $q_t$ ) ranged from 10 to 30 MPa in the upper 6.5m and 30 to 45 MPa from 6.5m to 8m followed by a decrease in ( $q_t$ ) with average of 20 MPa. The SBT chart proposed by Robertson (1990) indicated that the soil is mainly sand with some seams of silt and sandy silt. The sand relative density was evaluated using the correlations proposed by Kulhawy and Mayne (1990), and the obtained relative density profile is plotted in Figure 3.3a.

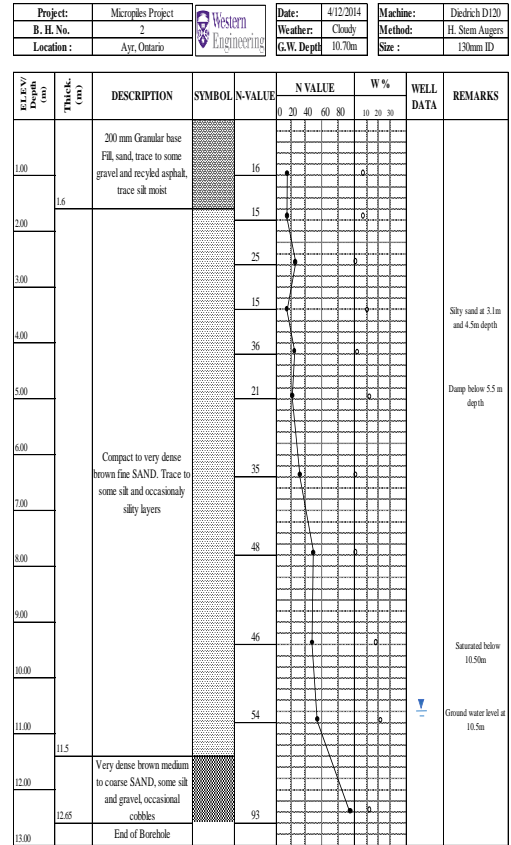
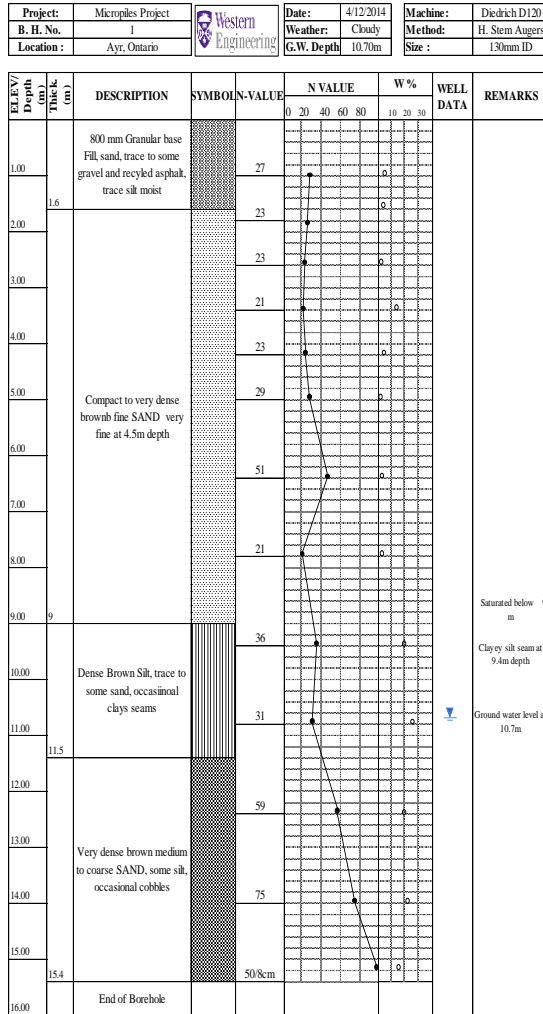

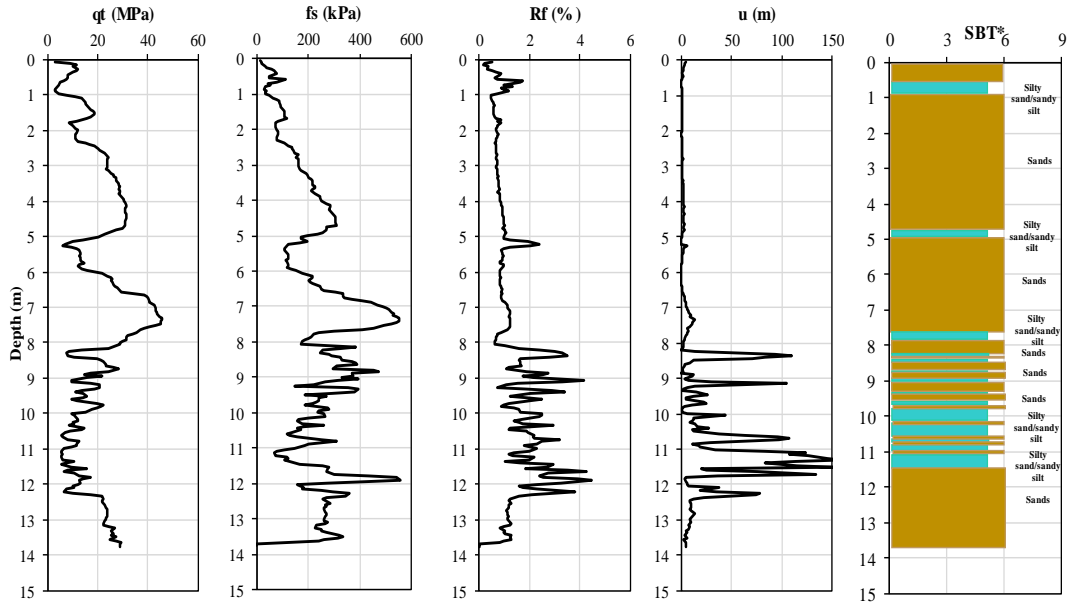
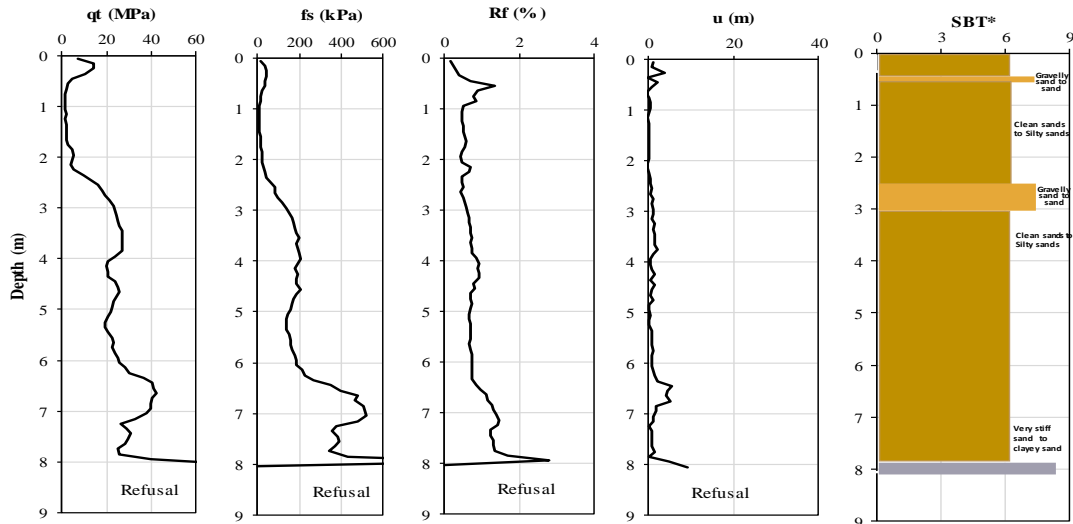


Figure 3-1 BH1 and BH2 log with SPT N values and water content

<b>Project:</b>	Micropiles Project		<b>Date:</b>	13/07/2015	<b>Max Depth:</b>	13.75 m
<b>Sounding:</b>	1		<b>Weather:</b>	Sunny	<b>Depth Inc:</b>	0.050 m
<b>Location:</b>	Ayr, Ontario		<b>G.W. Depth:</b>	9.0 m	<b>AVG Int :</b>	0.10 m



<b>Project:</b>	Micropiles Project		<b>Date:</b>	13/07/2015	<b>Max Depth:</b>	8.10 m
<b>Sounding:</b>	2		<b>Weather:</b>	Sunny	<b>Depth Inc:</b>	0.050 m
<b>Location:</b>	Ayr, Ontario		<b>G.W. Depth:</b>		<b>AVG Int :</b>	0.10 m

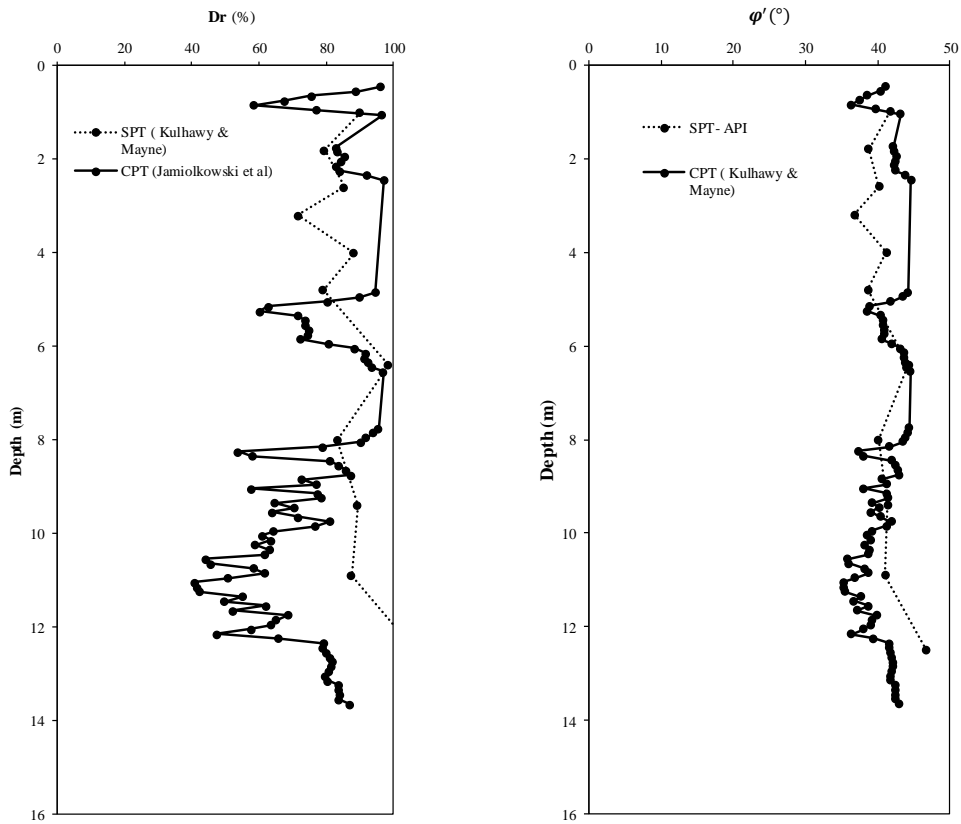


\* SBT: Robertson, 1990

Figure 3-2(a) CPT1 (b) CPT2 sounding with SBT

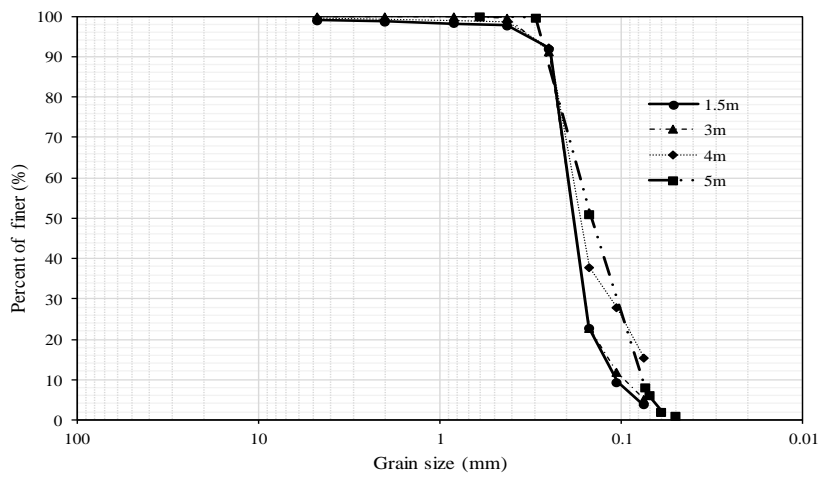


There is a good agreement between the two test results, which indicates that the sand is mainly dense up to the depth of interest, about 6m. The angle of internal friction was evaluated from direct shear tests and from two different correlations proposed by the American Petroleum Institute (1987) and Kulhawy and Mayne (1990). The calculated peak angle of internal friction profiles was compared with the direct shear test results in Figure 3.3b. As can be noted from Figure 3.3b, there is a good agreement between the computed values of the angle of internal friction using the two correlations with the measured values obtained from direct shear tests and that the average value of peak angle of internal friction is approximately  $42^\circ$ . The sieve analysis has shown that the soil along the piles is primarily fine sand as shown in Figure 3.3c.



(a)

(b)



(c)

**Figure 3-3 Properties of soil at test site: a) relative density; b) angle of internal friction; c) grain size distribution**

### 3.3 Micropile installation

Six hollow bar micropiles were constructed using an Ingersoll Rand ECM350 drill rig by HC Matcon. The hollow bars utilized were R51N with 51 mm outer diameter and 33 mm inner diameter. Tungsten carbide cross cut drill bits were employed for granular soils. A plan view of the test site showing the locations and distances between single micropiles and micropile groups along with the locations of SPTs and CPTs is presented in Figure 3.4. Four HBMPs (MP1, MP2, MP5 and MP6) were installed with a 152 mm drill bit diameter ( $D_b/D_h = 3$ ), and two (MP3 and MP4) were installed with 115 mm drill bit diameter ( $D_b/D_h = 2.25$ ). The total length of the micropiles was 6.0 m with 5.75 m embedded length.

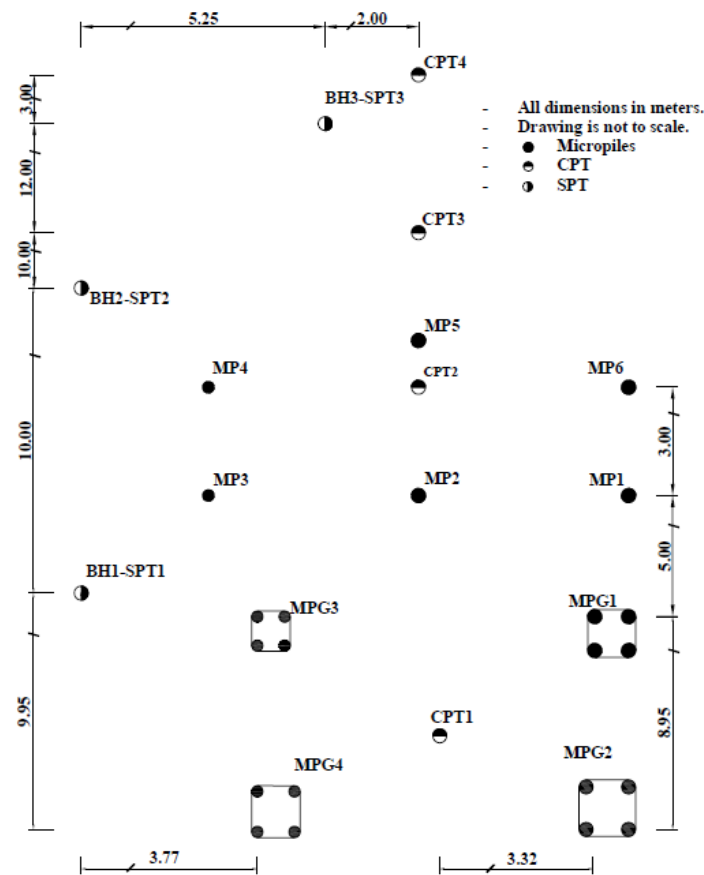


Figure 3-4 Plan view of single micropiles location

After attaching the drill bit to the hollow bar, rotary percussive drilling started simultaneously with a grout-flushing technique. The grout swivel allows the drilling and grouting operations to be performed as a single operation, which reduces the time of construction and ensures good bonding between the grout and ground. Grout with a specific gravity of 1.4 - 1.5 was employed as drilling fluid to install the hollow bars in place. As the hollow bars are typically manufactured in 3m length, once the first length (3.0 m) was installed, the drilling was stopped to allow for addition of the second segment; the two bars were attached using a 200 mm long coupler. The drilling was continued until the required depth was reached then the final competent structural grout was pumped under a pressure of between 0.8 to 1 MPa to displace the drilling grout. The final grout had specific gravity between 1.80 and 1.95, which is in compliance with (FHWA 2005) recommendation for micropile application.

The neat grout density was measured using the Baroid Mud Balance Test as per API Recommended Practice (RP) 13 B-1 (2009). The drilling and grouting rates were measured for each micropile. The drilling rate ranged between 0.45 to 0.60 m/min and the grouting rate was about 35 L/min. The drilling rates include the time period for adding the second segment of hollow bar with coupler which ranged between 1 to 2 minutes. The drilling and grout rates measured within this specific site can be used as useful tools to estimate the time required for the installation of hollow bar micropiles in a similar site and confirm the installation consistency.

The neat structural grout mix was designed with water to cement ratio,  $w/c = 0.45$ , in order to provide high strength, while being pumpable with minimum bleeding. Littlejohn and Bruce (1977) recommended  $w/c$  ratio in the range of 0.40 to 0.50 for micropile grout. They

indicated that the compressive strength for this range of w/c ratios is between 28 MPa to 37 MPa. FHWA (2013) required the grout compressive strength to be 21 MPa for 7 days and 35 MPa at 28 days for post-tensioning tendons for bridges. Grout cylinders were collected during the installation process using cylindrical molds of 100 mm by 200mm and 75 mm by 150mm. All specimens were de-moulded after 24 hours then placed in a control room with a relative humidity of 100% and constant temperature of 23oC. The cylinders were tested after 28 days to determine compressive strength and indirect tensile strength. The compressive strength was determined according to ASTM C39 and the tensile strength was obtained in according to ASTM C496. The average compressive strength after 28 days was 40 MPa and the average split tensile strength was 3.97 MPa. The results obtained for the compressive strength meet the minimum requirement set by FHWA (2013) for compressive strength of grout after 28 days.

The frictional capacity of the hollow bar – grout interface was evaluated in this study in order to establish the maximum possible size of grout column considering the grout-ground strength. A series of pull-out tests were conducted to investigate the frictional capacity of the hollow bar – grout interface.

Three hollow bars – grout specimens were prepared using the same hollow bar material employed in the construction of the HBMP and the grout was mixed with the same water to cement ratio. The hollow bar was placed in the mold and spacers were used to ensure the hollow bar was centralized during and after pouring the grout mix. The mixed grout of 0.45 water to cement ratio was then poured around and inside the hollow bar and were allowed to cure for 28 days. After the curing period, pull-out tests were conducted on the hollow bar-grout specimens with a loading rate of 40 kPa/min in accordance with ASTM

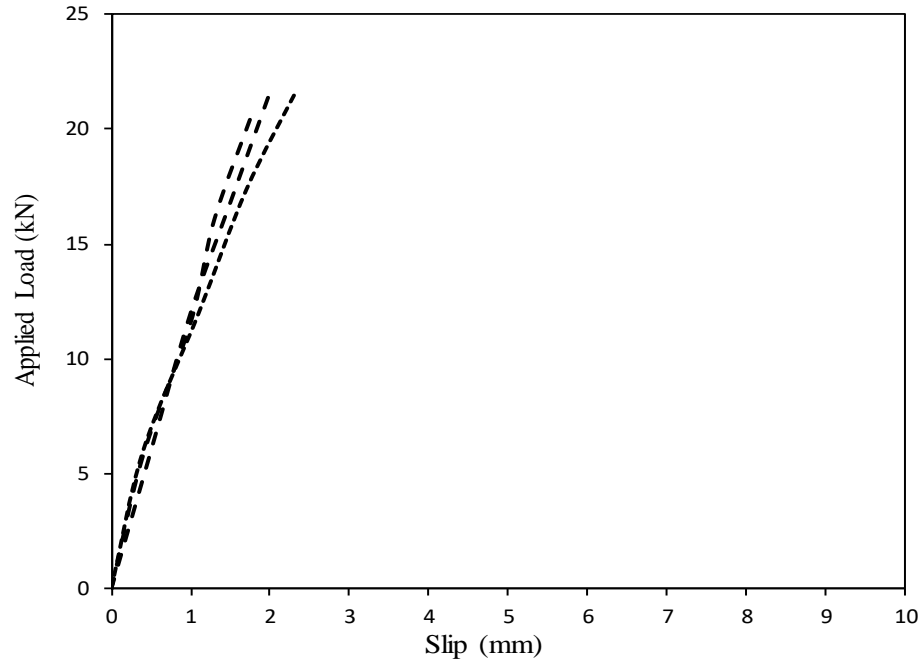
C900-15. The applied load and corresponding settlement were recorded simultaneously and the load – slip curves are obtained. Figure 3.5 presents the obtained results. The maximum load that caused slippage of the hollow bar from the grout was then used to determine the frictional resistance of the hollow bar – grout interface ( $f_{b-g}$ ).

The load transfer from the hollow bar to the grout column then to the adjacent soil is described in Figure 3.6. To ensure no structural failure happens, the optimum diameter of the grout column required in the design of HBMP for a given soil is given by:

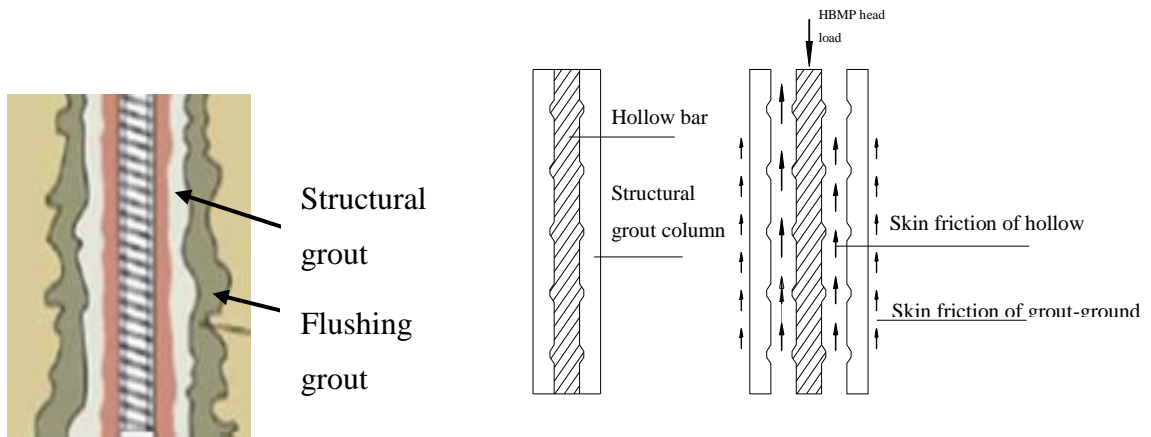
$$D_b = D_h (f_{b-g}/f_s) \quad (3.1)$$

in which  $D_h$  and  $D_b$  are the diameters of hollow bar and grout column;  $f_{b-g}$  and  $f_s$  are the peak frictional resistance of hollow bar – grout and grout – ground interfaces, respectively.

The diameter of the drill bit was optimized using Equation No. 3.1. The average peak frictional resistance of hollow bar – grout obtained from the pull-out tests was 745 kPa and the ultimate bond resistance was taken as the average value of the range provided by FHWA. The optimized diameter obtained from Equation No. 3.1 was 158 mm. Considering the availability drill bit sizes, the closest diameter of 152 mm was selected, which represented  $D_b/D_h = 3$ .



**Figure 3-5 Load-slip curves obtained from pull-out tests**

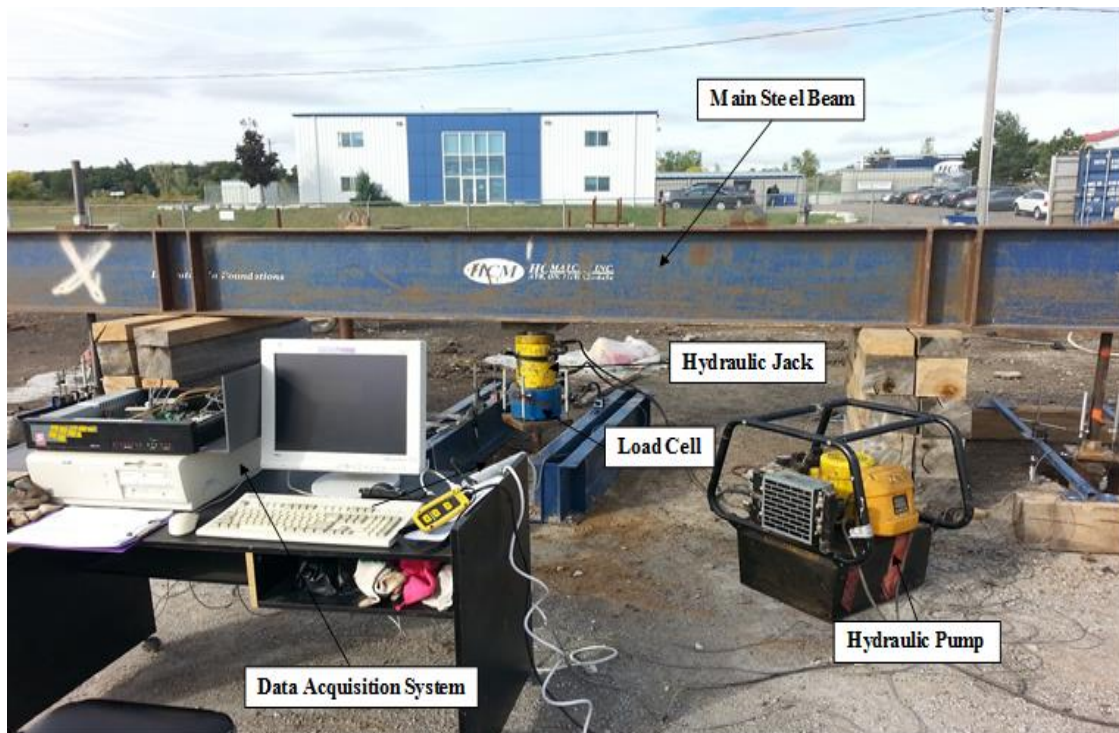


**Figure 3-6 Load transfer mechanism for HBMP**

### 3.4 Test Setup, Instrumentation and Procedures

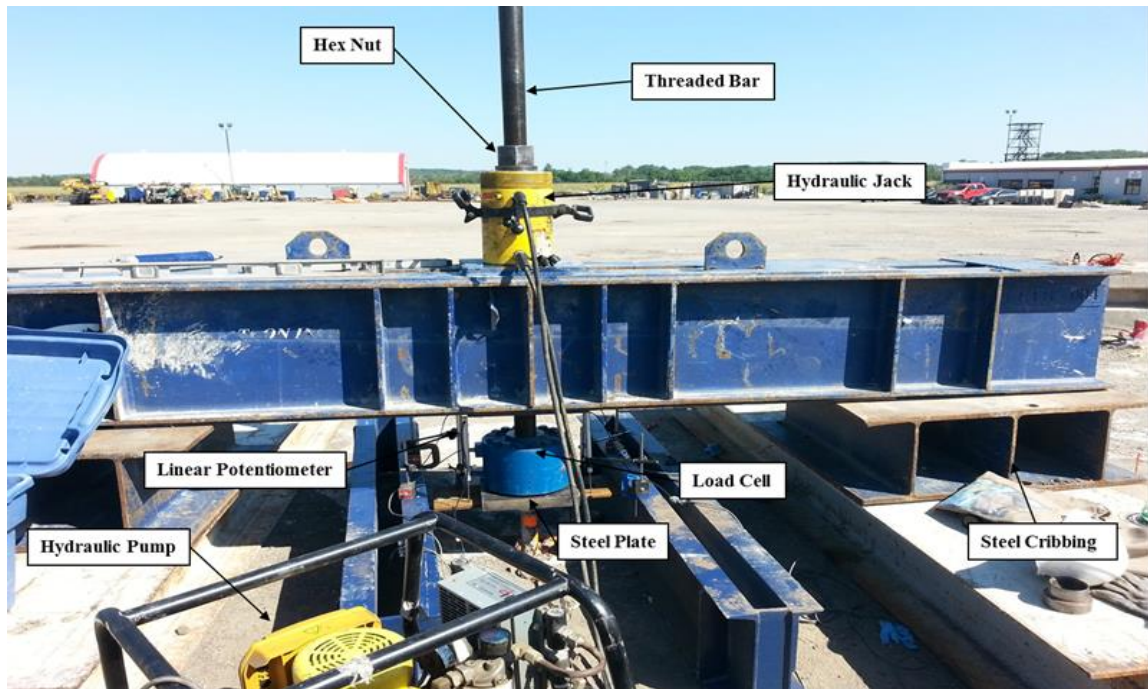
#### 3.4.1 Loading setup

A reaction frame system was used for both compression and tension tests. It comprised a steel reaction beam connected to two reaction piles (helical piles) in case of compression test and supported by cribbing for pull out testing. The reaction frame setups for compression and pull out tests are shown in Figure 3.7. The reaction (helical) piles consisted of a cylindrical shaft (114.3 mm in diameter and 17 mm thick wall) with one 300 mm helical plate. All reaction helical piles were placed at a distance of 2.25 m from the tested micropiles (15 times the diameter of the larger micropile). A hydraulic jack of 1100 kN advance capacity and a maximum stroke capacity of 150 mm was utilized for loading and a load cell of 1100 kN capacity was used to monitor the applied load.



(a)





(b)

**Figure 3-7 Load test setup: a) compression; and b) tension**

### 3.4.2 Pile instrumentation

Four HLP190 (hybrid Linear Potentiometers) were used to record the vertical pile head movement and their average reading was calculated. The HLP 190 has a 100 mm stroke and an accuracy of 0.01 mm. The potentiometers were attached to the loading steel plate in a square arrangement and clamped into two independent reference steel beams. Figure 3.8 shows the pile head instrumentation for micropile under compression loading. Two micropiles (MP2 and MP3) were instrumented with three vibrating wire strain gauges (VWSG) type EM-2 to investigate the load transfer mechanism along the micropiles. The VWSGs were placed at 0.80, 3.1 and 5.60 m from the ground surface, only one of the VWSG in MP3 was placed at 0.40 m instead of 0.80m from the ground surface in order to aid in determining the modulus of elasticity of the composite section. Based on experience

and recommendations proposed by Abd Elaziz and El Naggari (2012), VWSG were installed inside the hollow bar. The gauges were attached to a steel cage and installed immediately after grouting inside the hollow bar. Prior to and after the installation of the micropiles, the gauges were hooked to the vibrating wire readout Model Gk-404 to ensure that the VWSGs were working properly.

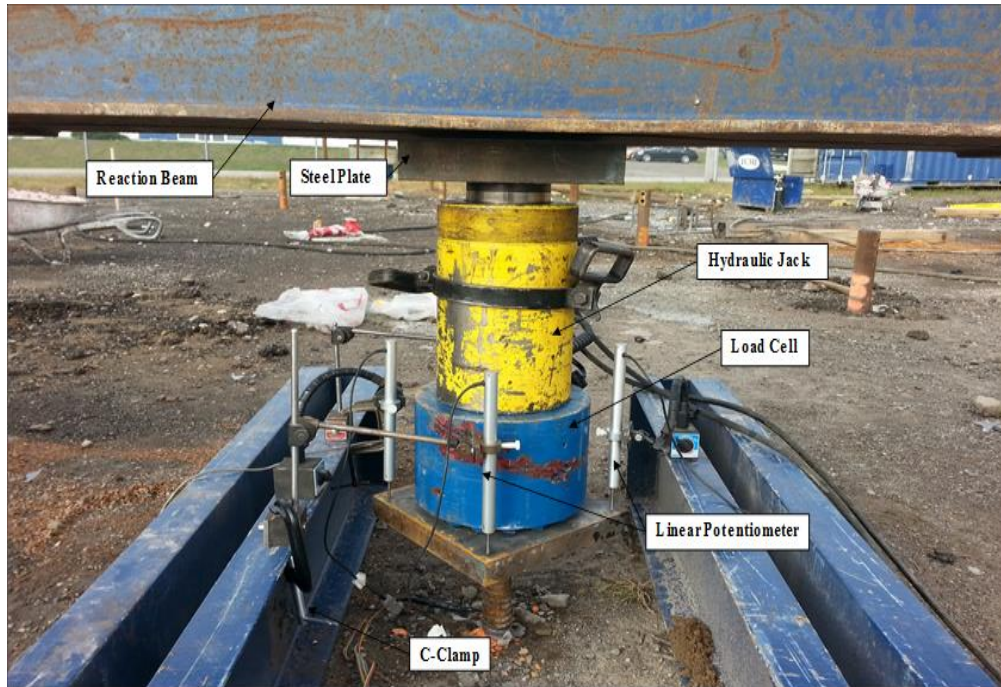
### 3.4.3 Load test procedure

The quick maintained load test method was employed in accordance with ASTM standards D1143-07 and D3689-07 (ASTM 2007a, b) for compression and tension tests, respectively. The load was applied in increments of 5% of the anticipated failure load and was maintained for 4-5 minutes before applying the next increment. The anticipated failure load was obtained by:

$$P_u = \alpha_{bond} \pi D_b L_b \quad (3.2)$$

Where:  $\alpha_{bond}$  = grout to ground ultimate bond strength;  $D_b$  = diameter of the drill hole; and  $L_b$  = bond length.

The grout-to-ground ultimate strength value was selected as the average value for Type B micropiles in medium to very dense sand. The predicated failure loads were 640 kN and 490 kN for 152 mm and 115 mm drill bit diameters, respectively. The load was increased incrementally until the pre-specified load or failure was reached; once the failure was reached, the unloading process took place in five approximately equal intervals.



**Figure 3-8 Micropile head instruments for compression test**

For cyclic loading, the load was applied up to the pre-specified design load before starting cycling. Quasi-static tension cyclic tests were conducted on MP1 and MP6. MP1 was first subjected to cyclic tension load test and then to cyclic compression load whereas MP6 was subjected to monotonic compression and tension load tests before starting the cycling loading test. In both cases, compression and tension cycling, MP1 and MP6 were subjected to 15 cycles of loadings and unloading of maximum 133% of the design load and minimum of 67% of the design load (the amplitude of the cyclic load is 100 kN, which is about 33% of design load). The pre-specified design load was 320 kN. The load was maintained for 2 minutes for each load cycle. Based on the efficiency of the hydraulic jack, the average time between loading and unloading was 9.5 sec.

### 3.4.4 Loading sequence

The compression and tension tests were conducted in three main stages. In the first stage, MP1 was subjected to cyclic tension test while MP2 and MP5 (with  $D_b/D_h=3$ ), and MP3 and MP4 (with  $D_b/D_h=2.25$ ) were subjected to monotonic tension loading; MP2 was loaded to failure while MP3, MP4 and MP5 were loaded up to the design load. In the second stage, six micropiles were subjected to monotonic compression loading; MP2, MP3, MP4, MP5, and MP6 were loaded to failure while MP1 was loaded to the design load and then subjected to 15 cycles of 100 kN load amplitude to investigate the behaviour of HBMP under compression cyclic loading conditions. In the third stage, four micropiles (MP3, MP4, MP5 and MP6) were subjected to tension loading; MP4, MP5 and MP6 were loaded to failure while MP3 was loaded to design load. The loading sequence is presented in Table 3.1.

**Table 3-1 Testing stages and loading sequences**

Stages	Type of test					
	MP1	MP2	MP3	MP4	MP5	MP6
<b>1<sup>st</sup> stage</b>	TC	MT-F	MT-DL	MT-DL	MT-DL	--
<b>2<sup>nd</sup> stage</b>	CC	MC-F	MC-F	MC-F	MC-F	MC-F
<b>3<sup>rd</sup> stage</b>	--	--	MT-DL	MT-F	MT-F	MT-F

TC, tension cyclic, CC, compression cyclic, MT-F, monotonic tension to failure, MC-F, monotonic compression to failure and MT-DL, monotonic tension to design load.

## **3.5 Test Results and Analysis**

### **3.5.1 Monotonic compression tests**

Compression load tests were conducted on MP2, MP3, MP4, MP5 and MP6. The micropiles were loaded to failure and the obtained load - settlement curves are presented in Figure 3.9. All micropiles displayed similar load -settlement response curves. It initiated with linear response followed by nonlinear behaviour, which is attributed to the start of yielding along the micropile-soil interface. The nonlinear response continued until failure (plunging) occurred, which was manifested by excessive increase in micropile settlement corresponding to small increase in applied load. This failure is attributed to exceeding the shear resistance of the micropile-soil interface.

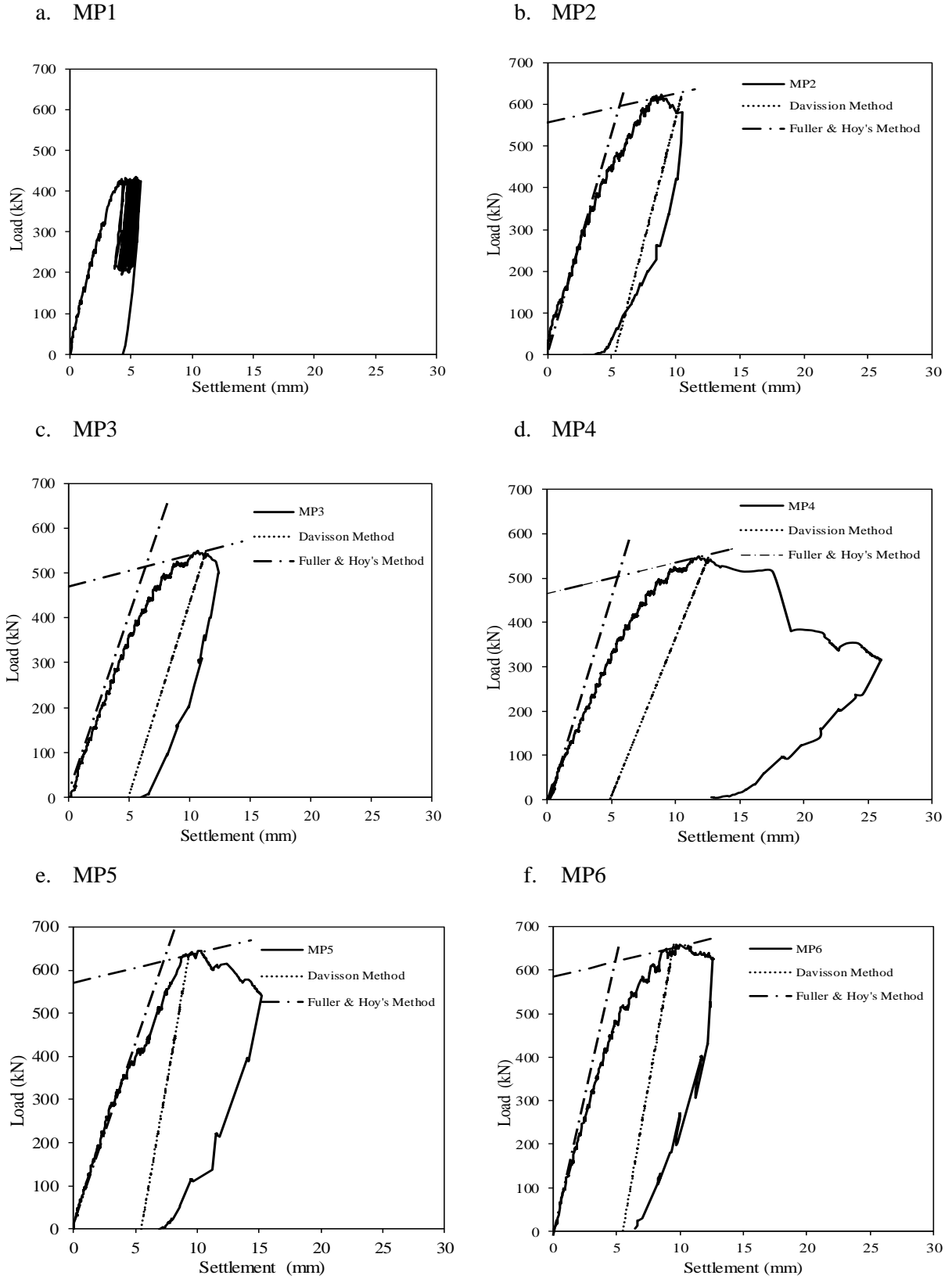
The micropile stiffness is important for evaluating the performance of the foundation and supported structure. The slope of the initial segment of the load- settlement curve represents the micropile stiffness up to its design capacity. The evaluated average stiffness values of the micropiles were 97 MN/m and 70 MN/m for micropiles with  $D_b/D_h=3$  and 2.25, respectively. These results demonstrate that the micropiles with  $D_b/D_h=3$  exhibited 38% higher stiffness than those with  $D_b/D_h=2.25$ .

### **3.5.2 Ultimate compressive capacity**

The load – settlement curves of MP2 and MP6 presented in Figure 3.9 show plunging failure at approximately 620 kN and 640 kN, respectively. The response curve of MP5 shows some softening at around 415 kN followed by nonlinear behaviour until plunging occurred at 630 kN. The load – settlement curves for MP3 and MP4 indicated failure load of 540 kN and 542 kN, respectively. These results indicate that the micropiles with  $D_b/D_h$

= 3 have higher failure load (approximately 17%) than the micropiles with  $D_b/D_h = 2.25$ . These results show that the increase in capacity is not linearly proportional to increase in drill bit (and micropile) diameter. This may be attributed to the fact that for the same grouting pressure, the permeation of the flushing grout into the surrounding soil (see Fig. 6a) is anticipated to be higher for the smaller diameter micropile than for the larger diameter micropile. This would result in relatively smaller improvement in strength of soil farther from the large diameter micropile, and consequently the increase in its capacity would not be proportional to the increase in its diameter.

There are several methods proposed in the literature to interpret the failure load from the load – settlement curve in case of plunging failure does not occur. Generally, interpreted failure load criteria presented in the literature are based on: mathematical modelling, settlement limitation or graphical construction. In this study, three interpreted failure load criteria are used, and their predictions are compared with the plunging failure load.



**Figure 3-9 Load- settlement curves for compression tests**

Davisson (1972) proposed a criterion for driven piles in which the failure load corresponds to a pile head settlement that has three main components: elastic pile compression, intercept equal to 3.8 mm and an empirical component related to tip resistance and is given by  $D/120$  mm (for SI units), i.e.

$$\Delta = \frac{QL}{A_p E_p} + 3.8 + \frac{D}{120} \quad (3.3)$$

Where  $\Delta$  = Settlement,  $Q$  = Applied load,  $L$  and  $D$  are the pile length and diameter, respectively,  $A_p$  = cross-sectional area of pile and  $E_p$  = elastic modulus of pile.

Reese and O'Neill (1988) defined the failure load as the load corresponding to pile head settlement equal to 5% of the pile diameter. Fuller and Hoy (1970) defined the interpreted failure load as the minimum load occurs for a rate of total settlement of 0.14 mm/kN. This method is recommended by FHWA (2005) for micropiles. Butler and Hoy (1977) proposed a criterion for interpreted failure load, which is given by the intersection of line with slope equal to 0.14 mm/kN with the line tangent to the initial straight-line portion of the load settlement curve. These methods are illustrated in Figure 3.9 and the determined interpreted failure loads are presented in Table 3.2.



**Table 3-2 Interpreted failure load methods and plunging failure**

<b>Method</b>	<b>Interpreted Failure Load (kN)</b>				
	<b>MP2</b>	<b>MP5</b>	<b>MP6</b>	<b>MP3</b>	<b>MP4</b>
<b>Plunging</b>	620	630	640	540	542
<b>Davisson</b>	580	628	635	540	540
<b>Reese and O'Neill</b>	607	500	604	450	405
<b>Fuller and Hoy's</b>	615	630	642	533	545
<b>Butler and Hoy's</b>	600	615	621	520	520

As it can be noted from Table 3.2, Fuller and Hoy's method provided the closest values to the observed failure (plunging) load for all micropiles while Davisson's method yielded conservative interpreted failure load for MP2. Kulhway and Hirany (2009) noted that the Davisson method gives a conservative interpreted ultimate load compared to other interpreted failure criteria.

Considering the capacity values presented in Table 3.2, the average ultimate capacity of micropiles with drill bit diameter,  $D_b = 152$  mm was 630 kN while the average ultimate capacity of the two micropiles with  $D_b = 115$  mm was 541 kN. Thus, increasing  $D_b$  from 115 mm to 152 mm using the same hollow bar diameter for both cases resulted in an increase in the ultimate capacity of the micropile by about 17%. The ultimate skin friction was back calculated from the average ultimate capacity of micropiles. The ultimate skin friction was estimated by subtracting the toe resistance from the load that caused plunging

failure. The calculated ultimate skin friction is 186 and 200 kPa for micropiles with drill bits of 152 and 115 mm, respectively. The higher skin friction for the smaller diameter micropile is due to the larger permeation of grout into the surrounding soil as discussed earlier.

### 3.5.3 Distribution of axial forces in micropiles

The axial compression stiffness of micropile can be simplified using the following formula,

$$E_p A_p = E_g A_g + E_s A_s \quad (3.4)$$

Where  $E_p$  = modulus of elasticity of the micropile,  $A_p$  = cross-sectional area of micropile,  $E_g$  = modulus of elasticity of the grout,  $E_s$  = modulus of elasticity of the steel bar,  $A_g$  = cross-sectional area of the grout and  $A_s$  = cross-sectional area of steel bar.

In order to obtain the actual diameter of micropiles, the top 2.0 m along all micropiles was excavated and the diameter of each micropile was measured. The measurement interval of the actual diameters was 200 mm and was reduced to 100 mm when the change in diameter was noticeable. Furthermore, MP3 and MP5 were carefully pulled out from the soil after load testing was completed in order to take measurement of the diameter along the micropile. It was found that the average diameter of micropiles with drill bit 115 and 152 mm was 132 and 172 mm, respectively, i.e. the diameter increased by 14.8% and 13.1% over the diameter of the drill bit. The ratio of the grout body diameter to the drill bit diameter was larger for smaller diameter drill bit. Figure 3.10 shows the exhumed micropile (MP3) and diameter measurement along its length.

In order to confirm the increase in diameter, the quantities of competent grout used in micropile construction were tracked and the average volume of the grout was used to evaluate the actual average increase in the diameter.

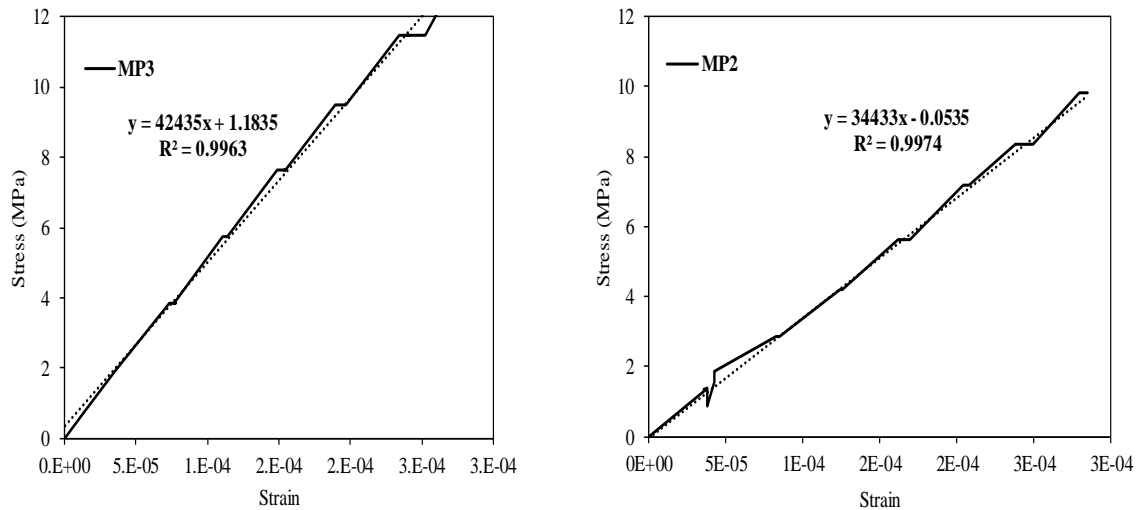


**Figure 3-10 Exhumed micropiles MP3 and diameter measurement along the depth**

For micropiles installed with,  $D_b = 152$  mm, the average back calculated diameter of the micropile was 177 mm while for micropiles installed with  $D_b = 115$  mm, the average micropile diameter was 145 mm. The average diameters back-calculated from the total volume of pressurized grout was higher than measured diameter. The difference in the diameters could be attributed to the fact that grout could permeate laterally through any seams of silt encountered occasionally during the grouting, which was noticed during the excavation around the micropiles. This further confirms the comments made earlier that

more grout permeated into the surrounding soil for the smaller diameter micropile, hence improved the ground strength relative to the case of the larger diameter micropile.

Using the strain gauge readings near the pile head for MP2 and MP3, which were placed 400 and 800 mm from the ground level, the modulus of elasticity of the micropiles was calculated by plotting the stress from the applied load over the area of micropile versus the strain gage measurement as illustrated in Figure 3.11.



**Figure 3-11 Stress-strain relationship for MP2 and MP3 from SG1**

Using the measurements obtained from the strain gauges installed in MP2 and MP3, the axial force distribution at different levels was calculated from:

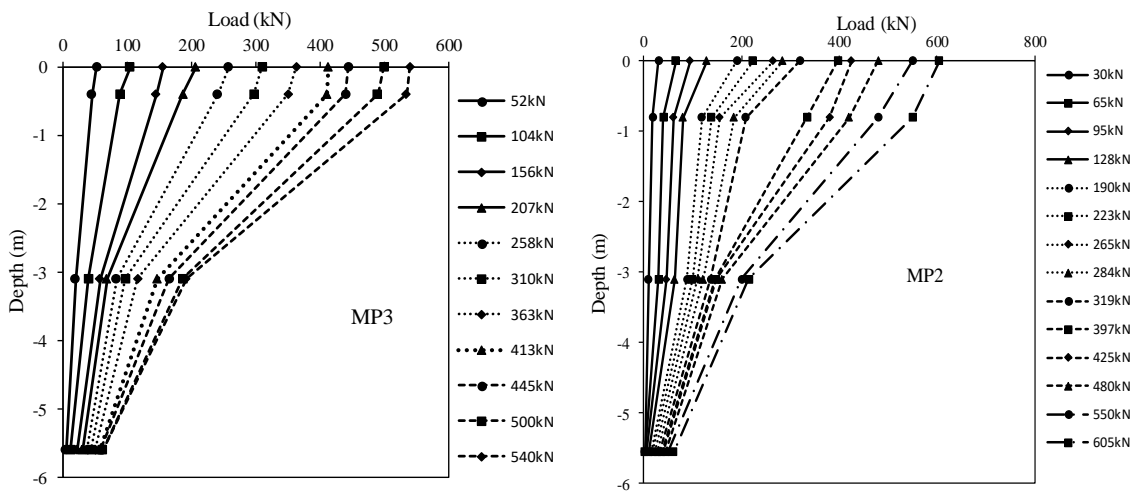
$$P = \varepsilon A_p E_p \quad (3.5)$$

Where  $P$  = axial force,  $\varepsilon$  = axial strain,  $A_p$  = cross sectional area of micropile and  $E_p$  = composite modulus of elasticity of micropile materials.

Figure 3.12 shows the distribution of axial forces with depth. As expected, the axial forces increased as the applied loads increased with most of the load transferred to the soil through the shaft, especially at lower applied loads. The load transferred through the shaft (skin) resistance accounted for 91% of the maximum applied load for MP2 and MP3, while the toe resistance accounted for 9% of the total resistance. The skin friction can be given by:

$$f_s = K_s \sigma'_v \tan \delta = \beta \sigma'_v \quad (3.6)$$

Where,  $f_s$  = ultimate unit side friction,  $K_s$  = coefficient of lateral earth pressure,  $\sigma'_v$  = The effective overburden pressure and  $\delta$  = the angle of friction between the pile and surrounding soil; and  $\beta$  is shaft friction coefficient.

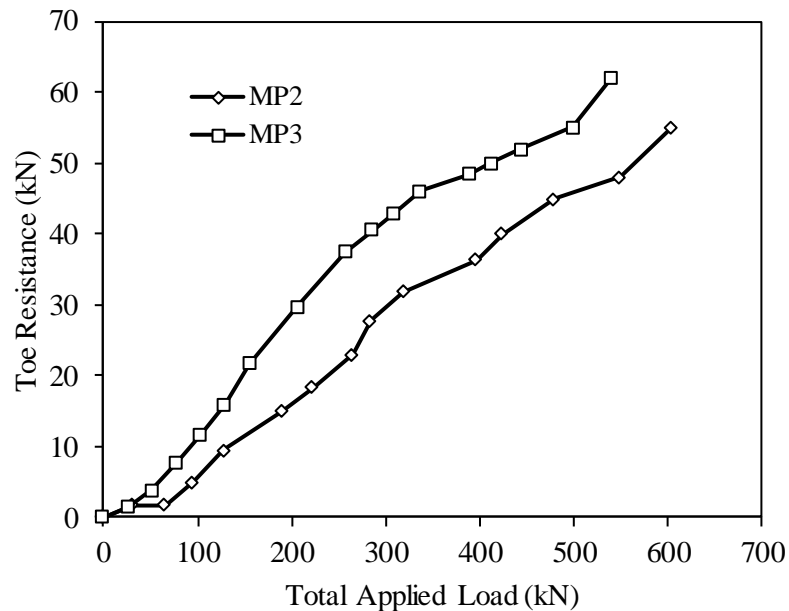


**Figure 3-12 Distribution of axial forces with depth for MP2 and MP3**

The  $K_s$  values were back calculated from the skin resistance values using equation 3.6. The  $K_s$  values ranges from 3.40 to 3.70. Based on the density of soil and type of pile, it was reported in the literature that the K-value ranges from 0.5 to 5 (Lancellotta, 1995 and Said, 2006).

### 3.5.4 Toe resistance of micropiles

Figure 3.13 presents the variation of the toe resistance with the total applied load at the micropile head for MP2 and MP3. It can be noted from Figure 3.13, the toe resistance increased sharply as the applied load approached the micropile ultimate capacity. As mentioned above, the readings of strain gauges placed close to the micropile toe demonstrated that the toe resistance accounted for about 9% of the total applied load. The toe resistance is usually ignored in the design of micropiles due to the small diameter of micropile, which may result in underestimating the micropile capacity by 9%. Han and Ye (2006) reported similar results for small diameter micropiles.



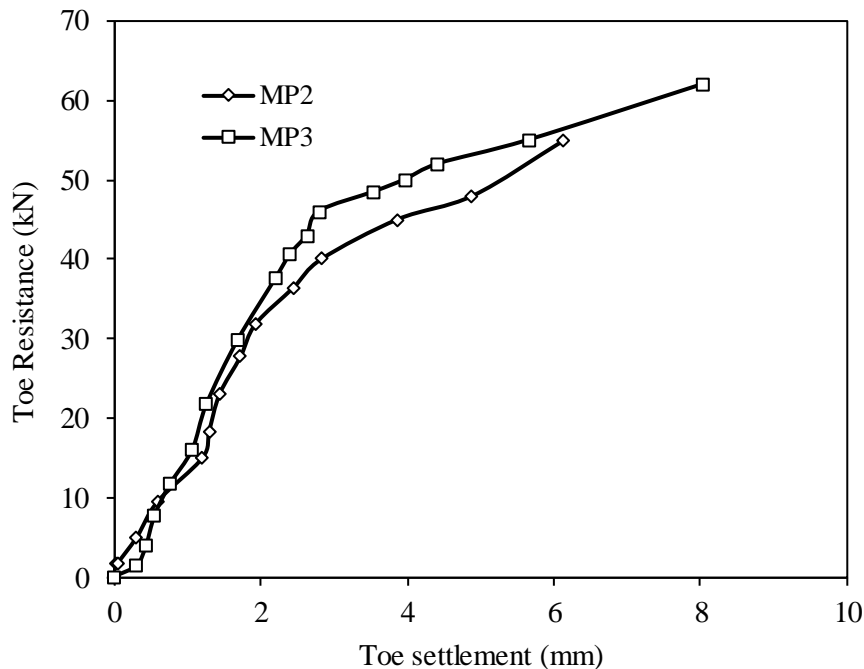
**Figure 3-13 Total applied load versus toe resistance for MP2 and MP3**

The toe settlement of micropile is equal to the total measured settlement minus the compression in the micropile shaft. The compression in the micropile shaft can be approximated using the following formula (Han and Ye, 2006):

$$\Delta_{sp} = \frac{(P_p + P_b) L}{2 E_p A_p} \quad (3.7)$$

Where,  $\Delta_{sp}$  is the compression of micropile shaft,  $P_p$  is the applied load on the micropile head measured from the load cell,  $P_b$  is the toe resistance obtained from the strain gauge close to the micropile toe,  $L$  is the micropile length,  $E_p$  is the elastic modulus of the micropile section and  $A_p$  is the cross-sectional area of micropile.

Figure 3.14 shows the variation of the toe settlement calculated from Equation 3.7 and the toe resistance obtained from strain gauge readings. As it can be noticed from Figure 3.14, the toe resistance- settlement relationship is nonlinear. Figure 14 also shows that MP2, with actual diameter of 171 mm, displayed slightly higher toe stiffness than micropile MP3 with 132 mm diameter due to increased micropile diameter.

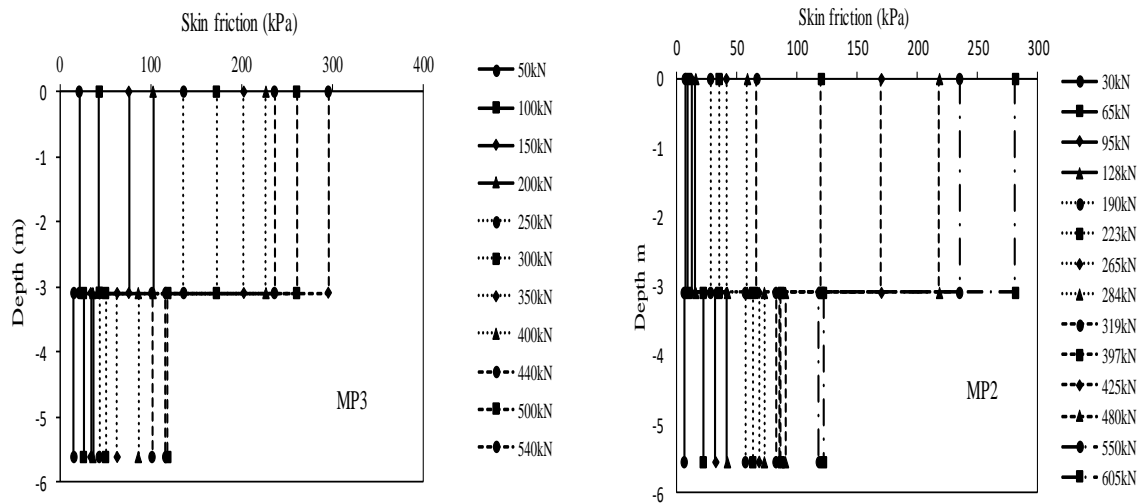


**Figure 3-14 Toe resistance versus toe settlement for MP2 and MP3**

### 3.5.5 Unit skin friction of micropiles

The unit skin friction within a layer is evaluated by dividing the load transferred by unit area to soil within this layer over a length of micropile (i.e. difference in axial forces obtained from two consecutive strain gauges within this layer) divided by the surface area between the gauges. The distribution of unit skin friction along MP2 and MP3 is shown in Figure 3.15. The unit skin friction along the upper 3 m of MP2 was 281 kPa while for the lower part the unit skin friction was only 122 kPa (similar trend was observed for MP3). This may be attributed to two factors: 1) the top layer is gravelly sand, which allows more grout permeation than the lower layer, which is silty sand, and consequently ground improvement and grout-ground strength are higher; 2) skin friction was mobilized fully for the top layer, but not developed fully for the bottom layer. This explains why plunging failure was not observed for micropiles MP2 and MP3 as shown in Figures 3-9b and c. The ultimate skin friction was back calculated by deducting the toe resistance estimated from the lower strain gauges from the failure load. The average value of skin friction for each micropile was slightly higher than the values suggested by FHWA (2005) for Type B micropiles as can be noted from Table 3.3.





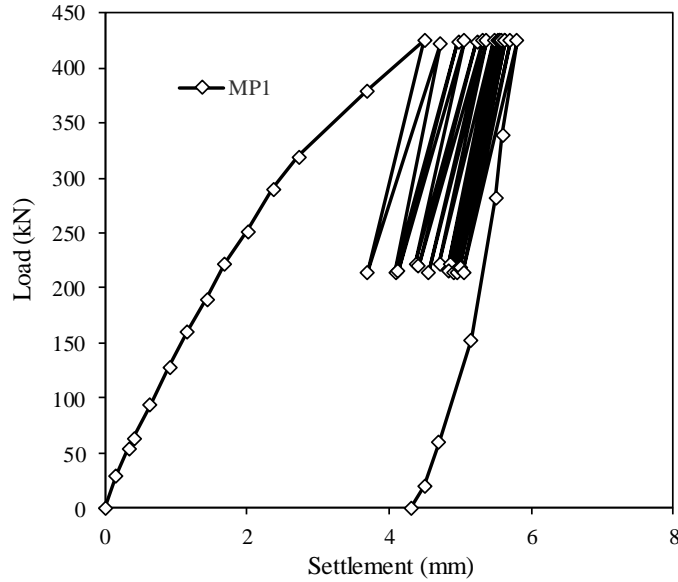
**Figure 3-15 Distribution of unit skin friction for MP2 and MP3**

**Table 3-3 Ultimate skin friction for MP2 and MP3**

<b>Elevation</b>	<b>MP2</b>	<b>MP3</b>
<b>Upper part</b>	281	295
<b>Lower part</b>	122	116
<b>Average</b>	202	206
<b>FHWA</b>	186	200

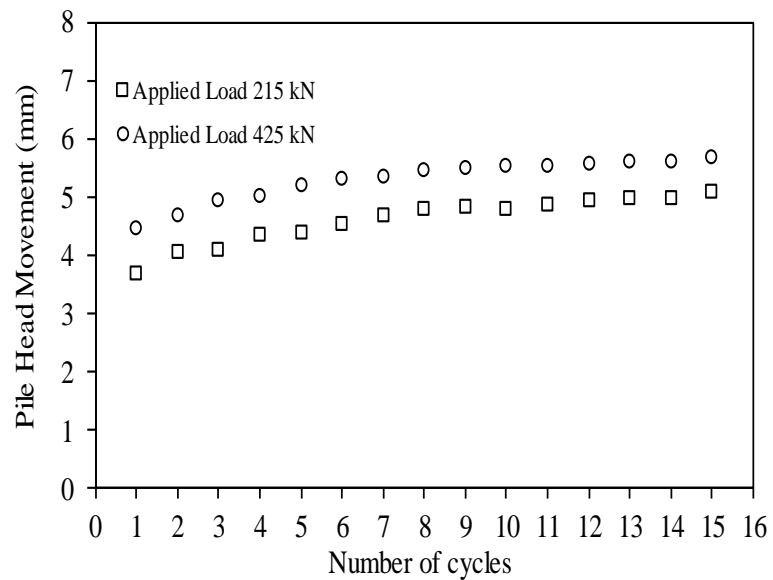
### 3.5.6 Cyclic compression tests

To shed some light on the effect on the effect of cyclic compression loading on HBMP performance, MP1 was subjected to 15 compression cycles of loading and unloading of maximum 133% of the design load and minimum of 67% of the design load (the amplitude of the cyclic load is 100 kN, which is about 33% of design load). Figure 3.16 shows the cyclic applied load versus vertical settlement for MP1.



**Figure 3-16 Cyclic compression loading for MP1**

The micropile head settlement increased with increasing the number of cycles as it can be seen in Figure 3.17. The difference between the initial micropile head settlement before and after applying 15 load cycles is 1.2 mm.



**Figure 3-17 Micropile (MP1) head movement versus number of cycles.**

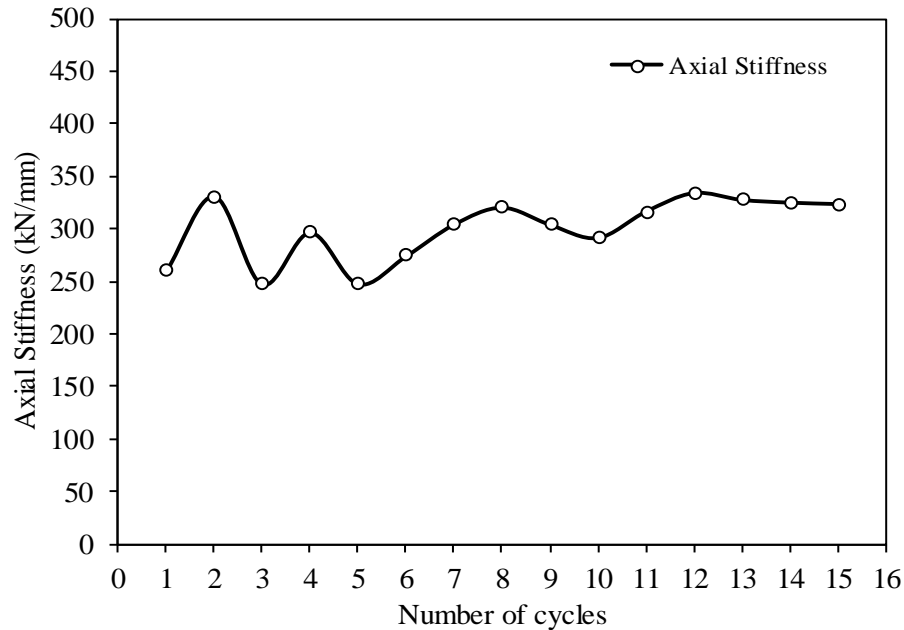
The micropile head stiffness is calculated as:

$$K = \left[ \frac{P_{max} - P_{min}}{\Delta_{max} - \Delta_{min}} \right] \quad (3.8)$$

Where;

$P_{max}$  &  $P_{min}$  are the maximum and minimum applied loads for each cycle, respectively, while  $\Delta_{max}$  &  $\Delta_{min}$  are the maximum and minimum vertical settlements for each cycle, respectively.

Figure 3.18 shows the effect of increasing the number of load cycles on the axial micropile head stiffness. There was a variation in the axial head stiffness in the first five cycles as the axial stiffness varies between 330 kN/mm and 250 kN/mm, this variation may be attributed to the effect of cyclic tension test which was performed before the compression cyclic tests. However, the axial micropile stiffness stabilized at 330 kN/mm after the seven cycles.



**Figure 3-18 Axial stiffness of MP1 with number of cycles**

### 3.5.7 Monotonic tension tests

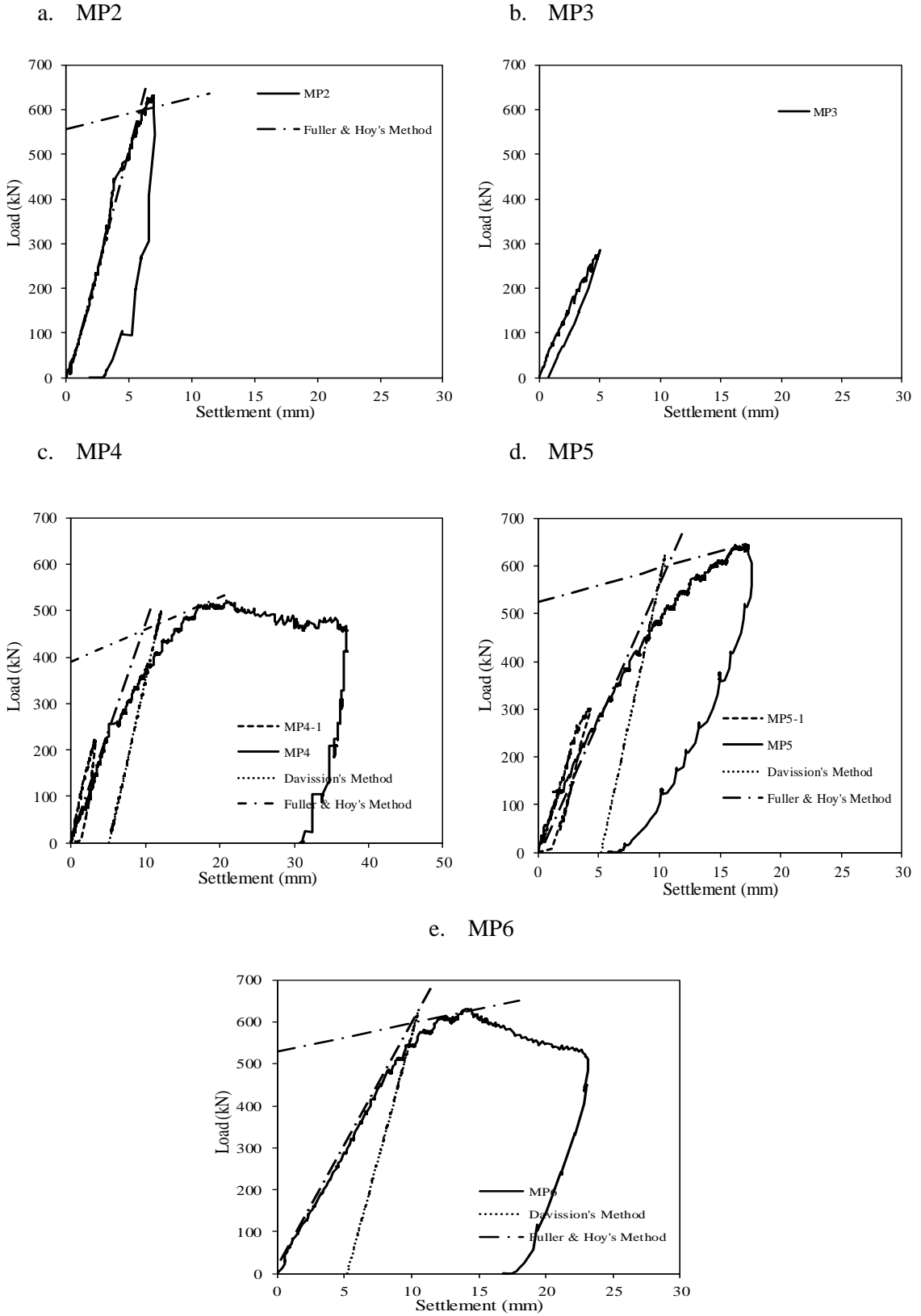
The tension load tests were conducted in stages 1 and 3. In stage 1, MP2 was loaded to failure while micropiles MP3, MP4 and MP5 were loaded up to the design load. In stage 3, after compression loading was completed, MP4, MP5 and MP6 were loaded to failure while MP3 was loaded up to the design load.

The load – settlement curves are plotted in Figure 3.19. The response of MP2 was stiffer than that of MP5 and MP6 because MP2 was loaded first in tension while MP5 and MP6 were tested under compression prior to tension loading. The load – settlement curves for MP5 and MP6 indicated a plunging failure at 638 and 612 kN, respectively. MP3 was loaded twice to the design load and the response during both tests were very similar. MP4 was tested twice under tension loading: first, loaded up to the design load prior to

compression loading; and second loaded up to failure after compression loading. The plunging failure occurred at 510 kN.

As MP4 and MP5 were initially loaded in tension up to the design load prior to compression loading to failure followed by tension loading to failure, the effect of loading sequence can be evaluated by comparing the tension responses before and after compression loading as presented in Figure 3.19. The comparison shows that the micropile stiffness in the initial part of second tension loading is lower than the stiffness in the virgin tension loading. Figure 3.19 also shows that the load – settlement curves for initial tension loading and compression loading cases are similar, indicating the micropiles derive their load resistance mainly from skin friction. The micropile stiffness up to the design load was calculated from the virgin tension load-settlement curves. The evaluated average stiffness of the micropiles are 86 MN/m and 65 MN/m for micropiles with  $D_b/D_h=3$  and 2.25, respectively.

These results demonstrate that the micropiles with  $D_b/D_h=3$  exhibited 32% higher stiffness than those with  $D_b/D_h=2.25$ .



**Figure 3-19 Load- settlement curves for tension tests**

### 3.5.8 Uplift capacity

Four failure criteria were used to interpret the uplift failure load: Davisson (1972), Reese and O'Neill (1988), Fuller and Hoy (1970) and Butler and Hoy (1977) and the results are summarized in Table 3.4. As suggested by (FHWA 2005), Fuller and Hoy's method gives closest estimate of the failure load compared to other failure criteria while Davisson method provides conservative estimate and Reese and O'Neill overestimated the failure load. The results indicated that the micropiles tension capacity increased by about 22.5% as the ratio of  $D_b/D_h$  increased from 2.25 to 3. Comparing the uplift capacity of the micropiles presented in Table 3.4 with their ultimate compressive capacity presented in Table 3.2 shows that their values are close.

The ultimate skin friction values under tension loading were back calculated considering the loads that caused plunging failure. The estimated ultimate skin frictions were found to be 204 and 214 kPa for micropiles with drill bits of 152 and 115 mm, respectively. FHWA (2005) gives a wide range for ultimate skin friction values for Type B micropile installed in medium to very dense sand between 120 - 360 kPa. The ultimate skin friction of grouted micropiles obtained from this study lie within the range values suggested by FHWA (2005).

**Table 3-4 Interpreted failure load methods and plunging failure for tension tests**

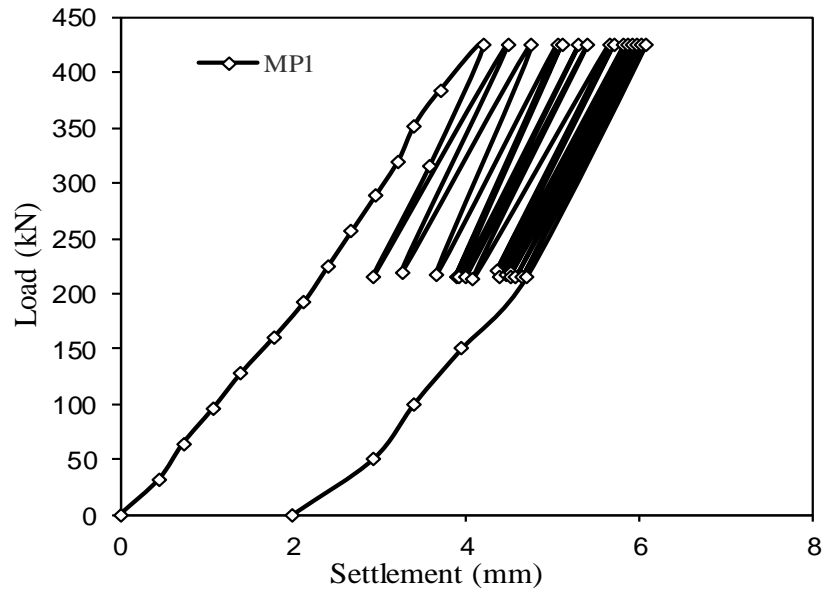
<b>Method</b>	<b>Interpreted Failure Load (kN)</b>			
	<b>MP2</b>	<b>MP5</b>	<b>MP6</b>	<b>MP4</b>
<b>Plunging</b>	NA	638	612	510
<b>Davisson</b>	NA	420	485	380
<b>Reese &amp; O'Neill</b>	NA	425	480	360
<b>Fuller &amp; Hoy's</b>	620	635	610	508
<b>Butler &amp; Hoy's</b>	610	300	600	470

### 3.5.9 Cyclic Tension Tests

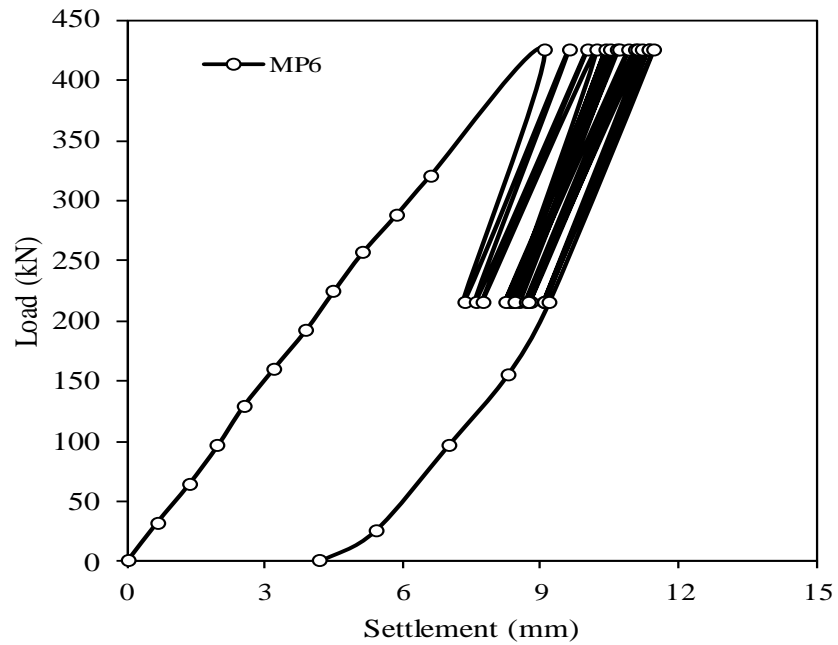
The cyclic load test results are presented in terms of the cyclic load- settlement curves and the effect of cycling loading on the micropile stiffness. The load- settlement curves for MP1 and MP6 are plotted in Figure 3.20 and Figure 3.21, respectively.

Figure 3.20 shows that MP1 displayed almost linear behavior up to the maximum applied load of 420 kN (1.33 of design load). It also shows that the pile head movement increased as the number of load cycles increased. However, the stiffness of the pile through the different cycles remained almost the same as manifested by the slope of load- settlement curve for the different cycles. MP6 exhibited similar behavior as can be noted from Figure 3.21. However, MP6 experienced larger pile head settlement and reduced stiffness due to the monotonic loading to failure prior to applying the cyclic loading.





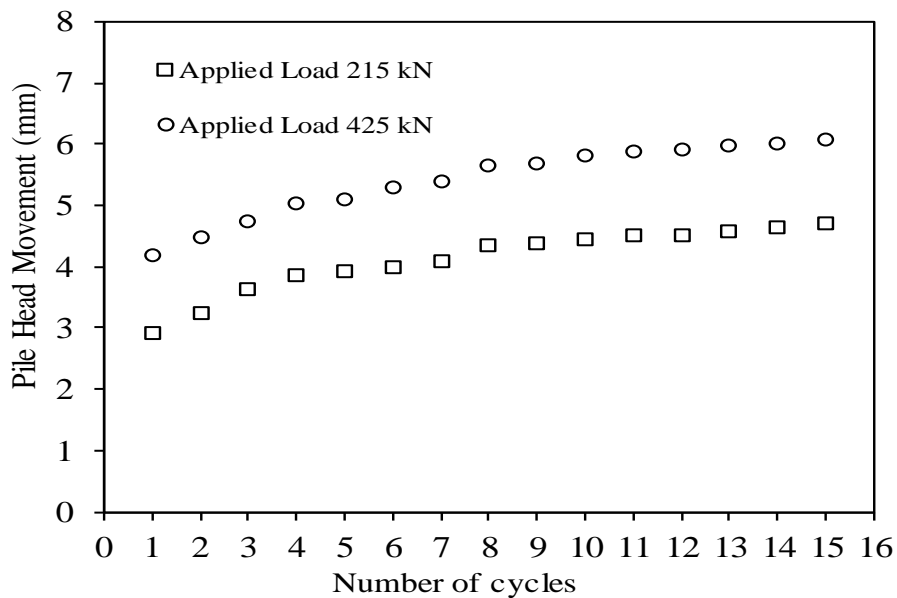
**Figure 3-20 Load – settlement curve for MP1**



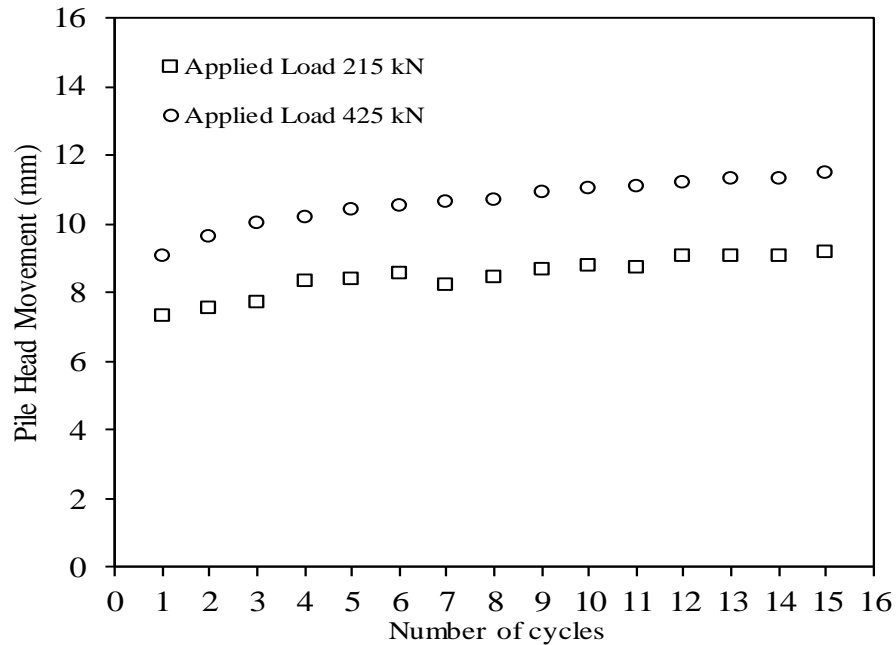
**Figure 3-21 Load settlement curve for MP6**

The differences between the initial head settlements before starting the cyclic loading on both micropiles and the final head settlements after applying 15 load cycles were 1.88 and 2.38 mm for MP1 and MP6, respectively. The rebound settlements after applying 15 load cycles were 2 and 4.2 mm for MP1 and MP6, respectively.

Figure 3.22 and Figure 3.23 show the cumulative head settlement after each cycle of loading. They clearly demonstrate that the cumulative micropile head increased after each load cycle, but at decreasing rate. Figure 3.22 shows that the vertical head settlement of MP1 increased with the number of load cycles. Moreover, the head settlement for the first four cycles accounted for 53% of the total head settlement after 15 cycles.

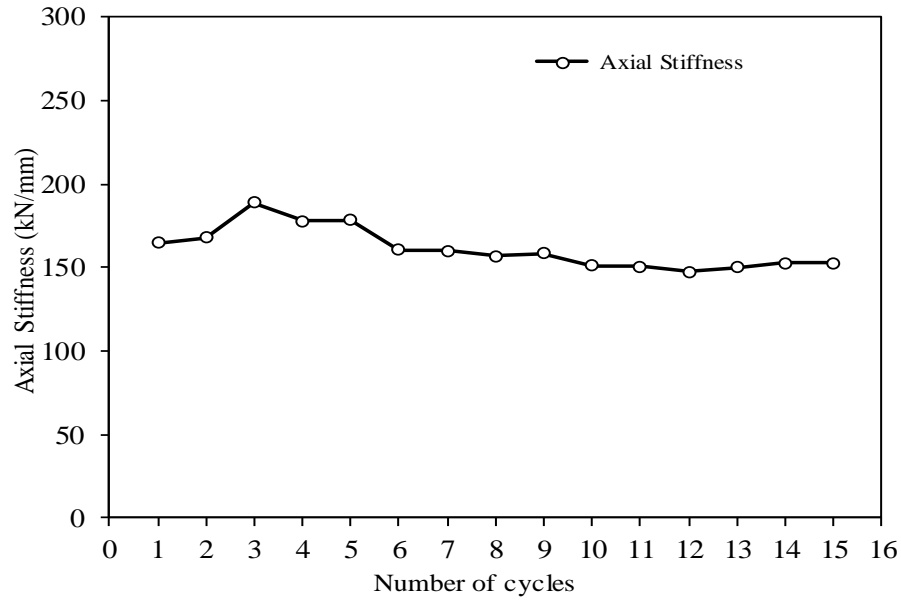


**Figure 3-22 Head micropile settlement vs number of cycles for MP1**

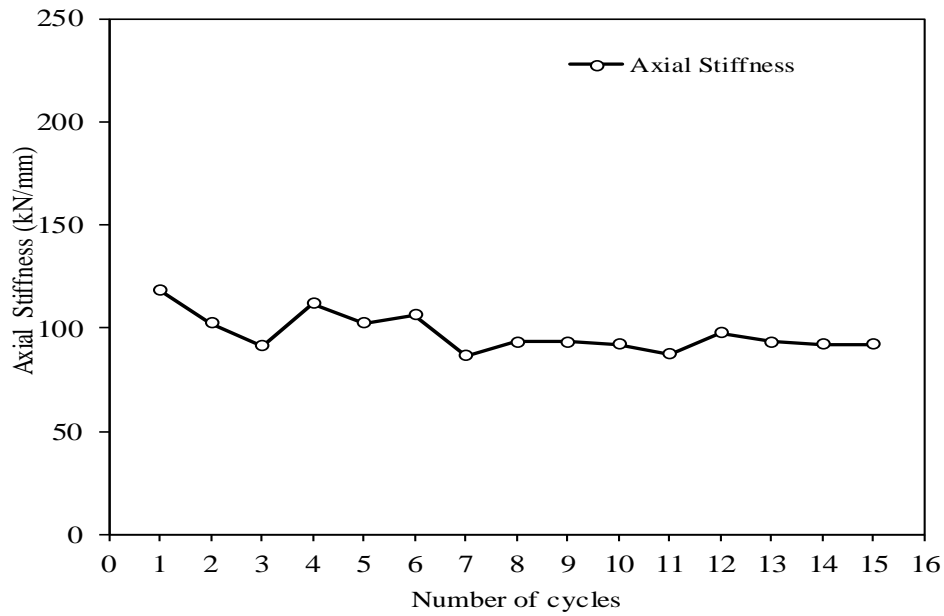


**Figure 3-23 Head micropile settlement vs number of cycles for MP6**

MP6 displayed the same pattern as can be noticed in Figure 3.23. The first four load cycles accounted for 47% of the total head settlement after applying load 15 cycles. The difference between the initial and final settlement indicates that the soil surrounding the micropiles undergone irrecoverable strains, which is usually accompanied with a change in sand density. Failure of foundations are usually associated with irrecoverable strains in soils. To evaluate the effect of cyclic loading on the micropile head stiffness, Figure 3.24 and Figure 3.25 show the calculated head stiffness with the number of load cycles.



**Figure 3-24 MP1 axial micropile head stiffness vs number of cycles**



**Figure 3-25 MP6 axial micropile head stiffness vs number of cycles**

In general, MP1 showed higher axial stiffness than MP6 because of the initial monotonic of MP6. Figure 3.24 shows that the axial stiffness of MP1 increased slightly in the first

three cycles and then started to decrease slightly as the number of load cycle continued to increase. However, no cumulative degradation of the MP1 stiffness was observed over the 15 load cycles. On the other hand, MP6 showed stiffness degradation in the first few cycles. Afterwards, it exhibited almost constant stiffness over the last eight cycles. The axial stiffness of MP6 initially varied between 118 and 86 kN/mm for the first six cycles and then stabilized at around 93 kN/mm for the rest of load.

### **3.6 Discussions and Conclusions**

Compression and tension loading tests were performed on six full-scale hollow bar micropiles to investigate the performance and capacity of hollow bar micropiles constructed with different diameter ratios of drill bit/hollow bar ( $D_b/D_h$ ). Two micropiles (MP2 and MP3) were instrumented with three vibrating wire strain gauges each to evaluate the distribution of load transfer along the micropile. The micropiles were constructed using hollow bars R51N along with tungsten carbide cross cut drill bits. The OD (Outer diameter) of the hollow bar was 51 mm and the ID (Inner diameter) was 33 mm. Three micropiles (MP2, MP5 and MP6) were installed with 152 mm drill bit (i.e.  $D_b/D_h=3$ ) and two (MP3 and MP4) with 115 mm drill bit (i.e.  $D_b/D_h=2.25$ ). The total length of each micropile was 6m with 5.75m embedded length.

The performance of hollow bar micropiles with two different drill bit diameters, representing  $D_b/D_h= 2.25$  and 3.0, installed in sand was investigated. Based on measurements of diameter of exhumed micropiles, the micropiles diameter increased by approximately 14% over the drill bit diameter. The micropile surface area was increased by 33% as  $D_b/D_h$  increased from 2.25 to 3. Meanwhile, the load test results showed that as

$D_b/D_h$  increased from 2.25 to 3, the micropile stiffness increased by 38% and 32% in compression and uplift, respectively. The load test results also showed that the compression and tension capacity of the micropiles increased by about 17% and 22.5%, as  $D_b/D_h$  increased from 2.25 to 3 respectively. In current practice, if the target micropile diameter is 152 mm, a hollow bar diameter of 76 mm would be used. Employing the proposed  $D_b/D_h = 3.0$ , this diameter can be achieved by using hollow bar diameter of 51 mm, which means the quantity of steel can be reduced by 50% by increasing the drill bit diameter to achieve  $D_b/D_h = 3.0$ . For micropiles installed in cohesive soil, Drbe and El Naggar (2014) suggested that increasing the  $D_b/D_h$  from 2.25 to 3 has small influence on the axial compression capacity of micropiles.

The values of ultimate bond resistance of grouted micropiles obtained from this study form both compression and tension tests lie within the wide range values provided by FHWA (2005) for dense sand soil between 120 and 360 kPa. For the dense sand examined herein, the ultimate bond resistance for the range of grout pressure applied in this study varied from 150 to 250 kPa rather than the wide range of 120 to 360 kPa suggested by FHWA.

Finally, the load- settlement response of micropiles under compression loading was slightly stiffer than the tension loading case and the ultimate compressive capacity of the micropiles was slightly higher than their uplift capacity. The conclusions obtained from this study are based on the load tests data and the soil profile encountered in this site.

### 3.7 References

- AASHTO. (2012). *AASHTO LRFD Bridge Design Specification, Customary U.S. Units*. The American Association of State Highway and Transportation Officials (AASHTO). Section 10.
- Abd Elaziz, A.Y., & El Naggar, M. H. (2012). Axial Behaviour of Hollow Bar Micropiles under Monotonic and Cyclic Loading. *Geotechnical Testing Journal*, 35(2), 249–260.
- Abd Elaziz, A. Y., & El Naggar, M. H. (2014). Geotechnical Capacity of Hollow-Bar Micropiles in Cohesive Soils. *Canadian Geotechnical Journal*, 51(10), 1123–1138.
- American Petroleum Institute (API) (1987). *Recommended Practice for Planning, Designing and Constructing Fixed Offshore Platforms*. API Recommended practice 2A, 17 Ed.
- American Petroleum Institute (API) (2009). *Recommended Practice for Field Testing Water-Based Drilling Fluids*. API Recommended practice RP 13B-1.
- ASTM International. (2013). *Standard Test Methods for Deep Foundations under Static Axial Compressive Load*. D1143/D1143M-07 (Reapproved 2013). American Society for Testing and Materials, West Conshohocken, Pa.
- ASTM International. (2015). *Standard Test Methods for Deep Foundations under Static Axial Compressive Load*. C900-15. American Society for Testing and Materials, West Conshohocken, Pa.
- ASTM International. (2013). *Standard Test Methods for Deep Foundations under Static Axial Tensile Load*. D3689/3689M-07(Reapproved 2013). American Society for Testing and Materials, West Conshohocken, Pa.

- Bruce, D.A., & Nicholson, P.J. (1989). The Practice and Application of Pin Piling. *Proceedings of the ASCE Foundation Engineering*, Evanston, IL, 19pp.
- Bruce, D. A., Dimillio, A. F., & Juran, I. (1997). Micropiles: The State of Practice. Part1 Characteristics, Definitions and Classifications. *Ground Improvement*. p. 25-35.
- Butler, H. D., & Hoy, H. E. (1977). *User Manual for the Texas Quick-Load Method for Foundation Load Testing*. Federal Highway Administration, Office of Development, Washington, DC.
- Cavey, J.K., Lambert, D. V., Miller, S.M., & Krhounek, R.C. (2000). Observations of Minipile Performance under Cyclic Loading Conditions, *Ground Improvement*, 4: 23-29.
- Chan, S.F. & Hanna, T.H. (1980). Repeated Loading on Single Piles in Sands, *Journal of Geotechnical Engineering*, ASCE, 106: 171-188.
- Davisson, M. T. (1972). High capacity piles. *In Proceedings of Soil Mechanics Lecture Series on Innovations in Foundation Construction*, American Society of Civil Engineers, Illinois Section, Chicago. 81–112.
- Drbe. O. E., & EL Naggar M. H. (2014). Axial Monotonic and Cyclic Compression Behaviour of Hollow Bar Micropiles. *Canadian Geotechnical Journal*. 52: 426-441.
- FHWA. (2005). *Micropiles Design and Construction*. Federal Highway Administration, U.S. Department of Transportation, Washington, D.C. FHWA-NHI-05-039.
- FHWA. (2013). *Post- Tensioning Tendon Installation and Grouting Manual*. Federal Highway Administration, U.S. Department of Transportation, Washington, D.C. Publication No. FHWA-NHI-13-026.
- Fuller, F. M., & Hoy, H.E. (1970). Pile Load Tests Including Quick-Load Test Method Conventional Methods and Interpretations. *Highway Research Board (HRB)*, Issue 333, 78-86.



- Gomez, J.E., Rodriguez, C.J., Robinson, H.D., Mikitka, J., & Keough, L. (2008). Bond Strength of Hollow-Core Bar Micropiles. *In Proceedings of 6th Annual Conference on Case Histories in Geotechnical Engineering*, Arlington, Va., August 2008.
- Han, J., & Ye, S.L. (2006). A Field Study on the Behavior of Micropiles in Clay under Compression or Tension. *Canadian Geotechnical Journal*, 43(1), 19-29.
- Jardine, R.J. (1991). *The Cyclic Behaviour of Large Piles with Special Reference to Offshore Structures*, Cyclic loading of soils, Eds. O'Reilly and Brown, Blackie, London.
- Juran, I. & Weinstein, G.M. (2009). Long-Term Performance Assessment of Micropiles under Monotonic and Cyclic Axial Loading, *In proceedings of 9th International Workshop on Micropiles*, London, UK.
- Kershaw, A. K., & Luna, R. (2014). Full-Scale Field Testing of Micropiles in Stiff Clay Subjected to Combined Axial and Lateral Loads. *Journal of Geotechnical and GeoEnvironmental Engineering*. 140 (1): 255-261.
- Kulhawy, F. H., & Mayne, P. W. (1990). *Manual on Estimating Soil Properties for Foundation Design*. Research project No. 1493-6, EL-6800, Electric Power Research Institute., Palo Alto, Calif.
- Kulhawy, F. H., & Hirany. A. (2009). Interpreted Failure Load for Drilled Shafts via Davisson and L1-L2. *Selected Papers of the 2009 Int. Foundation Congress and Equipment Expo*. ASCE, New York, 127-134.
- Li, J., & Kast, G. (2007). 30 Years of GEWI-Pile Applications in Canada. *In Proceedings of 8<sup>th</sup> International Workshop on Micropiles*, Toronto, Canada.
- Littlejohn, G. S., & Bruce, D. A. (1977). Rock Anchors State-of-the-Art. *Foundation Publications Ltd.*, Brentwood, Essex, England, 50 pages.
- Pearlman, S. L & Wolosick, J.R. (1992). Pin Piles for Bridge Foundations. *In Proceedings of 8th Annual Int. Bridge Conference*, Pittsburgh, Pennsylvania. p. 8.

- Poulos, H.G. (1988). Cyclic Stability Diagram for Axially Loaded Piles, *Journal of Geotechnical Engineering*, ASCE, 114: 887-895.
- Randolph, M.F. & Worth, C.P. (1978). Analysis of Deformation of Vertically Loaded Piles, *Journal of Geotechnical Engineering*, ASCE, 104: 1465-1488.
- Reese, L. C., & O'Neill, M. W. (1988). *Drilled Shafts: Construction Procedures and Design Methods*. Federal Highway Administration, McLean, Va. FHWA-HI-88-042.
- Robertson. P. K. (1990). Soil Classification Using Cone Penetration Test. *Canadian Geotechnical Journal*. 27(1), 151-158.
- Stuedlein, A. W., Gibson, M. D., & Horvits, G. E. (2008). Tension and Compression Micropile Load Test in Gravelly Sand. *6th International conference on case histories in geotechnical engineering*, Arlington, VA.
- Sulaiman, I.H. & Coyle, H.M. (1976). Uplift Resistance of Piles in Sand, *Journal of Geotechnical Engineering*, ASCE, 102: 559-562.
- Timothy, M. J., Bean, J. J. & Bolton, M. K. (2012). miniJET: a new Type of Micropile. *In Proceedings Grouting and Deep Mixing*. American Society of Civil Engineers (ASCE), New Orleans, Louisiana, 1095-1104.
- Tsukada. Y. & Ichimura, Y. (1997). Micropiles in Japan: Present Status and Future Prospects. *In Proceedings of 5th International Workshop on Micropiles*. Seattle, 265- 278.
- Turner, J.P. & Kulhawy, F.H. (1990). Drained Uplift Capacity of Drilled Shafts under Repeated Axial Loading, *Journal of Geotechnical Engineering*, ASCE, 116: 470-491.
- Wolosick. J. (2009). Ultimate Micropile Bond Stresses Observed During Load Testing in Clays and Sands. *Proceedings Selected Papers of the 2009 International Foundation Congress and Equipment Expo*. ASCE, New York, 12-22.

Yacyshyn, C.J.E. (2007). Cyclic Quasi-Static Load Tests on Micropiles. *In proceedings of 8<sup>th</sup> International Society of Micropiles Workshop*, Toronto, Canada.

## CHAPTER 4

# 4 Axial Performance of Micropile Groups in Cohesionless Soil from Full Scale Tests.

---

### 4.1 Introduction

A micropile is comprised of a steel reinforcement element centralized in a surrounding competent grout column. The grout can be injected under pressure or under gravity depending on the application and required load carrying capacity. The micropile industry is expanding rapidly, which is evident by the accomplishment of micropile foundations in a variety of applications (Cadden et al., 2004). This expansion motivated an advancement in drilling technology and growth in micropile types and applications, including using micropiles with a diameter up to 300 mm (Bruce et al. 1997 and Wolosick and Scott 2017).

Hollow bar micropile (HBMP) construction has become a popular option for pile foundations because it allows a faster installation process and ground improvement at the same time. Its construction utilizes hollow steel bars for drilling and acting as a grouting conduit, which eliminates the need for a casing during drilling. Because of its unique construction technique, Abdelaziz and El Naggar (2012) and Timothy et al. (2012) suggested designating hollow bar micropiles as Type E micropile, supplementing the four original micropile types designated by the US Federal Highway Administration (FHWA, 2005). The American Association of State Highway and Transportation Official (AASHTO 2012) classified the HBMP as Type E based on its method of installation where

grout with high water/cement ratio is initially utilized to stabilize the ground and then replaced by structural grout to form the grout column.

The pile group behaviour is usually represented in terms of the group efficiency factor defined as the ratio of load capacity of the pile group to the sum of the load capacity of single piles. For estimating the axial pile group capacity, Terzaghi and Peck (1948) proposed considering the lesser of (i) the sum of the ultimate capacities of the individual piles or (ii) the capacity of the equivalent composite pier of the pile group. Vesic (1969) reported a full-scale testing program of pile groups, which involved two groups of 4 and 9 driven piles in dry medium dense sand. The piles centre to centre spacing ( $S$ ) ranged from 2 to 6d (where d is the pile diameter). The author reported a group efficiency factor of 1.7 for a pile cap resting on the sand and pile spacing,  $s = 3d$ , and 1.3 for free standing piles. Prakash and Sharma (1990) stated that the optimum pile spacing is  $s = 3$  to  $3.5d$ , and that the piles behave individually for  $s > 7d$ . They also suggested that the load capacity of a pile group in cohesionless soils is the sum of single pile capacities unless the piles are installed in dense sand, it could be higher. Ismael (2001) conducted field tests to examine the behaviour of single and pile groups subjected to axial loading in cemented medium dense sands. Pile groups consisting of five piles were installed with  $s = 2$  and  $3d$ . He reported that the group efficiency factor ranged from 1.22 to 1.93. Dai et al. (2012) reported results for full-scale axial static load tests on single piles and pile groups installed in layered soil comprising clay and silt. They reported that for relatively large loads, the pile group settlement was generally larger than the corresponding single pile settlement at the same average load per pile. The Canadian Foundation Engineering Manual (2006) proposed using Meyerhof's (1976) reduction factor of 0.67 for bored pile groups installed in clean

sand and group efficiency of 1.0 for pile groups with  $s < 4.5d$  installed in sand with some fines and the pile cap in good contact with the soil. For drilled shafts installed in cohesionless soil, AASHTO (2012) suggested group efficiency factors of 0.67 and 1.0 for pile spacing to diameter ratios ( $s/D$ ) of 2.5 and 4 or more, respectively.

Juran et al. (1999) reviewed the state of practice and design methods of micropile groups. They evaluated several experimental studies on the behaviour of micropile groups and concluded that the group efficiency depends on the installation technique and the micropile inclination. They also reported that the empirical correlations relating the pile group settlement to the single pile settlement proposed by Fleming et al. (1992) and Skempton (1953) were consistent with their experimental results. However, they emphasized the need for further field studies and analytical simulations to develop guidelines for micropiles groups and reticulated network systems.

The FHWA (2005) commissioned a comprehensive study on micropile behaviour. The results of the study indicated that for micropiles installed in sand, the group efficiency ratio can be taken as 1.0 for  $s > 3d$ . However, the FHWA (2010) follows the AASHTO provisions for group efficiency. Similarly, the French National Research Project on Micropiles “FOREVER” was a major research project that investigated the behaviour of micropiles and involved both model and full-scale tests for micropile groups and micropile networks mostly in sand (Frank and Schlosser, 2009). The results of 54 load tests on micropile groups demonstrated that groups with a large number of micropiles provided a group efficiency factor  $> 1.0$ , whereas small groups had an efficiency factor less than or close to 1.0.

Bruce et al. (2005) suggested using an efficiency factor of 1.0 for micropile groups constructed by gravity grouting (i.e. Type A) with  $s > 3d$ . For micropiles constructed with pressurized grout (Types B, C and D), the efficiency factor is  $> 1$  because of the pressurized grout. However, there has been no evidence to support this potential advantage in North American practice (Bruce et al., 2005).

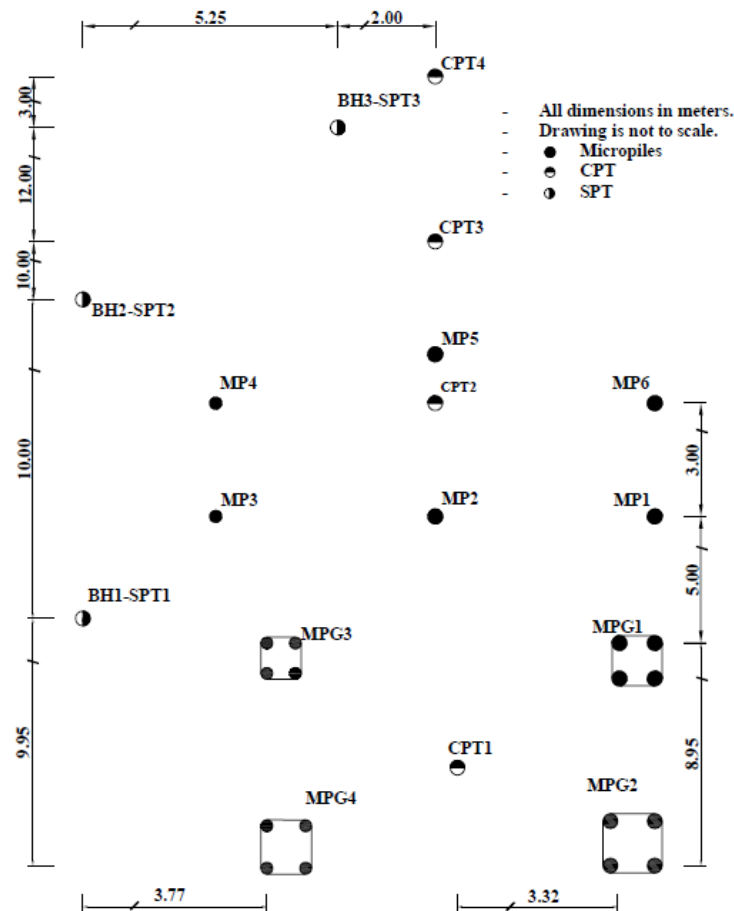
Rose and Taylor (2010) and Rose et al. (2013) investigated the behaviour of micropile perimeter groups in firm stiff clay using a geotechnical centrifuge and numerical modeling studies. The results showed that the group efficiency is greater than 1.0 for perimeter groups. They also indicated that the perimeter group provided larger efficiency than conventional grid groups. Abd Elaziz and El Nagggar (2014) conducted a full-scale load tests on single and pairs of hollow bar micropiles installed in soft soil. The test results were used to calibrate a three-dimensional finite element model and a parametric study was performed based on the calibrated model. A group efficiency factor of 1.0 was suggested for hollow bar micropile groups installed in cohesive soil. They also proposed a method of calculating the settlement of micropile groups and provided interaction factors to be used for evaluating group performance.

Despite the growing use of HBMP for many applications, there is a noticeable gap in literature on their performance in a group. Furthermore, the effect of several factors on the behaviour of HBMP groups such as the effects of increasing the drill bit/ hollow bar ( $D_b/D_h$ ) ratio and grouting pressure should be addressed. To fully investigate the constructional advantages of HBMP in different applications, this research effort attempts to evaluate the performance of HBMP groups and to establish some guideline for their design considering the most common spacings used in practice (i.e., 3 to  $5D_b$ ) and the effect

of increasing the ratio of commonly used  $D_b/D_h$  ratios of 2.25 to 3. Full-scale compression load tests are conducted on 4 HBMP groups and 6 individual HBMPs and the results are evaluated to gain better understanding of performance of HBMP groups installed in sand.

## 4.2 Geotechnical Site Characterization

A site investigation was carried out at the test site in Ayr, Ontario, Canada, which included both in-situ and laboratory testing. Figure 4.1 presents a plan view of the test site including the location of the in-situ testing along with micropile locations.



**Figure 4-1 Plan view of micropiles groups locations, BHs and CPTs (Dimensions in meters and Not to scale).**



Three exploratory boreholes were drilled to various depths using hollow stem augers of 130 mm, followed by standard penetration tests (SPT). Samples were extracted from the borings using a split spoon and transported to the laboratory for further testing. The boreholes showed that the top 200 - 300 mm consisted of granular base fill overlaying layers of brown medium dense to dense sand and silty sand up to a depth of 11m. Seams of silt and silty clay were observed at different levels. The ground water table elevation varied between 9.5 to 10.5m from the ground surface. Table 4.1 summarizes the SPT results, including N values and water content, for BH1 and BH2 that were conducted close to the test area.

Four cone penetration test (CPT) soundings were performed across the site. Figure 4.2 shows CPT1 and CPT2 soundings conducted within the test area along with the soil behaviour type (SBT) profile defined according to the classification chart proposed by Robertson (1990). The SBT profile confirmed that the soil is mainly sand with some seams of silt and sandy silt. The average cone tip resistance corrected to pore water pressure ( $q_t$ ) ranged from 10 to 30 MPa in the upper 6.5m and 30 to 45 MPa from 6.5m to 8m followed by a decrease in ( $q_t$ ) with an average of 20 MPa. The sand relative density,  $D_r$ , was obtained using the correlations proposed by Kulhawy and Mayne (1990) based on SPT and CPT data.

These results indicated that the sand is mainly medium dense to dense. In addition, sieve analyses conducted on samples retrieved from the test area has shown that the soil along the micropiles was primarily fine sand.

**Table 4-1 Summary of SPT N values for BH1 and BH2**

Depth (m)	Borehole No. 01		Borehole No. 02	
	N (blows/30cm)	Water content (%)	N (blows/30cm)	Water content (%)
1.00	27	6.0	16	7.0
1.80	23	5.0	15	6.0
2.60	23	4.0	25	3.0
3.20	21	13.0	15	10.0
4.00	23	5.0	36	3.0
4.80	29	2.0	21	12.0
6.40	51	4.0	35	3.0
8.00	21	4.0	48	4.0
9.40	36	20.0	46	18.0
10.90	31	25.0	54	22.0
12.50	59	20.0	93	12.0
14.00	75	22.0		
15.40	200	17.0	End of borehole	
	End of borehole			
<b>Note</b>	N is blow count to advance standard split spoon sampler 30cm with a 63.5 kg hammer			

The angle of internal friction,  $\phi$ , was measured using direct shear tests on soil samples retrieved at different elevations and reconstituted to the same in-situ relative density,  $D_r$ , evaluated from SPT and CPT soundings.

$$D_r = \left[ \frac{(N_1)_{60}}{40} \right]^{0.5} \quad (4.1)$$

$$D_r = \left[ \frac{\left( \frac{q_{ti}}{p_a} \right)}{305} \right]^{0.5} \quad (4.2)$$

Where,

$(N_1)_{60}$  = the measured N-value corrected for field procedures and effective overburden pressure of 100 kPa,  $P_a$  = the reference stress = 100 kPa and  $q_{ti}$  = normalized cone resistance.


Figure 4.3a shows the shear box test results in terms of horizontal displacement versus vertical displacement at four different confinement pressures, which indicates dilative dense sand behaviour. The results showed peak angle of internal friction  $\phi_p = 43.5^\circ$  and the residual angle of internal friction  $\phi_r = 33^\circ$  as shown in Figure 4.3b. In addition,  $\phi_p$  is correlated to  $D_r$  using the relationship proposed by American Petroleum Institute (1987), i.e.

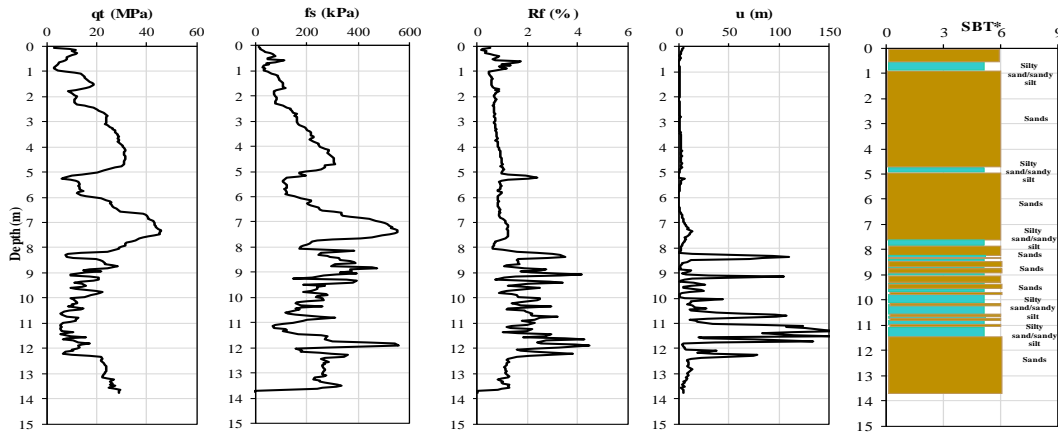
$$\phi = 16D_r^2 + 0.17D_r + 28.4 \quad (4.3)$$

The internal peak friction angle  $\phi_p$  was also correlated to normalized cone resistance,  $q_{t1} = (q_t/\sigma_{atm}) / (\sigma'_{vo}/\sigma_{atm})$  using relationship proposed by Kulhawy and Mayne (1990), i. e.

$$\phi_p = 17.6 + 11 \log(q_{t1}) \quad (4.4)$$

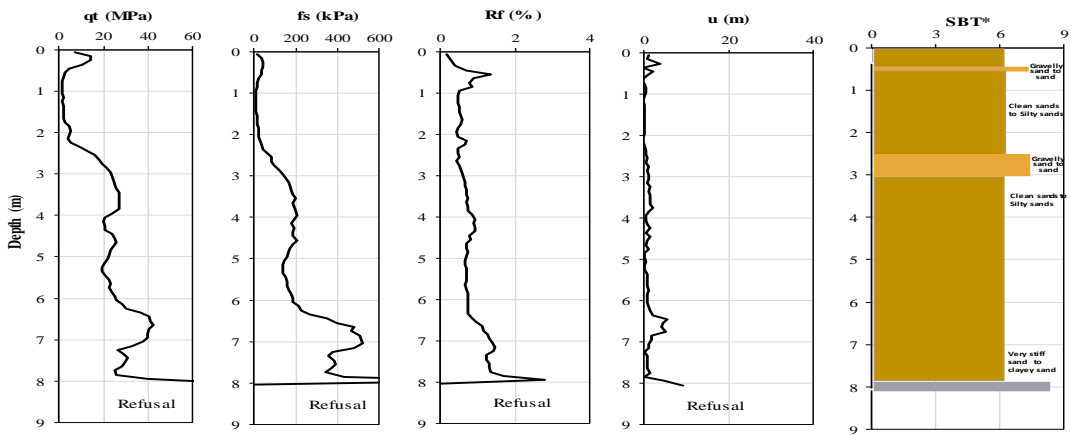
The average  $\phi_p$  over the top 6.0 m obtained from correlations with SPT and CPT was 42°, which is in reasonable agreement with measured  $\phi_p = 43.5^\circ$ .

<b>Project:</b>	Micropiles Project		<b>Date:</b>	13/07/2015	<b>Max Depth:</b>	13.75 m
<b>Sounding:</b>	1		<b>Weather:</b>	Sunny	<b>Depth Inc:</b>	0.050 m
<b>Location:</b>	Ayr, Ontario		<b>G.W. Depth:</b>	9.0 m	<b>AVG Int :</b>	0.10 m



(a)

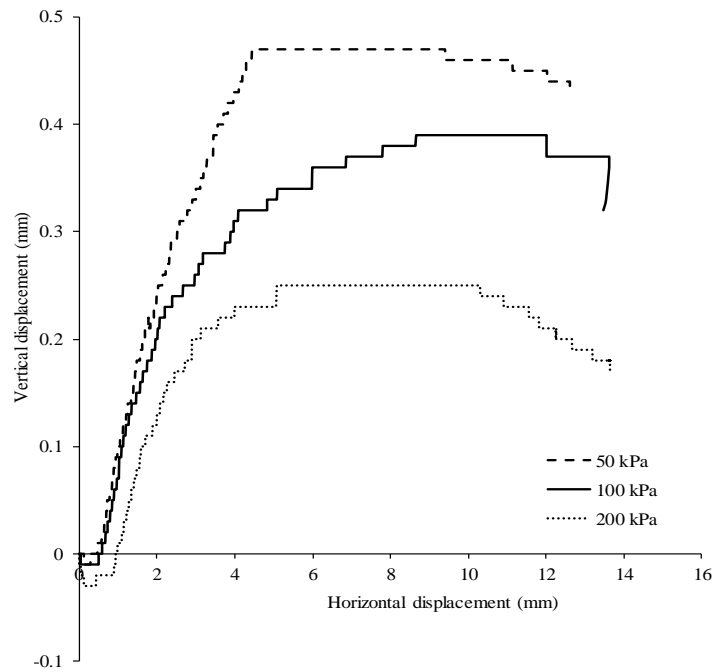
<b>Project:</b>	Micropiles Project		<b>Date:</b>	13/07/2015	<b>Max Depth:</b>	8.10 m
<b>Sounding:</b>	2		<b>Weather:</b>	Sunny	<b>Depth Inc:</b>	0.050 m
<b>Location:</b>	Ayr, Ontario		<b>G.W. Depth:</b>		<b>AVG Int :</b>	0.10 m



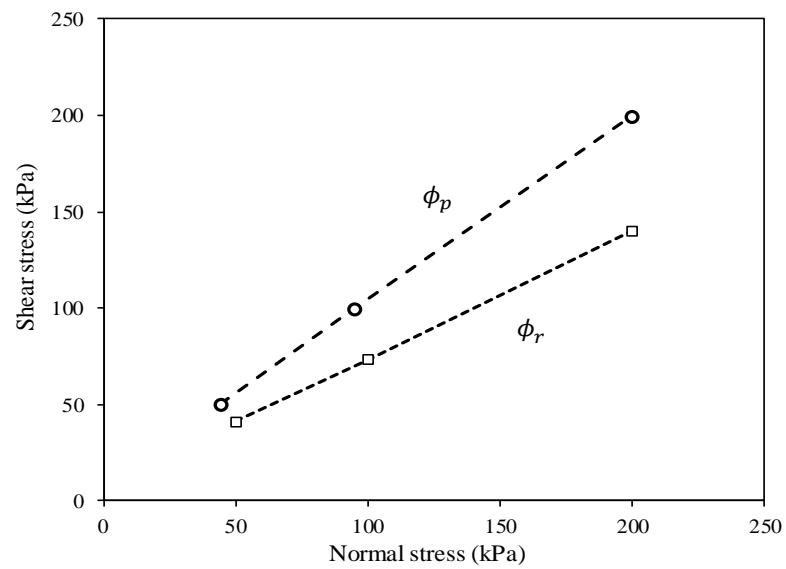
\* SBT: Robertson, 1990

(b)

Figure 4-2 CPT soundings with SBT: a) CPT1; b) CPT2



(a)



(b)

**Figure 4-3 Direct shear test results: a) horizontal settlement vs. vertical settlement;  
b) measured angle of internal friction**

### **4.3 Installation of Micropiles**

Four micropile groups (MPG1 to MPG4) and 6 individual micropiles (MP1 to MP6) were constructed and tested in this study. Each group was comprised of four hollow bar micropiles installed in a square arrangement, with two commonly used micropile spacings,  $3 D_b$  and  $5 D_b$ . All micropiles were 6.0 m long (with a 5.75 m embedded length). They were constructed utilizing R51N hollow bars with a 51 mm outer diameter and 33 mm inner diameter, and Tungsten carbide cross cut drill bits. Two groups, MPG1 and MPG2, were installed using a drill bit with  $D_b = 152$  mm (i.e.  $D_b/D_h=3$ ) and two groups, MPG3 and MPG4, were installed using  $D_b = 115$  mm (i.e.  $D_b/D_h=2.25$ ). Groups MPG1 and MPG3 had micropile spacings of  $3 D_b$ , while MPG2 and MPG4 had a spacing of  $5 D_b$ .

### **4.4 Micropiles Installation Procedure**

The drill bit was attached to the R51N hollow bar and set into the required position. Rotary percussive drilling was then started simultaneously with a grout-flushing technique. Drilling and grouting operations were performed in one step owing to a grout swivel, which accelerated the construction schedule and ensured a good grout/ground bond strength. During drilling, grout with a specific gravity of about 1.4-1.5 was employed to facilitate installing the hollow bars. Once the first hollow bar segment (3m in length) was installed, the drilling stopped to add the second segment and the two bars were attached using a 200mm long coupler. The drilling was continued until the required depth was reached, at which point the final competent structural grout was pumped under a pressure of between 0.8 to 1 MPa to displace the drilling grout.

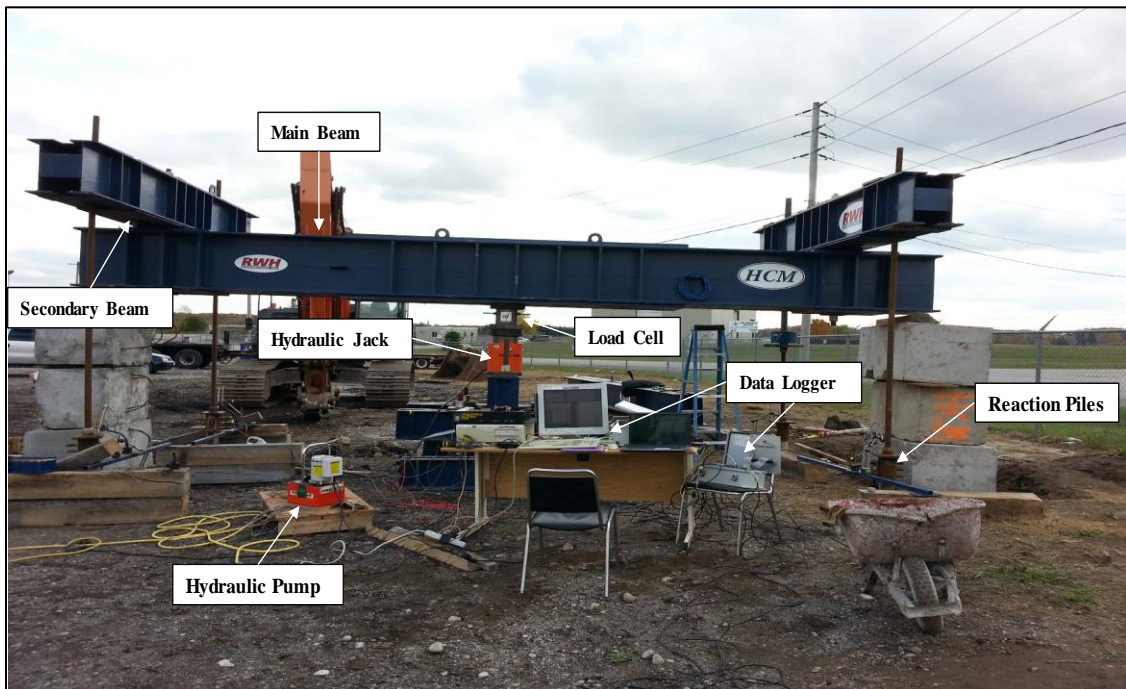
The final neat grout had a specific gravity between 1.80 and 1.95 in accordance with the FHWA (2005) recommendation for micropile applications, and had water to cement ratio,  $w/c = 0.45$  to provide high strength and suitable pumpability with minimum bleeding. The grout density was measured employing the Baroid Mud Balance Test as per API Recommended Practice (RP) 13 B-1. FHWA (2013) specifies a minimum compressive strength of 21 MPa for 7 days and 35 MPa at 28 days. The drilling rates ranged between 0.45 to 0.60 m/min and the grouting rate was about 35 L/min. The drilling rates, including the time period for adding the second segment of hollow bar with coupler, ranged between 1 to 2 minutes. The drilling and grout rates measured within this specific site can be used as useful tools to estimate the time required for the installation of hollow bar micropiles in a similar site and confirm the installation consistency.

Grout cylinders were collected during the installation process using a cylindrical mold of 100 mm by 200mm and 75 mm by 150mm. All specimens were de-moulded after 24 hours then placed in a control room with a relative humidity of 100% and constant temperature of 23°C. After four weeks, the cylinders were tested under compression and indirect tension. The compressive strength was determined according to ASTM C39 and the tensile strength was obtained in accordance with ASTM C496. The average compressive strength after 28 days was 40 MPa and the average split tensile strength was 3.97 MPa, which meet FHWA (2013) requirements.

## **4.5 Test Setup, Instrumentation and Procedures**

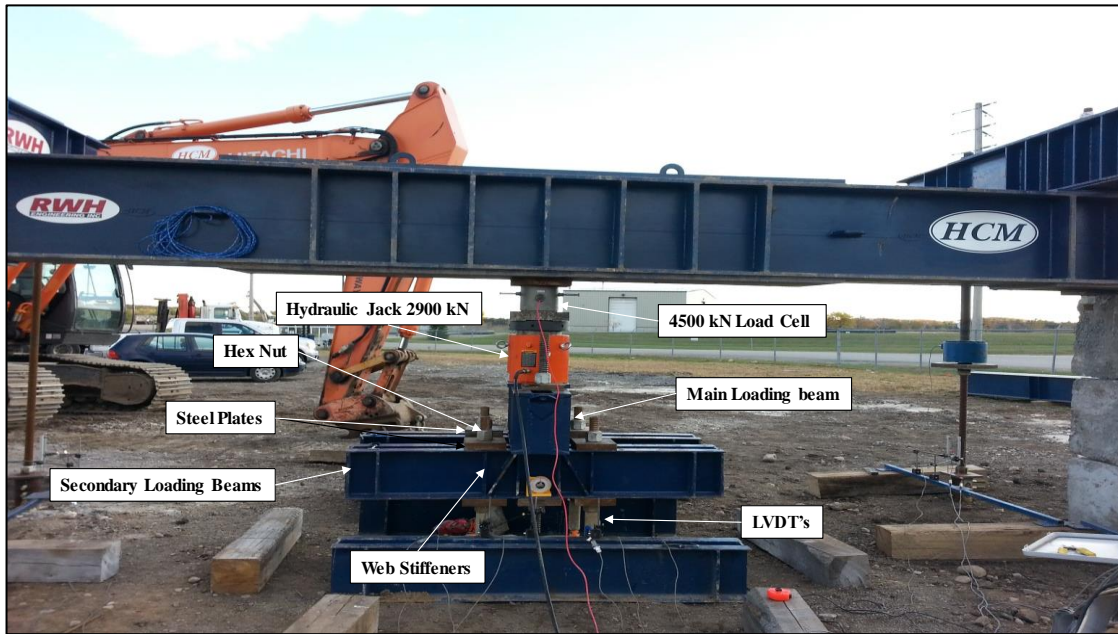
The testing program consisted of compression quick load tests for six single micropiles and four micropile groups. A reaction frame system was employed to perform the loading tests,

which comprised a main steel reaction beam and two secondary steel reaction beams. The main beam reacted against the two secondary beams, which were connected to four reaction helical piles. The helical piles consisted of a steel pipe (114.3 mm outer diameter and 97 mm inner diameter) welded to three 300 mm helical plates. The reaction piles were placed away from the test micropiles at a distance of more than 15 times the larger micropile diameter. A pile cap was used to transfer the load to the micropiles consisted of three I – beams configured in ‘H’ pattern as shown in Figure 4.4. The top I-beam was centered and seated on the two bottom I-beams.



(a)





(b)

Figure 4-4 a) Compression test setup; b) head instruments of micropile groups.

#### 4.5.1 Loading Equipment and Micropile Instrumentation

A hydraulic jack with 2900 kN advance capacity and a maximum stroke of 150 mm powered by a hydraulic pump was employed to apply the loading to the micropile groups. The applied load was monitored using a load cell with a 4500 kN capacity. Six HLP 190 linear potentiometers (100 mm stroke and 0.01 mm accuracy) were used to record the vertical micropile head movement and the average value was taken. The potentiometers were attached to the loading steel plates and clamped to two independent reference steel beams. Figure 4.4b shows the pile head instruments for micropile groups under compression loading.

To investigate the load transfer mechanism along the micropiles, two of the single micropiles (MP2 and MP3) were instrumented with strain gauges and each of MPG1, MPG3 and MPG4 had one instrumented micropile and MPG2 had two instrumented micropiles. Each instrumented micropile had three vibrating wire strain gauges (VWSGs) type EM-2 placed at 0.80, 3.1 and 5.60 m from the ground surface. The VWSGs were attached to a steel cage, which was installed inside the hollow bar immediately after grouting as recommended by Abd Elaziz and El Naggar (2012). Prior to and after the installation of the micropiles, the gauges were connected to the vibrating wire readout Model Gk-404 to ensure that they were working properly. To account for the environment effects on the vibrated wire strain gauges reading, no-stress gauges (dummy gauge) were hooked to the data acquisition system in order to measure the change in the strain in the same environment conditions without any load effect. The vertical settlements of the four reaction helical piles were observed during the tests using HLP 190 linear potentiometers.

#### **4.5.2 Load Test Procedure**

The quick load test procedure was employed in accordance with ASTM (2013) D1143-D1143M-07 (reapproved 2013), the standard for compression tests. The load was applied in increments; each increment was 5% of the anticipated failure load (estimated using the shaft shear resistance recommended by FHWA (2005) for Type B micropiles installed in sand) and was maintained for 5 minutes before applying the next increment. The load was increased until the pre-specified load or failure was reached, or when one of the reaction piles displayed a large and continuous settlement with a small increase in the applied load. Once one of these conditions were reached, unloading took place in five approximately equal increments. Only one micropile, MP1, was loaded to design load, not to failure. In

addition, loading for MPG2 could not reach the anticipated failure load due to the limitation of the reaction piles.

## **4.6 Test Results and Analysis**

### **4.6.1 Load – settlement curves**

For comparison, the load test results for the single micropiles are provided along with those for the micropile groups. Figure 4.5 displays the load - settlement curves for all single micropiles. As can be noted from Fig. 5, the response curves of all tested micropiles exhibited the same pattern: an initial linear segment followed by a nonlinear segment, and a final linear segment leading to failure (except for MP1, which was only loaded to its design capacity). The slope of the initial part represented the micropile stiffness under compressive loading. The average stiffness of micropiles with  $D_b/D_h = 2.25$  was 70 MN/m, while the average stiffness of micropiles with  $D_b/D_h = 3.0$  was 97 MN/m. This demonstrates that increasing the drill bit diameter improved the stiffness of the micropile by 39%.

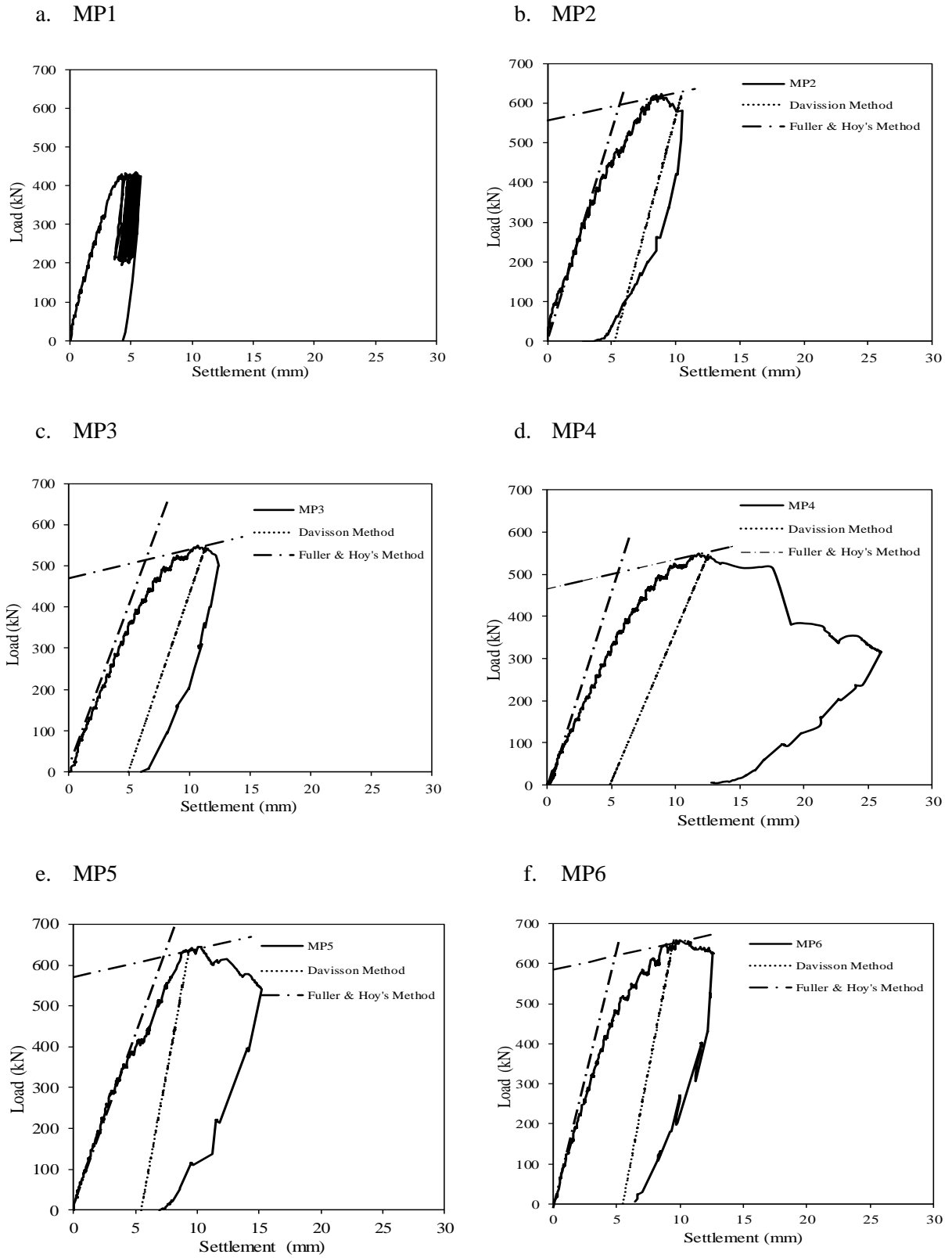
In the absence of plunging failure during load tests, the ultimate capacity can be evaluated by using a suitably chosen interpreted failure load criterion. Abdelaziz and El Naggar (2014) and Drbe and El Naggar (2014) demonstrated that the ultimate capacity of individual HBMP established from load test results using the Butler and Hoy (1977) criterion was in excellent agreement with the observed failure load. In this criterion, the interpreted failure load is defined by the intersection of the initial linear part of the load - settlement curve and the tangent to the nonlinear part of the response curve with slope equal to 0.14 mm/kN. Table 4.2 provides the ultimate capacity for the tested single micropiles. As can be noted from Table 4.2, the average ultimate capacity of micropiles

with  $D_b/D_h = 2.25$  was 541 kN, while the average ultimate capacity for micropiles with  $D_b/D_h = 3.0$  was 630 kN (i.e. 17% increase).

In order to delineate the effect of drill bit diameter on the behaviour of micropile groups, the results of micropile groups installed at the same micropile spacing but constructed with different drill bit size are compared in Figure 4.6. Figure 4.6a compares the load- settlement curves for micropile groups with  $S = 3 D_b$  but constructed with a different drill bit size (i.e. MPG1,  $D_b = 152$  mm; and MPG3,  $D_b = 115$  mm); while Figure 4.6b compares the results for micropile groups with  $S = 5D_b$  but constructed with a different drill bit size (i.e. MPG2,  $D_b = 152$  mm; and MPG3,  $D_b = 115$ ).

**Table 4-2 Interpreted failure load for single micropiles**

Method	Interpreted Failure Load (kN)				
	MP2	MP5	MP6	MP3	MP4
<b>Plunging</b>	620	630	640	540	542
<b>Fuller and Hoy's</b>	615	630	642	533	545
<b>Butler and Hoy's</b>	600	615	621	520	520

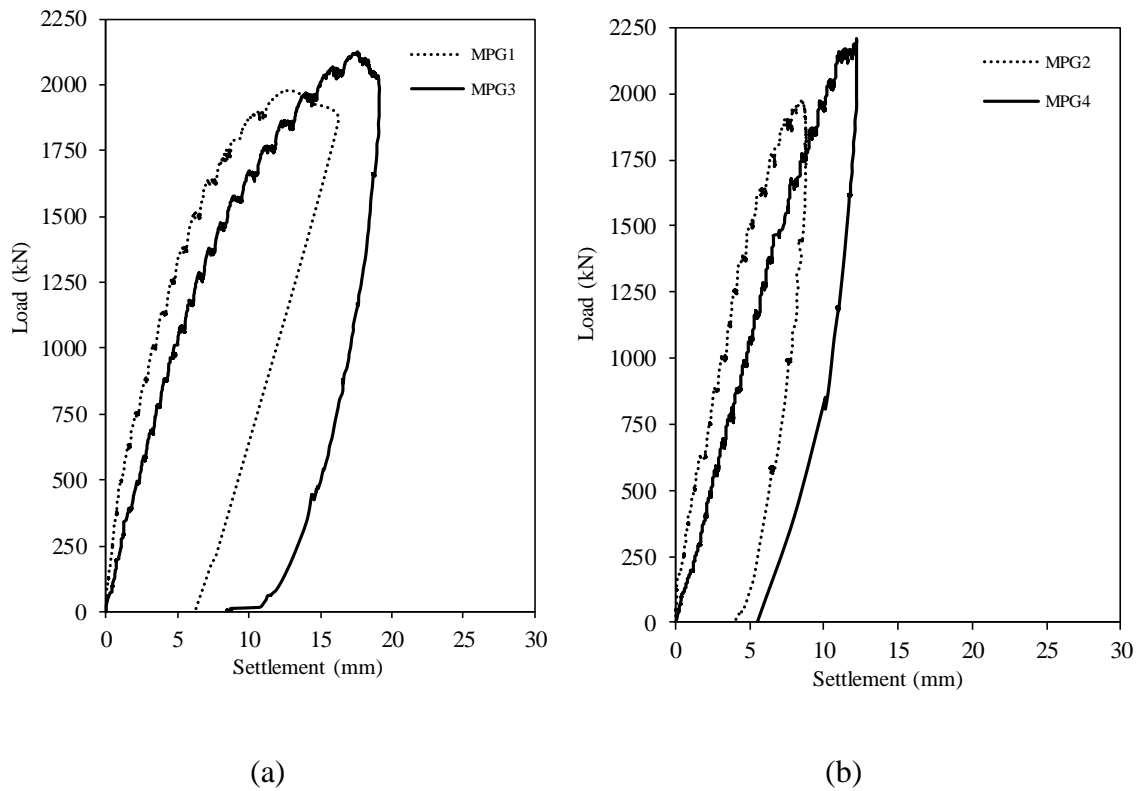


**Figure 4-5 Compression load – settlement curves for single micropiles**

As can be noted from Figure 4.6, all load- settlement curves displayed an initial linear part, which almost extended to the end of loading. The slope of the linear part represents the group stiffness. Table 4.3 compares the group stiffness for the four tested micropile groups. As can be noted from Table 4.3, the groups comprising micropiles constructed with  $D_b = 152$  displayed higher stiffness. For example, MPG1 had a stiffness of 275 MN/m while MPG3 had a stiffness of 195 MN/m, i.e. an increase of 41%. Similarly, MPG2 had a stiffness of 335 MN/m while MPG4 had a stiffness of 210 MN/m, i.e., an increase of 59%. These results show that the average group stiffness increased by about 50% due to the increase in drill bit diameter (i.e. micropile diameter).

As the applied load increased, the load- settlement curves for all groups displayed a slightly nonlinear part. However, for MPG1, the loading connection (i.e. extended hollow bar connecting the micropile head to the top of the secondary loading beam) shown in Figure 4.7 failed at an applied load of 1880 kN.

To avoid this premature structural failure of the loading bar when testing other groups, a hex nut and a coupler were added to stiffen the extended hollow bar. Furthermore, during the testing of MPG2, one of the reaction piles experienced sudden movement at an applied load of 1975 kN, at which point unloading started for safety reasons.



**Figure 4-6 Effect of increasing  $D_b/D_h$  on group behaviour for groups with: a)  $s/D_b = 3$ ; b)  $s/D_b = 5$**

**Table 4-3 Micropile groups stiffness**

<b>File Group Number</b>	<b>Stiffness (MN/m)</b>
<b>MPG1</b>	275
<b>MPG2</b>	335
<b>MPG3</b>	195
<b>MPG4</b>	210

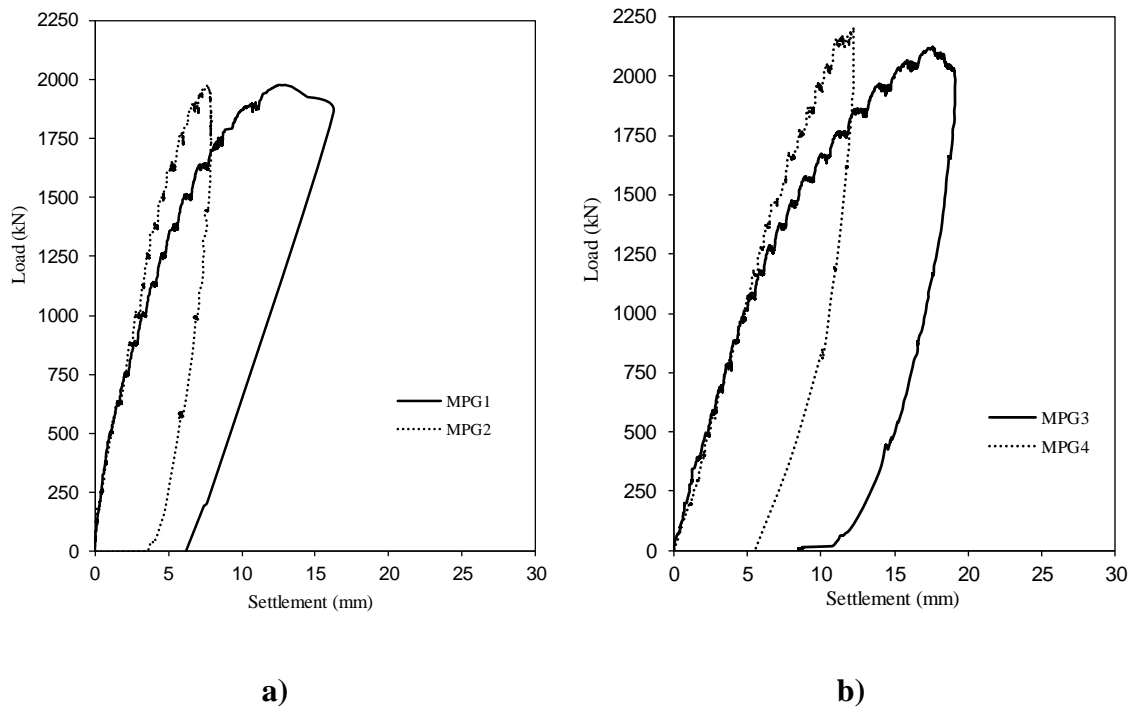
To discern the effect of micropile spacing on group behaviour, Figure 4.8a compares load-settlement curves of micropile groups constructed with  $D_b = 152$  mm but with a different micropile spacing (i.e. MPG1 ( $s = 3D_b$ ) and MPG2 ( $s = 5D_b$ )) and Figure 4.8b compares

response curves of groups constructed with  $D_b = 115$  mm (i.e. MPG3 ( $s = 3D_b$ ) and MPG4 ( $s = 5D_b$ )). The initial responses of MPG1 and MPG2 were approximately identical up to an applied load of 800 kN. As the loading continued, MPG1 exhibited a slightly softer response, which indicates slightly higher group effect for MPG1. Similarly, the initial response of MPG3 and MPG4 with  $s = 3D_b$  and  $5D_b$ , respectively, were almost identical up to 1050 kN. As the load continued to increase above this level, MPG3 exhibited a softer load - settlement response as shown in Figure 4.8b. It is interesting to note from Figure 4.8 that the initial response of groups with same diameter micropiles but spacing of 3D and 5D were identical up to 800 and 1050 kN with vertical settlements of 2.5 and 5.1 mm, respectively. For micropile groups installed with a micropile spacing of 3D, the micropile-soil-micropile interaction started to influence the group behaviour at a smaller load and settlement than in groups with a micropile spacing of 5D.



**Figure 4-7 Structural failure of loading bar for MPG1**





**Figure 4-8 Effect of spacing to diameter ratio on group behaviour for groups with:**  
**a)  $D_b/D_h = 2.25$ ; and b)  $D_b/D_h=3.0$**

There are no published criteria or recommendations for the interpretation of load tests of micropile groups to evaluate their axial capacity. Even though Fuller and Hoy (1970) and Butler and Hoy (1977) graphical methods were proposed to obtain the interpreted failure load of single piles, they are potentially suitable for the interpretation of micropile group tests because they are not a function of the pile diameter or a specified settlement. Rather, they are based on the shape of the load-settlement curve. Fuller and Hoy (1970) defined the ultimate load as the minimum load, which results in a rate of total settlement of 0.14 mm/kN, while Butler and Hoy (1977) gave the capacity by the intersection of the initial linear part of the load-settlement curve and a line tangent to the nonlinear part of the response curve with a slope equal to 0.14 mm/kN. The ultimate capacity values determined using the two criteria are compared in Table 4.4 with the failure (plunging) load.

**Table 4-4 Interpreted failure load methods for micropile groups**

Method	Interpreted Failure Load (kN)/ Associated settlement			
	MPG1	MPG2	MPG3	MPG4
<b>Plunging</b>	NA*	NA*	2125/18.13	2150/11.4
<b>Fuller and Hoy's</b>	NA*	NA*	2100/18	2140/11
<b>Butler and Hoy's</b>	NA*	NA*	2070/10	2130/10

Table 4.5 summarizes the test results for the four groups, including the group efficiency when applicable. The group efficiency of MPG3 and MPG4 at the ultimate load was close to unity. The capacity of micropile groups will be further evaluated from the interpretation of numerical modeling of the group load tests as will be discussed later.

**Table 4-5 Summary of group efficiency**

Micropile groups	Drill bit/Hollow bar diameters	Center-to-center distance	Failure load (kN)	Group efficiency
<b>MPG1</b>	3	3	2640*	1.04
<b>MPG2</b>	3	5	2682*	1.06
<b>MPG3</b>	2.25	3	2100	0.97
<b>MPG4</b>	2.25	5	2150	0.99

\*Values obtained from FE analysis.

#### 4.6.2 Unit skin friction and toe resistance of individual micropiles

The axial force distribution can be obtained using the strain gauge measurements at different levels by utilizing the measured area and equivalent modulus of elasticity. The axial force distribution at different levels along the micropile was calculated using measured strains, i.e.:

$$P = \varepsilon A_p E_p \quad (4.5)$$

Where  $P$  = axial force,  $\varepsilon$  = axial strain,  $A_p$  = cross sectional area of micropile and  $E_p$  = composite modulus of elasticity of micropile materials.

The equivalent axial compression stiffness of the micropiles can be obtained using the following formula,

$$E_p A_p = E_g A_g + E_s A_s \quad (4.6)$$

Where  $E_p$  = modulus of elasticity of the micropile,  $A_p$  = cross-sectional area of the micropile,  $E_g$  = modulus of elasticity of the grout,  $E_s$  = modulus of elasticity of the steel bar,  $A_g$  = cross-sectional area of the grout and  $A_s$  = cross-sectional area of the steel bar.

All micropile groups were excavated to at least a 2 m depth and the actual diameters were measured. It was observed that the micropile profiles for the excavated depth are similar to the profile of single micropiles. It was found that the average diameter of micropiles with drill bit 115 and 152 mm were 132 and 172 mm, respectively, i.e. the diameter increased by 14.8% and 13.1 % over the diameter of the drill bit. The actual diameters were used throughout the analysis to interpret the field test results.

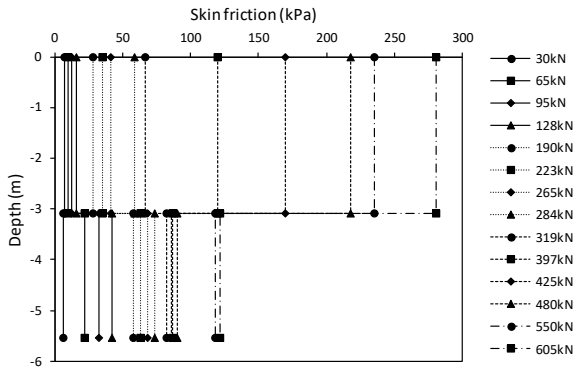
The ultimate skin resistance along the shaft between the levels of strain gauges can be calculated as the axial forces obtained from strain gauges readings divided by the surface area between the gauges. Figure 4.9 shows the distribution of skin friction along the instrumented micropiles MPG2-1, MPG2-2, MPG3-1 and MPG4-1 along with the single micropiles MP2 and MP3. The lower strain gauge for instrumented micropile MPG1 did not give reasonable results and was ignored.

The average values of skin friction for the upper and lower layers was computed and are compared to the suggested value by FHWA (2005) for ultimate skin friction. The computed results are summarized in Table 4.6. Table 4 demonstrates the skin friction values for the upper part is higher than the skin friction values for the lower part. This may be attributed to two factors: 1) the top layer is gravelly sand, which allows more grout permeation than the lower layer, which is silty sand, and consequently ground improvement and grout-ground strength are higher; 2) skin friction was mobilized fully for the top layer, but not developed fully for the bottom layer. The average ultimate skin friction for MPG3 and MPG4 are 202 kPa and 197 kPa, respectively, which were close to the ultimate skin friction of single micropile with the same diameter, MP3, 209 kPa, indicating that the group efficiency for MPG3 and MPG4 is close to unity. Moreover, these ultimate skin friction values are within the range of values suggested by FHWA (2005) for Type B micropiles installed in medium dense sand.

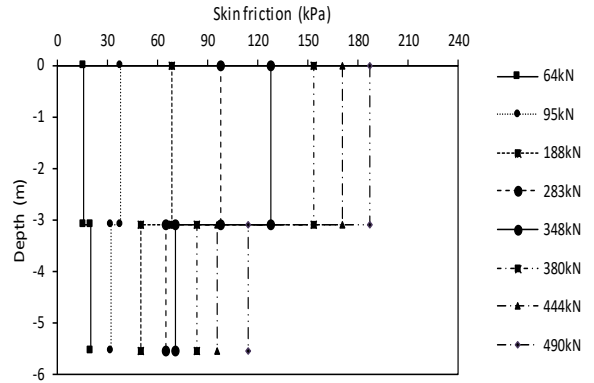
**Table 4-6 Ultimate skin friction of instrumented micropiles in the groups**

<b>Elevation</b>	<b>MP2</b>	<b>MPG1</b>	<b>MPG2</b>	<b>MP3</b>	<b>MPG3</b>	<b>MPG4</b>
<b>Upper part</b>	281	--	--	295	278.4	245.0
<b>Lower part</b>	122	--	--	123	124.9	148.9
<b>Average</b>	202	--	--	209	201.6	196.9
<b>FHWA</b>	186	179.9*	182.1*	200	197.7	199.9

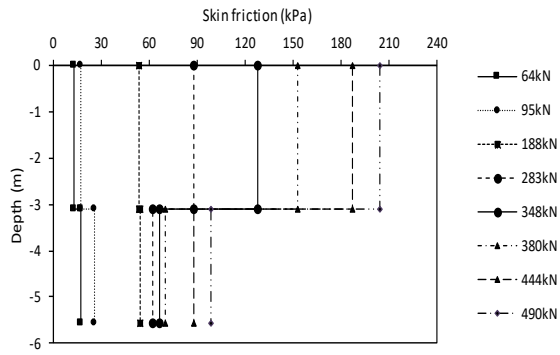
MP2



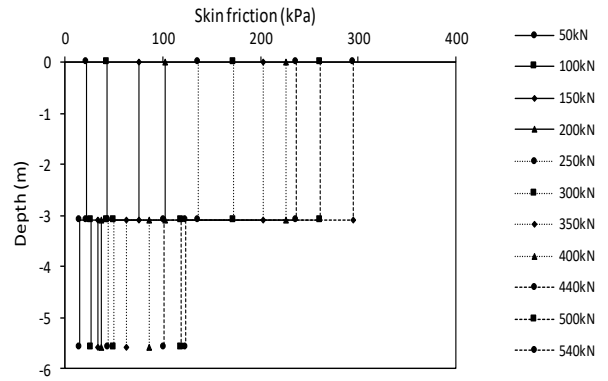
(MPG2-1)



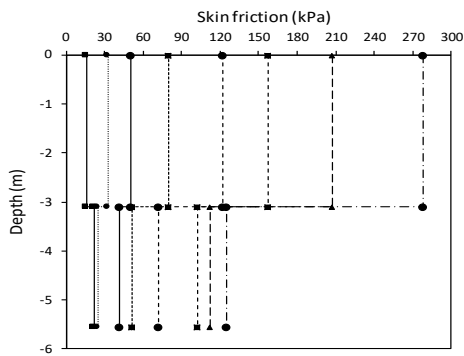
(MPG2-2)



MP3



(MPG3)



(MPG4)

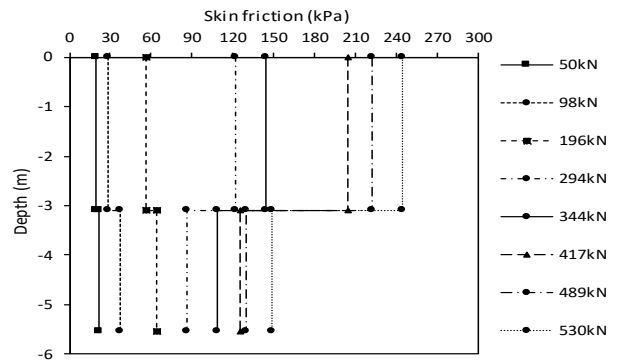
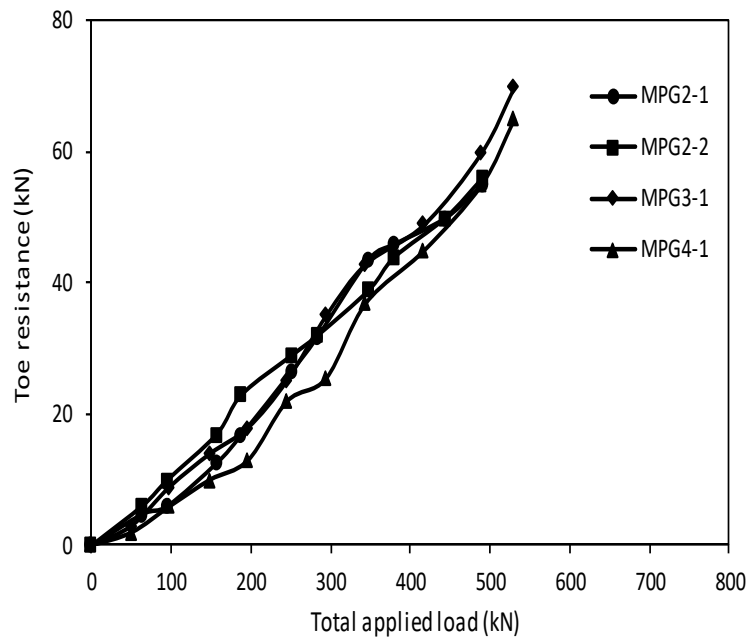


Figure 4-9 Distribution of unit shaft resistance for micropile groups

The toe resistance of instrumented micropiles was evaluated using the reading of the lower strain gauge placed near the micropile toe. The toe resistance is plotted against the total applied load in Figure 4.10. The average toe resistance accounted for about 12% of the total resistance of the tested micropiles. Accordingly, ignoring the toe resistance contribution to the total micropile resistance as suggested by FHWA seems to be conservative. Han and Ye (2006) and Drbi and El Naggar (2014) reported similar results.

To evaluate the group effect, the readings of strain gauges attached to single micropiles and micropile groups were used to calculate the distribution of the load along the micropiles and the results are compared in Figure 4.11. Additionally, the transferred loads at different depths for micropile groups are compared to the transferred loads of single micropiles with the same diameters in Table 4.7. For micropiles with  $D_b/D_h = 2.25$ , the results indicated that the group efficiency ratio is almost 1.



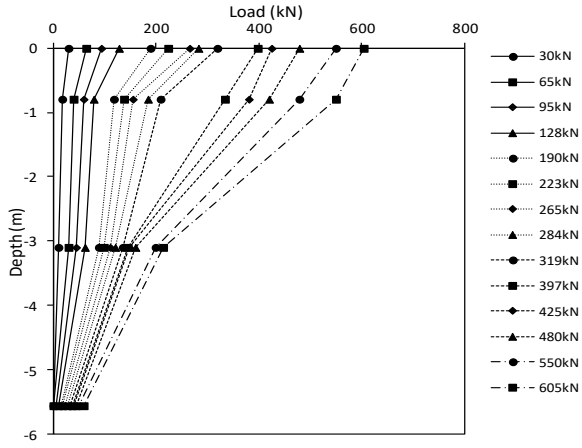
**Figure 4-10 Total applied load versus toe resistance of instrumented micropiles**

In addition, for micropile groups with  $D_b/D_h = 3$  (MPG1 and MPG2) in which the load was terminated prior to any noticeable sign of failure, the transferred loads for an applied load up to 425 kN were close to the transferred load of single micropiles, indicating that the group efficiency ratio is close to unity as well.

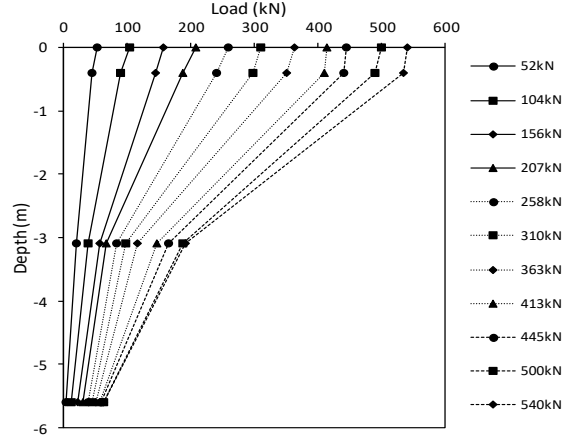
Even though every precaution was taken to ensure the loading system used in the current study would facilitate loading the micropile groups to failure, it was realized during the testing program that it was not possible. For example, the loading hollow bar failed during loading MPG1 and one of the reaction piles failed during testing MPG2. However, there is a need to establish the ultimate load from incomplete load tests. Several techniques were proposed for the interpretation of incomplete pile load tests (e.g. Chin, 1970) and are widely used in practice for that purpose. Although it has been widely used, the Chin's method gave inconsistent results for the interpreted failure load of MPG1 and MPG2, which was about 2500 kN and 5000 kN, respectively. Furthermore, Chin's method interpreted the failure load as 5000 kN for both MPG3 and MPG4. However, signs of failure were noticed during the loading tests at around 2100 kN at different levels of settlement. Therefore, numerical modeling was used to evaluate the pile group response of the incomplete load tests.



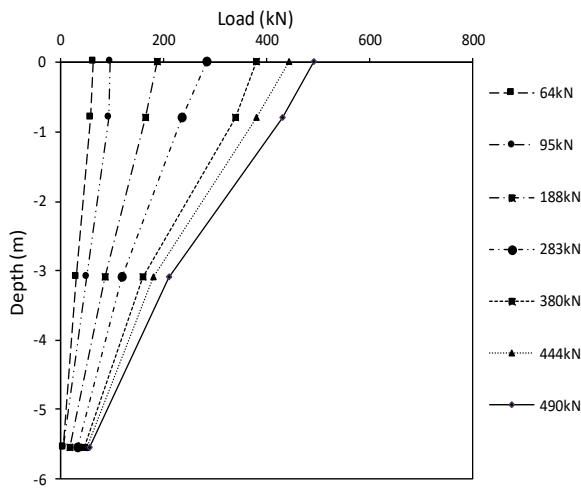
MP2



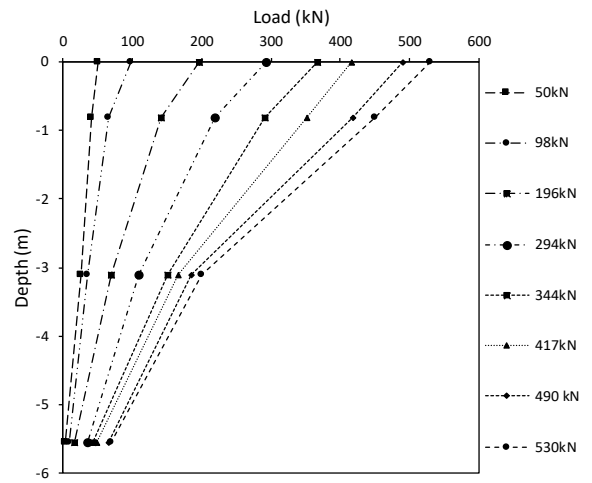
MP3



(MPG2-1)

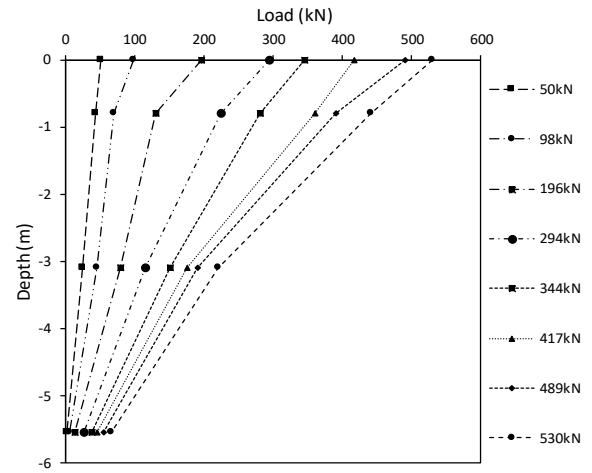
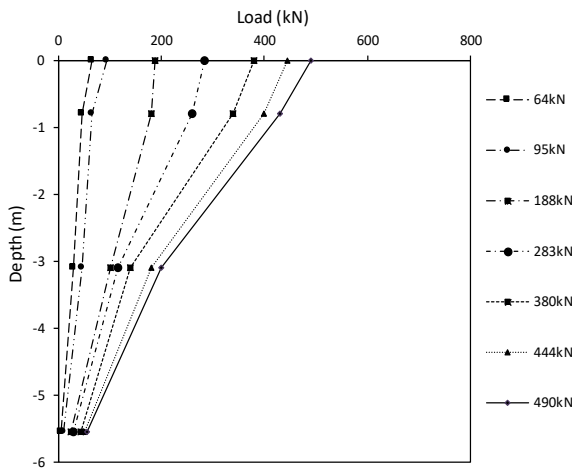


MPG3



MPG2-2

(MPG4)



(a)

(b)

**Figure 4-11 Load distribution along the micropile depth; single and groups: a)  $D_b/D_h = 2.25$ ; and b)  $D_b/D_h=3.0$**

**Table 4-7 Comparison between transferred load at different depths**

Elevation (m)	MP2 (Applied Load, kN)			MPG2-1/ MP2-2 (Applied Load, kN)			MP3 (Applied Load, kN)			MPG3 (Applied Load, kN)			MPG4 (Applied Load, kN)		
	285	425	605	285	425	605	245	417	530	245	417	530	245	417	530
-0.8	185	380	550	235/260	380/340	--	210	365	480	186	355	450	190	360	440
-3.1	121	150	215	120/115	180/183	--	85	147	192	95	166	200	90	176	220
-5.55	28	40	60	32/30	51/50	--	38	56	62	25	49	70	22	45	65

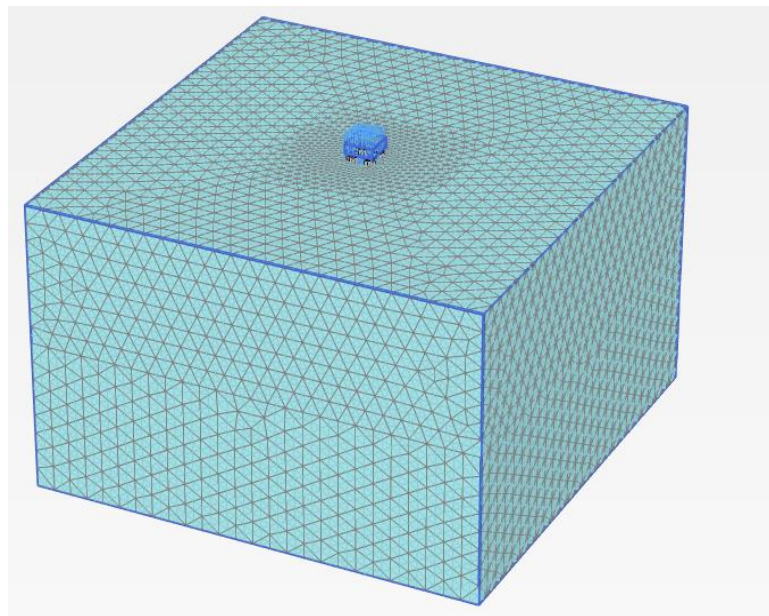
## **4.7 Numerical Modelling**

Numerical modeling can be used as a tool to extend the load test data to the anticipated failure load. This could be accomplished by developing a numerical model for the load test experiment, calibrated and verified with the available soil and pile load test data. This calibrated numerical model can then be used to conduct the test numerically until failure is attained.

### **4.7.1 3D Mesh Geometry**

The soil and pile, including all its components, were simulated in three-dimensional (3D) space. The geometry of the soil-pile model simulated the full-scale micropile test setups as close as possible. The 3D finite-element model was developed using PLAXIS 3D software and the model was calibrated using the field test results. The 3D mesh dimensions are selected to ensure that the boundaries are placed far enough from the test specimens so as not to affect the results. This was ascertained through a mesh sensitivity study. The locations of the boundaries were optimized by moving the boundaries until there is no noticeable change in the stresses at the boundaries. Based on the sensitivity analysis, the vertical boundaries were placed at distance  $8S$  measured from the center of the micropiles while the bottom boundaries were extended to a distance of two times the micropile length. The finite element model geometry and the devolved mesh are shown in Figure 12. The top boundary of the model was considered as a stress-free boundary while the translation of the bottom boundary was restrained in three directions X, Y and Z. The vertical boundaries of the soil block were set to move freely in the Z direction and constrained in the horizontal directions, X and Y.

The mesh was refined around the micropile circumference and the micropile base where non-linear behaviour was anticipated to reach the optimum solution and capture the system performance. As a result of the mesh refinements, the total number of model elements ranged from 141237 to 168385 and the average element size ranged from 0.153 to 0.173 m.



**Figure 4-12 Finite element model geometry**

## **4.7.2 Material Models**

### **4.7.2.1 Pile Material Model**

The micropiles were modeled using non-porous linear elastic volume elements. The linear elastic model, suitable for modeling stiff volumes in soil such as concrete elements (Brinkgreve et al., 2015), was used to simulate the structural micropile behaviour. It is

based on Hook's law of isotropic elasticity, which is defined in terms of the piles Young's modulus and Poisson's ratio. The Young's modulus was obtained from the applied load and strain readings of the strain gauges close to the ground surface (about -0.80 m). The micropiles cap was modeled using a linear elastic model and placed 20 cm above the ground so that there is no contact between the cap and beneath soil.

#### 4.7.2.2 Soil Material Model

The soil was modeled using 10-node tetrahedral elements utilizing the Hardening Soil model (HS). The tetrahedral elements have three degrees of freedom per node,  $u_x$ ,  $u_y$  and  $u_z$ , and provide a second-order interpolation of settlements. The soil behaviour is simulated using an elasto-plastic hardening soil model, which is incorporated in PLAXIS (Schanz and Vermeer, 1998). This model requires the following soil parameters: unit weight, ( $\gamma$ ), cohesion ( $c$ ), friction angle, ( $\phi$ ), dilation angle, ( $\psi$ ), Poisson's ratio ( $\nu$ ), triaxial loading stiffness,  $E_{50}^{ref}$ , the triaxial unloading stiffness,  $E_{ur}^{ref}$  and the oedometer loading stiffness,  $E_{oed}^{ref}$ .

The triaxial loading stiffness,  $E_{50}^{ref}$  was obtained by performing a drained triaxial test on sand samples under 100 kPa confining pressure, which is referred to as the reference stress for stiffness,  $p^{ref}$ . The triaxial unloading stiffness,  $E_{ur}^{ref}$  and the oedometer loading stiffness,  $E_{oed}^{ref}$  were calculated from (Brinkgreve et al., 2015):

$$E_{oed}^{ref} = \frac{2}{3} E_{50}^{ref} \quad (4.7)$$

$$E_{ur}^{ref} = 3E_{50}^{ref} \quad (4.8)$$

### 4.7.2.3 Soil - Micropile Interface Model

The soil-micropile interface was modeled using 12-noded interface elements (6 pairs of nodes); 6 nodes are connected to the 6 nodes of the soil element and 6 nodes are connected to the micropile element. They are numerically integrated using 6-point Gauss integration; the distance between a node pair is zero. Each node has three translational degree of freedom ( $u_x$ ,  $u_y$  and  $u_z$ ). The interface parameters are simulated using the shear strength properties of the surrounding soil and a strength reduction interface parameter,  $R_{int}$ , which is defined as a percentage of the shear strength of the soil. Table 4.8 summarizes the geotechnical parameters assigned to the hardening soil model for both soil and the soil-pile interface along with the linear elastic model parameters for micropiles.

### 4.7.3 Model Calibration and Verification

The soil properties utilized in the initial calibration were obtained from the site investigation, which included field boreholes, SPT, CPTu, and laboratory tests. The micropile material properties were back calculated from the strain gauges results. The initial properties of the soil obtained from the site investigation were employed initially as representative values in the numerical modelling. These initial values were adjusted slightly to calibrate the model by comparing the load-settlement curves obtained from the field load tests with the model prediction. The effective friction angle was selected as equal to  $42^\circ$  and the dilation angle obtained from the direct shear test was used  $10^\circ$ .

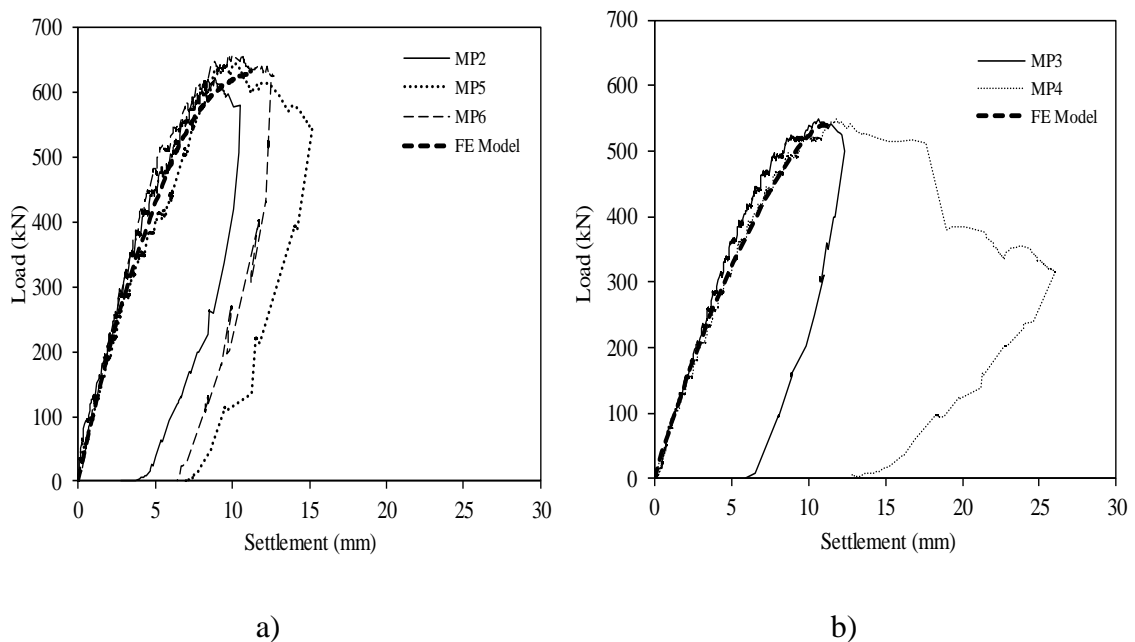
**Table 4-8 Geotechnical parameters used in FEM**

<b>Parameter</b>	<b>Unit</b>	<b>Soil</b>	<b>Soil -Pile Interface</b>	<b>Micropile</b>
<b>Constitutive model</b>	--	Hardening Soil	Hardening Soil	Linear Elastic
<b>Effective friction angle, <math>\varphi</math></b>	°	42	42	--
<b>Effective cohesion, c</b>	kN/m <sup>2</sup>	1	1	--
<b>Dilatancy angle, <math>\psi</math></b>	°	10	10	--
<b>Modulus of elasticity</b>	kN/m <sup>2</sup>	--	--	42e7
<b>Triaxial loading stiffness, <math>E_{50}^{ref}</math></b>	kN/m <sup>2</sup>	65e3	65e3	
<b>Triaxial unloading stiffness, <math>E_{ur}^{ref}</math></b>	kN/m <sup>2</sup>	43e3	43e3	--
<b>Oedometer loading stiffness, <math>E_{oed}^{ref}</math></b>	kN/m <sup>2</sup>	195e3	195e3	--
<b>Poisson's ratio (<math>\nu</math>)</b>	--	0.3	0.3	0.2
<b>Unit Weight (<math>\gamma_d</math>)</b>	kN/m <sup>3</sup>	19.5	19.5	24
<b>Interface reduction factor, <math>R_{int}</math></b>	--	--	0.90	--

An equivalent elastic modulus,  $E_p = 42 \times 10^7 \text{ kN/m}^2$  was used in the calibration process as a representative value for the non-porous linear elastic volume element. This value was obtained from the readings of the top strain gauges (close to the ground surface). The values of lateral earth pressure coefficient,  $K_s$ , were back figured from the frictional resistance of the micropile shafts. The back calculated values from the field load test results varied from 3.5 to 3.7.

The numerical modeling involved three main stages. Initially, geostatic stresses were applied to replicate the in-situ stresses. In the second stage, the volume of the pile was installed, and its properties were defined. In the third stage, the load was applied until failure occurred. In the numerical modeling calibration process, the coefficient of lateral earth pressure was varied to match the load – settlement curves. The coefficient of lateral earth pressure was found to be between 3.4 to 3.71, which gives a best match of the load-settlement curve to the field load test results. The developed model was initially calibrated using the load-settlement curves for single micropiles: MP2, MP5 and MP6 with diameter,  $D = 172 \text{ mm}$ . To verify the developed model, the calibrated model with the same parameters and boundary conditions was employed to analyze the load- settlement response for micropiles MP3 and MP4 with  $D = 132 \text{ mm}$ . The results obtained from the analysis are compared with the experimental observations in Figure 4.13.

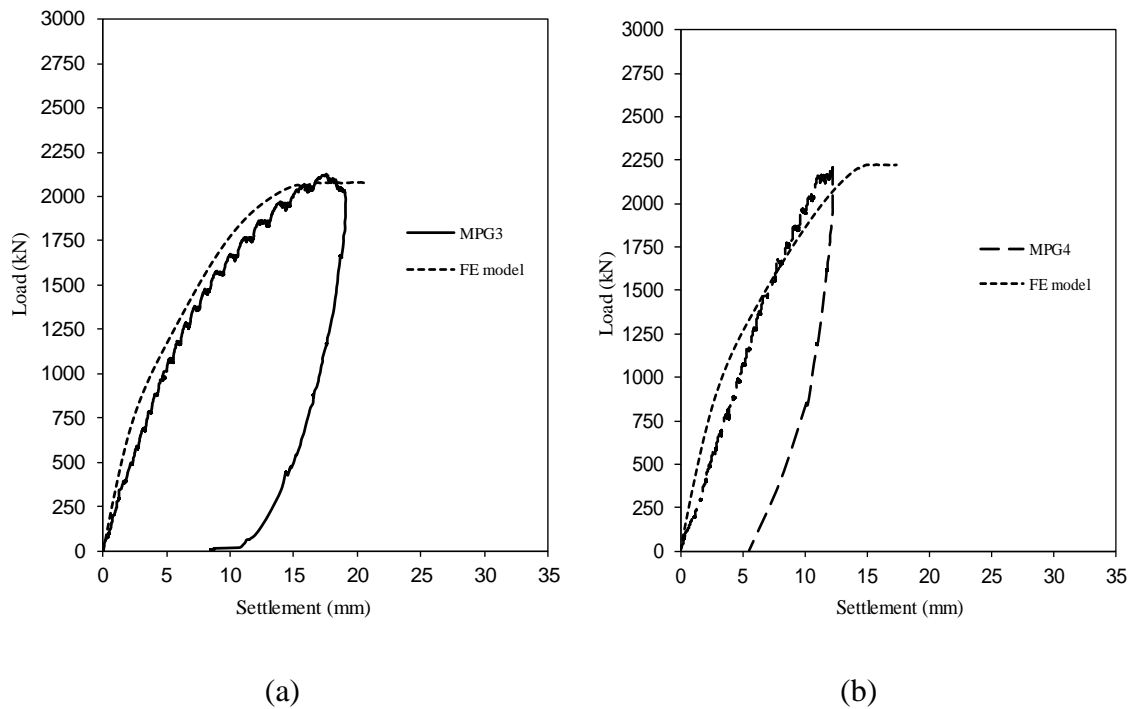




**Figure 4-13 (a) FE model calibration for micropiles with  $D_b/D_h=3$ ; and (b) model verification for micropiles with  $D_b/D_h=2.25$**

As can be noted from Figure 4.13, the calculated response agrees well with the field test results, which verifies the ability of the numerical model to predict the response of micropiles during axial load testing.

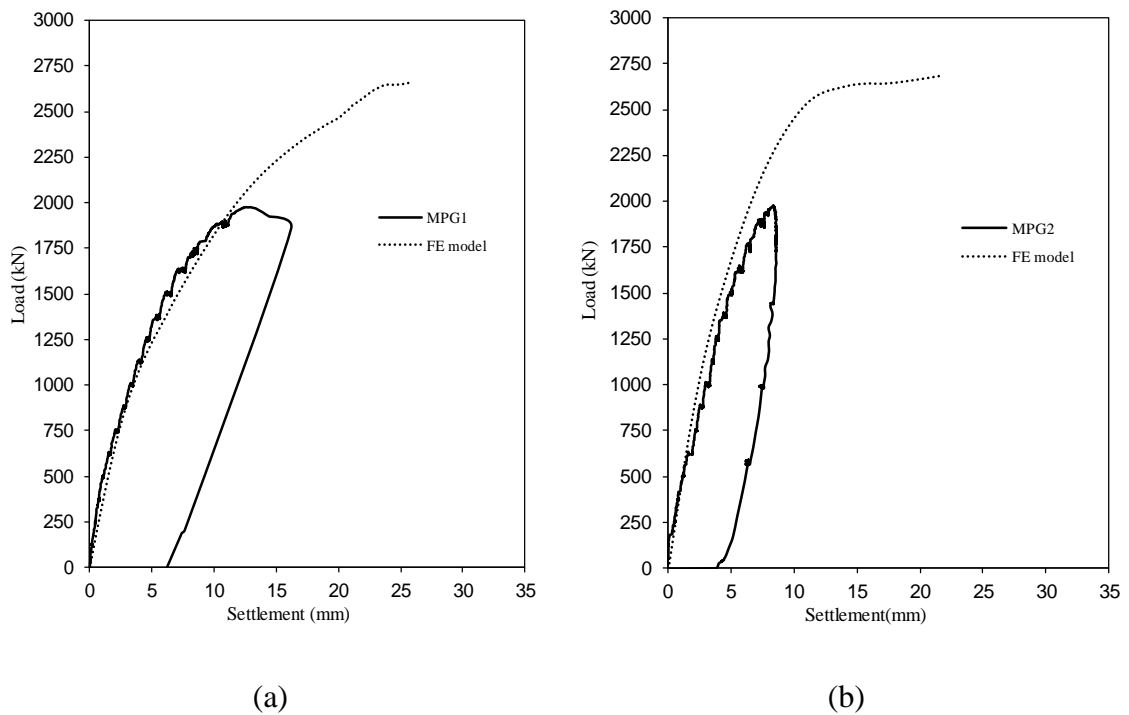
The same geotechnical parameters used in the analyses of the single micropile load tests were assigned to the micropile groups to calculate the load- settlement curves of the two groups, MPG3 and MPG4. The results are compared with those obtained from the field load tests in Figure 4.14. The calculated and measured responses agree well, which further verifies the ability of the numerical model to predict the response of micropile groups to axial loading. However, the numerical model predicts a slightly stiffer response during the initial part of loading. As can be noted from Figure 4.14, the calculated response extended the applied load until plunging failure was predicted to facilitate the evaluation of the group ultimate capacity.



**Figure 4-14 Comparison between Load-settlement curves for MPG1 and MPG2 field and FE model**

The same numerical model was then employed to analyze the response of micropile groups MPG1 and MPG2. Similar to the numerical modeling of groups MPG3 and MPG4, the loading was extended until plunging failure was predicted. The load - settlement curves obtained from the field loading tests for the MPG1 and MPG2 are plotted in Figure 4.15 along with the load - settlement curves obtained from the developed finite element model. In general, the predicted response is in good agreement with the measured response.

The calculated load - settlement curves of micropile groups can be utilized to establish their ultimate axial load capacity. The results of the FE model confirm that the group efficiency for the groups installed with  $s = 3D_b$  or  $5D_b$  is between 0.97 and 1.06.

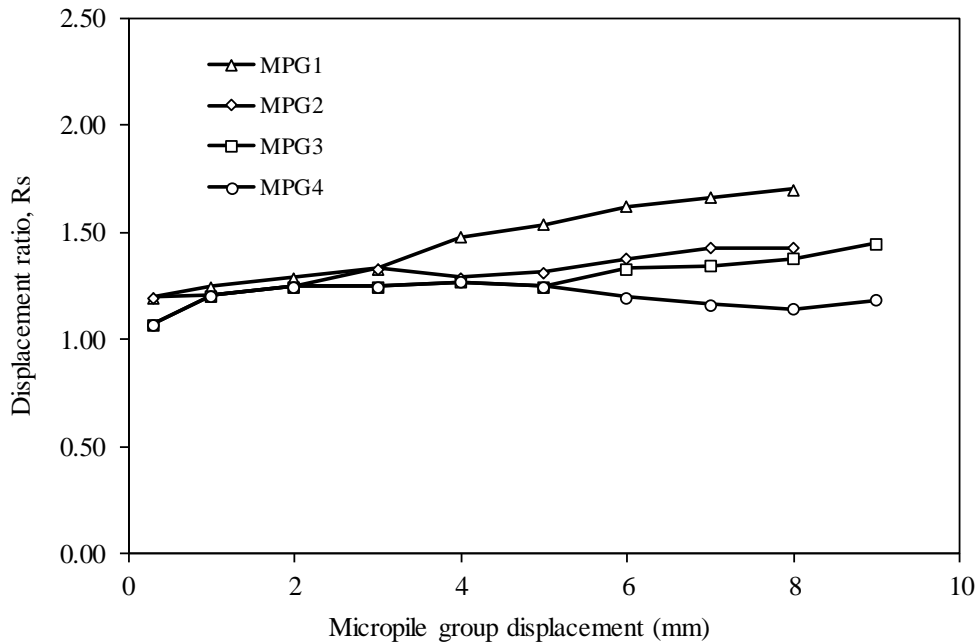


**Figure 4-15 Comparison between Load-settlement curves for MPG1 and MPG2 field and FE model**

## 4.8 Settlement Ratio

The design of pile groups installed in sand is generally controlled by the serviceability limit state (i.e. settlement) rather than the ultimate capacity. The group settlement ratio,  $R_s$ , (Poulos and Davis, 1980) is used to quantify the settlement of pile groups compared to single piles at the same average applied load. The settlement ratio at different levels of micropile group settlements are plotted in Figure 4.16. The group settlement ratio varied at a small group settlement and then increased with the increase in micropile group settlement. MPG1 and MPG3 with  $s = 3D_b$  displayed a higher group settlement ratio with increasing the applied load which indicates more interaction between the micropiles in groups with  $s = 3D_b$ . For micropile groups with  $s = 5D_b$  (MPG2 and MPG4), the group

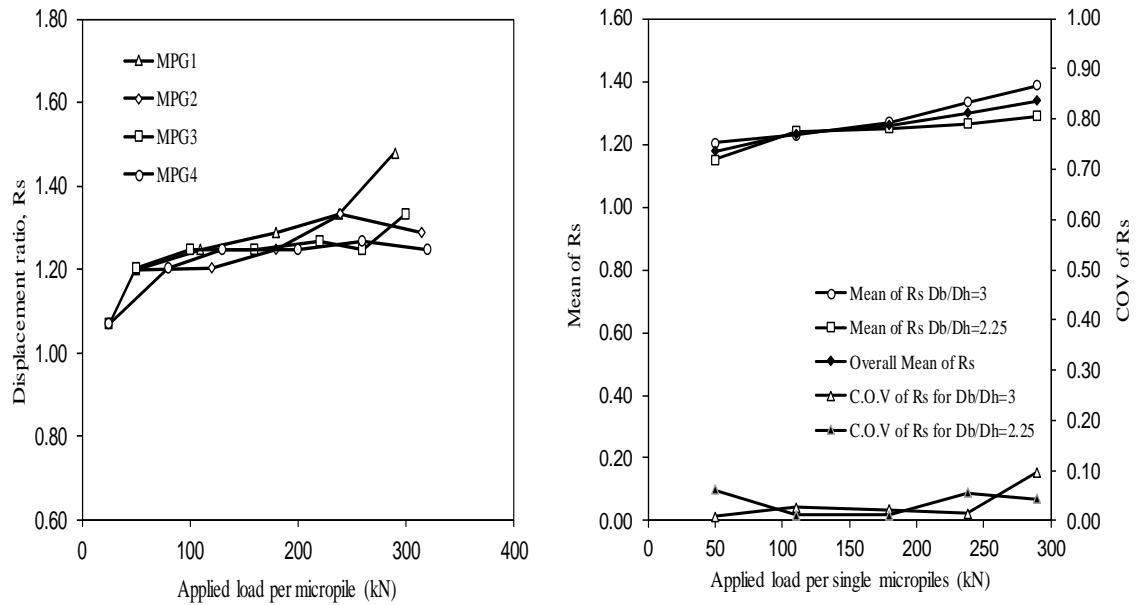
settlement ratio varied at small settlements and then decreased slightly with an increase in the total group settlement.



**Figure 4-16 Settlement ratio versus micropile group settlement**

For further investigation of the settlement ratio of micropile groups in dense soils, the group settlement ratio along with the mean and COV (Coefficient of variation) values of  $R_s$  versus the applied load per single micropile are plotted in Figure 4.17.

According to Mandolini and Viggiani (1997), the group interaction factor should be applied to the elastic settlement as the plastic portion of total settlement is not transmitted to the adjacent piles. At large applied loads, the response of a pile is dominated by nonlinear behaviour, which led to a lesser effect on the group interaction.



**Figure 4-17 Mean and COV of  $R_s$  of micropile groups with applied loads**

The group settlement ratio was considered up to the working load of about 300 kN per micropile, i.e., the linear portion of the load-settlement curves. The settlement ratio of MPG3 and MPG4 with drill bit/hollow bar diameters of 2.25 is 1.07 with a COV of 0.06 at small loads. Increasing the load to the working load resulted in a COV of 0.04 and settlement ratios of 1.25 and 1.33 for MPG3 and MPG4, respectively. At small loads for MPG1 and MPG2 with drill bit/hollow bar diameters equal to 3,  $R_s$  is almost 1 with a COV of 0.008. However, by increasing the applied load to the working load, the mean value of the settlement ratio became 1.39 with only a COV of 0.1. As it can be seen from Figure 4.17, the COV values of settlement ratio tend to decrease with increasing the applied load up to 200 kN, with only a small amount of variation within the considered range of loading. Table 4.9 compares the values of group settlement ratio obtained from this study with the empirical equations proposed by Vesic (1969) and Fleming et al. (1992).

The calculated values of settlement ratio showed in Table 4.9 are obtained for small loads (50 kN) and up to the working load (250 kN). By comparing the measured values of settlement ratio to the empirical correlations in Table 4.9, the proposed formulas did not give a good estimation for the settlement ratio. The value of settlement ratio depends on the number of piles in the group as well as the micropile diameter and the width of the group. This is indicated by the varying results of micropiles with varying diameters from 115 mm to 152 mm. The density of the sandy soil is another factor that can affect the group interaction. O'Neill (1983) recognized the influence of group geometry and soil type on the group settlement ratio based on full-scale tests results.

**Table 4-9 Comparison between empirical formulas for  $R_s$  with the measured values**

Method	Vesic (1969)		Fleming et al. (1992)		Measured Values	
Formula	$*R_s = \sqrt{\frac{B}{d}}$		$R_s = N^e$		Test date	
	3D	5D	Upper limit	Lower limit	$D_b/D_h = 2.25$	$D_b/D_h = 3$
Calculated values	2	2.45	1.74	2.30	1.25 - 1.33	1.29 - 1.48

\*B is the outer distance of the micropile groups

## 4.9 Conclusions

Full-scale loading tests were conducted on four groups of micropiles and six single micropiles to investigate the performance of micropile groups with the different drill bit/

hollow bar diameter ratios of 2.25 and 3, and two different common spacings between the micropiles in groups,  $s = 3D_b$  and  $5D_b$ . At least one micropile in each group was instrumented with three vibrating wire strain gauges to evaluate the force distribution along the micropile length. R51N Hollow bars with an OD of 51 mm and ID of 33 mm were installed with two different drill bit diameters,  $D_b = 115\text{mm}$  and  $152\text{ mm}$ . The total length of each micropile was 6.0 m with a 5.75 m embedded length. In addition to field load testing, a finite element analysis was conducted to complement the experimental results and further evaluate the micropile group axial capacity when the ultimate load was not reached. The following conclusions can be drawn from the obtained results:

- The micropile groups constructed with a drill bit/hollow bar diameter ratio,  $D_b /D_h = 3$  displayed a 50% stiffer response than the groups constructed with  $D_b /D_h = 2.25$ . In addition, groups constructed with  $D_b /D_h = 3$  displayed a 25% increase in capacity compared to groups constructed with  $D_b /D_h = 2.25$ . This demonstrates the benefit of using  $D_b /D_h = 3$  when larger a capacity or stiffer response is required.
- The group efficiency at both working load and interpreted failure load are close to unity; between 0.97 and 1.06 for dense sand soils for both a  $3D_b$  and  $5D_b$  center-to-center distance. This was confirmed by the results obtained from the finite element model.
- The mean value of group settlement ratio at working load for groups with  $D_b /D_h = 2.25$  was 1.29 while for groups with  $D_b /D_h = 3$ , the mean value of group settlement ratio was 1.39. The C.O.V of group settlement ratio for both cases was less than 0.10 at the working load.

- The ultimate skin friction values of grouted micropiles obtained from this study were slightly higher than the values suggested by FHWA (2005) for medium to very dense sand.
- The average toe resistance accounted for about 12% of the total resistance of micropiles. Ignoring the toe resistance contribution to the total micropile resistance may be conservative.
- For hollow bar micropile groups constructed with spacing,  $s \geq 3D_b$ , the group efficiency ratio can be taken as 1.0.



## 4.10 References

- AASHTO. (2012). *AASHTO LRFD Bridge Design Specifications*, Customary U.S. Units. The American Association of State Highway and Transportation Officials (AASHTO). Section 10.
- Abd Elaziz, A. Y., & El Naggar, M. H. (2012). Axial Behaviour of Hollow Bar Micropiles under Monotonic and Cyclic Loading. *Geotechnical Testing Journal*, 35(2), 249–260.
- Abd Elaziz, A. Y., & El Naggar, M. H. (2014). Geotechnical Capacity of Hollow-Bar Micropiles in Cohesive Soils. *Canadian Geotechnical Journal*, 51(10), 1123–1138.
- American Petroleum Institute (API). (2009). *Recommended Practice for Field Testing Water-Based Drilling Fluids*. API Recommended practice RP 13B-1.
- ASTM International (2013). *Standard Test Methods for Deep Foundations under Static Axial Compressive Load*. D1143/D1143M-07 (Reapproved 2013). American Society for Testing and Materials, West Conshohocken, Pa.
- Brinkgreve, R. B. J., Engin, E. & Swolfs, W. M. (2012). *Plaxis 3D 2011 Manual, 2012*.
- Bruce, D. A., Dimillio, A. F., & Juran, I. (1997). Micropiles: The State of Practice. Part1 Characteristics, Definitions and Classifications. *Ground Improvement*. Vol. 1(1). pp. 25-35.
- Bruce, D. A., Cadden, A. W., & Sabatini, P. J. (2005). Practical Advice for Foundation Design – Micropile for Structural Support. *Conference GeoFrontiers 2005. Contemporary Issues in Foundation Engineering* (GSp 131), ASCE, Austin, Texas: pp. 1-25.
- Cadden, A., Gomez, J., Bruce, D., & Armour, T. (2004). Micropiles: Recent Advances and Future Trends. In *Current practices and future trends in deep foundations*. Edited

by J.A. DiMaggio, and M.H. Hussein. *American Society of Civil Engineers*, Reston, Va., 140-165.

CCTG (1993). French code. *Technical Rules for the Design and Calculation of the Foundations of the Civil Engineering Works*. Fascicule 62, Titre V. CCTG.

CFEM. (2006). *Canadian Foundation Engineering Manual*. 4th edition, BiTech publishers Ltd. The Canadian Geotechnical Society.

Dai, G., Salgado, R., Gong, W., & Zhang, Y. (2012). Loads Tests on Full-Scale Bored Pile Groups. *Canadian Geotechnical Journal*, 49, pp 1293-1308

Davisson, M. T. (1972). High Capacity Piles. Proceedings, Soil Mechanics Lecture Series on Innovations in Foundation Construction, *American Society of Civil Engineers*, Illinois Section, Chicago. 81–112.

Drbe. O. E., & EL Naggar M. H. (2014). Axial Monotonic and Cyclic Compression Behaviour of Hollow Bar Micropiles. *Canadian Geotechnical Journal*. Vol. 52: pp. 426-441.

FHWA. (2005). *Micropiles design and construction*. Federal Highway Administration (FHWA), U.S. Department of Transportation, Washington, D.C. Publication No. FHWA-NHI-05-039.

FHWA. (2010). *Drilled Shafts: Construction Procedures and LRFD Design Methods*. Federal Highway Administration (FHWA), U.S. Department of Transportation, Washington, D.C. Publication No. FHWA-NHI-05-039.

FHWA. (2013). *Post - Tensioning Tendon Installation and Grouting Manual*. Federal Highway Administration (FHWA), U.S. Department of Transportation, Washington, D.C. Publication No. FHWA-NHI-13-026.

Feld, J. (1943). Discussion on Frictional Pile Foundation. *Transactions of the American Society of Civil Engineers*, Vol, 108, pp143-144.

- Frank, R. & Schlosser, F. (2009). Some Lessons Learnt from the 'FOREVER' French National Research Project on Micropiles. *In Proceedings of 9th International Society of Micropiles Workshop*, London, UK.
- Fleming, W.G.K., Weltman, A.J., Randolph, M.F. & Elson, W.K. (1992). *Pilling Engineering*. Wiley, New York.
- Fuller, F. M., & Hoy, H. E. (1970). Pile Load Tests Including Quick-Load Test Method Conventional Methods and Interpretations. *Highway Research Board (HRB)*, Issue 333, 78-86.
- Garg, K. G. (1979). Bored Pile Groups under Vertical Load in Sand. *Journal of Geotechnical Engineering*. ASCE, 105(8), 939–956.
- Han, J., & Ye, S.L. (2006). A Field Study on the Behavior of Micropiles in Clay under Compression or Tension. *Canadian Geotechnical Journal*, 43(1), 19-29.
- Ismael, N. F. (2001). Axial Load Tests on Bored Piles and Pile Groups in Cemented Sands. *Journal of Geotechnical and Geoenvironmental Engineering*, 127(9), 766–773.
- Juran, I., Bruce, D. A., Dimillio, A., & Benslimane, A. (1999). Micropiles: The State of Practice. Part II: Design of Single Micropiles and Groups and Networks of Micropiles. *Ground Improvement*, 3, 89-110.
- Kishida, H. (1967). Ultimate Bearing Capacity of Piles Driven into Loose Sand. *Soils and Foundation*, Japanese Geotechnical Society. Tokyo, VII (3), pp 20–29.
- Kulhawy, F. H., & Mayne, P. W. (1990). *Manual on Estimating Soil Properties for Foundation Design*. Research project No. 1493-6, EL-6800, Electric Power Research Institute., Palo Alto, Calif.
- Littlejohn, G. S., & Bruce, D. A. (1977). *Rock Anchors State-of-the-Art*. Foundation Publications Ltd., Brentwood, Essex, England, 50 pages.

- Mandolini, A., & Viggiani, C. (1997). Settlement of Piled Foundations. *Geotechnique*, 47(4), 791 –816.
- O'Neill, M. W. (1983). Group Action in Offshore Piles. *Proceedings, ASCE Conference of Geotechnical practice in offshore engineering*. Austin, Texas, pp. 25-64.
- Prakash, S. & Sharma, H.D. (1990). *Pile Foundations in Engineering Practice*. John Wiley and Sons, NY.
- Poulos, H. G., & Davis, E. H. (1980). *Pile Foundation Analysis and Design*. Wiley, New York.
- Reese, L. C., & O'Neil, M. W. (1988). *Drilled Shafts: Construction Procedures and Design Methods*. Federal Highway Administration, McLean, Va. FHWA-HI-88-042.
- Robertson, P. K. (1990). Soil Classification Using Cone Penetration Test. *Canadian Geotechnical Journal*. 27(1), 151-158.
- Rose, A.V. & Taylor, R. N. (2010). Modelling the Axial Capacity of Micropiles at Close Spacing. *In Proceedings of 10th International Society of Micropiles Workshop*. Washington, DC, USA.
- Rose, A.V., Taylor, R. N. & El Naggar, M. (2013). Numerical Modelling of PerimeterPile Groups in Clay. *Canadian Geotechnical Journal*, 50(3): 250-258.
- Skempton, A. W. (1953). Discussion: Piles and Pile Foundations. *Proceedings of, 3rd International Conference of Soil Mechanics and Foundation Engineering* ICSMFE, Zurich. Vol. 3, pp. 172.
- Skempton, A. W. (1959). Cast in Situ Bored Piles in London Clay. *Geotechnique*. 9, 4, 153-173.

- Timothy, M. J., Bean, J. J. & Bolton, M. K. (2012). MiniJET: A New Type of Micropile. *Proceedings, Grouting and Deep Mixing*. American Society of Civil Engineers (ASCE), New Orleans, Louisiana, 1095-1104.
- Terzaghi, K & Peck, R.B. (1948). *Soil Mechanics in Engineering Practice*. 1st Edition, Wiley, New York.
- Vesic, A.S. (1969) Experiment with Instrumented Pile Groups in Sand. Performance of deep foundations, *ASTM special technical publication*, No. 444, Pa., 172-222.
- Wolosick, R. J. & Scott, F. R. (2017) Loading Effects on Battered Micropiles Supporting Lateral and Compression Forces. The 9th Lizzi Lecture, *In Proceedings of 13th International Workshop on Micropiles*. Vancouver. Canada.
- Whitaker, T. (1957). Experiments with model piles in groups. *Géotechnique*, 7(4): 147-167

## CHAPTER 5

# 5 Lateral Performance of Single and Groups of Hollow Bar Micropiles in Cohesionless Soil.

---

## 5.1 Introduction

Micropiles can carry a considerable amount of axial load but only moderate lateral load due to their small diameter. The installation procedure of conventional micropiles involves two main steps: drilling and grouting. The construction technique of hollow bar micropile (HBMP) combines both steps, drilling and grouting, in one-step process, which facilitates fast installation, increased productivity and less soil disturbance. In addition, the high grouting pressure used in HBMP construction results in efficient load transfer mechanism. This has been well documented for HBMP installed in sand, however, its effect on the load transfer and micropiles response to lateral load need to be investigated.

Reese et al. (1975) performed lateral load tests on three pipe piles; two with 610 mm diameter and one with 152 mm diameter driven into stiff clay. Piles were subjected to monotonic and cyclic loads. The results were used to obtain  $p$ - $y$  curves and compared with computed  $p$ - $y$  curves. The results showed a good agreement between the measured and calculated  $p$ - $y$  curves. Brown et al. (1987) conducted full scale cyclic lateral load tests on single and pile group. The pile groups were arranged in 3 by 3 with a spacing between the piles equal to three times the pile diameter. The results showed that under the load equal to the average load per pile, the pile groups experienced a greater deflection than single pile. Brown et al. (1988) conducted a full scale two-way cyclic lateral load on single and pile

groups of steel pipe piles installed in dense sand compacted around the piles. It was concluded that the deflection in the pile group were greater than single pile under equal average load that was attributed mainly to the shadowing effect. Rollins et al. (2005a and b) conducted full-scale lateral load tests on single pile and pile group. The piles were driven into a loose to medium dense sand underlain by clay. The results showed a clear group interaction effects as the single piles showed a stiffer lateral resistance compared to the pile in the group. Also, it was shown that the lateral resistance in the pile group is a function of the pile location in the group.

Long et al. (2005) reported the results of lateral load tests on micropiles installed in medium-strength clay overlying sand. The micropiles were installed to 15.2 m depth and were reinforced with a high-strength threaded bar. The upper 9 m was stiffened by steel casing with 224 mm outer diameter and 13.8 mm wall thickness. The measured horizontal displacements were compared to the predicated values employing LPILE software. They concluded that the measured and predicated load-displacement curves agreed well. Anderson and Babalola (2014) conducted five lateral load tests to evaluate the impact of joints and casing embedment on micropiles behaviour in shallow rock. They concluded that micropiles embedded 0.6 m, 1.5 m and 3.0 m into rock were able to carry more than 180 kN lateral load. Kershaw and Luna (2014) performed load tests on six micropiles to investigate the effect of combined (i.e. axial and lateral) loading. The test micropiles were subjected to axial, lateral and combined loads. They concluded that the axial load has an insignificant effect on lateral performance of micropiles installed in stiff clay. Bruce and Janes (2014) reported the use of Case 2 micropile networks to support a steep temporary cut required for a tunnel construction. They claimed that using Case 2 micropile networks

saved a significant volume of excavation. On the other hand, Wolosick and Scott (2017) emphasized the need for reconsidering battered micropiles in USA after the Technical Council of Lifeline Earthquake Engineering recommendation in 1998 that discouraging the use of Batter piles at ports due to their poor performance during the past earthquakes.

Richards and Rothbauer (2004) compared the results of lateral load tests performed on micropiles installed as part of eight different projects to the methods recommended by NAVFAC and Characteristic Load Method (CLM). The test results were also compared to the response predicted by LPILE program. They concluded that the LPILE results were in reasonable agreement with the measured responses while CLM and NAVFAC methods significantly underestimated the response. They also reported that the soil properties along the top 2 to 5 m (10 to 15 micropile diameter) controlled the micropiles response.

Despite the rapid growth of HBMP construction fueled by advancement in hollow bar technology and bar size leading increased design axial capacity, a few studies were dedicated to evaluating their lateral performance. Abd Elaziz and El Nagggar (2015) studied the performance of HBMP under monotonic and cyclic lateral loads installed in stiff silty clay. The load test results were employed to calibrate a numerical model that was used to perform a parametric study. They concluded that the properties of soil along a depth of 10 times the HBMP diameter govern the load-displacement curve. They demonstrated the ability of HBMP to carry moderate lateral loads with appropriate reinforcement configuration and pile head fixity.

There is a high level of uncertainty in obtaining the lateral capacity of hollow bar micropiles compared to conventional piles due to several factors associated with the



construction method of hollow bar micropile such as the grouting pressure, type of soils and the drill bit/ hollow bar diameter ratio as they should be considered in the design of hollow bar micropiles under lateral loads. Given the scarcity of test data on lateral performance of hollow bar micropiles, there is a demonstrated need to evaluate the performance of laterally loaded single and groups of HBMPs installed in different ground conditions. In the current study, six full-scale HBMPs were installed in cohesionless soil and subjected to monotonic lateral load tests followed by applying cyclic lateral loads on four of the six micropiles. Additionally, five HBMPs were subjected to monotonic lateral loads to investigate the performance of micropiles after applying the cycling loads. Finally, a group of four HBMP was subjected to monotonic lateral loading to evaluate the group effect on the lateral response.

## **5.2 Geotechnical Site Characterization**

An extensive site investigation was carried out at the test site in Ayr, Ontario, Canada. Three boreholes were drilled to various depths using hollow stem auger (130 mm in diameter), followed by standard penetration tests (SPT). Samples were extracted from the borings using the split spoon sampling method and transported to the laboratory for further testing. BH1 and BH2 that were conducted close to the test area indicated that the first 200 mm consisted of granular base fill with some gravel and recycled asphalt overlaying layers of brown medium dense to dense sand and silty sand up to 11 m depth. Seams of silt and silty clay were observed at different levels. The SPT blow count (N value) along the top 6 m varied between 15 and 35 with an average of 21, and increased substantially beyond 6 m below the ground surface as shown in Table 5.1. The ground water table elevation varied between 9.5 to 10.5 m below the ground surface.

**Table 5-1 Boreholes logs and N values**


<b>Borehole</b>	<b>Depth (m)</b>	<b>Overburden stress (kPa)</b>	<b>Overburden stress correct factor (<math>C_n</math>)</b>	<b>N (blows/30cm)</b>	<b><math>N_{1,60}</math></b>
<b>1</b>	1	19.6	1.5	27	41.4
	1.8	34.3	1.3	23	30.9
	2.6	51.0	1.2	23	27.9
	3.2	62.8	1.1	21	24.0
	4	78.5	1.1	23	24.6
	4.8	94.2	1	29	29.2
	6.4	125.6	0.9	51	46.5
	8	157.0	0.8	21	17.6
	9.4	184.4	0.8	36	28.2
	10.9	213.9	0.7	31	22.8
	12.5	245.3	0.7	59	40.6
	14	276.8	0.6	75	50
15.4	306.2	0.6	200	50	
<b>2</b>	1	19.6	1.5	16	24.5
	1.8	34.3	1.3	15	20.2
	2.6	51.0	1.2	25	30.3
	3.2	62.8	1.1	15	17.2
	4.0	78.5	1.0	36	38.5
	4.8	94.2	0.9	21	21.2
	6.4	125.6	0.8	35	31.9
	8.0	157.0	0.8	48	40.2
9.4	184.4	0.7	46	36.0	

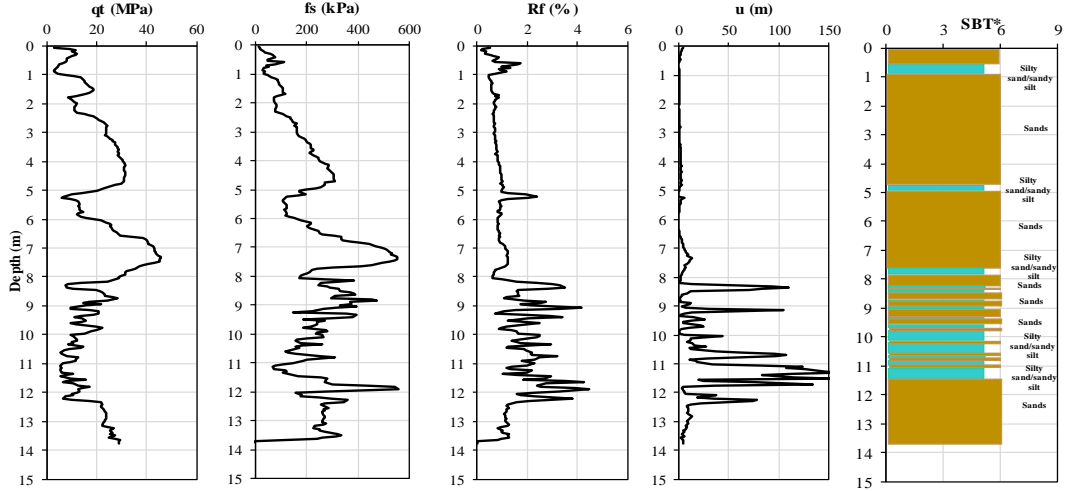
\* N is blow count to advance standard spit spoon sampler 30 cm with a 63.5 hammer.

\*\* Increasing values of N over 50, of overburden soils, do not substantially differentiate reliable soil strength and are normalized to a value of 50 for  $N_{1,60}$ .

Four CPT soundings were performed across the site. The results of the CPT1 and CPT2 soundings conducted within the test area are shown in Figure 5.1 along with the soil behaviour type according to the classification chart proposed by Robertson (1990). The average cone resistance corrected to pore water pressure ( $q_t$ ) ranged from 10 to 30 MPa in the upper 6.5m and 30 to 45 MPa from 6.5m to 8m followed by a decrease in ( $q_t$ ) with an average of 20 MPa. The soil behaviour type indicated that the soil is mainly sand with some seams of silt and sandy silt. The relative density,  $D_r$ , of sand was obtained using the correlations proposed by Kulhawy and Mayne (1990) based on SPT and CPT data, which indicated that the sand is mainly medium dense to dense.

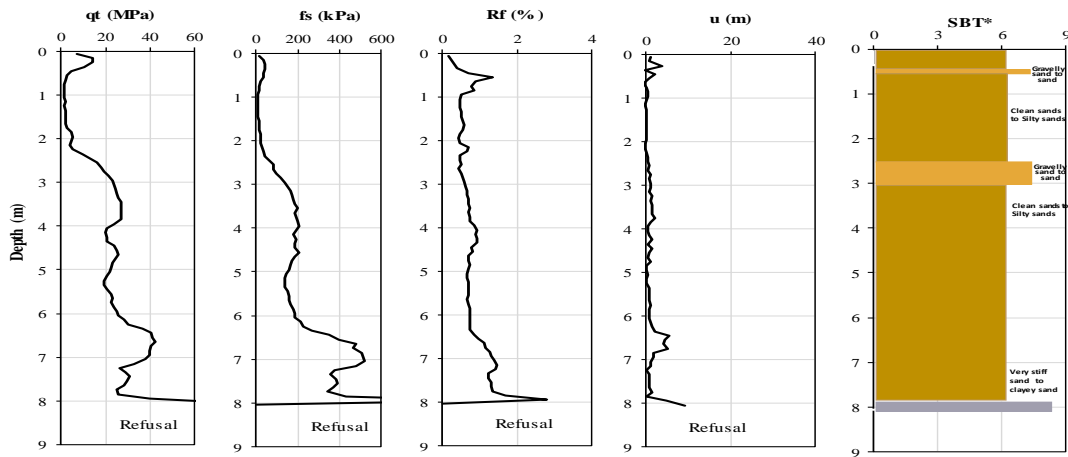
The peak angle of internal friction,  $\phi$ , was obtained from direct shear tests conducted on samples retrieved at different elevations and reconstituted to the same in-situ  $D_r$ . In addition,  $\phi$  was correlated to measured cone tip resistance,  $q_{t1}$ , using relationship proposed by Kulhawy and Mayne (1990); the average value of the peak angle of internal friction was found to be  $42^\circ$ . BH3 and CPT3 and CPT4 provided similar soil profile and same range of soil properties. The sieve analysis has shown that the soil along the piles is primarily fine sand as shown in Figure 5.2.

<b>Project:</b>	Micropiles Project		<b>Date:</b>	13/07/2015	<b>Max Depth:</b>	13.75 m
<b>Sounding:</b>	1		<b>Weather:</b>	Sunny	<b>Depth Inc:</b>	0.050 m
<b>Location:</b>	Ayr, Ontario		<b>G.W. Depth:</b>	9.0 m	<b>AVG Int :</b>	0.10 m



(a)

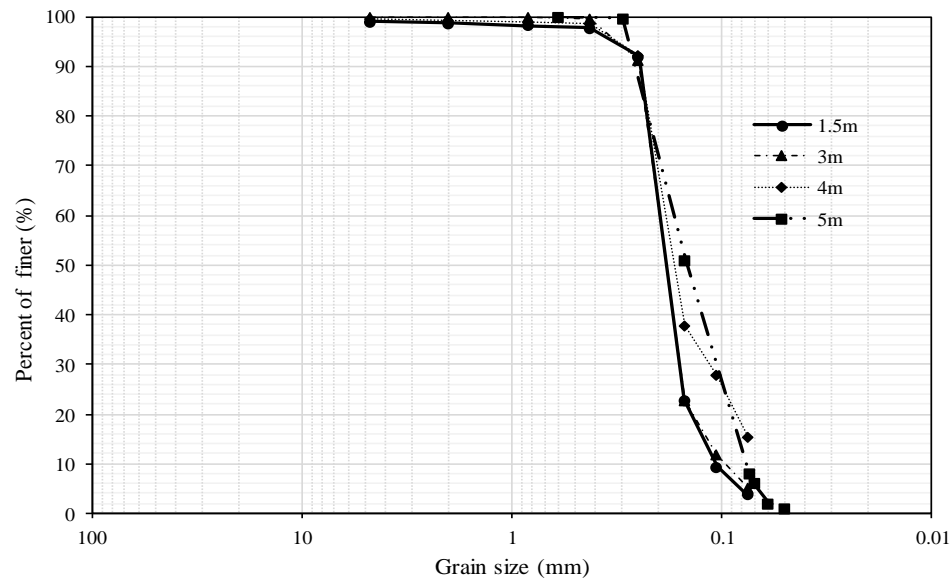
<b>Project:</b>	Micropiles Project		<b>Date:</b>	13/07/2015	<b>Max Depth:</b>	8.10 m
<b>Sounding:</b>	2		<b>Weather:</b>	Sunny	<b>Depth Inc:</b>	0.050 m
<b>Location:</b>	Ayr, Ontario		<b>G.W. Depth:</b>		<b>AVG Int :</b>	0.10 m



\* SBT: Robertson, 1990

(b)

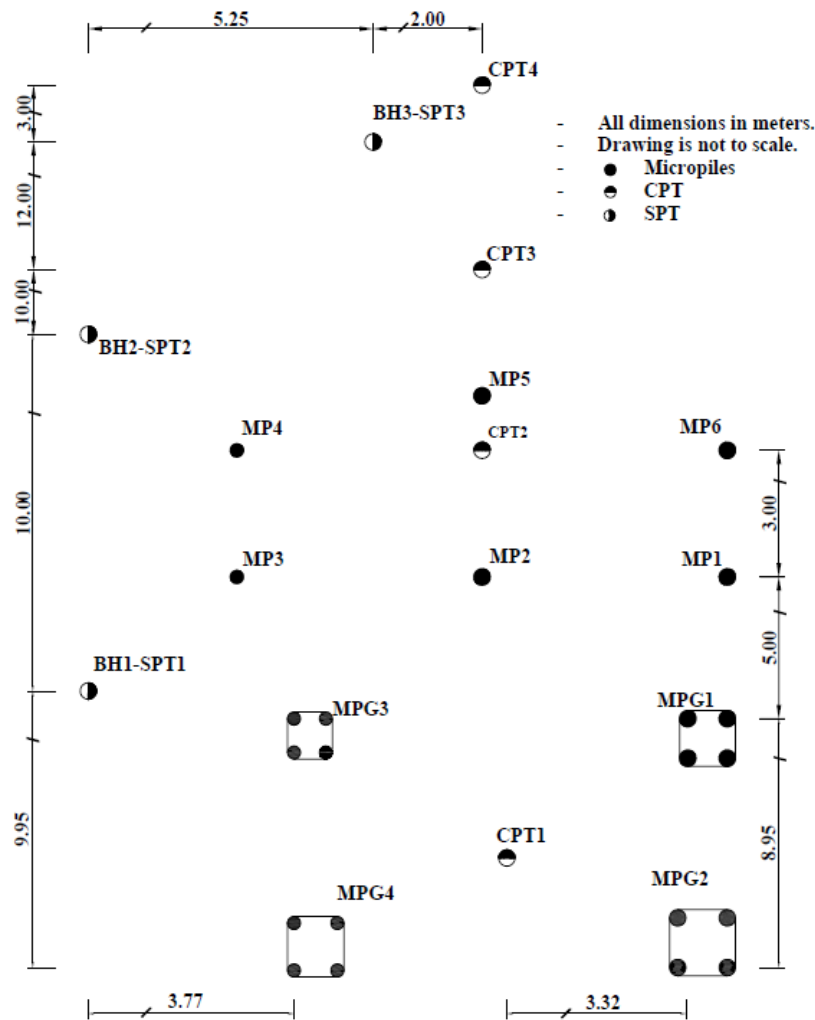
Figure 5-1 CPT soundings with SBT: a) CPT1; b) CPT2



**Figure 5-2 Grain size distribution of soil at test site**

### 5.3 Installation of Micropiles

Six hollow bar micropiles (MP1 to MP6) were constructed and tested in this study. The hollow bars utilized were R51N with 51 mm outer diameter and 33 mm inner diameter. Given the site granular soil, Tungsten carbide cross cut drill bits were employed for the HBMPs construction. Figure 5.3 presents a plan view of the test site showing the locations and distances between micropiles, as well as the locations of the boreholes and CPT soundings. Four HBMPs (MP1, MP2, MP5 and MP6) were installed with a 152 mm drill bit diameter resulting in diameter ratio of drill bit/ hollow bar ( $D_b/D_h=3$ ), and two (MP3 and MP4) were installed with 115 mm drill bit diameter (i.e.  $D_b/D_h=2.25$ ). The size of the larger drill bit was selected considering the hollow bar-grout and grout ground interface strengths.



**Figure 5-3 Plan view of micropiles locations along with boreholes and CPT soundings locations.**

After attaching the drill bit to the hollow bar into the required position, rotary percussive drilling started simultaneously with a grout-flushing technique. The drilling and grouting operations were performed as a single operation, which reduced the time of construction and ensured good bonding between the grout and ground. Grout with a specific gravity of 1.4 - 1.5 was employed as drilling fluid to install the hollow bars in place. As the hollow bars used were 3m long, once the first length (3.0 m) was installed, the drilling was stopped

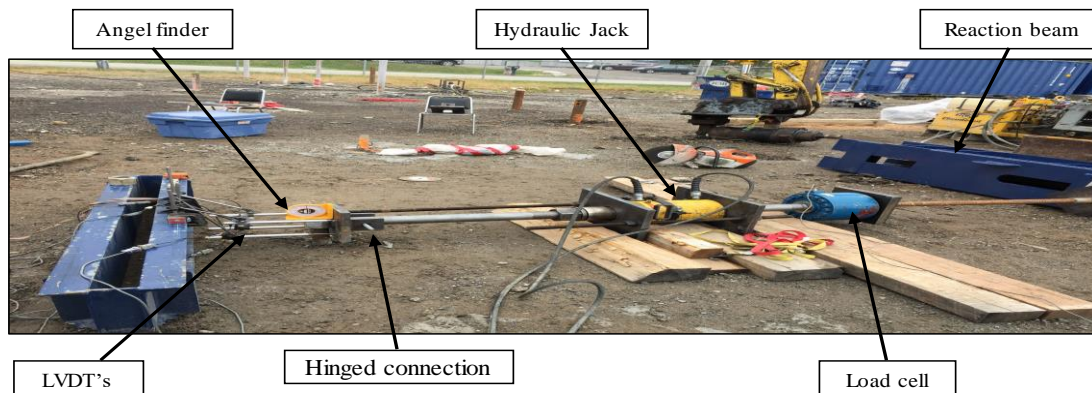
to allow for adding the second segment; the two bars were attached using a coupler 200 mm long. The drilling was continued until the required depth was reached then the final competent structure grout was pumped under a pressure of between 0.8 to 1 MPa to displace the drilling grout. The final grout had specific gravity between 1.80 and 1.95, which is in compliance with (FHWA 2005) recommendation for micropile application. The total length of each micropile was 6m with 5.75m embedded length.

The structural (neat) grout mix was designed with water to cement ratio,  $w/c = 0.45$ , in order to provide high strength, while being pumpable with minimum bleeding. FHWA (2013) required the grout compressive strength to be 21 MPa for 7 days and 35 MPa at 28 days for post-tensioning tendons for bridges. Grout cylinders were collected during the installation process using a cylindrical mold of 100 mm by 200mm and 75 mm by 150mm. All specimens were de-moulded after 24 hours then placed in a control room with a relative humidity of 100% and constant temperature of 23°C. The cylinders were tested after 28 days to determine compressive strength, indirect tensile strength and static modulus of elasticity. The compressive strength was determined according to ASTM C39 and the tensile strength was obtained in according to ASTM C496. The average compressive strength after 28 days was 40 MPa and the average split tensile strength was 3.97 MPa.

In order to explore the potential improvement in lateral response of HBMP utilizing fibre-reinforced grouts, MP6 was constructed using structural grout reinforced with micro-steel fibers of 1% dosage. The reinforced grout was added manually to the top 2 m of the micropile and the drilling machine was rotated in order to help redistribute the fibers evenly within the grout. Details of steel fibres and reinforced grout are given in AbdIbrahim and El Naggar (2015).

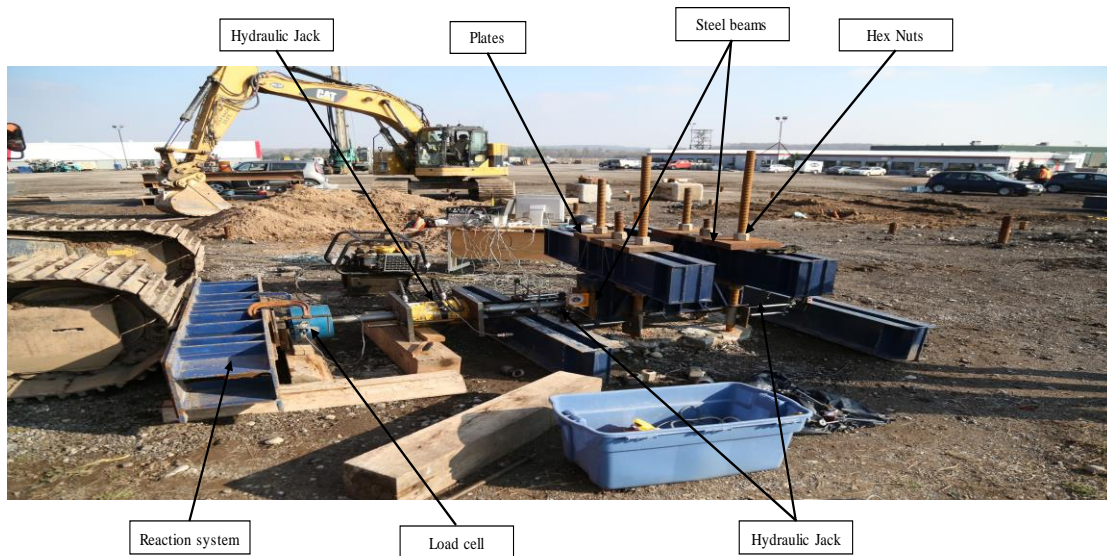
## 5.4 Test Setup, Instrumentation and Loading Procedures

A special test setup was designed and manufactured to facilitate applying both monotonic and cyclic loads to single micropiles as shown in Figure 5.4a. A reaction frame was used to support the loading system, which consisted of steel rod threaded to the load cell from one end and attached to the micropile head using hinged connection to apply the lateral load with zero moment. The load frame was designed to be rigid in comparison with the micropile stiffness. A square steel plate of 250x250x30 mm was welded to a hex nut (ID 51 mm) and threaded to the hollow bar head to facilitate applying the lateral loads to the micropile head. The load was applied through a hollow cylinder hydraulic jack with a capacity of 900 kN and recorded via a load cell capacity 900 kN. Four HLP190 (hybrid Linear Potentiometers) were attached to the steel plate in square arrangement to measure the lateral deflection for single micropiles and six HLP190 were used to measure the group deflection, one on each micropile and two were attached to the connection beam. The load cell and the LVDT's were connected to a data logger to acquire the reading every one second.



(a)





(b)

**Figure 5-4 Load test setup: a) Single micropiles; and b) Micropiles group**

Four foil strain gauges were attached to each micropile to measure the strain at different level and then use the measured data to obtain the  $p$ - $y$  curves. Unfortunately, due to the harsh installation procedure of HBMP on the strain gauges and to the pretesting program (Compression and pullout tests) on the micropiles, no foil strain gauge survived. The four micropiles comprising group MPG4 were installed with center-to-center spacing of 5 D (where D micropile diameter = 132 mm). The heads of the test micropiles were attached to three steel beams that were connected together using steel plates on top and bottom of the beams and secured with hex nuts as shown in Fig. 5.4 b. The three steel beams formed a pile cap connecting the four micropiles.

The testing program encompassed three phases of loading for the single micropiles: Phase 1, six HBMPs (MP1 to MP6) were subjected to monotonic lateral loads; Phase 2, four HBMPs (MP2, MP4, MP5 and MP6) were subjected to cyclic lateral load tests; Phase 3,

five HBMPs (MP1, MP2, MP3, MP5 and MP6) were subjected to monotonic lateral loading. All single micropiles were loaded monotonically in equal increments of 3 kN, each increment was maintained for 5 minutes. The cyclic loading involved five one-way load cycles at each load increment of 3 kN increment. The time for each load cycle was about 30 seconds. The effect of applying five cycles on the monotonic lateral performance of HBMPs was evaluated by subjecting five micropiles (MP1, MP2, MP3, MP5 and MP6) to another round of monotonic lateral loads. In order to investigate the group effect of HBMPs, the micropiles group was subjected to monotonic lateral loading only. The same monotonic loading scheme utilized for single micropiles was used for the micropiles group but with equal increments of 10 kN, and the load was applied through the main beam at 150 mm above the ground surface. Table 5.2 presents the main stages of lateral load tests performed in this study.

**Table 5-2 Testing stages and loading sequences**

Stages	Type of test					
	MP1	MP2	MP3	MP4	MP5	MP6
<b>1<sup>st</sup> stage</b>	ML	ML	ML	ML	ML	ML
<b>2<sup>nd</sup> stage</b>	--	CL	--	CL	CL	CL
<b>3<sup>rd</sup> stage</b>	ML	ML	ML	--	ML	ML

ML, monotonic lateral test and CL, cyclic lateral test

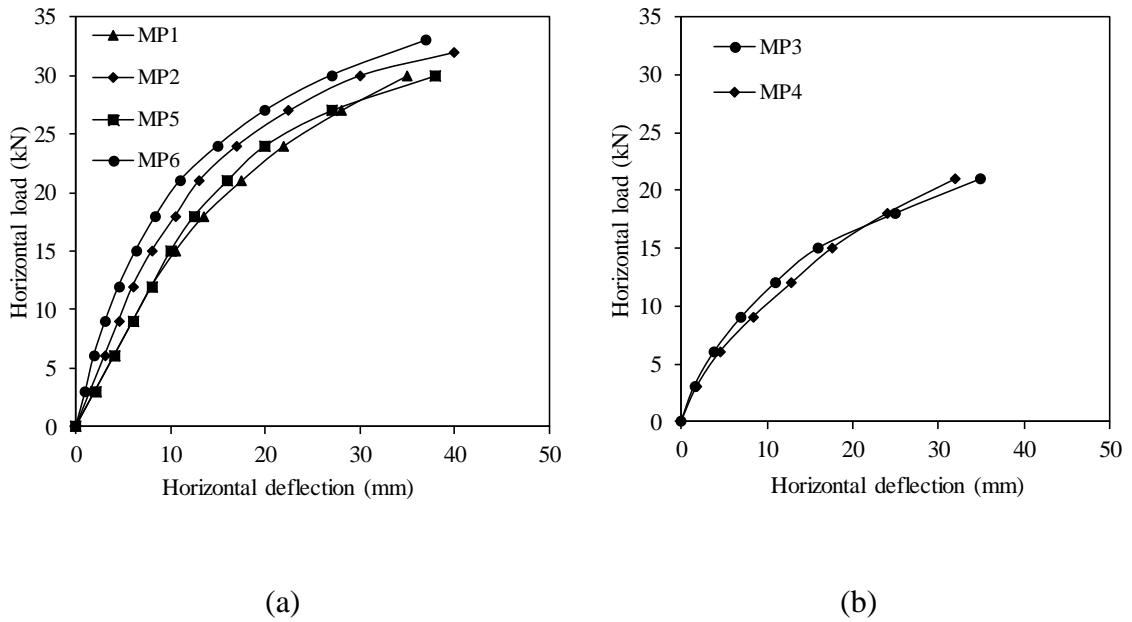
## 5.5 Test Results and Analysis

### 5.5.1 Monotonic Load – Deflection Curves for Single Micropiles

Figures 5.5a and 5.5b present the load– deflection curves for micropiles with  $D_b/D_h=3$  and  $D_b/D_h=2.25$ , respectively. It is noted from Fig. 5 that the load-deflection curves exhibited three main regions: linear elastic response up to a deflection of about 5 to 7% of the micropiles diameter; followed by a non-linear region that extended to a deflection of 20 - 25 mm; and a final linear region that extended to the test termination.

Two different mechanisms can define the pile failure: short pile behavior, which involves yielding of surrounding soil along the pile length; and long pile behavior, which involves yielding of the pile materials when the maximum applied moment reaches the moment capacity of the pile section. Bierschwale et al. (1981) defined the pile rigidity in terms of its slenderness ratio, and hence the potential failure mechanism; pile with slenderness ratio less than 6 is considered short pile, while a pile with slenderness ratio greater than 20 is considered to be long.

The micropiles tested in this study had slenderness ratio of 44, and accordingly are considered long piles. Tomlinson and Woodward (2008) and Viggiani et al. (2012) adopted the stiffness factor  $T$  and characteristic length  $\lambda$  to categorize the rigidity of the pile, i.e.



**Figure 5-5 Load – deflection curves; a)  $D_b/D_h=3$  and b)  $D_b/D_h=2.25$**

$$T = \sqrt[5]{\frac{EI}{n_h}} \quad \text{where } k = n_h \frac{x}{B} \quad (5.1)$$

$$\lambda = \sqrt[4]{\frac{4 E_p J}{k_h d}} \quad \text{for } k_h \text{ constant with depth} \quad (5.2)$$

$$\lambda = \sqrt[5]{\frac{E_p J}{n_h}} \quad \text{for } k_h = n_h \frac{z}{d} \quad (5.3)$$

Considering all the above criteria, the micropile is considered as a flexible pile due to the large slenderness ratio.

Several interpretation criteria of ultimate lateral capacity of piles are presented in the literature. Five criteria are considered in this paper: three are based on absolute displacement limits, including McNulty (1956), Walker and Cox (1966), New York City (1981); and two are based on specified displacement as a function of pile diameter, i.e.,

Pyke (1984) and Briaud (1984). Table 5.3 summarizes the ultimate lateral capacities obtained by using the above-mentioned methods. It should be noted that the micropiles were exhumed after testing and the measured average diameter was found to be 171 and 132 mm for the large and small drill bits (i.e. 115% and 112.5% of the drill bit diameter).

**Table 5-3 Interpreted ultimate lateral capacity of micropiles**

Method	Definition of failure load	Failure load (kN)					
		$D_b/D_h = 3$				$D_b/D_h = 2.25$	
		MP1	MP2	MP5	MP6	MP3	MP4
<b>McNulty (1956)</b>	Load at 6.25 mm head displacement	9	12	9.2	15.2	8.2	7.5
<b>Walker and Cox (1966)</b>	Load at 13.0 mm head displacement	17.5	21	18.5	22.5	13.5	12
<b>New York City (1981)</b>	Load at 25.0 mm head displacement	25.5	27	26	29	18	18.5
<b>Pyke (1984)</b>	Load at 5% the shaft diameter	13	16	13	19	9.5	8.5
<b>Briaud (1984)</b>	Load at 10% the shaft diameter	20.5	24	22	25.2	14.5	13.8

The results will be evaluated herein considering the load that causes 25 mm deflection at the micropile head as the ultimate load and the load that causes 6.25 mm as the design load. The two criteria were selected to present the pure elastic deflection and the end of the nonlinear region in case of 6.25 mm and 25 mm, respectively. The average ultimate load for micropiles with  $D_b/D_h = 3$  is 26.8 kN. The average ultimate load for micropiles with  $D_b/D_h = 2.25$  is 18.25 kN. These results indicate that increasing  $D_b/D_h$  from 2.25 to 3

improved the ultimate lateral load of the micropiles by about 47%. Correspondingly, the average stiffness of HBMPs with  $D_b/D_h = 3$  was 1912 kN/m, while the average stiffness of HBMPs with  $D_b/D_h = 2.25$  was 1183 kN/m. This indicates an increase in the HBMP stiffness by 61% due to increasing  $D_b/D_h$  from 2.25 to 3. It is also noted from Figure 5.5 that MP6 provided the stiffest response and the largest ultimate lateral resistance because of the fibre reinforced grout used in its construction. Adding steel fibers to the grout mix increased the grout elastic modulus, the pile flexural rigidity and its bending moment capacity (Abdlrahem and El Naggar, 2015). This improved the lateral resistance of the micropile.

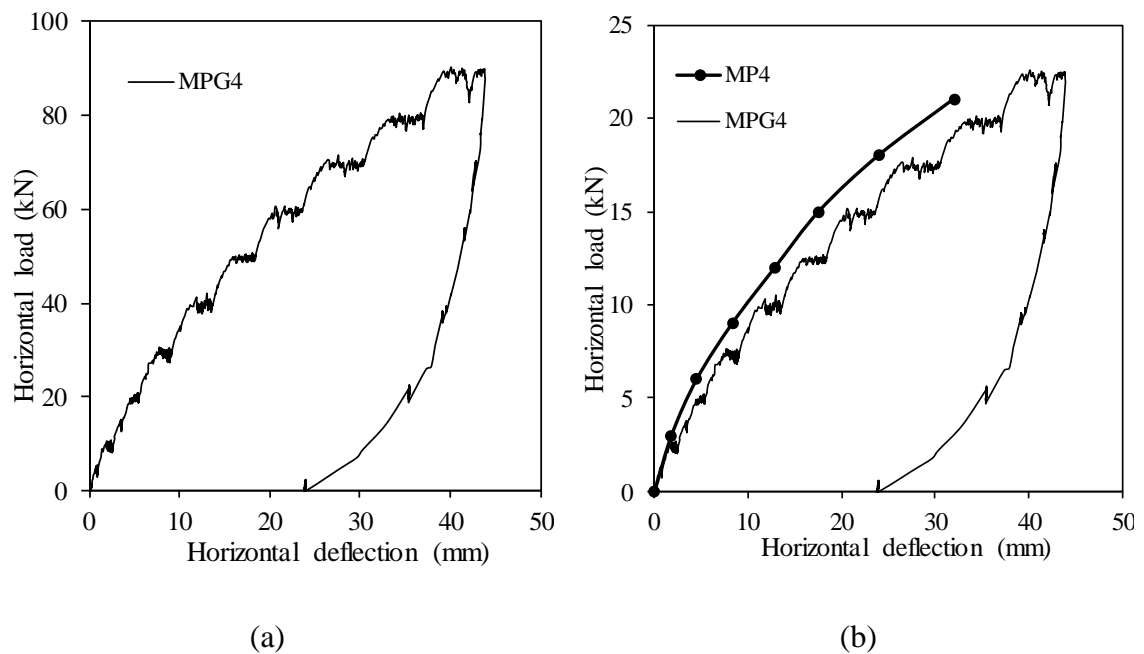
Table 5-3 shows that the failure lateral load interpretation can vary dramatically based on the utilized failure criteria. For example, using McNulty's (1956) criteria the average lateral load failure for micropiles with  $D_b/D_h=3$  is about 10 kN while utilizing Briaud's (1984) criteria, the lateral failure load is 21.1 kN. In this comparable case, the difference in the interpreted failure load is more than 100%. Generally, it is not recommended to utilize a failure criterion that related a hollow bar micropile diameter to the failure load due to the uncertainty of the increase in the micropile diameter during installation. However, in this case, the interpreted failure load at 10% of the measured shaft diameter is close to the criteria that interpreted the failure load as the load at 25 mm head displacement.

### **5.5.2 Monotonic Load – Deflection Curve for Micropile Group.**

The load - deflection curve for micropile group MPG4 is shown in Figure 5.6. For comparison purpose, the load versus deflection for single micropile MP4 was plotted in

Figure 5.6 b. As it can be noted from Figure 5.6, the response of single micropile is stiffer than the response of the micropile group.

At the same lateral load per pile, the group experienced higher displacement than the single micropile due to the group effect. Considering the 25 mm deflection as an ultimate lateral load criterion, the group efficiency for micropile groups with spacing equal to five diameters is 89%. McVay et al. (1995) reported results, as he calculated group efficiency of 93% for piles installed in cohesionless soil at spacing equal to five pile diameters.



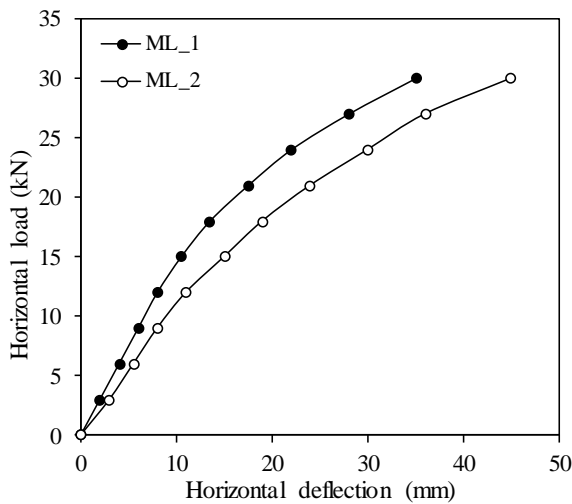
**Figure 5-6 Load – deflection curves: a) Micropile groups MPG4 and b) Comparison with single micropile**

### 5.5.3 Cyclic Load-Deflection Curves for Single Micropiles.

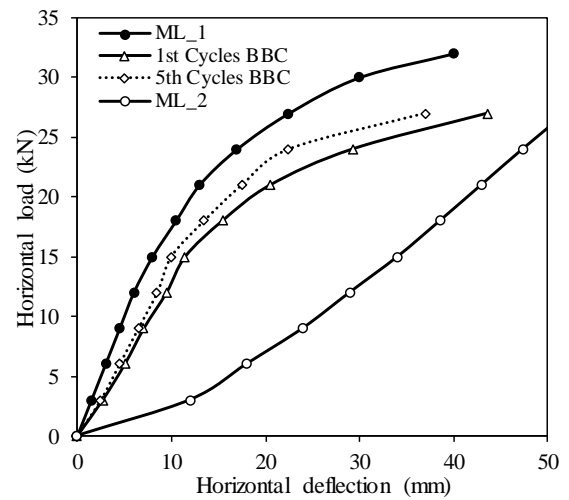
As described previously, four HBMPs (MP2, MP4, MP5 and MP6) were subjected to cyclic loading that comprised five cycles of one-way loading at each load increment of 3 kN. In addition, the effect of applying five cycles on the monotonic lateral performance of

HBMPs was evaluated by subjecting five micropiles (MP1, MP2, MP3, MP5 and MP6) to another round of monotonic lateral loads. Four HBMPs (MP2, MP4, MP5 and MP6) were subjected to cyclic loading (i.e. Phase 2) that comprised five cycles of one-way loading at each load increment of 3 kN, then three of micropiles (MP2, MP5 and MP6) were subjected to a repeated monotonic lateral loading in Phase 3. Figure 5.7 shows the load - deflection curves for the three loading stages that includes the load - deflection curves for the first stage of monotonic lateral loading and the back-bone curves for the first and last cycles of lateral cyclic tests to illustrate the effect of applying five cyclic at each load steps on the performance of micropiles.

a. MP1

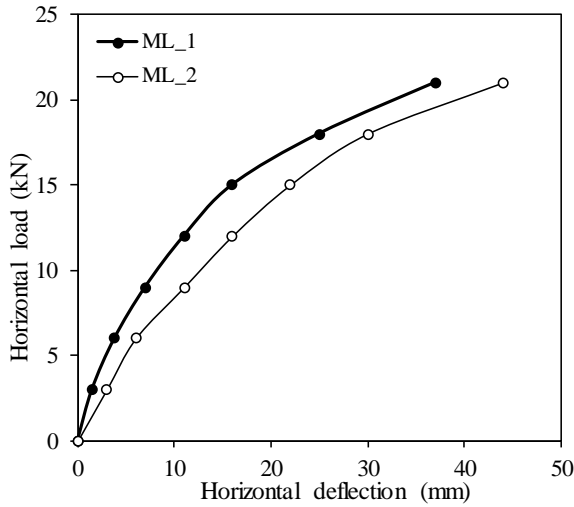


b. MP2

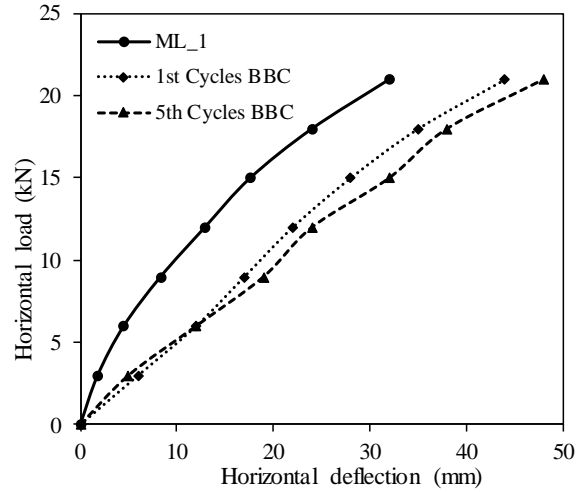




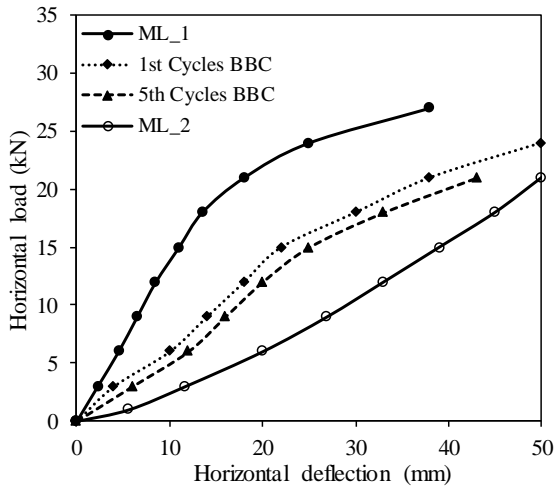
c. MP3



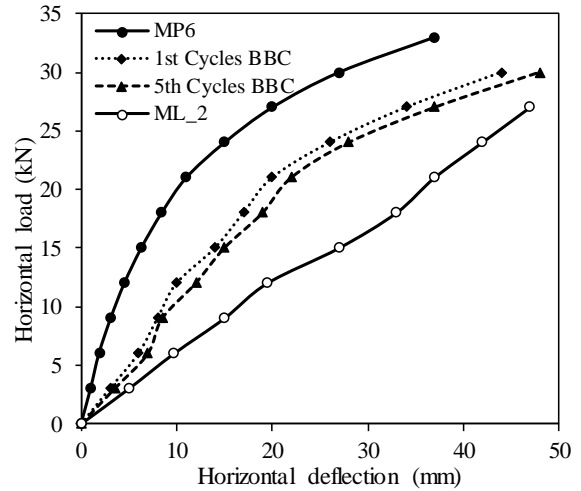
d. MP4



e. MP5



f. MP6



**Figure 5-7 Load – deflection curves for lateral monotonic and cycle tests.**

Moreover, the load - deflection curves for micropiles retested under monotonic lateral loads in the third stage are also shown in Figure 5.7. It can be noted from Figure 5.7 that the lateral stiffness decreased dramatically for micropiles MP2, MP5 and MP6 that were

subjected to cyclic loading prior to the second monotonic loading, whereas the stiffness for micropiles MP1 and MP3 decreased slightly because they were not subjected to cyclic loading in the second phase which shows the effect of applying five cycles on the micropile performance. The degradation of the lateral stiffness is more obvious at larger deflection, similar to observations made by Matlock (1970).

Field observations demonstrated that HBMBs exhibited local failure during cyclic loading, which was manifested in radial cracks and separation between the hollow steel bar and the surrounding grout as shown in Figure 5.8. This failure mechanism due to cyclic loading has affected the micropiles response in the third loading stage as it was clearly demonstrated in cases of micropiles MP2, MP5 and MP6.



**Figure 5-8 Local failure mechanism due to cyclic loading**

To examine the stiffness degradation of micropiles due to cyclic loading, the lateral stiffness for each cycle was calculated from:

$$K = \left[ \frac{P_{max} - P_{min}}{\Delta_{max} - \Delta_{min}} \right] \quad (5.4)$$

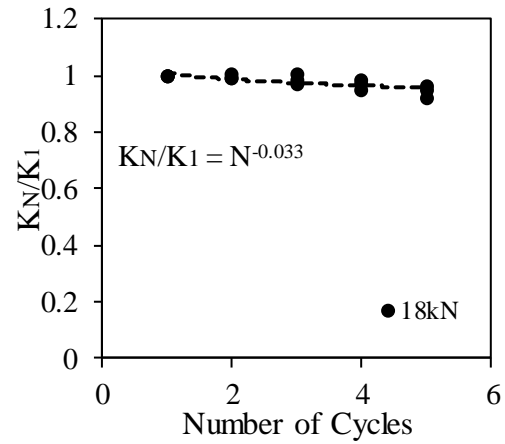
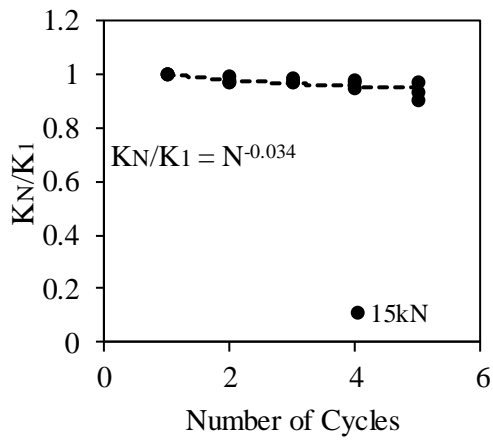
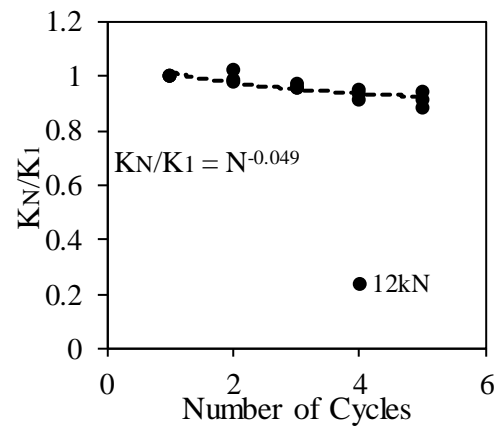
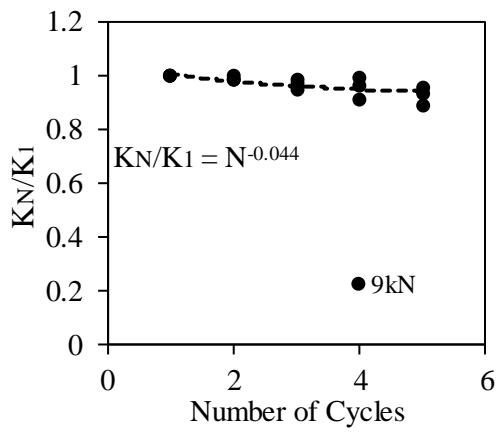
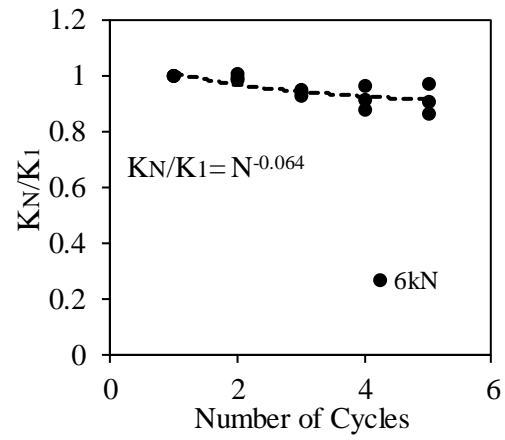
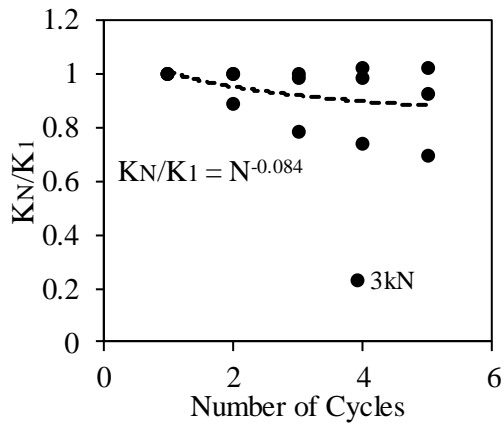
where  $P_{max}$  &  $P_{min}$  are the maximum and minimum applied loads for each cycle, respectively, while  $\Delta_{max}$  &  $\Delta_{min}$  are the maximum and minimum lateral deflections for each cycle, respectively.

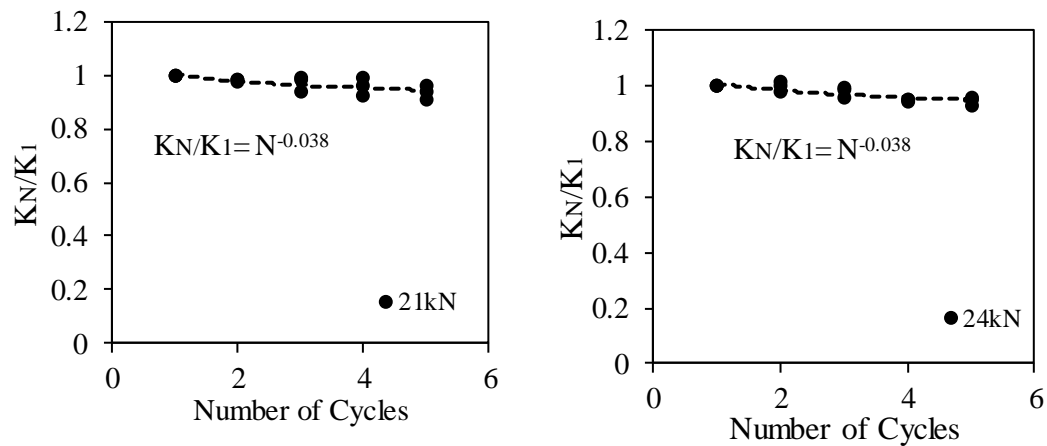
The change in the stiffness for each cycle may be presented by the stiffness ratio  $K/K_i$ , where  $K_i$  is the initial stiffness. Little and Briaud (1988) related the degradation of pile head stiffness to the number of applied cycles by a degradation parameter,  $t$ , i.e.

$$\left( \frac{K_{hN}}{K_{h1}} \right) = N^{-t} \quad (5.5)$$

Where  $K_{hN}$  and  $K_{h1}$  are the stiffness values for 1 and N cycles, respectively and  $a$  is the degradation parameter and usually donated in the literature as  $t$ .

The normalized micropile head stiffness versus the number of loading cycles along with the best fitting curves are plotted in Figure 5.9. Based on the best fitting curves of measured results, the degradation parameter  $t$  varies from 0.084 to 0.033 and from 0.062 to 0.031 for micropiles with  $D_b/D_h = 3$  and  $D_b/D_h = 2.25$ , respectively. The degradation parameter  $t$  reaches the peak value at the first few cycles and then decreases with increasing the number of cycles and the load amplitude.

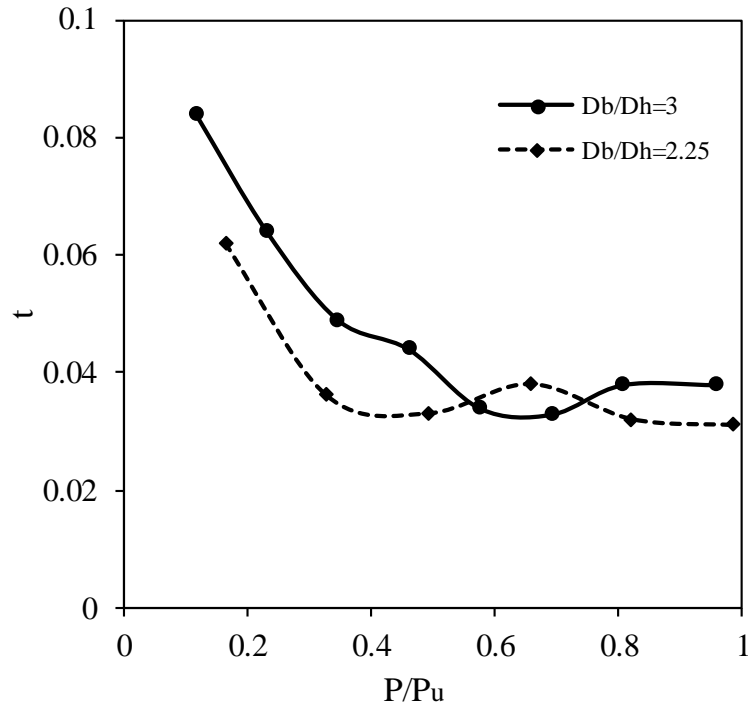




**Figure 5-9 . Normalized micropile head stiffness versus number of cycles for micropiles with  $D_b/D_h=3$ .**

Long and Vanneste (1994) reported the results of 34 cyclic load tests, the value of the degradation parameter for one-way cyclic loading ranged between 0.52 and 0.00 with an average near 0.22. They noticed that the effect of cyclic loading was more noticeable at the first cycle of loading and as the cycling continued the effect of cycles weakened.

The degradation parameter,  $t$ , versus the stress level  $P/P_u$ , where  $P$  is the applied load and the  $P_u$  is the ultimate lateral resistance which was selected as the load corresponding to 25 mm lateral deflection are plotted in Figure 5.9. As it can be seen from Figure 5.9, the degradation parameter decreases with increasing the stress levels then it plateaued.



**Figure 5-10 Degradation parameter at different stress levels for micropiles with  $D_b/D_h=3$  and 2.25**

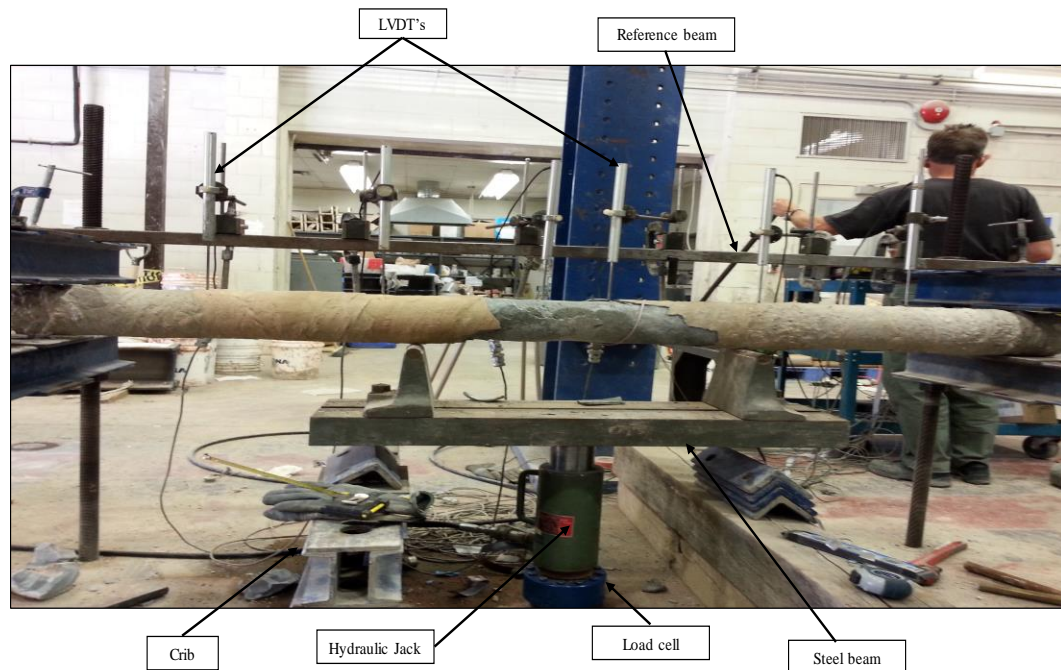
#### 5.5.4 Pure Bending Tests

Two single micropiles MP3 and MP5 were carefully pulled out from the soil after the load testing was completed in order to measure the actual diameter along the micropiles. The average diameter of micropiles with drill bit 115 and 152 mm were found to be 132 and 171 mm, respectively, i.e. the diameter increased by 14.8% and 12.5% over the diameter of the drill bit. Figure 5.11 shows the exhumed micropile (MP3) and the diameter measurement along its length. MP3 was taken to the structural lab and pure bending test was performed.



**Figure 5-11 Exhumed micropile MP3 and diameter measurement along the depth**

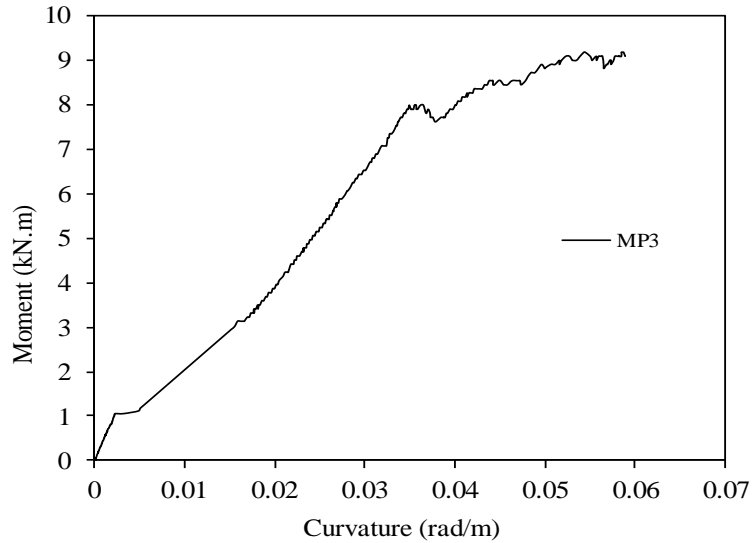
The exhumed micropile was subjected to four- point pure bending test to establish the actual moment curvature curve, which will be used later to establish a numerical model for the analysis of the micropiles to lateral loading. The four- point setup is shown in Figure 5.12. The total length was divided to three equal spans and the load was applied at the one third and two thirds of the total length. Six LVDT's were utilized to measure the deflection along the micropile length. Two of the LVDT's were installed around the half distance of the specimen where the large deflection was anticipated. The load was applied in very slow manner using a hydraulic jack with 250 kN capacity and a maximum stroke of 152.4 mm. The applied load was measured using a load cell with a capacity of 220 kN. All the LVDT's and the load cell were connected to a data acquisition system to record the readings every second.



**Figure 5-12 Pure bending test on the exhumed micropile MP3**

The deflection along the micropile was obtained via the LVDT's readings, and curve fitting was used to extract the deflection along the micropile prior to start the double-differentiation process. The curve was fitted using quadratic function and the double-differentiation process was utilized to convert the deflection to curvature. The moment - curvature curve obtained using the above-mentioned procedure is plotted in Figure 5.13. The ultimate bending moment and the corresponding curvature are 9.1 kN.m and 0.058 rad/m, respectively.





**Figure 5-13 Moment-Curvature curve for the exhumed micropile MP3**

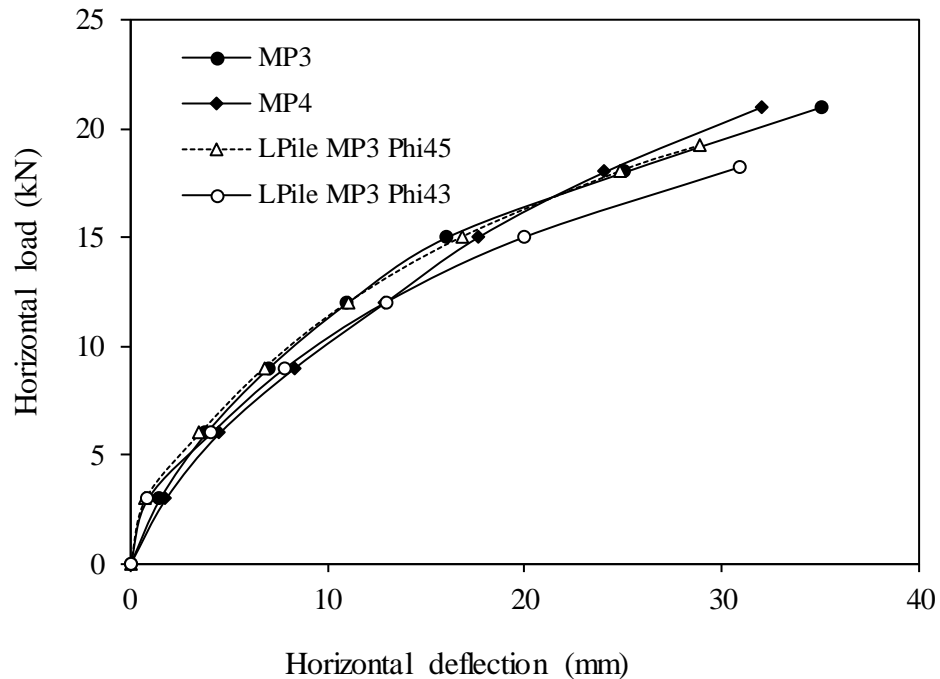
## 5.6 Numerical Modeling

LPile is a special purpose computer program that can be utilized to analyze the response of a pile under lateral loading. The program incorporates the  $p$ - $y$  method and can be used to compute deflection, shear, bending moment and nonlinear soil response (Wang and Isenhower, 2012). The  $p$ - $y$  method is based on the modification of the beam-on-Winkler foundation approach in which the soil is simulated by nonlinear Winkler-type springs. Using this method, the pile deflection can be calculated as function of the lateral load applied at the pile head. The  $p$ - $y$  approach is widely used to examine the serviceability of the piles under lateral loading.

The nonlinear bending properties and associated curves extracted from pure bending tests can be employed in the LPile software to simulate the nonlinear flexural behavior of the micropiles. The bending moment versus bending curvature curve shown in Figure 5.13 was incorporated in LPile along with the actual micropile diameter. To simulate the nonlinear

lateral soil resistance, LPile offers 14 different internal  $p$ - $y$  curves for different soil conditions. The soil resistance was simulated using the Sand model (Reese) with effective unit weight,  $\gamma'=19.5$  kN/m<sup>3</sup> and angle of internal friction  $\phi'=43^\circ$ .

Figure 5.14 compares the load - deflection curves of field test results of micropiles with  $D_b/D_h=2.25$  and the load-deflection curves obtained from LPile. As it can be noticed from Figure 5.14, the calculated response is stiffer than the measured response at small deflection. However, the response becomes softer than the measured values at higher deflection. Increasing the angle of internal friction  $\phi'$  from  $43^\circ$  to  $45^\circ$ , it improved the response of calculated load - deflection curve at higher deflection, resulting in good agreement with the measured response as can be seen in Figure 5.14.



**Figure 5-14 Comparison between load -deflection curves for micropiles MP3 and MP4 with LPile results**

To simulate the results of micropiles with  $D_b/D_h=3$ , LPILE model was created for micropiles with  $D_b/D_h=2.25$  and validated by comparing the outcome results with the actual response of micropiles.

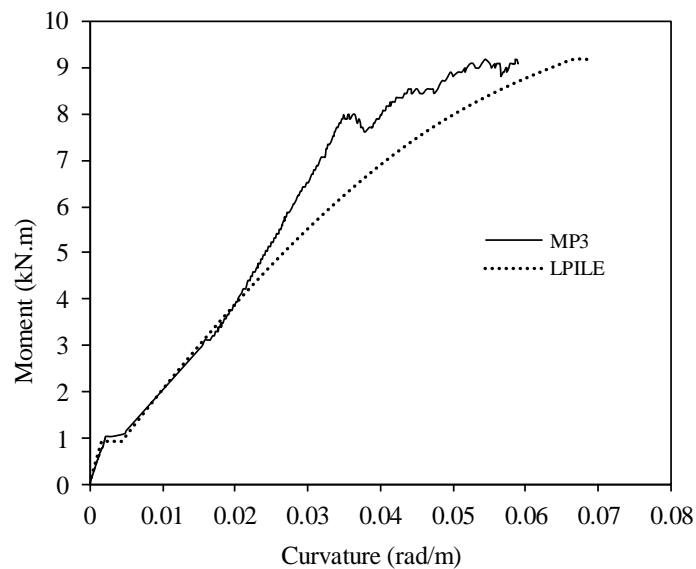
LPILE program does not incorporate a built-in cross-section that represents a hollow bar surrounded by grout with no permanent casing. In order to overcome this issue, a round shaft with a permanent casing and hollow core was selected. The permanent casing wall thickness was set equal to zero as the hollow bar micropile installs with no casing. Abd Elaziz and El Naggar (2015) used the same technique to model the hollow bar micropile embedded in cohesive soil, which provided good results.

Table 5.4 summarizes the material properties of the grout and the steel employed in the analysis. The nonlinearity of soil-pile system response to lateral loading is attributed to two main factors; the nonlinearity of the pile materials under loading, which was accounted for in this study by extracting the actual bending moment-curvature of the micropile section; and the second factor is the nonlinearity of the surrounding soil. As the strain gauges did not work properly, it was not possible to extract the p-y curves from the test results.

**Table 5-4 Material properties used in LPILE**

Type of material	Young's modulus, E (kPa)	Yield stress, $f_y$ (kPa)	Compressive strength, $f'_c$ (kPa)
Steel	$200 \times 10^6$	$600 \times 10^3$	--
Grout	$27 \times 10^6$	--	$40 \times 10^3$

Consequently, the Sand model available in the LPILE library was employed in the analysis to simulate the soil behaviour. The soil effective unit weight,  $\gamma' = 19.5 \text{ kN/m}^3$  and angle of internal friction  $\phi' = 45^\circ$  were used in the soil. The moment-curvature curves obtained from LPILE model and the exhumed MP3 are compared in Figure 5.15, which shows that the measured moment-curvature curve and that predicted by LPILE model are in good agreement.

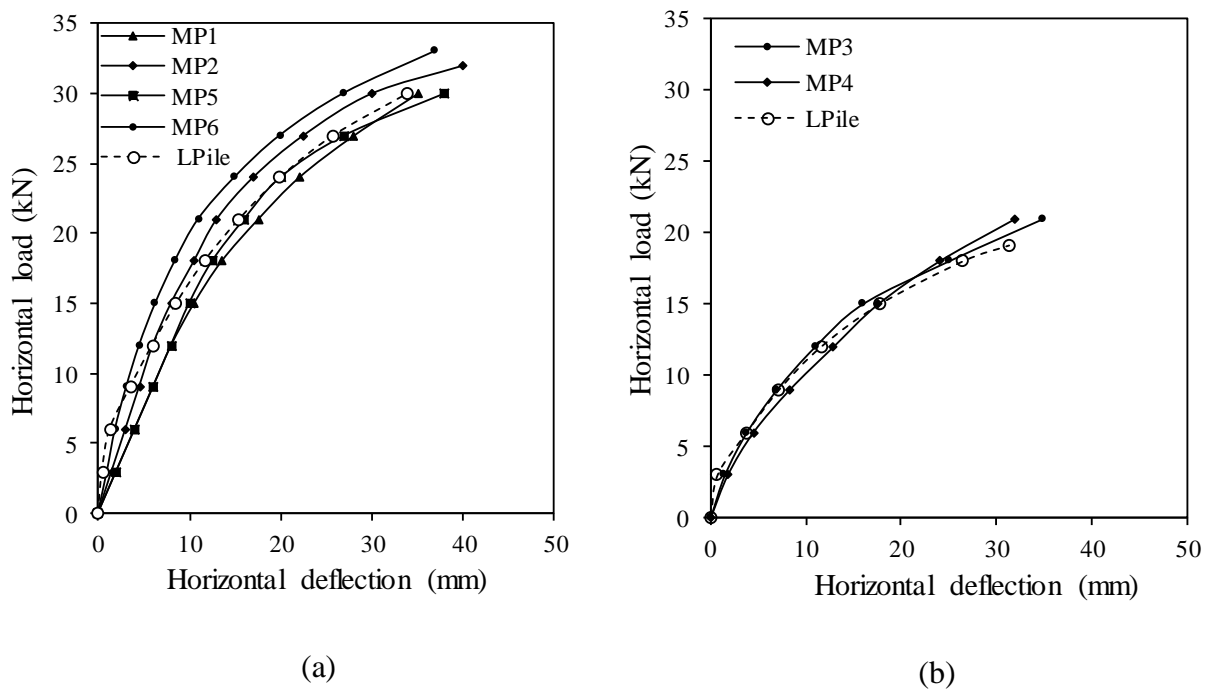


**Figure 5-15 Moment-Curvature curves for the exhumed micropile MP3 and Lpile model**

To validate the LPILE model, the same properties of soil and micropile materials used for micropile with  $D_b/D_h = 2.25$  were employed to generate LPILE model for micropiles with  $D_b/D_h = 3$ . Figure 5.16 compares the results of the field test with those obtained from LPILE models for both  $D_b/D_h = 2.25$  and 3. As it can be seen in Figure 5.16, the computed response employing the LPILE model is in agreement with the measured response from the field scale

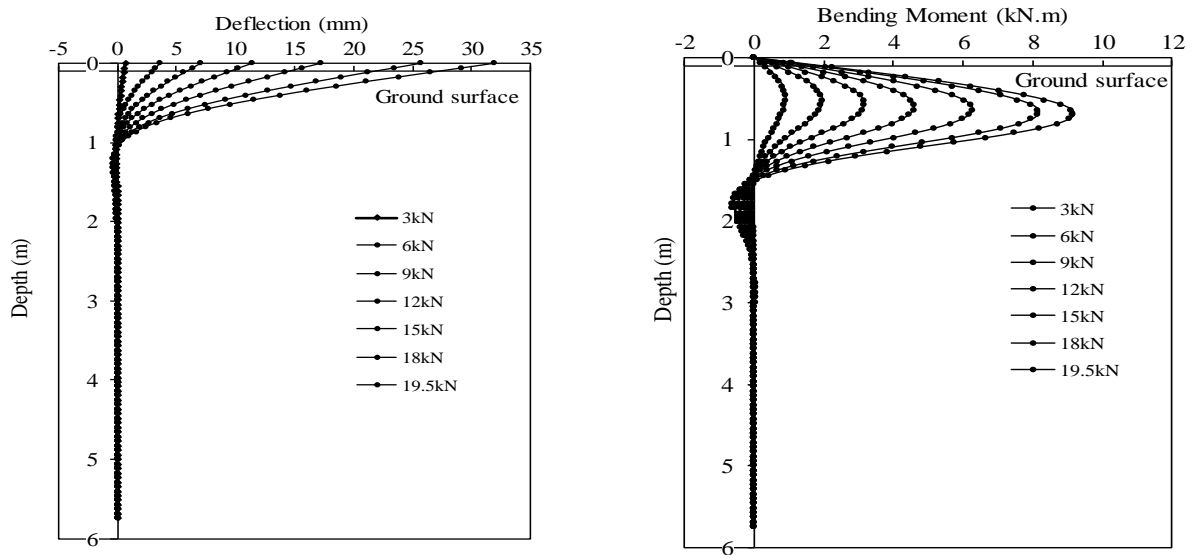
lad test. However, the angle of internal friction  $\phi' = 45^\circ$  was used, which is higher than the average correlated value using Kulhawy and Mayne proposed equation (1990) by  $3^\circ$ .

Sensitivity analysis was performed to investigate the extent of soil layers whose properties influence the performance of hollow bar micropiles. It was found that the properties of soil layers up to 1.2 m and 1.5 m below the ground surface influenced the lateral response for micropiles with 132 mm and 172 mm diameters, respectively. Below these depths, varying the soil properties had no effect on the calculated micropile lateral response. Accordingly, it can be concluded that the properties of the soil at depth within eight to nine times micropile diameters has the largest influence on the hollow bar micropiles performance under lateral loading.

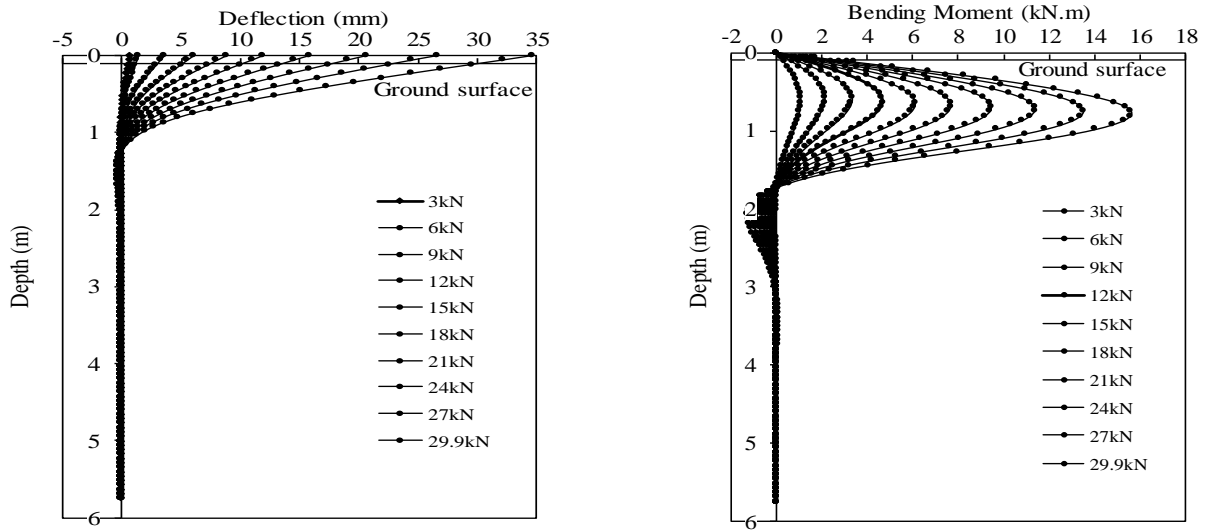


**Figure 5-16 (a) Calibration and (b) validation of L-Pile model.**

Figures 5.17 (a and b) show the micropiles deflection and bending moment with depth obtained from LPILE for both micropiles with  $D_b/D_h = 2.25$  and 3, respectively. As it was expected, both micropiles behaved as flexible piles with the deflection limited to the top 2.0m of the micropile. It is also noted that the maximum bending moment occurred at a depth between 4.5 and 4.35 of micropiles diameters. The results also show that the moment capacity is 9.18 kN.m and 15.6 kN.m for micropiles with  $D_b/D_h = 2.25$  and 3, respectively. This represented an increase of the moment capacity by 70% due to the increase in the diameter of the drill bit, and associated increase in the micropile diameter.



(a)



(b)

**Figure 5-17 Deflection and bending moment versus depth (LPile model); a)**

**$D_b/D_h=2.25$  and b)  $D_b/D_h=3$**

## 5.7 Conclusions

Fifteen full-scale loading tests were conducted on hollow bar micropiles to investigate the performance of micropiles under monotonic and cyclic lateral loads with different drill bit/hollow bar diameter ratio of 2.25 and 3. One group of four micropiles with common spacing between the micropiles in groups, 5D was tested under lateral monotonic loading. Hollow bars R51N with OD of 51 mm and the ID is 33 mm were installed with two different drill bit diameters 115 and 152 mm. The total length of micropiles is 6 m with 5.75 m embedded length. Based on the obtained results and the analysis performed, the following can be concluded,

- The load - deflection response of single micropiles indicated a stiffer response for micropiles with drill bit/hollow bar diameter ratio equal to 3 than the response of ratio of 2.25 which presents the current practice.
- Increasing the drill bit/hollow bar diameter ratio from 2.25 to 3, improved the lateral capacity by about 32%.
- Adding micro-steel fiber (1%) to the grout mix seems to improve the lateral performance of micropiles under lateral loads.
- Considering the 25mm lateral deflection as a failure criterion for micropiles under lateral loads, the group efficiency of micropiles group with five diameters center-to-center distance is about 89%.
- The degradation parameter  $t$  varies from 0.084 to 0.033 and from 0.062 to 0.031 for micropiles with  $D_b/D_h = 3$  and  $D_b/D_h = 2.25$ , respectively. The degradation parameter  $t$  reaches the peak value at the first few cycles and then decreases with increasing the number of cycles and the load amplitude.
- It was demonstrated that the LPILE software can be used to analysis the hollow bar micropiles under lateral loading following the procedure mention above.
- The first eight to nine micropile diameters depth have the major impact on the hollow bar micropiles performance under lateral loading.
- The maximum bending moments occurred at depth about 4.5 and 4.35 of micropiles diameters.



## 5.8 References

- AASHTO. (2012). *AASHTO LRFD Bridge Design Specifications*, Customary U.S. Units. The American Association of State Highway and Transportation Officials (AASHTO). Section 10.
- Abd Elaziz, A.Y. & El Naggar, M.H. (2014a). Evaluation of Geotechnical Capacity of Hollow Bar Micropiles in Cohesive Soils. *Canadian Geotechnical Journal*, Vol. 51, No. 10, pp. 1123-1138.
- Abd Elaziz, A.Y. & El Naggar, M.H. (2014b). Group Behaviour of Hollow Bar Micropiles in Cohesive Soils. *Canadian Geotechnical Journal*, Vol. 51, No. 10, pp. 1139-1150.
- Abd Elaziz, A.Y., & El Naggar, M.H. (2015). Performance of Hollow bar Micropiles under Monotonic and Cyclic Lateral Loads. *Journal of Geotechnical and GeoEnvironmental Engineering*. 141 (5).
- American Petroleum Institute (API). (2009). *Recommended Practice for Field Testing Water-Based Drilling Fluids*. API Recommended practice RP 13B-1.
- Abdraham, M. & El Naggar, M.H. (2015). Investigation of Mechanical Properties of Fibre-Reinforced Grouts for Micropile Application. *In Proceedings of the 15th Pan-American Conference on Soil Mechanics and Geotechnical Engineering*, Buenos Aires, Argentina. 1607 -1614.
- Anderson, J. B. & Babalola, M. R. (2014). Lateral Load Testing Micropiles to Evaluate the Impact of Threaded Joints and Casing Embedment on Short Micropiles in Shallow Rock. *DFI Journal*, Vol 5, issue 2.
- Brown, D. A., Morrison, C., & Reese, L. C. (1988). Lateral Load Behavior of Pile Group in Sand. *ASCE Journal of Geotechnical Engineering*, 114(11), 1261-1276.
- Brown, D. A., Reese, L. C., & O'Neill, M. W. (1987). Cyclic Lateral Loading of a Large-Scale Pile Group. *ASCE Journal of Geotechnical Engineering*, 113(11), 1326-1343

- Bruce, D. A. & Janes, M. (2014). A Case 2 Micropile Network Employed at a Rapid Excavation Railway Project. *In Proceedings of 12<sup>th</sup> International Workshop on Micropiles*. Krakow, Poland.
- Bierschwale, M.W., Coyle, H.M. & Bartoskewitz, R.E. (1981). Field Tests and New Design Procedure for Laterally Loaded Drilled Shafts in Clay. *Research Report 211- 3F, Texas transportation Institute*, Texas A&M University, Collage Station, 116p.
- Brettmann, T. & Duncan, J. M. (1996). Computer Application of CLM Lateral Load Analysis to Piles and Drilled Shafts. *ASCE Journal of Geotechnical Engineering*, Vol. 122, No. 6, 496-500
- Briaud, J. L. (1984). Panel Discussion, Laterally Loaded Deep Foundation. Philadelphia: *American Society for Testing and Materials (ASTM)*.
- Drbe, O.H. and El Naggar, M.H. 2015. Monotonic and Cyclic Compression Behaviour of Hollow Bar Micropiles. *Canadian Geotechnical Journal*, Vol. 52, No. 4, pp. 426-441.
- FHWA. (2005). *Micropiles Design and Construction*. Federal Highway Administration (FHWA), U.S. Department of Transportation, Washington, D.C. Publication No. FHWA-NHI-05-039.
- FHWA. (2010). *Drilled Shafts Construction Procedures and LRFD Design Methods*. Federal Highway Administration (FHWA), U.S. Department of Transportation, Washington, D.C. Publication No. FHWA-NHI-05-039.
- FHWA. (2013). *Post- Tensioning Tendon Installation and Grouting Manual*. Federal Highway Administration (FHWA), U.S. Department of Transportation, Washington, D.C. Publication No. FHWA-NHI-13-026.
- Juran, I., Bruce, D. A., Dimillio, A. & Benslimane, A. (1999). Micropiles: The State of Practice. Part II: Design of Single Micropiles and Groups and Networks of Micropiles. *Ground Improvement*, 3, 89–110.

- Kershaw, A. K. & Luna, R. (2014) Full-Scale Field Testing of Micropiles in Stiff Clay Subjected to Combined Axial and Lateral Loads. *Journal of Geotechnical and GeoEnvironmental Engineering*. 140(1): 225-261.
- Kulhawy, F. H., & Mayne, P. W. (1990). *Manual on Estimating Soil Properties for Foundation Design*. Research project No. 1493-6, EL-6800, Electric Power Research Institute., Palo Alto, Calif.
- Littlejohn, G. S., & Bruce, D. A. (1977). *Rock Anchors State-of-the-Art*. Foundation Publications Ltd., Brentwood, Essex, England, 50 pages.
- Little, R. L., & Briaud, J-L. (1988). Full Scale Cyclic Lateral Load Tests on Six Single Piles in Sand. *Miscellaneous Paper GL-88-27, Geotechnical Div.*, Texas A&M Univ., College Station, Texas.
- Long, J., Maniaci, M., & Menezes, G. (2004). Results of Lateral Load Tests on Micropiles. Geotechnical Special Publication, no. 124, Geosupport 2004 - Drilled Shafts, Micropiling, Deep Mixing, Remedial Methods, and Specialty Foundation Systems, *In Proceedings of Sessions of the GeoSupport Conference*, p 122-133.
- Long, J. H. & Vanneste, G. (1994). Effects of Cyclic Lateral Loads on Piles in Sand. *Journal of Geotechnical and Geoenvironmental Engineering*. 120(1): 225-244.
- LPILE. (2006). *A program for the analysis of piles and drilled shafts under lateral loads*. Version 6.0.27 [computer program]. Austin, Tex: Ensoft Inc.
- McVay, M., Casper, R., & Shang, T. (1995). Lateral Response of Three-Row Groups in Loose to Dense Sands at 3D and 5D Pile Spacing. *Journal of Geotechnical Engineering*, ASCE Vol. 121, No. 5, pp. 436- 441.
- McNulty, J. F. (1956). Thrust Loading on Piles. *Journal of Soil Mechanics and Foundations Division*, 82(SM2), 1-25.
- NAVFAC. (1986). *Foundation and Earth Structure, Design Manual 7.02*. Naval Facilities Engineering Command (NAVFAC).

- New York City. (1981). *Building Code of the City of New York*. Binghamton.: Gould Publications.
- Pyke, R. (1984). Panel Discussion, Laterally Loaded Deep Foundation. Philadelphia: *American Society for Testing and Materials (ASTM)*.
- Reese, L. C., Cox, W. R., & Koop, F. D. (1975). 'Field Testing and Analysis of Laterally Loaded Piles in Stiff Clay. *Proceedings, 7th Offshore Technology Conference*, Paper No. OTC 2312, 672–690.
- Rollins, K.M., Gerber, T.M., Lane, J.D., & Ashford, S.A. (2005). Lateral Resistance of a Full-Scale Pile Group in Liquefied Sand. *Journal of Geotech. Geoenviron Eng.*, ASCE, Vol. 131, No. 1, 115-125.
- Robertson. P. K. (1990). Soil Classification using Cone Penetration Test. *Canadian Geotechnical Journal*, 27(1), 151-158.
- Richards, T. D., & Rothbauer, M. J. (2004). Lateral Loads on Pin Piles (Micropiles). *Drilled shafts, Micropiling, Deep Mixing, Remedial Methods, and Specialty Foundation Systems*, Vol. 124, ASCE, Orlando, FL, 158–174.
- Tomlinson, M. & Woodward, J. (2008). *Pile Design and Construction Practice*. Taylor and Francis. London and New York.
- Viggiani, C., Mandolini, A. & Russo, G. (2012). *Piles and Pile Foundations*, Spon Press. New York.
- Walker, J. N., & Cox, E. H. (1966). Design of Pier Foundations for Lateral Loads. *Transactions of the ASABE*, 9(3), 417-427.
- Wang, S.-T & Isenhower, W. M. (2012). *Technical Manual for LPile*, Version 6, Ensoft.
- Wolosick, R. J. & Scott, F. R. (2017) Loading Effects on Battered Micropiles Supporting Lateral and Compression Forces. 9th Lizzi Lecture, *In Proceedings of 13th International Workshop on Micropiles*. Vancouver. Canada.

## CHAPTER 6

# 6 Improving the Mechanical Properties of Grout for Micropile Application

---

## 6.1 Introduction

In recent years, micropiles technology has been growing rapidly for both retrofitting existing foundations and supporting new structures. Micropiles can carry a considerable amount of axial loads; however, its lateral capacity is relatively small when compared with other pile types due to its small cross-sectional area. This represents the main limitation to its application in structures subjected to relatively large lateral loads. In order to further exploit their several advantages related to constructability, ground improvement effects, and efficient load transfer mechanism, there is an interest in introducing micropiles to support laterally loaded structures.

In current practice, steel casings are used along the upper part of micropiles to increase the lateral resistance. Wolosick and Scott (2017) illustrated the need for reconsidering battered micropiles when large lateral loads are anticipated. They advised that when lateral loads on micropiles anticipated, a steel pipe section in with a length equal to 20 - 25 times the drill - hole diameter should be used in the upper portion of the micropile. However, this increases the cost and construction time. Alternatively, adding reinforcing fibers to the grout can enhance the lateral performance of micropiles by increasing the flexural strength and improving the post-cracking behaviour. However, this potentially effective method for enhancing the flexural strength of the grout was not attempted.

Steel-fiber reinforced concrete is used in many structural applications, specifically when the structure subjected to loads over the serviceability limit in bending and shear (Bencardino, et al., 2008). Fibers can control crack initiation and subsequent crack development. Extensive research efforts were focused on the behavior of the fiber reinforced concrete (Mansur et al., 1999). Thomas and Rasmuswamy (2007) reported experimental results and an analytical model to evaluate the influence of fibers on the mechanical properties of concrete. They concluded that fibers can improve the mechanical properties significantly.

Neat grout, which is a mix of cement and water, is commonly used in North America for the construction of micropiles. However, sand can be added to the grout mix in some parts of the world (FHWA, 2005). However, adding fibers to the grout to enhance its flexural capacity has not been investigated to strengthen grouts used in micropiles construction. Because of the high slenderness ratio, micropiles are relatively flexible and when subjected to lateral loads they may experience structural failure (i.e. failure occurs in the micropile materials rather than in the surrounding soil). Thus, enhancing the flexural strength of micropile grout can improve its lateral resistance.

## **6.2 Objective and Scope of Work**

The aim of this study is to investigate the mechanical properties of fiber-reinforced grout for potential use in micropile applications. The study was divided into four main stages; in the first stage, the mechanical properties of the reinforced grout comprising four different fibers were evaluated: plastic fibers (PF), basalt fibers (BF) and micro-steel fibers (MSF) of steel fibers (SF). This stage involved testing cylindrical specimens of plain grout and

grouts reinforced with different types and dosages of fibers for tensile strength, compressive strength, and modulus of elasticity. Beams were also cast and tested under flexural loading conditions. Based on the obtained results from the first stage and the constructability of the fiber-reinforced grout, steel fibers were selected for further investigation. In the second stage, the flexural strength of micropile models was investigated. Models of micropiles were cast with two different steel fibers and tested under pure bending. The deflection along the micropile was measured and the moment-curvature was consequently established. In the third stage, the established moment-curvature curves were implemented in LPILE software to evaluate the lateral capacity of micropiles comprising the fiber-reinforced grouts. The fourth stage involved constructing a full-scale micropile in cohesionless soil utilizing 1% micro-steel fiber to investigate its lateral performance in comparison with a micropile constructed with same diameter and in the same environment using conventional grout.

### **6.3 Mechanical Properties of Fiber-Reinforced Grout**

The mechanical properties of reinforced grouts were investigated by casting specimens with four different types of fibers and three different volume contents dosages for each type. Two hundred and thirty-four cylinders 100 x 200 mm were cast and tested to evaluate the compressive strength, tensile strength and modulus of elasticity. Twelve cylindrical samples for each mix containing different volume contents of different types of fibers were tested after seven and twenty-eight days. Six cylinders were tested to evaluate compressive strength and six for indirect tensile strength. Cylindrical reinforced grout specimens were selected to enable casting the reinforced grout along the vertical direction to account for the orientation of the fibers in relation to the applied load. The compressive strength was

determined according to ASTM C39 and the tensile strength was obtained according to ASTM C496. In addition, six control cylinders (grout without fibers) were cast. Six cylinders for each volume content of different fiber dosage were evaluate for static modulus of elasticity and tested according to ASTM C469. To evaluate the effect of fiber dosage on the flexural strength, seventy-eight beams with dimensions 100 mm by 100 mm by 380 mm were cast. Six beams for each type of fibers with different dosages were cast and tested under Third-Point loading in a flexural testing machine to evaluate the effect of fibers on the flexural strength of different mixtures. The Third-Point Loading was performed in accordance to ASTM C1609.

The mixing procedure was performed as follows: the required quantity of water was added to the cement and mixed for four minutes, then fibers were sprinkled gradually by hand while continuous mixing for additional four minutes. Mixtures were prepared using a colloidal mixer to ensure proper consistency was achieved. The mixtures were poured in 100 mm diameter by 200 mm length cylindrical molds and 100 mm by 100 mm by 380 mm beams. All specimens were de-moulded after 24 hours then placed in a control room with a relative humidity of 100% and a constant temperature of 23°C.

According to FHWA (2005), the water to cement (w/c) ratio for micropile application should be between 0.4 to 0.5 by weight unless admixtures are used. In the current study, Portland cement Type 10 and w/c ratio of 0.45 were used. The properties of the four different types of fibers employed in this study are illustrated in Table 6.1. Figure 6.1 shows the four types of fibers used in this study.



**Table 6-1 Properties of fibers used in this study**

Type of Fiber	L(mm)	D(mm)	Aspect Ratio	Unit Weight kN/m <sup>3</sup>
<b>Steel Fiber (Micro-Steel Fiber)</b>	12	0.2	60	78.5
<b>Steel Fiber</b>	33	0.55	60	78.5
<b>Basalt Fibers (MiniBar)</b>	20	0.65	30.8	18
<b>Plastic Fiber (Fibermesh 650)</b>	Graded	Graded	96.5	9.1



a) Micro-steel fiber



b) Steel fiber



c) Plastic fiber



d) Basalt fiber

**Figure 6-1 Four different type of fibers**

### 6.3.1 Mechanical Properties of Tested Fiber-Reinforced Grouts

This section presents the results obtained from the experimental program including the compressive strength, tensile strength, elastic modulus of elasticity, and flexural strength.

#### 6.3.1.1 Compressive Strength and Tensile Strength

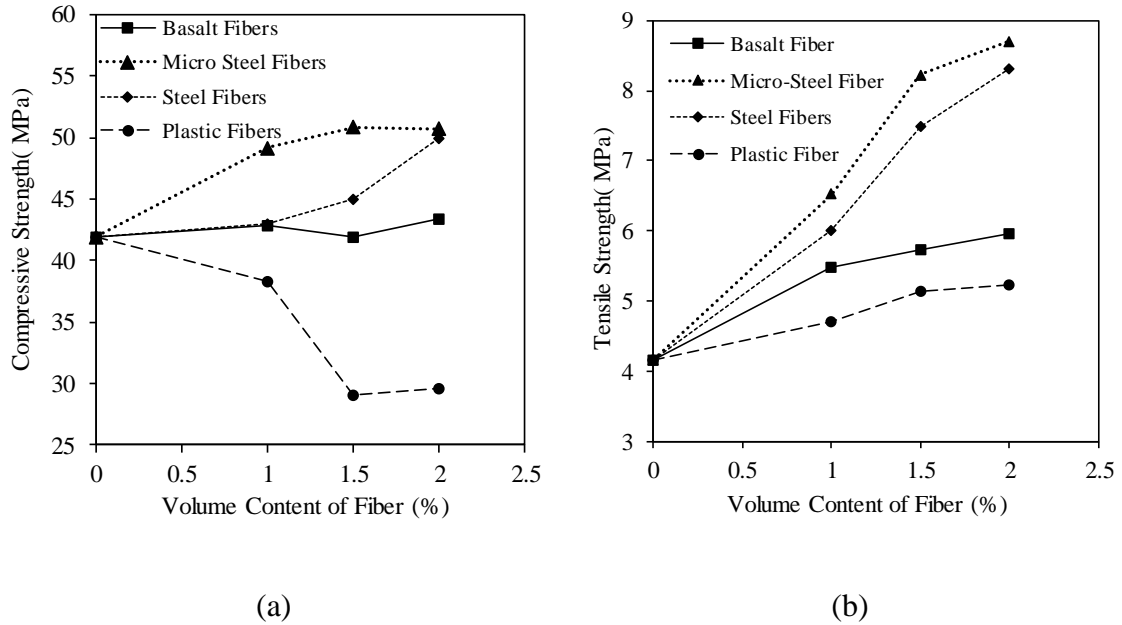
The average compressive strength measured for neat grout was 42 MPa, which is higher than the specified limit of 30 to 35 MPa by FHWA (2005) for micropile applications (Littlejohn and Bruce, 1977). The results of the compressive strength are presented in

Figure 6.2(a). The compressive strength of micro-steel fiber and steel fiber mixtures increased as the volume content of the fibers increased from 1% to 2%. For basalt fiber mixtures, the compressive strength changed slightly with the increase of the volume content while the compressive strength of the plastic fiber mixtures decreased by about 20% as the volume content of the fibers increased from 1% to 2%.

It was noted that the compressive strength for grout reinforced with plastic fibers decreased with the increase in the fiber dosage (34% reduction for 2% dosage of plastic fibers compared to just neat grout mix). However, the compressive strength for micro-steel fiber mixtures increased up to 16% with the increase in volume content of the fibers. For the plastic fiber mixtures, the decrease in compressive strength as the fiber dosage increases is attributed to a decrease in the cement content of the mixture. The fibers replaced a percentage of the cement in the mixture which was not fully compensated by the additional strength due to the fibers themselves.

The tensile strength of the micro-steel fiber and steel fiber mixtures showed significant increase with increasing dosages up to 2% as presented in Figure 6.2(b). It increased by more than 100% when compared to neat grout mixtures. The tensile strength of the plastic fiber mixtures increased by about 20% when the dosage increased to 2% of volume content. The mixture with 2% of basalt fibers demonstrated an increase in the tensile strength by about 30% compared to neat grout. Even though the grout compressive strength decreased by adding a certain percentage of plastic fiber; the tensile strength for plastic fiber mixtures increased by adding the same percentage of fibers. It was noted that adding a certain percentage of micro-steel fibers or steel fibers to the cement-based grout enhanced both

compressive and tensile strength. Generally, the tensile strength increased dramatically with a slight increase in compressive strength.



**Figure 6-2 (a) compressive strength; (b) tensile strength for four types of fibers with different dosages**

### 6.3.1.2 Static Modulus of Elasticity

The average measured static modulus of elasticity of neat grout for six cylinders was 13.5 GPa. For design calculations, FHWA 2005 recommended Equation No. 6.1 to estimate the modulus of elasticity of grout, i.e.

$$E_{grout} = 4732 \sqrt{(f'_c)} \quad (6.1)$$

$E_{grout}$  : is the modulus of elasticity of grout (MPa).

$f'_c$  : is the compressive strength of the grout (MPa).

Equation 6.1 is adopted in ACI code 318- 08 to correlate the compressive strength of concrete to the static modulus of elasticity is specified for use in concrete. However, it overestimates the modulus of elasticity for neat grout.  $E_{grout}$ . The calculated value of static modulus of elasticity based on Equation 6.1 is 31 GPa, which is higher than the value obtained from the test results. Based on experimental data, Drbe (2013) and Aboutabikh (2016) evaluated static modulus of elasticity of neat grout from extensive testing programs and they reported the modulus of elasticity for neat grout to be about 15 GPa which is in good agreement with the test results. Therefore, it is recommended to modify Equation 6.1 to estimate the static modulus of elasticity for neat grout, i.e.,

$$E_{grout} = 2200 \sqrt{(f'_c)} \quad (6.2)$$

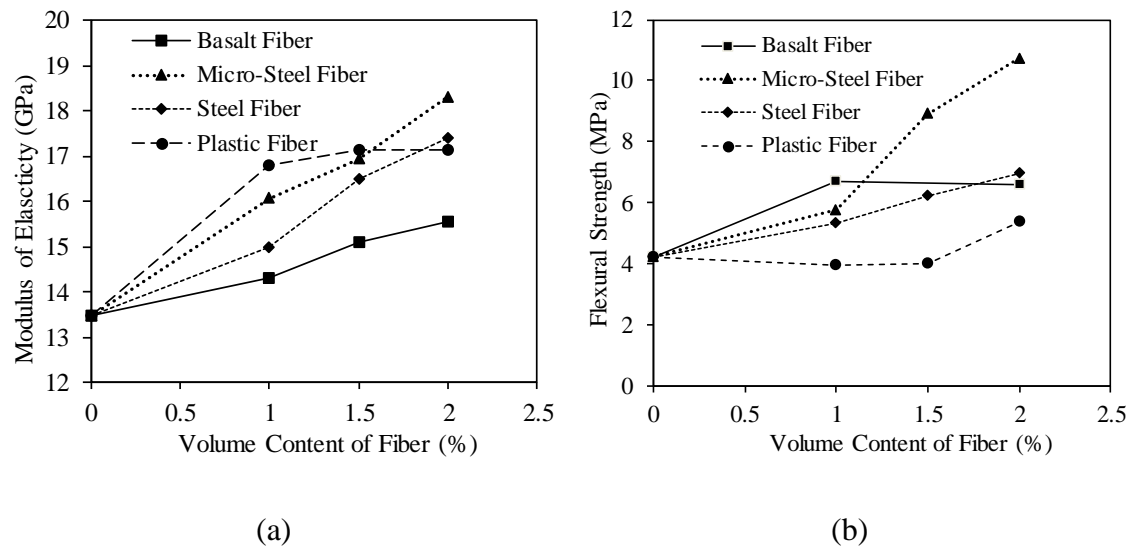
Equation No.6.2 agrees with US Army Corps of Engineers, which recommends that the modulus of elasticity of neat grout is about half of the concrete modulus of elasticity.

The mixtures with basalt fibers exhibited an increase in the modulus of elasticity of 15% for 2% of volume content of fibers as shown in Figure 6.3(a). The 1% dosage of plastic fibers recorded the highest percentage increase equal to 24.7% among the four types of fibers for this dosage. However, further increase in dosage did not result in further enhancement of the elastic modulus. The micro-steel fiber and basalt fiber mixtures showed a steady increase in modulus of elasticity with the increase in fibers dosage. The micro-steel fiber and steel fiber mixtures showed a linear increase in the modulus of elasticity with the increase of the volume fibers dosage. The mixtures of 2% of micro-steel fibers

recorded the highest value of modulus of elasticity among the four types of fibers tested equal to 18.3 GPa.

### **6.3.1.3 Flexural Strength**

To assess the flexural strength of different types of mixtures, six beams were cast and tested after 7 and 28 days. Four different percentages of fiber dosage were used for each type of fiber except for basalt fiber only 1 and 2% were used. All tests were carried out according to ASTM C78. Figure 6.8(b) summarizes the test results of the different mixtures with different fibers dosages. The flexural strength varied between 10 and 20% of the corresponding compressive strength, which is in agreement with US Army Corps of Engineers recommendations that the flexural strength should be between 10-20% of the compressive strength. The flexural strength of the micro-steel fiber mixture with 2% of volume content, however, was about 23% of its compressive strength. The micro-steel fibers mixtures showed a dramatic increase in the flexural strength by about 153% for 2% dosage. Plastic fiber mixtures exhibited slight decreases in flexural strength for a 1% dosage. However, a 2% dosage of the same fibers showed an increase in the flexural strength by about 28% for plastic fiber. The flexural strength of basalt fiber mixtures increased by 56% for a 2% dosage. It was noted that for basalt fiber mixtures the flexural strength changed slightly when the percentage of fiber increased from 1 to 2%.



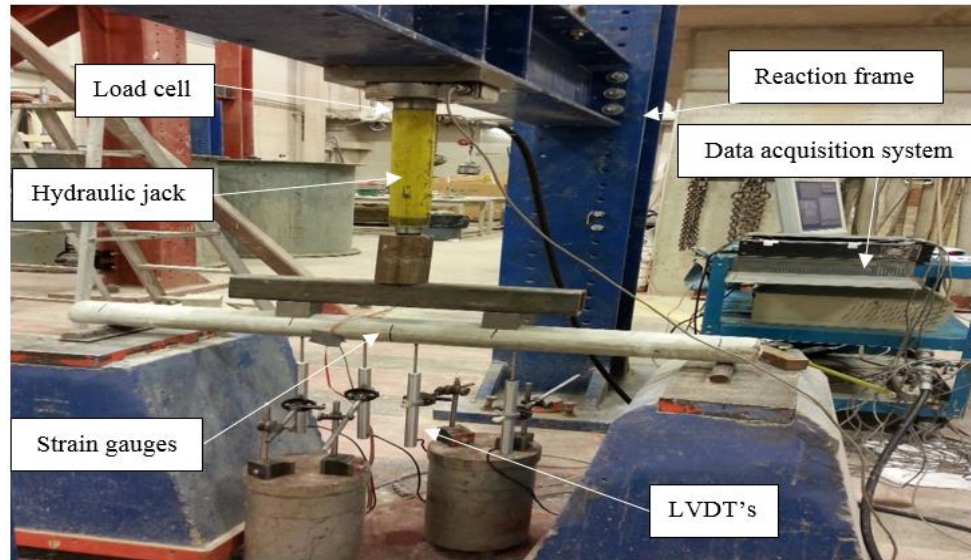
**Figure 6-3 (a) Modulus of elasticity; (b) Flexural strength for four types of fibers with different dosages**

## 6.4 Pure Bending Tests

Based on the results obtained from the first stage and practical consideration for the full-scale test in site, such as the pumpability of the grouted fiber and the nozzle diameter, two types of fibers with 1% dosage were selected for this stage to evaluate the effect of adding fibers on the bending moment capacity of micropiles. Nine model micropiles were cast: three with neat grout, three with 1% of steel fiber and three with 1% of micro-steel fiber. The model micropile length was 1000mm and its diameter was 76mm. The Threaded hollow steel bar (R38N/21) used to construct the models had an outer diameter of 38 mm and inner diameter of 22 mm. The ultimate (structural) axial load of the hollow bar is 500 kN and the thread type is ISO 10208. The neat grout was mixed with 0.45 w/c ratio as per the recommendation of FHWA for micropile application. All micropiles models were de-

moulded after 24 hours and kept in a controlled room with a relative humidity of 100% and constant temperature of 23°C. The models were left for 28 days in the controlled room before testing. The model was divided to three equal spans and the load was applied at the one third and two thirds of the total length to produce a pure bending moment at the middle third of the model. Four LVDT's were utilized to measure the deflection along the micropile length. The load was applied in very slow fashion using a 100 kN hydraulic jack capacity with a maximum stroke of 152.4 mm. The applied load was measured using a load cell with a capacity of 100 kN. All the LVDT's and the load cell were hooked to a data acquisition system to obtain a reading for each second. To facilitate applying the load on a curved surface, a special piece of solid steel was designed with the same micropile diameter. The load test setup is shown in Figure 6-4.

Micropiles were subjected to pure bending tests and their deflections were measured along the micropile model. The deflection along the micropile was obtained via the LVDT's readings. Curve fitting was used to establish the deflection along the micropile. The deflection curves were then fitted using a quadratic function to establish a continuous function of deflection. The deflection fitted curve was then subjected to double-differentiation to calculate the curvature profile along the micropile. The moment – curvature curves were established from the measured bending moments and the corresponding curvature profile. The cracking behaviour was monitored during the tests and the results are also reported.

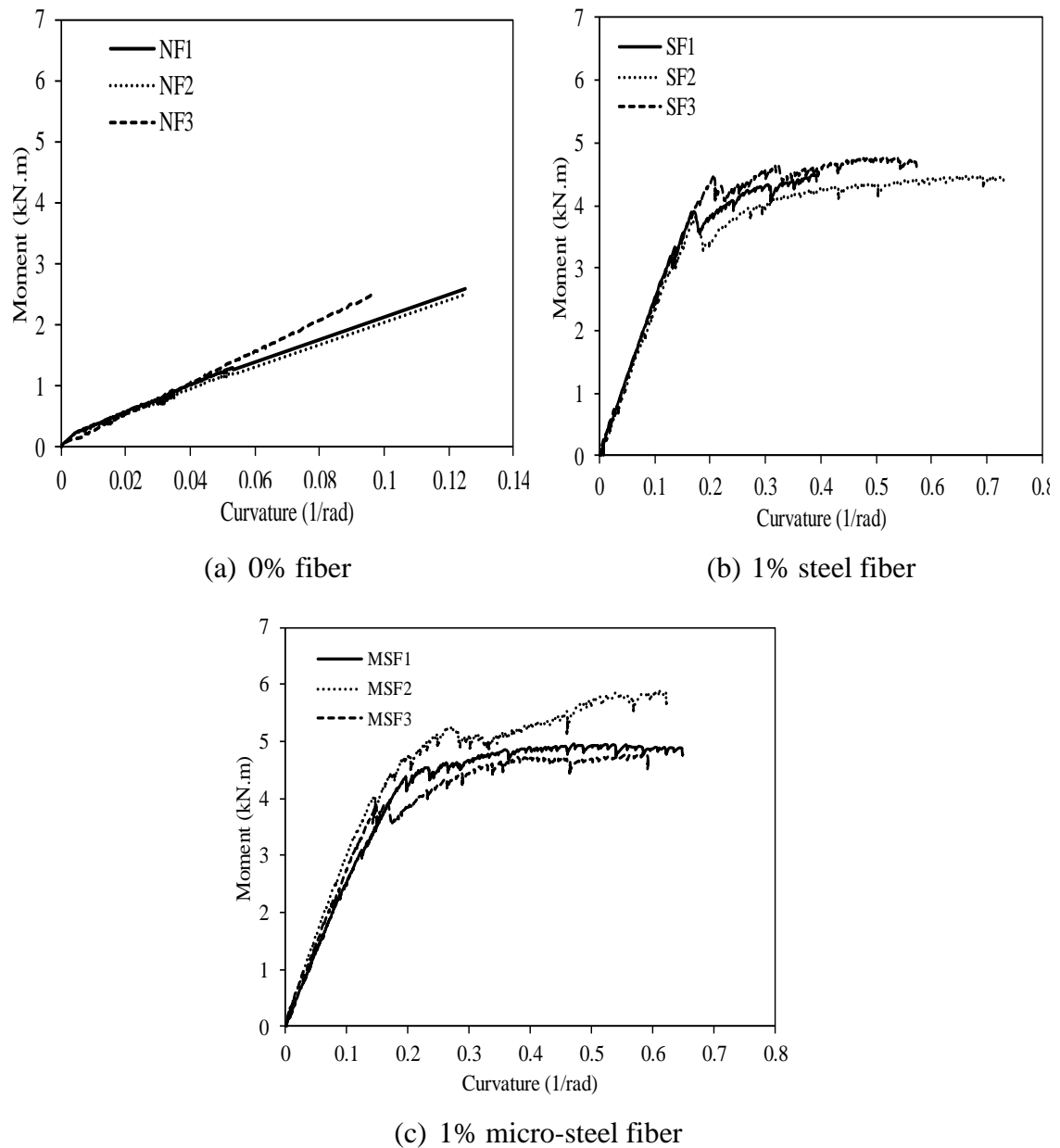


**Figure 6-4 Load test setup**

#### **6.4.1 Results of Pure Bending Tests**

The moment-curvature curves for the nine micropile models are plotted in Figure 6-5. As shown in Figure 6-5, model micropiles with no steel fiber failed at low bending moment (less than 2.5 kN.m) and the failure was brittle and occurred at low curvature compared to the model micropiles with steel fibers. The moment – curvature curves indicated that the moment capacity of micropiles increased and the post-cracking behaviour improved by adding steel fibers to the grout mix. The bending moment capacity of the micropiles increased significantly by about 100% as a result of adding 1% by volume of micro-steel fibers. In addition, micropiles with steel fibers exhibited ductile behaviour as the applied moment exceeded its yield bending moment.





**Figure 6-5 Moment-curvature curves obtained from pure moment tests**

Figure 6-6 shows the tested model micropiles after completing the pure bending tests. As can be observed from Figure 6-6, the micropiles cast with neat grout exhibited grout crushing and separation from the central hollow bar experienced total loss of grout due to the brittle behaviour of neat grout. On the other hand, micropiles constructed with reinforced grout maintained the grout form, with some cracks, owing to its enhanced

ductility. This is more evident in the larger deformation of the micropiles constructed with fiber-reinforced grout compared to the micropile constructed with neat grout, which failed at minimal reinforcing bar deflection.



**Figure 6-6 Post cracking behaviour of fiber reinforced and non-reinforced grouted micropiles**

## 6.5 Numerical Modeling

LPile is a special purpose program used to analyze a single pile under lateral loading. The program utilizes the  $p$ - $y$  method for analyzing the nonlinear lateral load transfer of piles. Lateral deflection, bending moment, shear force and soil response over the pile length can be computed using LPile program. The program uses various types of published and well documented lateral load-transfer curves ( $p$ - $y$  curves) to model different type of soils (Isenhower, et al., 2017). LPile offers the option to incorporate the bending moment versus

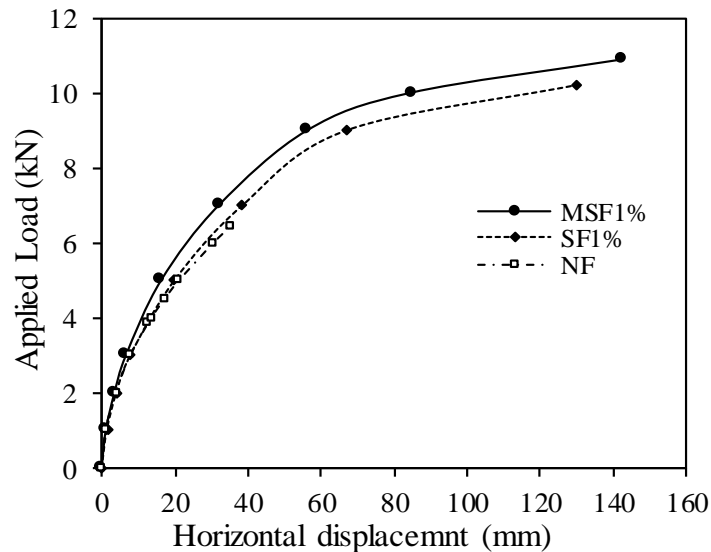
bending curvature in the analysis when they are available. The nonlinearity of lateral response of soil-pile system can be attributed to two main factors: first, the response of soil to lateral loading is nonlinear; and second, structural nonlinearity associated with the pile material. The soil nonlinearity is accounted for by incorporating an appropriate  $p$ - $y$  curve; LPILE offers 14 different internal  $p$ - $y$  curves for soil modeling. The pile material nonlinearity can be accounted for by incorporating the bending moment versus bending curvature behaviour obtained from pure bending tests. For the lateral load transfer mechanism,

To investigate the effect of reinforcing fibers in the grout mix and how it improves the performance of micropiles under lateral loading, the moment-curvature curves obtained from pure bending moment tests were incorporated in LPILE. The  $p$ - $y$  Sand model (Reese et al., 1974) was used to perform the analysis. The soil was modeled with the following parameter values: effective unit weight,  $\gamma' = 19.5 \text{ kN/m}^3$  and angle of internal friction  $\phi' = 42^\circ$ . The soil properties were obtained from the site investigation performed as part of this thesis.

### **6.5.1 Results of Numerical Modeling**

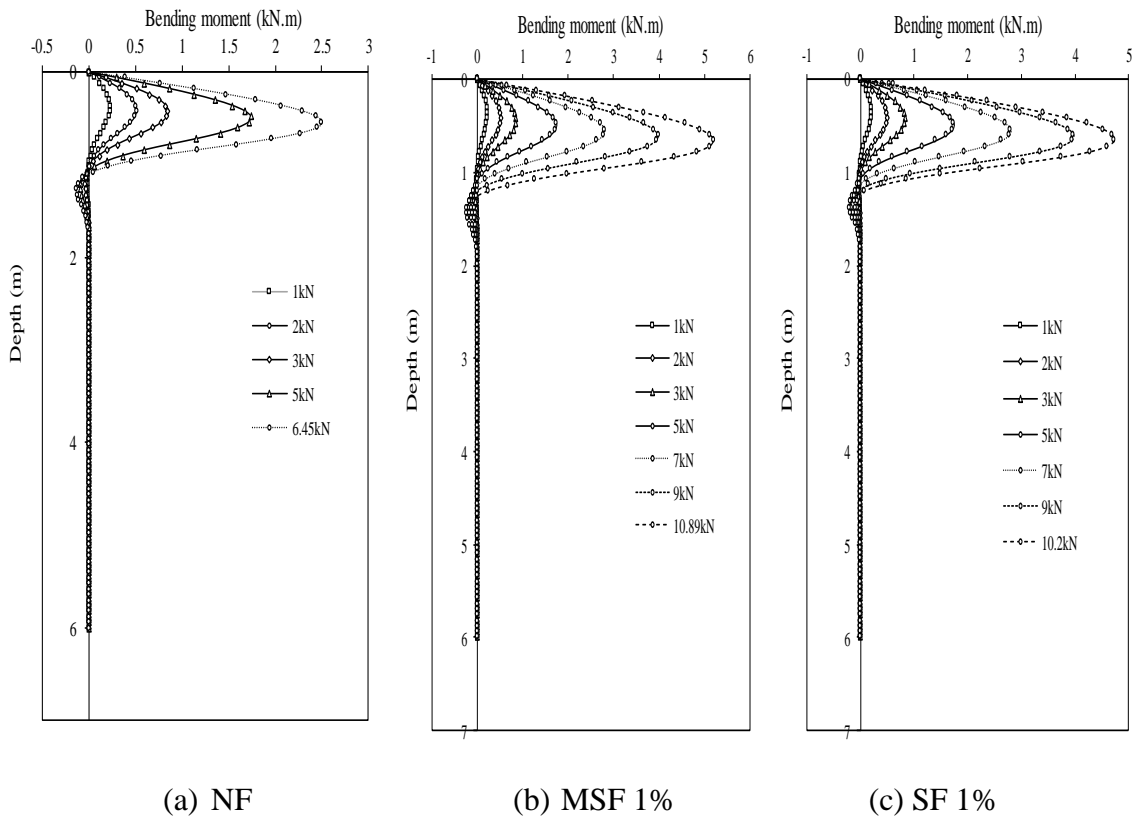
The load-deflection curves were obtained from LPILE analyses for the three types of micropiles: neat grout, no fibers (NF); 1% micro-steel fibers (MSF); and 1% steel fibers (SF) and the results are shown in Figure 6-7. It is noted from Figure 6-7 that micropiles constructed with reinforced grout could sustain larger applied loads compared to micropiles cast with neat grout without steel fibers. For example, MSF 1% sustained an applied lateral load greater than 11 kN before failure occurred, while the NF micropile failed at a

maximum load of 6.5 kN. It is also noted that the MSF micropile displayed very ductile behaviour with large lateral displacement of up to 140 mm (i.e. almost twice the micropile diameter).



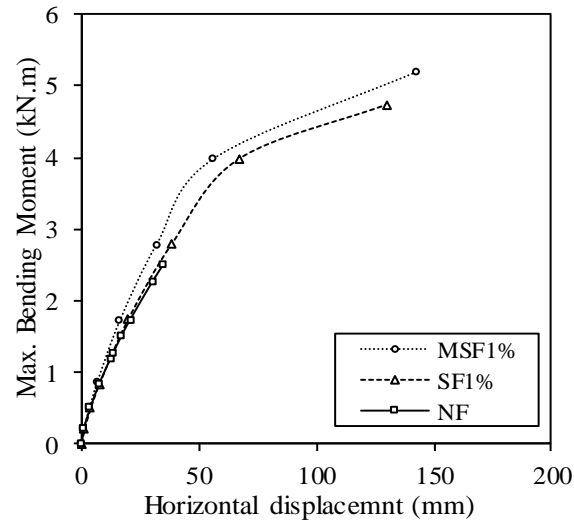
**Figure 6-7 Load-deflection curves using Reese model for the three micropiles; NF, MSF1% and SF1%**

Considering the lateral capacity of micropiles to be the load corresponding to 25 mm of pile head deflection, the capacities of the three micropiles were evaluated. The lateral capacity of micropiles cast with MSF and SF increased by 12.9% and 3.6 %, respectively, when compared to micropiles constructed with NF. The bending moments along the depth of micropiles are shown in Figure 6-8. The maximum bending moment where the plastic hinge is expected to occur was observed at depth equal to 7.1 times the micropile diameter for micropiles constructed with no fibers while for micropiles cast with steel fibers the plastic hinge encountered at depth equal to 8.7 times micropile diameters.



**Figure 6-8 Bending moment along the depth of the three micropiles using Reese model**

Figure 6-9 displays the variation of the maximum bending moment with the maximum micropile head deflection. It is evident from Figure 6-9 that the bending moment capacities of micropiles cast with steel fibers was higher than the micropile constructed with NF, and the response of the fiber—reinforced micropiles was stiffer.



**Figure 6-9 Maximum bending moment versus maximum head deflection curves for three micropiles**

## 6.6 Full-Scale Test

A full-scale micropile (designated MP6) was installed as part of large study to investigate the performance of micropiles installed in cohesionless soil. Micro-steel fiber with a 1% of volume dosage was added to the neat grout mix which had a w/c ratio of 0.45 to investigate the effect of adding micro-steel fibers on the lateral performance of micropiles. Adding the micro-steel fiber was made manually for the top 2.25 m (about 15 times the micropile diameter) where the influence of adding fibers to the grout was anticipated. The total micropile length was 6m with a 5.75m embedded length. The micropile was installed with a drill bit diameter 152mm, and the hollow bar utilized was R51N with 51mm outer diameter and 33mm inner diameter. The final grout had a specific gravity between 1.80 and 1.95, which is in compliance with (FHWA 2005) recommendation for micropile application. The final competent structure grout was pumped using a pressure of between

0.8 to 1 MPa to displace the drilling grout. Grout cylinders were collected during the installation process using cylindrical molds of 100 mm diameter by 200mm length and 75 mm diameter by 150mm length. All specimens were de-moulded after 24 hours and then placed in a control room with a relative humidity of 100% and constant temperature of 23°C. The cylinders were tested after 28 days to determine compressive strength and indirect tensile strength. The compressive strength was determined according to ASTM C39 and the tensile strength was obtained in according to ASTM C496. The average compressive strength after 28 days was 40 MPa and the average spilt tensile strength was 3.97 MPa. The results obtained for the compressive strength met the minimum requirement set by FHWA (2013) for compressive strength of grout after 28 days.

### **6.6.1 Site Exploration**

The site is located near Ayr, Ontario. The site exploration program included in-situ and laboratory tests to characterize the soil and obtain the soil strength parameters. Three boreholes were drilled which included standard penetration tests (SPT). Soil samples were extracted using the spilt spoon method and tested in a laboratory environment. Additionally, four piezocone penetration tests (CPT) were performed across the site, two of them were in the vicinity of the test locations (CPT1 and CPT2).

The relative density  $D_r$  was obtained using the correlations proposed by Kulhawy and Mayne (1990) based on SPT and CPT data and are summarized along the depth in Table 6.2. The site investigation was covered extensively in the previous chapters three and four.

**Table 6-2 Correlated relative density from SPT and CPT**

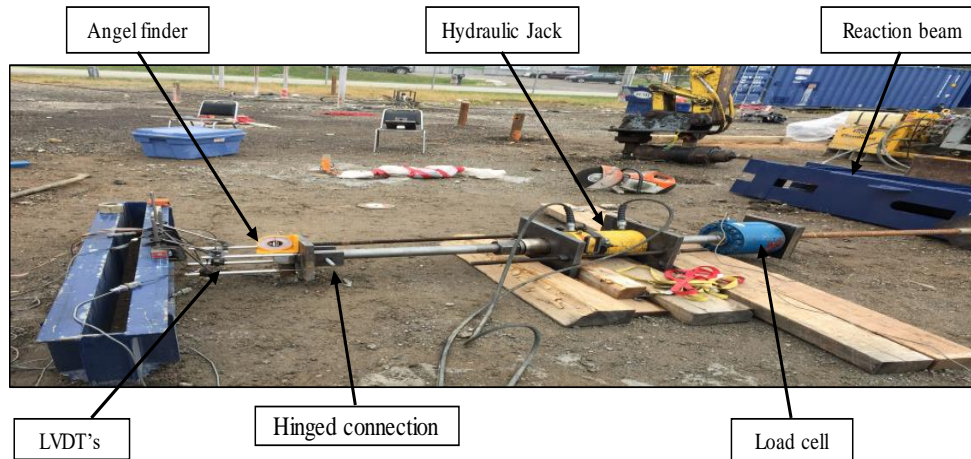
<b>Depth (m)</b>	<b>Relative density (%) from SPT</b>	<b>Relative density (%) from CPT</b>
<b>1</b>	89.9	82.3
<b>1.8</b>	79.4	83.2
<b>2.6</b>	85.2	92.1
<b>3.2</b>	71.5	93.3
<b>4</b>	88.2	94.2
<b>4.8</b>	79.1	88.5
<b>6.4</b>	98.5	94.2
<b>8</b>	83.3	90.1
<b>9.4</b>	89.4	71.2
<b>10.9</b>	87.5	60.1

### **6.6.2 Loading setup and Pile Instrumentation**

A test setup was designed and manufactured to facilitate applying monotonic lateral loads on micropile head as shown in Figure 6.13. A reaction frame was used to support the loading system which consisted of steel rod threaded to the load cell from one end and attached to the micropile head using a hinged connection to apply the lateral load with zero moment. A square steel plate with a 250 mm side length and 30 mm thickness with a hex nut (ID 51 mm) welded to one side was threaded to the hollow bar head to facilitate



applying the lateral loads to the micropile. The load was applied through a hollow cylinder hydraulic jack with a capacity of 900 kN and recorded via a load cell capacity 900 kN.



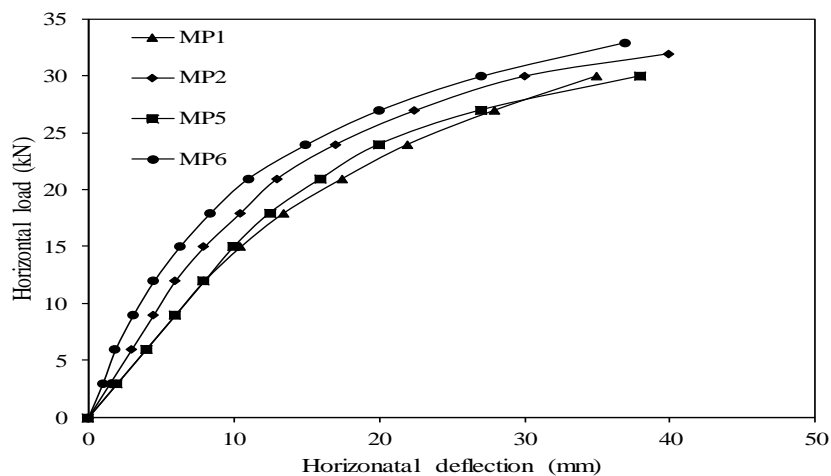
**Figure 6-10 Lateral load test setup**

Four HLP190 (hybrid Linear Potentiometers) were attached to the steel plate in square arrangement to measure the lateral deflection for single micropiles and six HLP190 were used to measure the group deflection; one on each micropile and two were attached to the connection beam. The load cell and the LVDT's were connected to a data logger to acquire the readings every one second. MP6 was equipped with eight foil strain gauges concentrated on the top two and half meters of the pile where a large deflection and bending moment were expected. All necessary precautions were taken in consideration to ensure the survivability of the strain gauges; that includes proper attaching and coating procedure. However, due to the harsh installation procedures of hollow bar micropiles, that involves drilling through the soil and grouting simultaneously, no strain gauges survived. Micropile MP6 was loaded monotonically in equal increments of 3 kN, each increment was maintained for 5 minutes.

### 6.6.3 Results of Full-Scale Lateral Test

The load - deflection curves for micropile (MP6) installed with reinforced grout (1% of MSF) and micropiles installed with neat grout containing no fibers (MP1, MP2 and MP5) are shown in Figure 6-14.

The results of micropiles MP1, MP2 and MP5 are reported and discussed previously in more details in Chapter 5, addressing the effect of increasing the drill bit/ diameter ratio on the micropile lateral performance. Herein, the focus is on the effect of fiber reinforcement on the lateral behaviour of the micropiles. As can be observed from Figure 6-14, MP6 displayed a stiffer lateral response when compared to the other three micropiles. In addition, considering the lateral capacity of micropiles as the lateral applied load which causes 25 mm of lateral deflection at the micropile head, the lateral capacity of the fiber reinforced pile increased by 10% compared to the average capacities of the three micropiles installed with no fiber.



**Figure 6-11 Load vs deflection curves for MP6 with MSF 1% and MP1, MP2 and MP5 with No fibers**

## 6.7 Summary and Conclusions

The mechanical properties of neat grout and various reinforced grouts were investigated in this study by performing several laboratory tests for compressive strength, tensile strength, modulus of elasticity, and flexural strength. Furthermore, model micropiles 1000 mm long and 76 mm in diameter were cast and subjected to pure bending moment tests to investigate the effect of adding fibers on the bending moment capacity of micropiles. An LPile model was developed utilizing the moment-curvature curves obtained from the pure bending moment tests results and was used to further evaluate the beneficial effects of using fiber-reinforced grouts on the micropile lateral behaviour. The optimum dosage of fibers was suggested based on the results of the experimental investigation and parametric study. The optimum steel fibers dosage was then used to construct a full-scale micropile 6 m long and 172 mm in diameter in cohesionless soil. The micropile was tested under monotonic lateral loads. Based on the obtained results from this study, the following can be concluded:

- The compressive strength of plastic fiber mixtures decreased slightly when increasing the fiber dosage. However, the tensile strength increased by increasing the dosage.
- The compressive and tensile strengths of micro-steel fiber and steel fiber mixtures increased when increasing the volume content of fibers. The compressive strength increased by 21% for both fibers mixtures while the tensile strength increased by 110% and 100% for grout mixed with micro-steel fibers and steel fibers, respectively.

- The 2% dosage of micro-steel fiber mixtures displayed the highest value of static modulus of elasticity amongst the four types of fibers and dosages considered in this study.
- The flexural strength of micro-steel fiber and basalt fiber mixtures increased as fiber dosage increased. On the other hand, the flexural strength of plastic fibers mixtures decreased as the fiber dosage increased.
- The bending moment capacity of micropiles increased and the post-cracking behaviour improved by adding micro-steel fibers and steel fibers to the grout mix.
- Micropiles cast with steel fibers showed larger lateral capacity and greatly increased ductility compared to micropiles constructed with neat grout, which failed in a brittle manner.
- The plastic hinge developed at a depth equal to 7.1 and 8.7 times the micropile diameter for micropiles constructed with no fibers and micropiles casted with steel fibers, respectively.
- The lateral capacity of micropile constructed with 1% of MSF grout increased by 10% compared to micropiles constructed with neat grout.

## 6.8 References

- Abdraham, M. & El Naggar, M.H. (2015). Investigation of Mechanical Properties of Fibre-Reinforced Grouts for Micropile Application. *In Proceedings of the 15th Pan-American Conference on Soil Mechanics and Geotechnical Engineering*, Buenos Aires, Argentina. 1607 -1614.
- Aboutabikh, M. (2016). *Application of treated oil sands drill cuttings waste in micropiles construction. MSc thesis*. Western University, London, Canada.
- ASTM C78 (2010). *Standard test method for Flexural Strength of Concrete (Using Simple Beam with Third-Point Loading)*. West Conshohocken, PA: ASTM International.
- ASTM C496 (2011). *Standard Test Method for Splitting Tensile Strength of Cylindrical Concrete Specimens*. West Conshohocken, PA: ASTM International.
- ASTM C39 (2012). *Standard Test Method for Compressive Strength of Cylindrical Concrete Specimens*. West Conshohocken, PA: ASTM International.
- ASTM C1609 (2012). *Standard Test Method for Flexural Performance of Concrete (Using Simple Beam with Third-Point Loading)*. West Conshohocken, PA: ASTM International.
- ASTM C469 (2014). *Standard Test Method for Static Modulus of Elasticity and Poisson's Ratio of concrete in Compression*. West Conshohocken, PA: ASTM International.
- American Petroleum Institute (API). (1987). *Recommended practice for planning, designing and constructing fixed offshore platforms*. API Recommended practice 2A, 17 Ed.
- Bencardino, F., Rizzuti, L., Spadea, G. & Swamy, R. N., (2008). Stress-Strain Behavior of Steel Fiber-Reinforced Concrete in Compression. *Journal of Materials in Civil Engineering*, Volume 20, pp. 225-263.

- Bruce, D. A., Dimillio, A. F., & Juran, I. (1997). Micropiles: The State of Practice. Part1 Characteristics, Definitions and Classifications. *Ground Improvement*. p. 25-35.
- Bruce, D.A., & Nicholson, P.J. (1989). The Practice and Application of Pin Piling. *Proceedings of the ASCE Foundation Engineering*, Evanston, IL, 19pp.
- Butler, H. D., & Hoy, H. E. (1977). *User Manual for the Texas Quick-Load Method for Foundation Load Testing*. Federal Highway Administration, Office of Development, Washington, DC.
- Drbe. O. (2013). *Investigation of Hollow Bar Micropiles in Cohesive Soil*. MSc thesis, Western University, London, Canada.
- FHWA. (2005). *Micropiles design and construction*. Federal Highway Administration (FHWA), U.S. Department of Transportation, Washington, D.C. Publication No. FHWA-NHI-05-039.
- FHWA. (2013). *Post- tensioning tendon installation and grouting manual*. Federal Highway Administration (FHWA), U.S. Department of Transportation, Washington, D.C. Publication No. FHWA-NHI-13-026.
- Gomez, J. E., Rodriguez, C.J., Robinson, H. D. & Keough, L. (2007). Hollow Core Bar Micropiles- Design Parameters Interprets from 260 Load Tests. *In Proceedings of the 32nd Annual Conference on Deep Foundations*. Colorado, CO.
- Thomas, J. & Ramaswamy, A., 2007. Mechanical Properties of Steel Fiber-Reinforced Concrete. *Journal of Materials in Civil Engineering*, 5(19), pp. 385-392.
- Isenhower, W. M., Wang, S.-T. & Vasquez, L. G., (2017). *User's Manual for Lpile 2018*, s.l.: Ensoft, INC.
- Kulhawy, F. H., & Mayne, P. W. (1990). *Manual on estimating soil properties for foundation design*. Research project No. 1493-6, EL-6800, Electric Power Research Institute., Palo Alto, Calif.

- Littlejohn, G. S., & Bruce, D. A. (1977). *Rock Anchors State-of-the-Art*. Foundation Publications Ltd., Brentwood, Essex, England, 50 pages.
- Mansur, M. A. & Chin, M. S. (1999). Stress-Strain Relationship of High-Strength Fiber Concrete in Compression. *Journal of Materials in Civil Engineering*, Feb 1999.
- Reese, L.C., Cox, W.R. & Koop F.D. (1974). Field Testing and Analysis of Laterally Loaded Piles in Sand. *In Proceedings, VI Annual Offshore Technology Conference*, Houston, Texas, 2(OTC 2080): 473-485.
- Timothy, M. J., Bean, J. J. & Bolton, M. K. (2012). MiniJET: A New Type of Micropile. *Proceedings, Grouting and Deep Mixing*. American Society of Civil Engineers (ASCE), New Orleans, Louisiana, 1095-1104.
- Wolosick, R. J. & Scott, F. R. (2017) Loading Effects on Battered Micropiles Supporting Lateral and Compression Forces. 9th Lizzi Lecture, *In Proceedings of 13th International Workshop on Micropiles*. Vancouver. Canada.

**CHAPTER 7****7 Numerical Modelling of Hollow Bar Micropiles in Cohesionless Soils**

---

**7.1 Introduction**

Numerical modelling provides a powerful tool for analyzing a wide range of geotechnical problems and has increasingly gained acceptance in foundation design. Hollow bar micropiles (HBMP) are a relatively new type of micropile and are increasingly used as an effective foundation system. Based on their method of construction, the FHWA (2005) has classified micropiles into four categories. For Type A micropiles, the grout is placed under gravity and no pressure is required. For Type B micropiles, the grout is typically pressurized under a pressure range from 0.5 to 1 MPa as the temporary casing is withdrawn. For type C micropiles, the grout is placed in a two-step process. First, the grout is poured under gravity such as in Type A. Before the grout hardens, it is pressurized to at least 1 MPa without the use of a packer. Type D micropiles is also constructed following a two – step installation process. First, the grout is placed under gravity as in Type A or sometimes pressurized as in Type B. After hardening of the initial grout, additional grout is pressurized between 2 to 9 MPa through a sleeved pipe by using packers.

HBMP is classified as Type B according to the FHWA classification system even though its installation method is different from Type B micropile. The construction technique of HBMP combines drilling and grouting in a one-step process, which facilitates fast



installation, increased productivity, and less soil disturbance. In addition, the high grouting pressure used in HBMP construction results in an efficient load transfer mechanism.

Due to the cost of installation and testing, examining the effect of various parameters such as soil density, soil strength parameters, and slenderness ratios of piles could be quite expensive. On the other hand, numerical models can be utilized to conduct parametric studies covering these different parameters. Although sophisticated advanced numerical models are growing, and computer software is advancing rapidly, full-scale load tests remain the most valuable and reliable source of investigating a piles performance. A numerical model must be calibrated and validated against experimental data in order to obtain reliable results (Satibi et al., 2009).

Wehnert and Vermeer (2004) compared the results of a finite element model to the results of bored pile load tests in stiff clay. They emphasized the importance of using proper interface elements to simulate the realistic behavior of the pile-soil system. Furthermore, they concluded that the hardening soil model simulated the pile behavior better than the elastic-plastic Mohr-Coulomb model and the soft-soil model. Shahrour and Juran (2004) developed a three-dimensional finite element model for the analysis of micropiles and calibrated it using the experimental results from a centrifuge study on micropiles. They demonstrated the suitability of the developed numerical model to simulate the lateral behavior of the micropiles under seismic loading. Similarly, Sadek and Shahrour (2004) employed a calibrated three-dimensional finite element model to analyze the response of inclined micropiles to seismic loading. Rose et al. (2013) developed a three-dimensional finite element model and calibrated it employing the results of a centrifuge study on groups of small diameter piles. The calibrated model was then employed to investigate the relative

effectiveness of perimeter small diameter pile groups in comparison with the more common grid configuration. They reported that block type failure was noticed when piles were placed at a spacing of less than 2 times the pile diameter.

Elsherbiny and El Nagggar investigated the axial performance of helical piles installed in sand. The created model was calibrated and verified against the full-scale load tests. A bearing capacity reduction factor and helix efficiency factor were proposed for helical piles installed in sand. Abd Elaziz and El Nagggar (2014) investigated the behaviour of single hollow bar micropiles embedded in silty clay soil using a 2D axisymmetric finite element model. The numerical model was calibrated using field test results and then was utilized to perform a parametric study. From the results of the parametric study, an equation was proposed to estimate the axial capacity of HBMP installed in cohesive soil. Alnuaim et al. (2016) investigated numerically the performance of micropiled rafts in sand. FE model was developed and calibrated and with the centrifuge tests, the performance of micropiled raft was investigated. They reported that the micropile raft system increases the tolerable bearing pressure by 190% compared to the isolated raft. Fahmy and El Nagggar (2017) conducted a 3D FE model to analyze the axial static behaviour helical tapered piles installed in sand. The developed model was calibrated and verified using the load-displacement curves from the field load tests. The analysis confirmed the ability of the numerical model to predict the behaviour of the tapered helical piles, and its larger mobilized shaft resistance compared to the straight piles. It was also demonstrated that the tapered piles capacity and stiffness are higher than that of the straight piles due to the increased confining pressure attributed to the pile configuration. The cavity expansion theory was first developed by Bishop et al. (1945) for metal applications. Yu and Houlsby

(1991) developed a semi-analytical solution for the expansion of a cylindrical cavity in elasto-plastic soils, which was widely used in geotechnical applications. The cavity expansion technique was utilized to simulate the changes in stresses around embedded structures (Randolph et al. (1979), Dijkstra et al. (2006), Newson et al. (2009), Satibi et al. (2009), Castro and Karstunen (2010), El Naggar and El Naggar (2012)).

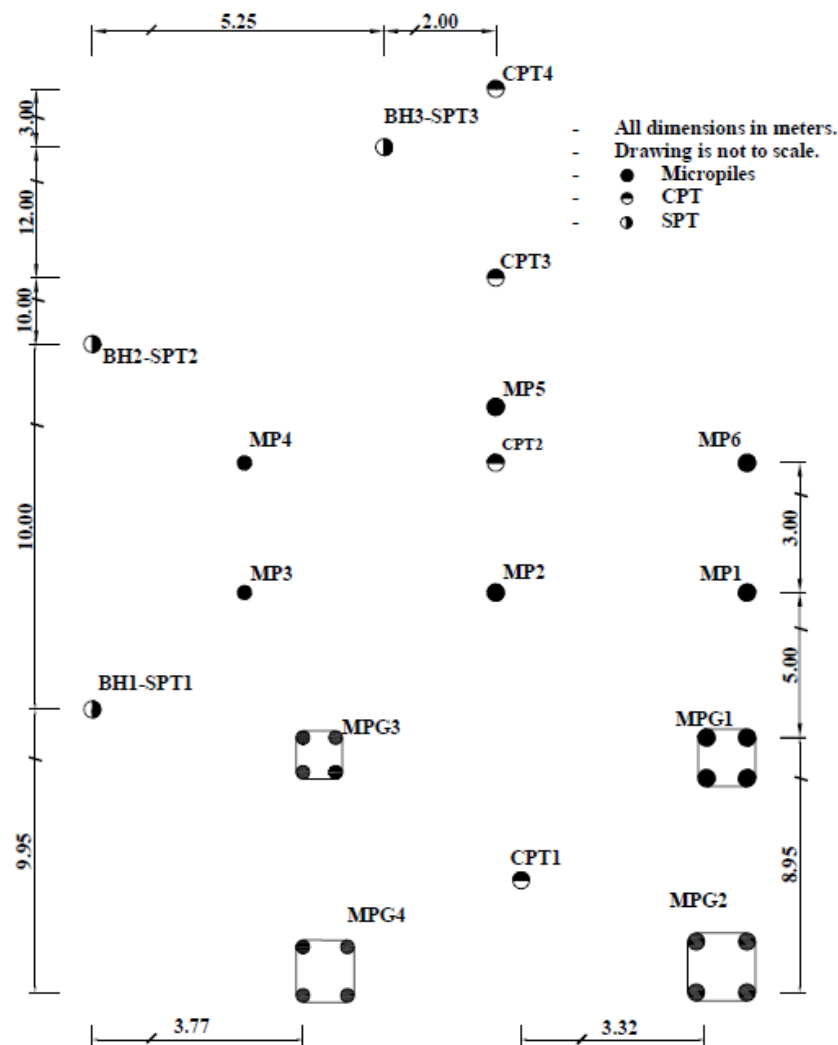
The performance of single micropiles and micropile groups installed in cohesionless soil was investigated through a full-scale field study as reported in previous chapters of this thesis. In this chapter, a three-dimensional finite element model was developed and calibrated using the soil properties and the field load tests results. To ensure that the calibrated model gave reliable results, the model was then validated using the field test results of micropiles installed with different diameters. The validated model was then used to perform a comprehensive parametric study.

The cavity expansion theory was used to simulate the installation effect and radial stress changes due to the micropiles installation. Displacement- controlled cavity expansion was used. A surface prescribed displacement was applied to a cylindrical cavity to replicate the increase in radial stresses during the micropile installation. The results obtained from the cavity expansion analysis were compared to the more common method of simulating the pile installation by increasing the  $K_0$  value to the back calculated value from the load test.

## **7.2 Installation of Micropiles**

As part of the experimental phase of this study, six hollow bar micropiles (MP1 to MP6) and four micropile groups (MPG1 to MPG4) were installed and subjected to axial centric loading. The micropiles were constructed utilizing R51N hollow bars with 51 mm outer

diameter and 33 mm inner diameter. Four single HBMP (MP1, MP2, MP5 and MP6) and two groups of HBMPs (MPG1 and MPG2) were installed with a 152 mm drill bit diameter resulting in diameter ratio of drill bit/ hollow bar ( $D_b/D_h$ ) of 3, and two HBMP (MP3 and MP4) along with two micropile groups (MPG3 and MPG4) were installed with a 115 mm drill bit diameter (i.e.  $D_b/D_h = 2.25$ ). Figure 7.1 shows the plan view for the location of single and groups of micropiles along with the SPT and CPT test locations.



**Figure 7-1 Plan view of micropiles locations, SPTs and CPTs (Dimensions in meters and Not to scale)**

### 7.3 Load Test Results

The single micropiles and micropile groups were subjected to axial loading to either failure or the limit of the reaction system and the load - settlement curves for the tested micropiles were obtained. The results of the field load tests are used to calibrate and validate the numerical models. Even though every precaution was taken to ensure the loading system used in the current study would facilitate loading the micropile groups to failure, it was realized during the testing program that it was not possible. Two groups, MPG3 and MPG4, were loaded to the ultimate load while the ultimate load for MPG1 and MPG2 was not reached. For MPG1, the loading hollow bar failed during loading and one of the reaction piles failed during the testing of MPG2. The soil parameters obtained from the site investigation are summarized in Table 7.1.

**Table 7-1 Soil parameters from the site investigation**

Parameter	Unit	Soil	Micropile
Effective friction angle, $\phi'$	°	42	--
Effective cohesion, $c$	kN/m <sup>2</sup>	1	--
Dilatancy angle, $\psi$	°	10	--
Modulus of elasticity	kN/m <sup>2</sup>	--	42e7
Triaxial loading stiffness, $E_{50}^{ref}$	kN/m <sup>2</sup>	65e3	
Unit Weight ( $\gamma_d$ )	kN/m <sup>3</sup>	19.5	24

## 7.4 Numerical Modeling

The finite element program PLAXIS 3D was used to develop the numerical model to study the performance of single micropiles and micropile groups. Full three-dimensional finite element models were developed in order to investigate the group interaction effects for micropile groups. The performed site investigation, including in-situ and laboratory tests, provided the soil parameters required for simulating the soil behavior in the numerical model. Additionally, the micropiles properties along with the strain gauges measurements obtained from the micropiles load tests provided the required information for developing and calibrating the finite element model. This information included the micropiles geometry and their mechanical strength parameters.

The pile installation method can have a significant impact on the stress field within the soil surrounding the pile. Based on several factors such as the soil density and type of pile, the lateral earth pressure coefficient after pile installation,  $K_s$ , can range from 0.5 to 5 (Lancellotta, 1995; Said, 2006; Satibi et al., 2009). This is particularly true for HBMP as its installation procedure can have a major effect on its performance as pressurizing the grout changes the initial geostatic field stress, which results in increasing the radial stresses around the micropile. The simplest method to account for the radial stress increase around the pile is to back figure an average value of  $K_s$  from the field load tests which can then be used to describe the appropriate stresses around the pile. However, this may result in unrealistic stress field around the micropile as the radial stresses are assumed to increase linearly with depth. On the other hand, the cavity expansion technique can provide a realistic stress field around the piles. The two methods are used to model the installation effect and the results will be discussed in detail.

## 7.4.1 Material Models

### 7.4.1.1 Soil Model

The soil was modeled using 10-node tetrahedral elements. The tetrahedral elements have three degrees of freedom per node,  $u_x$ ,  $u_y$  and  $u_z$ , and provide a second-order interpolation of settlements. The soil behavior is simulated using an elasto-plastic hardening soil model, which is incorporated in PLAXIS 3D (Schanz and Vermeer, 1998). This model requires the following soil parameters: unit weight, ( $\gamma$ ), cohesion ( $c$ ), friction angle, ( $\phi$ ), dilation angle, ( $\psi$ ), Poisson's ratio ( $\nu$ ), triaxial loading stiffness,  $E_{50}^{ref}$ , the triaxial unloading stiffness,  $E_{ur}^{ref}$  and the oedometer loading stiffness,  $E_{oed}^{ref}$ . The triaxial loading stiffness,  $E_{50}^{ref}$  was obtained by performing a drained triaxial test on sand samples retrieved from the test site under 100 kPa of confining pressure, which is referred to as the reference stress for stiffness,  $P^{ref}$ . The triaxial unloading stiffness,  $E_{ur}^{ref}$  and the oedometer loading stiffness,  $E_{oed}^{ref}$  were calculated from (Brinkgreve et al., 2015):

$$E_{oed}^{ref} = \frac{2}{3} E_{50}^{ref} \quad (7.1)$$

$$E_{ur}^{ref} = 3E_{50}^{ref} \quad (7.2)$$

### 7.4.1.2 Pile Model

The micropiles were modeled using non-porous volume elements. The linear elastic model, suitable for modeling stiff volumes in soil such as concrete elements (Brinkgreve et al.,

2015), was used to simulate the micropiles structural behaviour. It is based on Hook's law of isotropic elasticity, which is defined in terms of the micropiles Young's modulus and Poisson's ratio. The Young's modulus was obtained from the applied load and strain readings of strain gauges close to the ground surface (about -0.80 m). The micropile cap was modeled using a linear elastic model and placed 20 cm above the ground resulting in no contact between the cap and underlying soil.

### **7.4.1.3 Soil- Micropile Interface Model**

The soil-micropile interface was modeled using 12-noded interface elements (6 pairs of nodes); 6 nodes are connected to the 6 nodes of the soil element and 6 nodes are connected to the micropile elements. They are numerically integrated using 6-point Gauss integration. The distance between a node pair is zero. Each node has three translational degrees of freedom ( $u_x$ ,  $u_y$  and  $u_z$ ). The interface parameters are simulated using the shear strength properties of the surrounding soil and a strength reduction interface parameter,  $R_{int}$ , which is defined as a percentage of the shear strength of the soil. Table 7.2 summarizes the geotechnical parameters assigned to the hardening soil model for both soil and the soil-pile interface along with the linear elastic model parameters for micropiles.



**Table 7-2 Geotechnical parameters used in FEM**

Parameter	Unit	Soil	Soil -Pile Interface	Micropile
<b>Constitutive model</b>	--	Hardening Soil	Hardening Soil	Linear Elastic
<b>Effective friction angle, <math>\varphi</math></b>	°	42	42	--
<b>Effective cohesion, c</b>	kN/m <sup>2</sup>	1	1	--
<b>Dilatancy angle, <math>\psi</math></b>	°	10	10	--
<b>Modulus of elasticity</b>	kN/m <sup>2</sup>	--	--	42e7
<b>Triaxial loading stiffness, <math>E_{50}^{ref}</math></b>	kN/m <sup>2</sup>	65e3	65e3	--
<b>Triaxial unloading stiffness, <math>E_{ur}^{ref}</math></b>	kN/m <sup>2</sup>	43e3	43e3	--
<b>Oedometer loading stiffness, <math>E_{oed}^{ref}</math></b>	kN/m <sup>2</sup>	195e3	195e3	--
<b>Poisson's ratio (<math>\nu</math>)</b>	--	0.3	0.3	0.2
<b>Unit Weight (<math>\gamma_d</math>)</b>	kN/m <sup>3</sup>	19.5	19.5	24
<b>Interface reduction factor, <math>R_{int}</math></b>	--	--	0.90	--

### 7.4.2 3D Mesh Geometry

The soil and pile were simulated in three-dimensional (3D) space. The geometry of the soil-pile model simulated the full-scale micropile test setups as close as possible. The 3D

mesh dimensions are selected to ensure that the boundaries are placed far enough from the test specimens to not affect the results. This was ascertained through a mesh sensitivity study. The locations of the boundaries were optimized by extending the distance to the boundaries until there was no noticeable change in the stresses at the boundaries. Based on the sensitivity analysis, the vertical boundaries for single micropiles were placed at a distance of  $15D$  measured from the center of micropiles. The bottom boundaries were extended to a distance of two times the micropile length for the K-pressure method, while for the cavity expansion method the vertical boundaries were placed at a distance of  $25D_p$  (where  $D_p$  is micropile diameter). For the micropile groups, the vertical boundaries were placed at  $12S$  (where  $s$  is spacing between micropiles center-to-center) measured from the center of the micropile for cavity expansion method and  $9S$  for the K pressure method. The top boundary of the model was considered as a stress-free boundary while the translation of the bottom boundary was restrained in three directions: X, Y and Z. The vertical boundaries of the soil block were set to move freely in the Z direction and constrained in the horizontal directions, X and Y.

The mesh was refined around the micropile circumference and the micropile base where non-linear behaviour was anticipated in order to reach the optimum solution and capture the system performance. As a result of the mesh refinements, the total number of the model elements ranged from 141237 to 168385 and the average element size ranged from 0.153 to 0.173 m for micropile groups while for single micropiles the number of elements was around 43048 elements and the average size of the elements was 0.067.

### 7.4.3 Increasing $K_o$ Method

In this approach, the geostatic stresses were defined in the first step of analysis as the in-situ soil condition. The vertical effective stresses are increased linearly with depth below the ground surface while the radial stresses are increased as a function of vertical effective stresses and the coefficient of lateral earth pressure at rest,  $K_o$ , which is given by:

$$K_o = 1 - \sin \phi' \quad (7.3)$$

In the second step of analysis, the radial stresses are assumed to increase linearly with depth according to the lateral earth pressure coefficient after micropile installation,  $K$ , times the vertical stresses. The  $K$  value can be back calculated from the field load test results and. After applying the radial stresses using the  $K$  value, the load was applied in step number 3 of the analysis as a prescribed displacement until failure occurred. In this approach the radial stresses are increased for the whole soil volume and not just around the pile.

### 7.4.4 Cavity Expansion Method

In this method the pile installation is simulated by applying a uniform prescribed displacement on a cavity wall. The cylindrical cavity expansion is modeled as prescribed displacement because this approach ensures numerical stability of the analysis (Kirsch, 2006; Castro and Karstunen, 2010). In the first step of this analysis method, the in-situ condition is simulated by applying radial stresses which increase linearly with depth equal to the effective vertical stresses times  $K_o$ . In the second step of this analysis, the cavity is created by removing volume elements equal to the volume of the micropile using the original drill bit diameter and a prescribed surface radial displacement is applied to the cavity wall. By imposing the prescribed displacement on the cavity wall, the radial stresses

increased around the micropile volume. At the same time, vertical stresses are applied to the bottom part of the cavity equal to geostatic stresses at this level. The prescribed displacement in this step was selected based on the actual increase in micropile diameter over the drill bit diameter. Micropiles were exhumed and their actual size was measured and used in the analysis. The drill bit radius is denoted as  $a_o$  and was considered as the initial cavity radius while the actual measured radius was considered as the final target radius and denoted as  $a_f$ . In the final stage, after the cavity expanded to the required prescribed displacement, the micropile was placed in the cavity with the measured diameter and the prescribed displacement was removed. In the final step of analysis, the load was applied to the micropile head by means of a described displacement until failure occurred.

## **7.5 Numerical Analysis Procedure**

### **7.5.1 Model Calibration and Verification**

The micropile material properties were back calculated from the strain gauge results. The soil properties utilized in the initial calibration were obtained from the site investigation and were considered representative of the soil behaviour. These initial values were adjusted slightly in order to calibrate the model by comparing the load-settlement curves predicted by the numerical model with those obtained from the field load tests. The initial value of effective angle of internal friction was  $42^\circ$  and the dilation angle was  $10^\circ$  as obtained from direct shear test. The micropile equivalent elastic modulus,  $E_p = 42 \times 10^6 \text{ kN/m}^2$  was used in the calibration process as a representative value for the non-porous linear elastic volume elements. The values of the lateral earth pressure coefficient,  $K$ , were back figured from the frictional resistance of the micropile shafts during the field load tests and varied from 3.5 to 3.7.

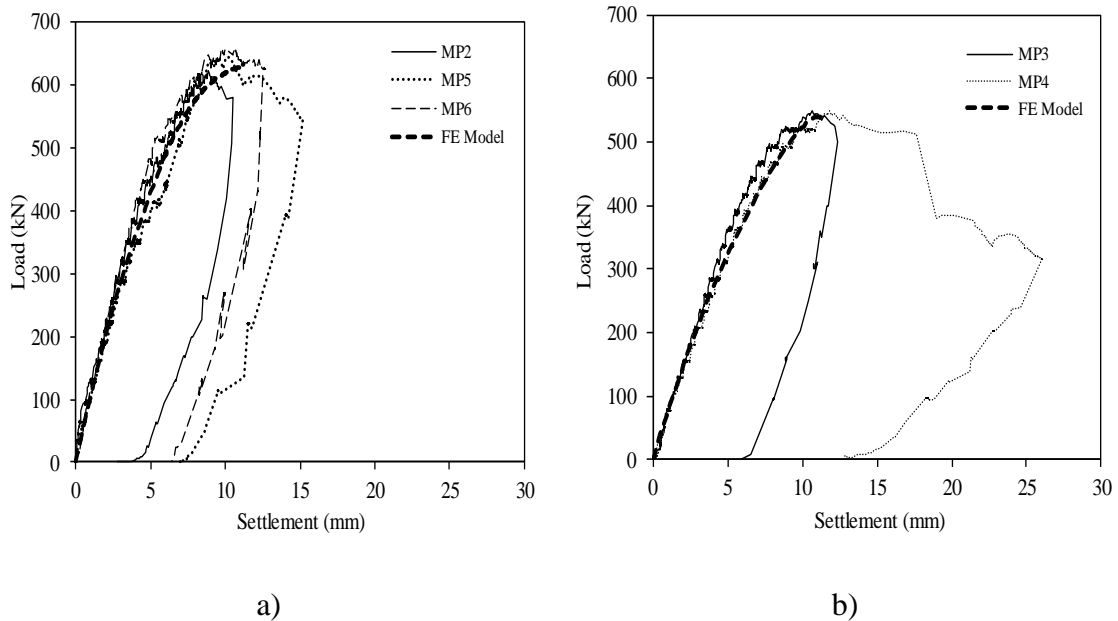
In the analysis that simulated by installation effect by increasing  $K$ , the coefficient of lateral earth pressure was varied in order to match the load – settlement curves. The coefficient of lateral earth pressure was found to be 3.4 and 3.71 for micropiles with  $D_b/D_h = 3$  and 2.25, respectively, which gave the best match of the load- settlement curves to the field load test results. For the cavity expansion method, prescribed horizontal displacements of 10 mm and 12 mm were applied to the cavity surface walls for micropiles with  $D_b/D_h = 3$  and  $D_b/D_h = 2.25$ , respectively. The reason for applying a larger prescribed displacement for micropiles installed with  $D_b/D_h = 2.25$  in the numerical analysis is due to the increase in the lateral earth pressure coefficient. The higher value for micropiles with  $D_b/D_h = 2.25$  replicated the observed increase in the micropile diameter from field tests. This is attributed to applying the same grouting pressure in the installation for all micropiles, but the smaller drill bit had smaller nozzles than the large drill bits, which resulted in increased grout velocity (and hence diameter increase) for micropiles installed with 115 mm drill bit.

### **7.5.2 Single Micropiles**

The developed model was initially calibrated using the load-settlement curves for single micropiles MP2, MP5, and MP6, which have a diameter  $D_p = 172$  mm. To verify the developed model, the calibrated model was used to predict the response of micropiles with  $D_p = 132$  mm using the same parameters and boundary conditions. The results were compared to micropiles MP3 and MP4.

The results obtained from the analysis that simulated pile installation by increasing  $K_o$  value are compared to the experimental observations in Figure 7.2 (a and b). As it can be noted from Figure 7.2, the calculated responses agree well with the field test results. This

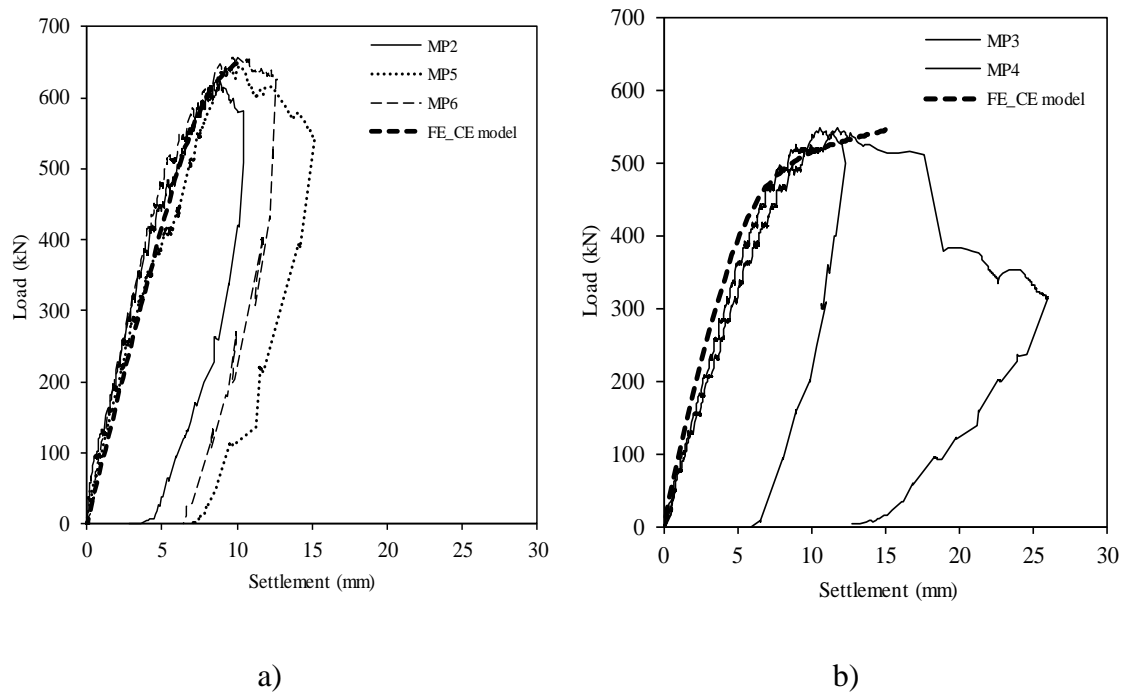
verifies the ability of the numerical model to predict the response of micropiles subjected to axial loading.



**Figure 7-2 FE model calibration and verification using increasing  $K_o$  method: a)  $D_b/D_h = 3$ ; and b)  $D_b/D_h=2.25$**

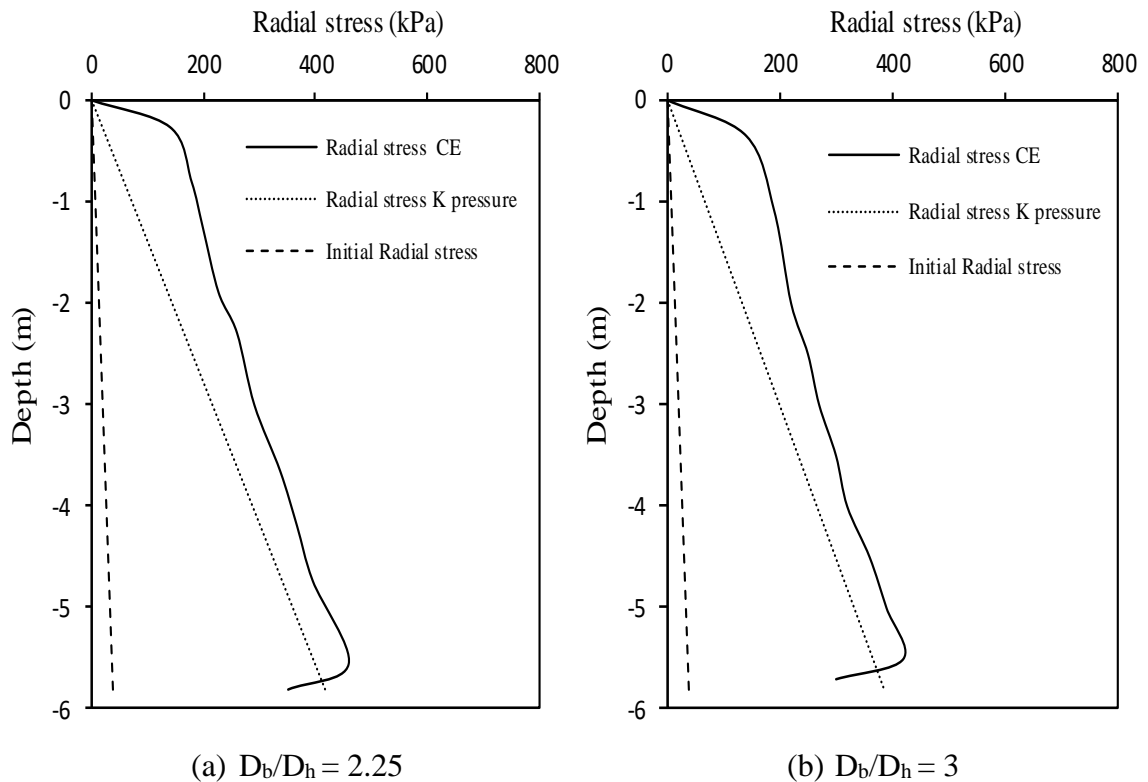
The load – settlement curves obtained using the cavity expansion technique are compared to the measured response in Figure 7-3. As shown in Figure 7-3, the load – settlement curves predicted from the numerical models agree well with the measured curves.

Both methods seem to give a reasonable match to the load – settlement curves. However, the variation of the radial stresses with depth varied between the two methods as shown in Figure 7-4.



**Figure 7-3 FE model calibration and verification using Cavity Expansion method: a)  $D_b/D_h = 3$ ; and b)  $D_b/D_h = 2.25$**

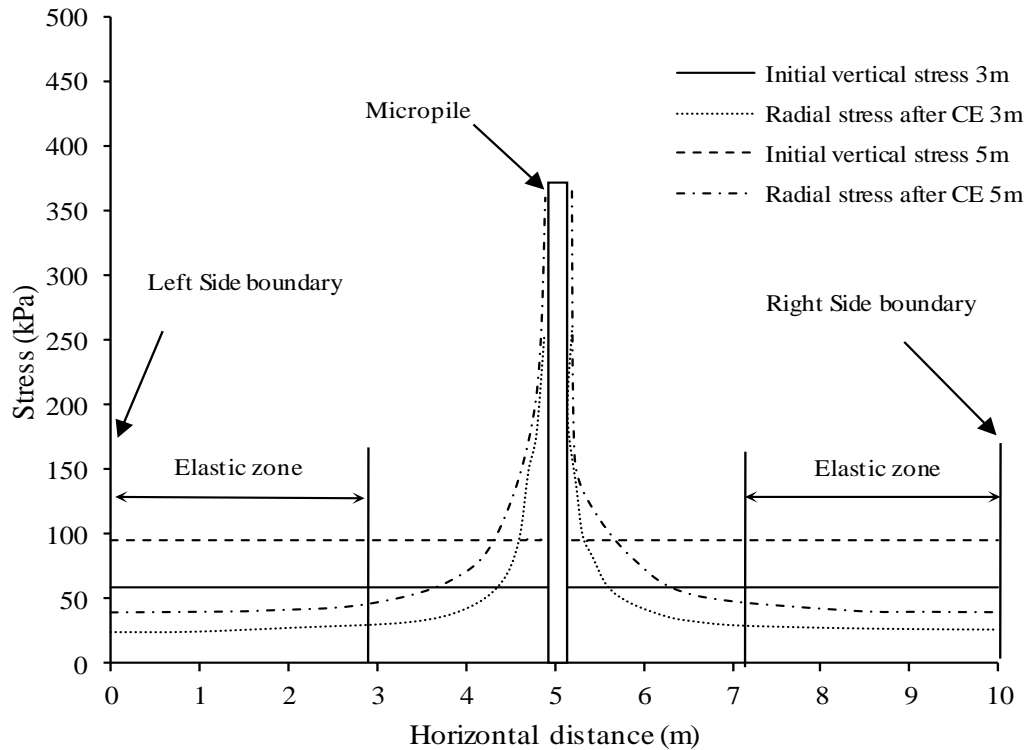
In the analysis simulating micropile installation by increasing  $K$ , the radial stresses increased linearly with depth. For the analysis that employed cavity expansion to simulate micropile installation, the radial stresses increased significantly close to the ground surface, then increased linearly with depth to an elevation slightly above the micropile toe, then decreased afterwards. The reduction of radial stresses close to the micropile toe could be attributed to the fact that the micropile toe settles during loading which can drag the surrounding soil. The soil beneath the toe tends to displace the adjacent soil which creates an arching effect. The same behaviour was observed by Vesic (1963); Touma and Reese (1974), and Satibi and Vermeer (2009).



**Figure 7-4 Radial stress vs depth at the interface using cavity expansion (CE) and  $K_0$  pressure method**

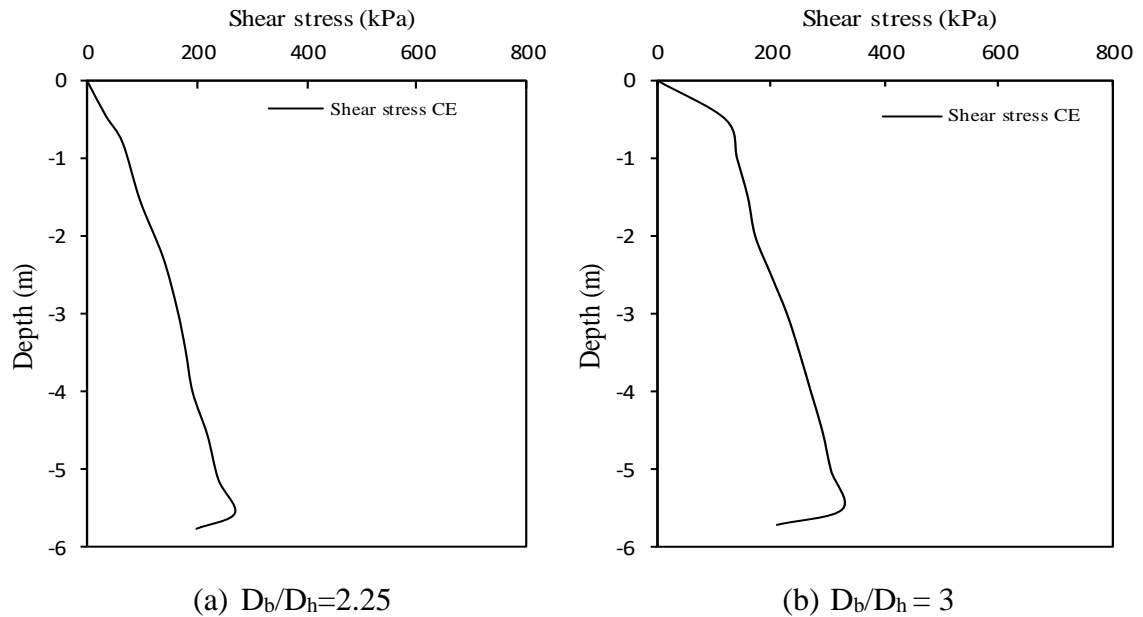
For micropiles with  $D_p = 172$  mm, the vertical and radial stresses at 3 m and 5 m depths are plotted in Figure 7-5. The plot shows that the elastic zone extended to about 12 times the diameter of the micropile from the center of the micropile. This highlights the importance of placing the side boundaries of the finite element model for a single HBMP at a distance not less than 15 times its diameter when using a prescribed displacement to simulate the installation effects.





**Figure 7-5 Stresses at 3m and 5 m depth using cavity expansion**

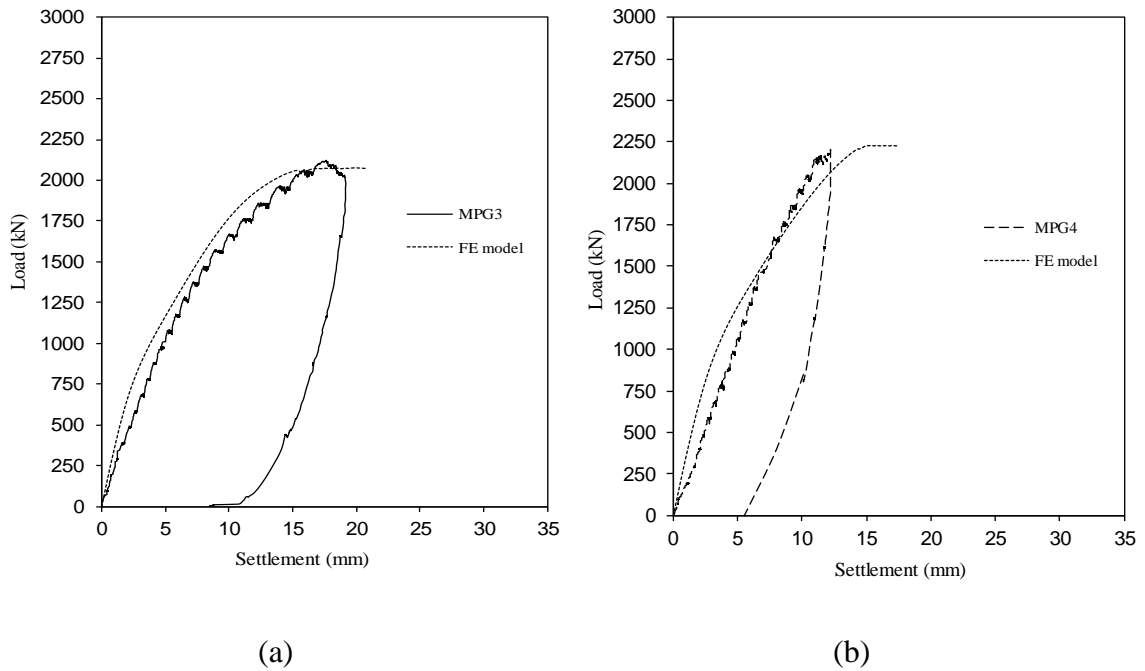
The interface shear stresses along the micropile depth obtained from the cavity expansion analysis are shown in Figure 7-6. As expected, the interface shear stresses follow the pattern of radial stresses presented in Figure 7-4. The increase in the interface shear stresses underscores the advantageous load transfer mechanism of hollow bar micropiles. It should be noted the curves shown in Figure 7-5 are obtained by curve fitting the results from the finite element analyses using fourth polynomial functions because the actual numerical predictions are zigzagging as a result of the numerical integration.



**Figure 7-6 Shear stress vs depth using Cavity Expansion (CE)**

### 7.5.3 Micropile Groups

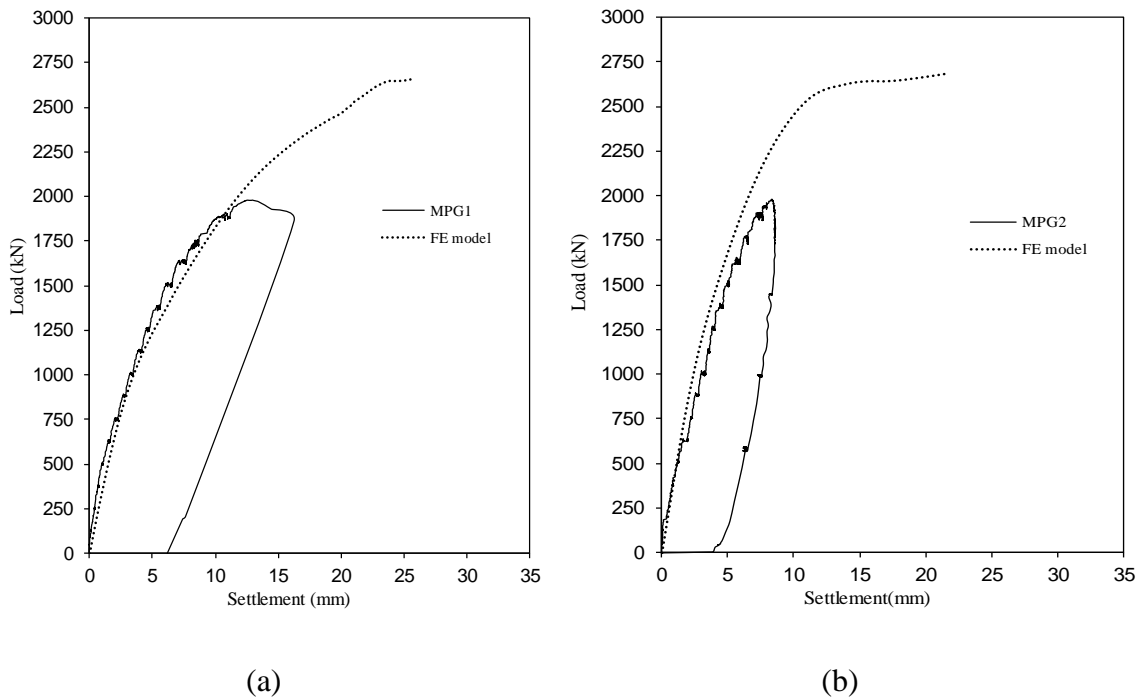
A numerical model was developed utilizing the same geotechnical parameters employed in the analysis of single micropiles and simulated the micropile installation by increasing the K value. As both methods gave similar load – displacement curves when analyzing the single micropiles, K pressure method was used to analyze the micropile group for the sake of time. The numerical model was utilized to calculate the load - settlement curves of two micropile groups, MPG3 and MPG4. The results were compared with those obtained from the field load tests in Figure 7-7. The calculated and measured responses agree well, which further verifies the ability of the numerical model to predict the response of micropile groups to axial loading. However, the numerical model predicts a slightly stiffer response during the initial part of loading. As can be noted from Figure 7-7, the calculated response extended the applied load until plunging failure was predicted to facilitate the evaluation of the pile group ultimate capacity.



**Figure 7-7 Comparison between Load-settlement curves for MPG3 and MPG4 from field tests and Increasing  $K_0$  Method**

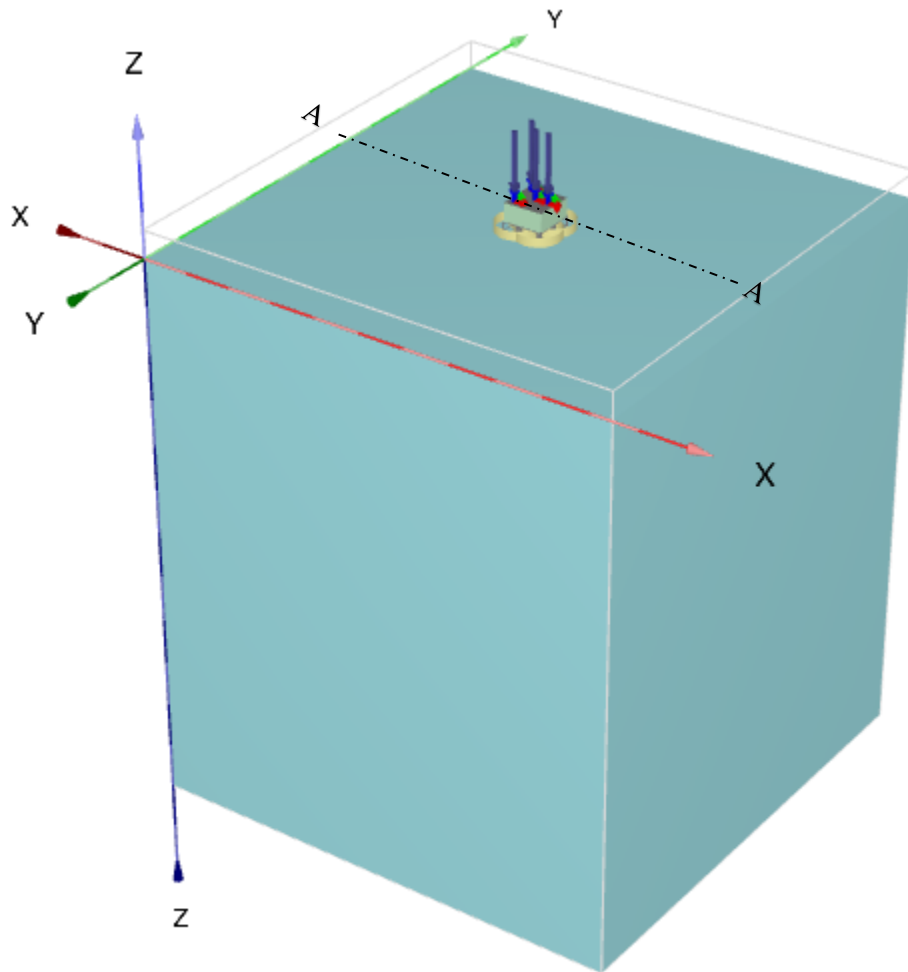
The same numerical model was then employed to analyze the response of micropile groups MPG1 and MPG2. The loading was also extended until plunging failure was predicted. The load- settlement curves obtained from the field loading tests for MPG1 and MPG2 are plotted in Figure 7-7 along with the load - settlement curves predicted from the developed finite element model. In general, the predicted response was in good agreement with the measured response.

The calculated load - settlement curves of micropile groups were utilized to establish their ultimate axial load capacity. The predicted ultimate capacity of the micropile groups obtained from the numerical results confirm that the group efficiency for groups installed with  $s = 3D_b$  or  $5D_b$  is between 0.97 and 1.06.

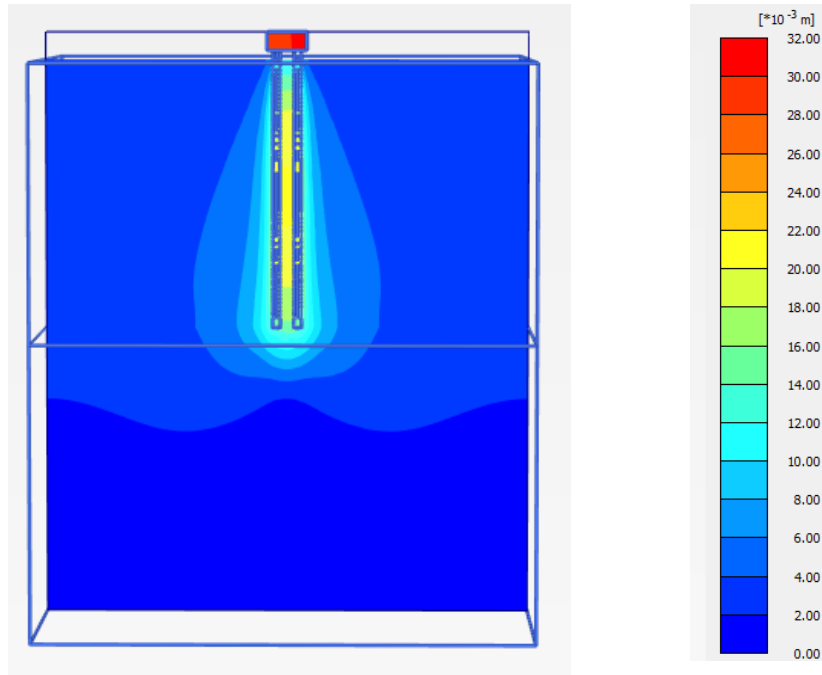


**Figure 7-8 Comparison between Load-settlement curves for MPG1 and MPG2 from field tests and Increasing  $K_0$  method**

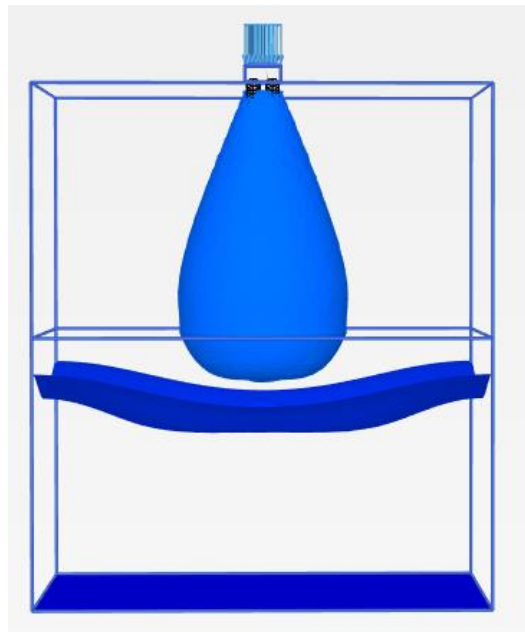
A cross-section through the soil volume in the center of MPG1 was taken to demonstrate the interaction among the micropiles within the group and the mobilized shear strength. The location of the cross-section is shown in Figure 7.9. The micropile group settlement at section A-A is shown in Figure 7.10. As it can be seen from Figure 7.10, the interaction is clear between the micropiles and the deformation contours show the displacement distribution around the micropile group. The Iso surface for the vertical displacement of MPG1 is shown in Figure 7.11, which indicates a clear contour of soil movement around the micropile group, which extends to almost 1.5 times the width of the micropile group on either side.



**Figure 7-9** Location of cross section A-A

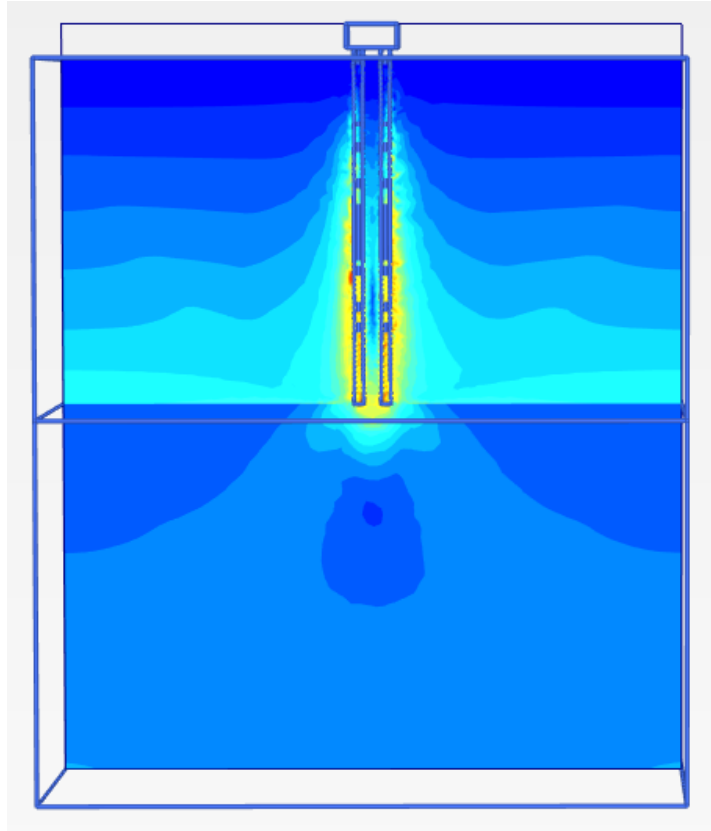


**Figure 7-10 Settlement contours for section A-A**



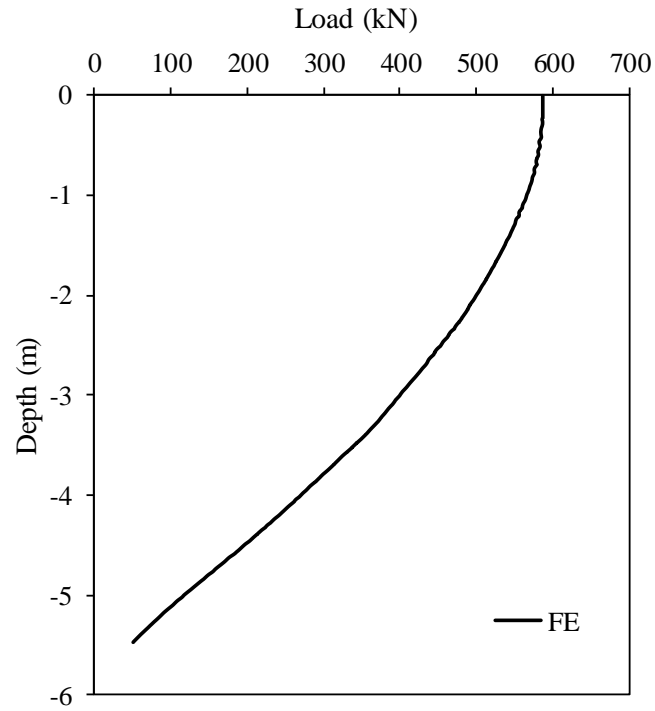
**Figure 7-11 Iso surface for vertical settlement of MPG1**

The mobilized shear strength of the soil around MPG1 is shown in Figure 7.12. As it can be seen from Figure 7.12, the failure occurred around the shaft surfaces along the micropile length and immediately beneath the micropile group.

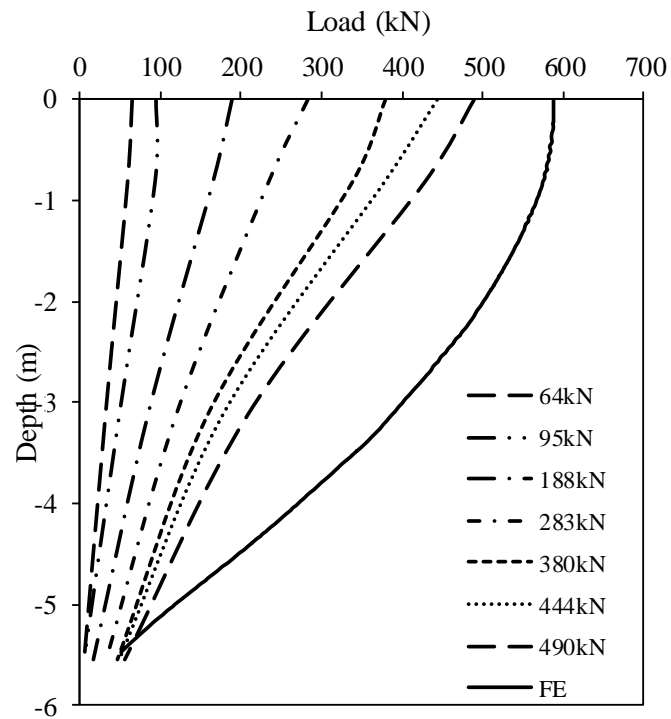


**Figure 7-12 Mobilized shear strength of MPG1**

As mentioned previously, the load test was stopped pre-maturely for MPG1 was stopped for safety reasons and failure was not achieved. Therefore, the loading was continued in the numerical model to mobilize the full resistance of the micropiles and achieve failure. The load distribution with depth obtained from the numerical model is presented in Figure 7.13. The load distribution obtained from the numerical model was used to establish the load distribution of MPG1 along the pile shaft and is shown in Figure 7.14.



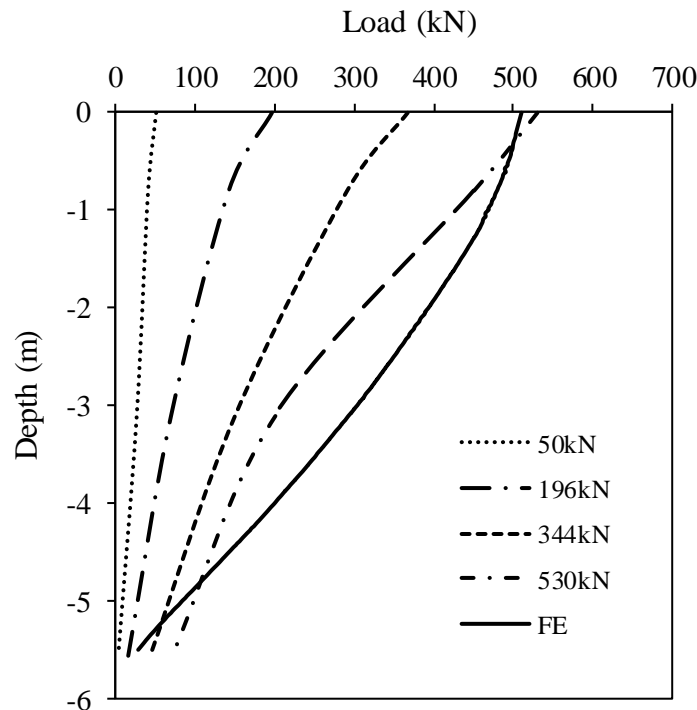
**Figure 7-13 Load distribution with depth obtain from FEM for MPG1**



**Figure 7-14 Completing the load distribution of MPG1 (FEM)**

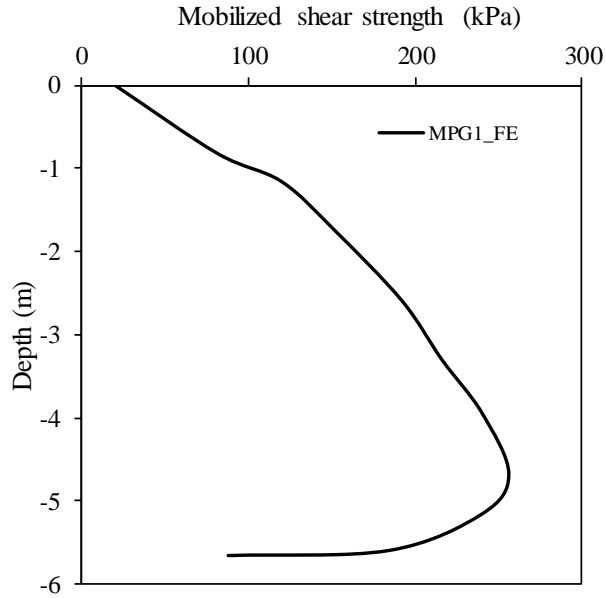


The variation of load distribution along the pile shaft obtained from finite element model is gradual, unlike that obtained from the load distribution evaluated from strain gauges during the load tests. This is because the strain gauges readings were recorded at only three different levels while for the numerical model there was continuous distribution with depth. The load distribution with depth for MPG3 is shown in Figure 7.15, which also demonstrates gradual variation with depth. Besides, it demonstrated a smaller toe resistance compared to the load distribution obtained from the strain gauges. It should be noted that the soil profile changed slightly from location to another as it can be seen from the SPT and CPT results. Thus, it is expected that the soil properties would be different and consequently the micropiles resistance would also differ.

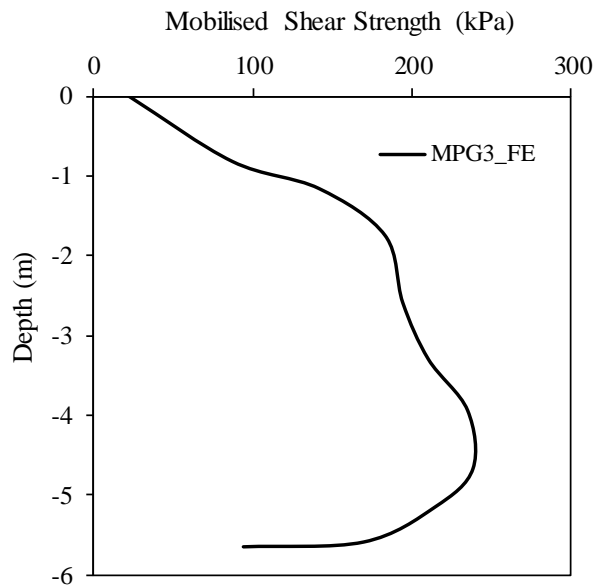


**Figure 7-15 Comparing load distribution from FEM and strain gauges**

The mobilized shear strength profiles at the pile-soil interface for MPG1 and MPG3 are presented in Figure 7.16 and 7.17, respectively.



**Figure 7-16 Mobilized shear strength of MPG1 at micropile-soil interface**



**Figure 7-17 Mobilized shear strength of MPG3 at micropile-soil interface**

The mobilized shear strength profiles for both micropiles groups are similar. The mobilized strength increased with depth, but declined towards the toe, which is in agreement with the skin friction distribution reported by O'Neil and Reese (1970). This decrease in shaft resistance close to the micropile toe is caused by the so-called trap-door effects as it was first explained by Terzaghi in 1936.

## **7.6 Parametric Study**

The calibrated and verified finite element models are utilized to perform a parametric study to investigate the effect of several factors that were not examined in the field testing program due to cost and time limitations. Specifically, this parametric study investigates the effect of soil strength parameters and micropiles slenderness ratio on their ultimate capacity. Furthermore, the effect of micropile-soil interface condition was investigated. The lateral earth pressure coefficient, Poisson's ratio, and micropile strength parameters were kept constant throughout the parametric study. The parametric study was performed on micropile MP1.

### **7.6.1 Soil Strength Parameters**

The analysis covered a practical range of the soil effective angle of internal friction angles and secant triaxial loading stiffness values, representing sand with different relative density (i.e. very loose, loose, medium dense, and dense). The soil properties of the six considered cases are based on Obrzud and Truty (2012) and are summarized in Table 7-3.

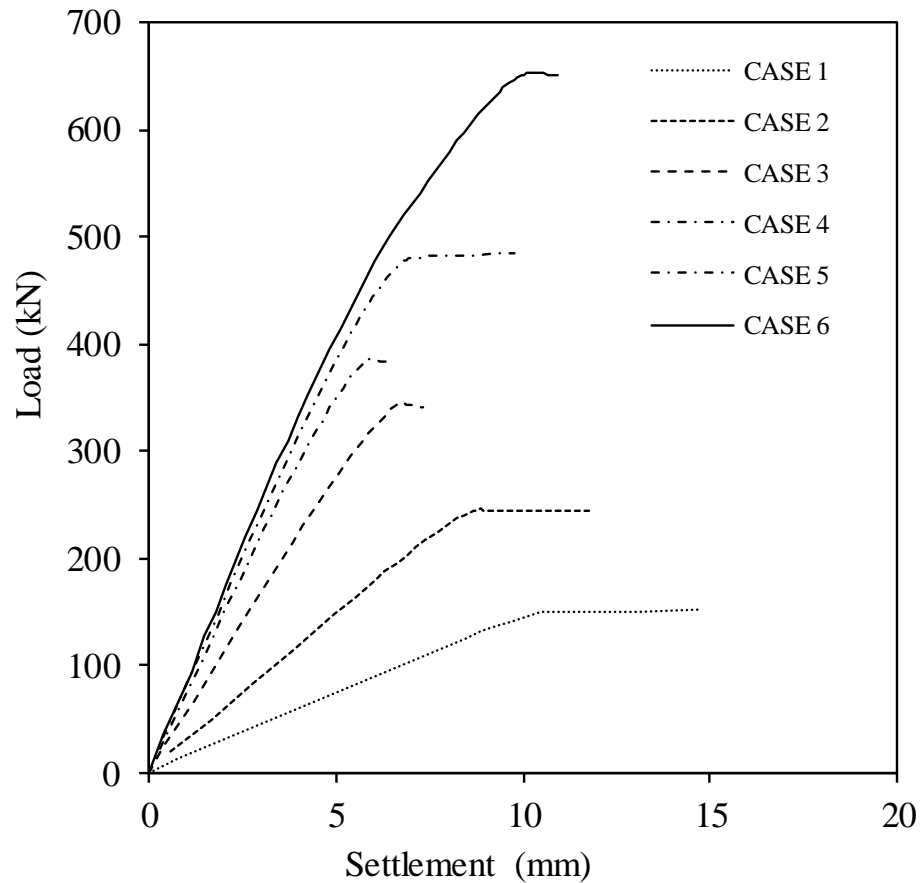
**Table 7-3 Soil Parameters used in the parametric study**

<b>CASE</b>	<b>Relative density D<sub>r</sub> (%)</b>	<b>Unit weight (kN/m<sup>3</sup>)</b>	<b>Effective friction angle</b>	<b>Triaxial loading stiffness (kN/m<sup>2</sup>)</b>
<b>CASE 1</b>	Very loose sand	16	25	10
<b>CASE 2</b>	Loose sand	17.5	30	20
<b>CASE 3</b>	Medium sand	18.5	35	40
<b>CASE 4</b>	Dense sand	19	37	55
<b>CASE 5</b>	Dense sand	19.2	40	60
<b>CASE 6</b>	Very dense sand	19.5	42	65

Figure 7- 18 shows the load – settlement curves for the six considered cases. As expected, the stiffness and ultimate capacity increase with the increase in soil strength parameters. The values of ultimate bond strength were back calculated and compared with the values suggested by FHWA for micropiles Type B in Table 7-4.

Inspecting Table 7-4, the predicted ultimate bond strength values for Cases 1 and 2 (very loose to loose sand) are less than the minimum value of ultimate bond strength suggested by FHWA for Type B micropiles. However, the values suggested by FHWA are for loose-medium dense sand not very loose sand. For cases 4 and 5, (i.e. medium to dense sand), the ultimate bond strength values are close to the lower boundaries suggested by FHWA for Type B micropiles. Comparing the average ultimate bond strength values provided by FHWA to the ultimate bond strength values obtained from the finite element models, the

average values provided by FHWA are higher than the values obtained from the finite element analysis.



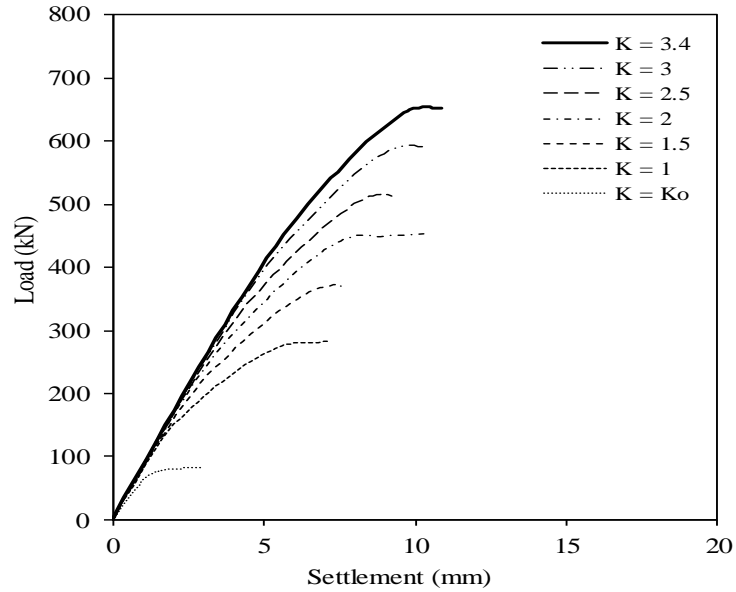
**Figure 7-18 Load vs settlement curves for different soil parameters**

On the other hand, the ultimate bond strength values obtained from the finite element models for Cases 3 to 6 are within the range of values suggested by FHWA for loose-medium dense sand and medium to very dense sand.

**Table 7-4 Comparison between ultimate bond strength values from FE and FHWA**

<b>CASE</b>	<b>Ultimate bond strength (FE), kPa</b>	<b>Ultimate bond strength, Type B (FHWA, 2005), kPa</b>	<b>Average ultimate bond strength (FHWA,2005), kPa</b>
<b>CASE 1</b>	48	70 - 190	130
<b>CASE 2</b>	64	70 – 190	130
<b>CASE 3</b>	99	70 – 190	130
<b>CASE 4</b>	112	120 – 360	240
<b>CASE 5</b>	131	120 – 360	240
<b>CASE 6</b>	190	120 – 360	240

The lateral earth pressure coefficient is an important pile design parameter and can be back figured from the numerical results. Figure 7-19 shows the effect of the lateral earth pressure coefficient on micropile performance and capacity. The value was increased from the lateral earth pressure coefficient at rest to the value back figured from the load test to show the effect of this parameter on the pile’s capacity. All other soil and pile parameters were kept constant during this analysis to investigate the effect of the lateral earth pressure coefficient. As expected, the micropile stiffness and ultimate capacity increased as K increased, underscoring the advantageous effect of the pressurized grout used in the construction of HBMP.



**Figure 7-19 Effect of Lateral earth pressure coefficient on micropile performance**

### 7.6.2 Slenderness ratio

To investigate the effect of the micropiles slenderness ratio,  $L/D$ , an analysis was performed for three values: 20, 33.5 and 50. The micropile diameter was kept constant and the length was increased from 3.45 m to 8.6 m. The results are summarized in Table 7.5 in terms of the ultimate failure load. The average failure load for micropiles with a diameter of 172 mm ( $L/D = 33.5$ ) is also included in Table 7.5. It is expected that the ultimate bearing capacity would increase as the pile length increase. However, the rate of increase in the ultimate capacity is not linear as the length of micropile increases. As the micropile length increased from 3.45 m to 5.75 m which is 67% of increase, the ultimate micropile capacity increased by 168.3%. Furthermore, as the micropile length increased from 5.75 m to 8.6 m which is 50% of increase, the ultimate micropile capacity increased by 70%.

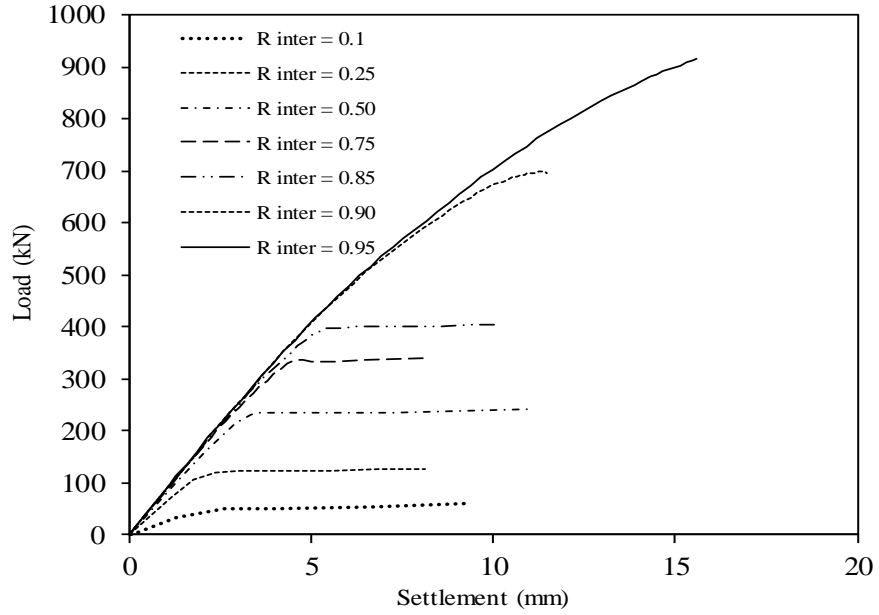
**Table 7-5 Summary of the effect of slenderness ratio on the failure load**

CASE	Failure load (kN)	Max settlement (mm)
L/D = 20	240	5.0
L/D = 33.5	644	10.2
L/D = 50	1100	15.4

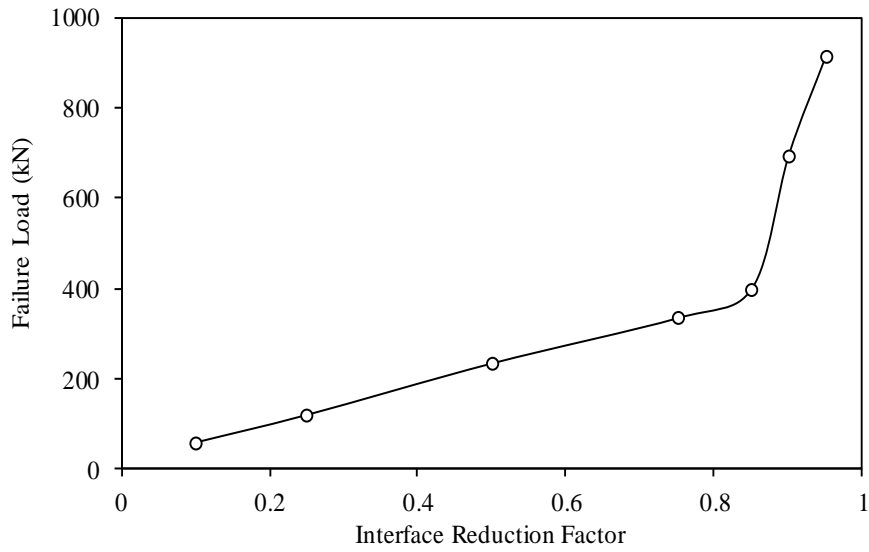
### 7.6.3 Interface Reduction Factor ( $R_{inter}$ )

The strength at the pile-soil interface is simulated using the shear strength properties of the surrounding soil and a strength reduction interface parameter,  $R_{int}$ , which is defined as a percentage of the shear strength of the soil. The interface reduction factor varied from 0.1 to 0.95. The load – settlement curves for various interface reduction factor values are shown in Figure 7-20. The figure shows the influence of the interface reduction factor on a micropiles performance and capacity. The failure load increased from about 60 kN for  $R_{inter} = 0.1$  to more than 915 kN for an interface reduction factor equal to 0.95,  $R_{inter} = 0.95$ . As expected, the failure load increased almost linearly as the interface reduction factor increased from 0.1 to 0.85. However, the failure load increased significantly as the interface reduction factor exceeded 0.85. The sudden increase in the failure load as the interface reduction factor exceeded 0.85 is believed to be as a result of changing the failure mechanism from the shear band failure at the pile-soil interface to form a block failure extended to the surrounding soil. The effect of increasing the interface reduction factor on the failure load is shown in Figure 7-21.





**Figure 7-20 Effect of the interface reduction factor on micropile performance**



**Figure 7-21 Effect of the interface reduction factor on the failure load of micropiles**

### 7.6.4 Number of Micropiles in the Group

To study the effect of different micropile group configurations, a full 3D FE model was created for a micropile group consisting of nine micropiles (3 X 3), each with a diameter of 172 mm, and spacing,  $s = 5D_b$ . The same soil parameters used in this model are the same used for modelling MPG1 and MPG2. Figure 7-22 shows the finite element model utilized with the dimension and the boundaries from the micropile group. The mesh was made finer around the micropiles where large stress changes was anticipated to occur.

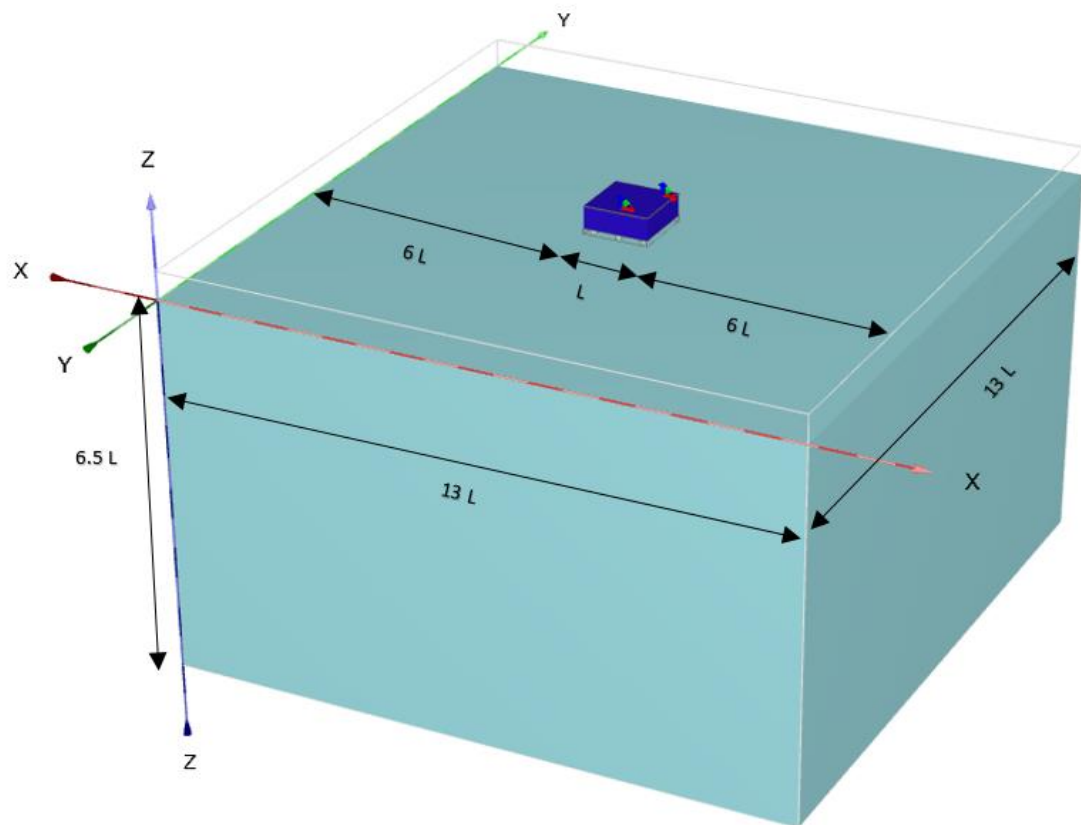
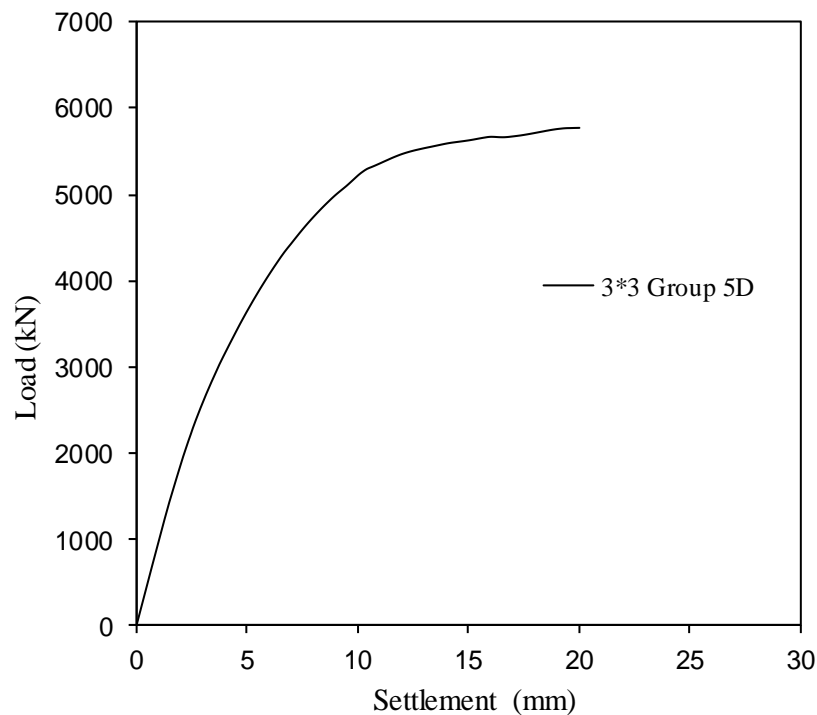


Figure 7-22 Full 3D model with deformed mesh.

Figure 7-23 shows the load - settlement curves for the nine-micropile group. The load – settlement curve shows three main regions. The first region is a linear elastic portion which extends up to a load of 2670 kN with a vertical settlement equal to 2.38 mm. The maximum linear elastic load is approximately 46% of the failure load, which is 5750 kN, and the elastic settlement is equal to 1.38% of the micropile diameter. The second region is the nonlinear portion, which extends to a vertical settlement of 15.2 mm at an applied load of 5620 kN of applied load. The final region extends to the failure load of 5750 kN, which occurred at 19.8 mm (i.e. 11.5% of the micropile diameter). The nine micropiles group efficiency (3\*3) is equal to unity which confirms the findings of the field test results of micropile groups with four micropiles (2\*2).



**Figure 7-23 Load vs settlement of 3\* 3 micropiles group**

### 7.6.5 Spacing to Diameter Ratio of Micropile in the Group

To investigate the effect of spacing between the micropiles in the group, two more spacing to diameter ratio were considered;  $2D_b$  and  $4D_b$  as micropile groups of  $3D_b$  and  $5D_b$  were modeled and used in the calibration and verification of the finite element model. The results are presented in terms of load – settlement curves in Figure 7-24. The effect of the interaction between the micropiles in the group is more evident at higher settlement due to the interaction effect as it can be seen in Figure 7-24. The group efficiency ranges from 0.99 for 2D spacing between the micropiles to up 1.06 for 5D spacing. Briaud et al. (1989) reported a similar finding of group efficiency equal to 0.99 for five pile group installed in medium dense sand with a spacing to diameter ratio of 3.4.

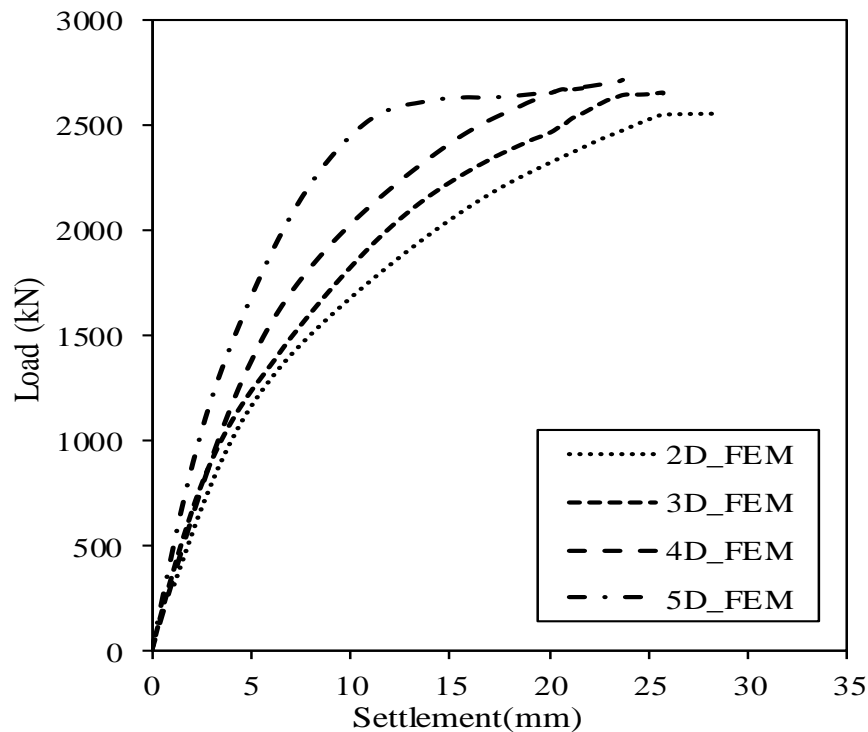
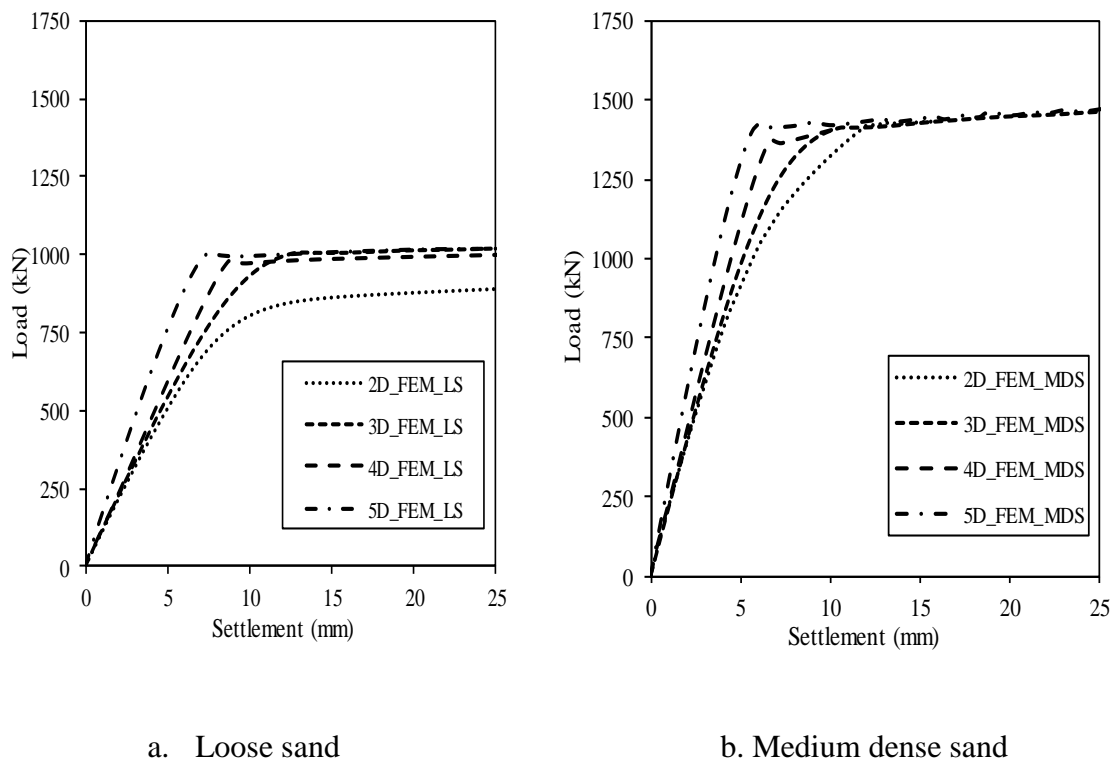


Figure 7-24 Load vs settlement for different spacing between micropile groups

### 7.6.6 Effect of Relative Density on Performance of Micropile Group

To investigate the effect of relative density on the group efficiency, two cases were considered; loose sand and medium dense sand as they are defined in Table 7.3 by Case 2 and Case3, respectively. Case 6 which represents the dense sand was analyzed in the previous section. Furthermore, each case was investigated considering four different spacing to diameter ratio ranged from 2D to 5D. The results are shown in Figure 7.25.



**Figure 7-25 Effect of relative density on the load - settlement curves of micropile group with different s/D ratios.**

Considering the load – displacement curves from Figure 7.25, the group efficiency for different spacing to diameter ratios were obtained. The group efficiency is close to unity for all the groups except for loose sand with spacing to diameter ratio equal to 2 where the

group efficiency was less than unity, 0.87 which can be contributed to stress overlapping between the micropiles. Using a factor of safety equal to 2, the design load was obtained as the failure load from Figure 7.24 and 7.25 divided by two. The micropile stiffness which defined as the ratio of the design load to the corresponding settlement was calculated and compared in Table 7.6.

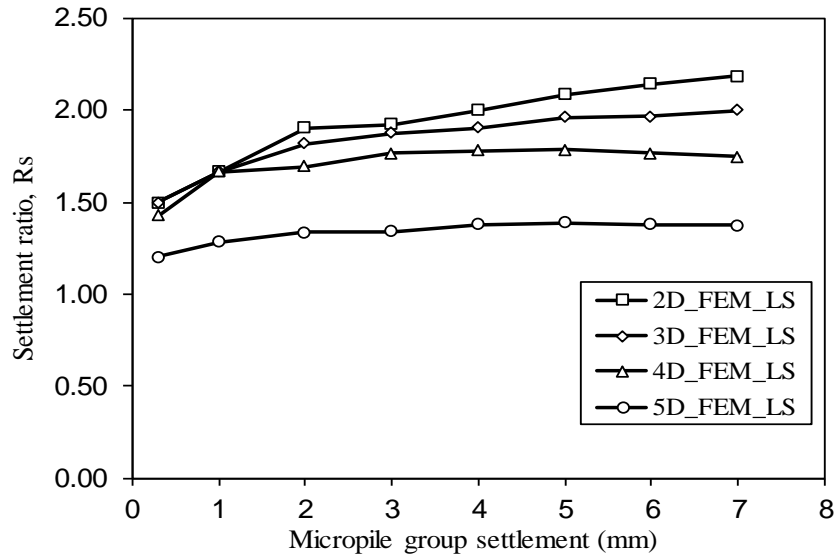
**Table 7-6 Micropile group stiffness with different s/D**

<b>Design micropile stiffness (MN/m)</b>			
	Loose sand	Medium dense sand	Dense sand
<b>2D</b>	99	201	212
<b>3D</b>	102	207	265
<b>4D</b>	125	235	305
<b>5D</b>	166	282	371

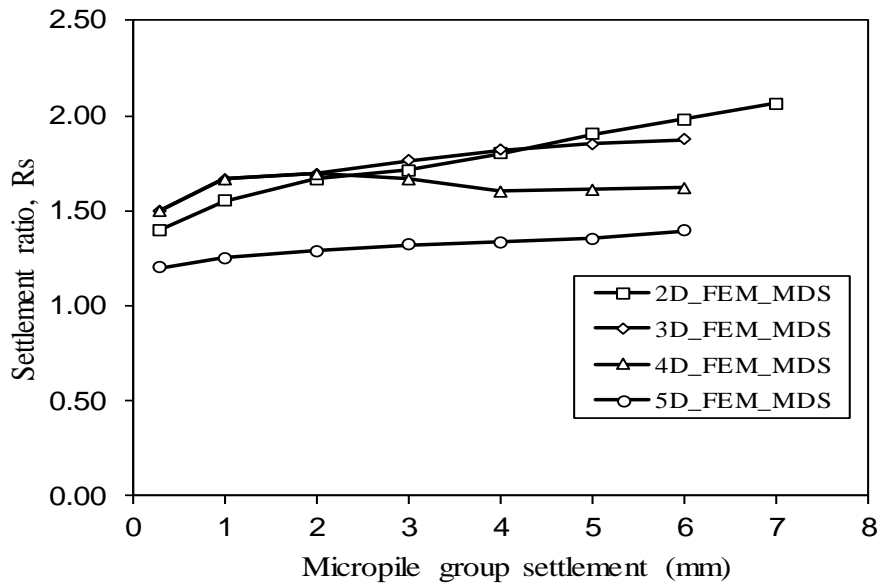
The group efficiency for most of the cases is close to unity; however, the micropile group stiffness increases as the spacing to diameter ratio increases. For example, the micropile group stiffness for s/D equal to 5 is larger than the micropile group stiffness for s/D equal to 2 by about 75%.

### **7.6.7 Settlement Ratio of Micropile Group**

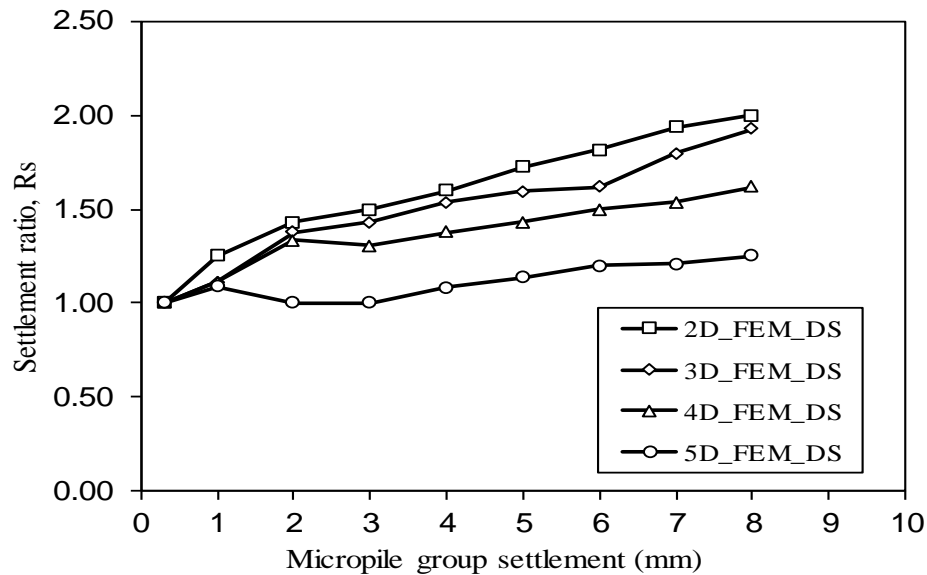
The settlement ratio of micropile groups was calculated for a range of spacing to diameter ratio from 2 to 5. The results are shown in Figure 7.26.



a. Loose sand



b. Medium dense sand



c. Dense sand

**Figure 7-26 Settlement ratio  $R_s$  for different relative densities and  $s/D$  ratios**

As it can be seen from Figure 7.26, the group settlement ratio increases as the total micropile group settlement increases at different rate based on the spacing between the micropiles in the group. For all micropile groups installed in sandy soil, the increase in group settlement ratio with the micropile group settlement becomes more pronounced at small  $s/D$  ratio and as the  $s/D$  increases the rate of increase the group settlement ratio decreases.

The group settlement ratio relates the settlement of single pile to the settlement of pile group at working load, which can be as a useful design tool in designing micropile groups. Therefore, the group settlement ratio is calculated and compared at the design load which is defined as the failure load divided by a factor of safety equal to 2. The results are summarized in Table 7.7 for the 9-micropile group. The results demonstrate that the



settlement ratio increases as the micropiles spacing decreases and the sand relative density increases

**Table 7-7 Comparison between Rs with different s/D ratio**

<b>Group settlement ratio at design load</b>			
	Loose sand	Medium dense sand	Dense sand
<b>2D</b>	2	1.76	1.72
<b>3D</b>	1.92	1.73	1.61
<b>4D</b>	1.80	1.67	1.40
<b>5D</b>	1.35	1.30	1.08

Neely (2008) revisited Berezantsev et al. (1961) work and reported that the group settlement ratio increases as the normalized load for groups of piles increases for piles installed with s/D equal to 3 and the rate of increase in group settlement ratio is clearer as the number of piles in the group increases. It was concluded that the group settlement ratio does not only depend on the average load per pile but also on the geometry of pile group. Briaud et al. (1989) reported a group settlement ratio of 1.29 for a group of five steel piles installed in medium dense sand at 3.4 spacing to diameter ratio.

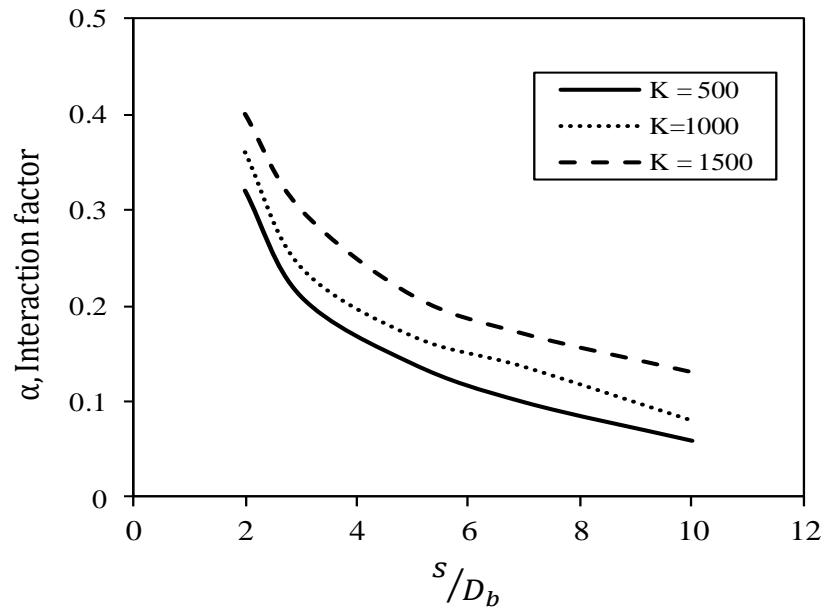
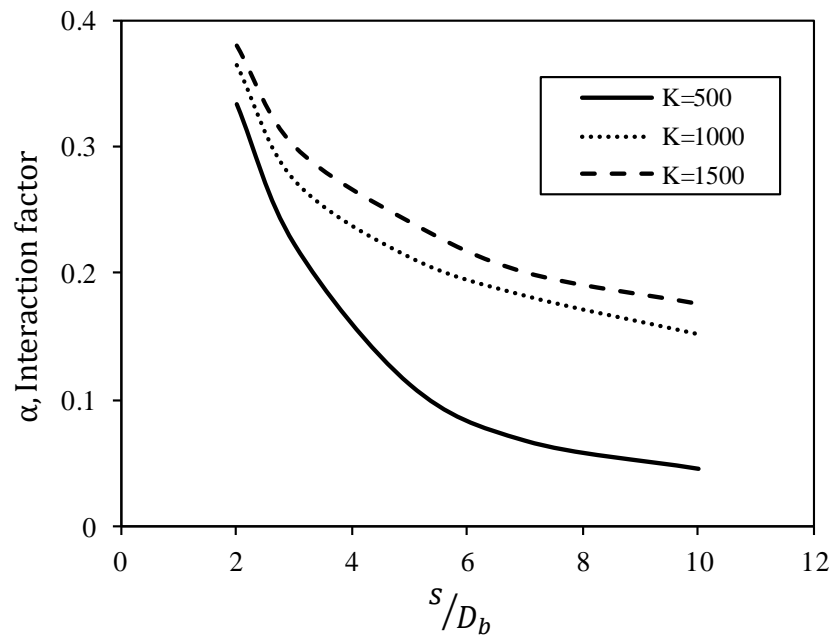
### **7.6.8 Interaction Factor between Two-Micropiles Group**

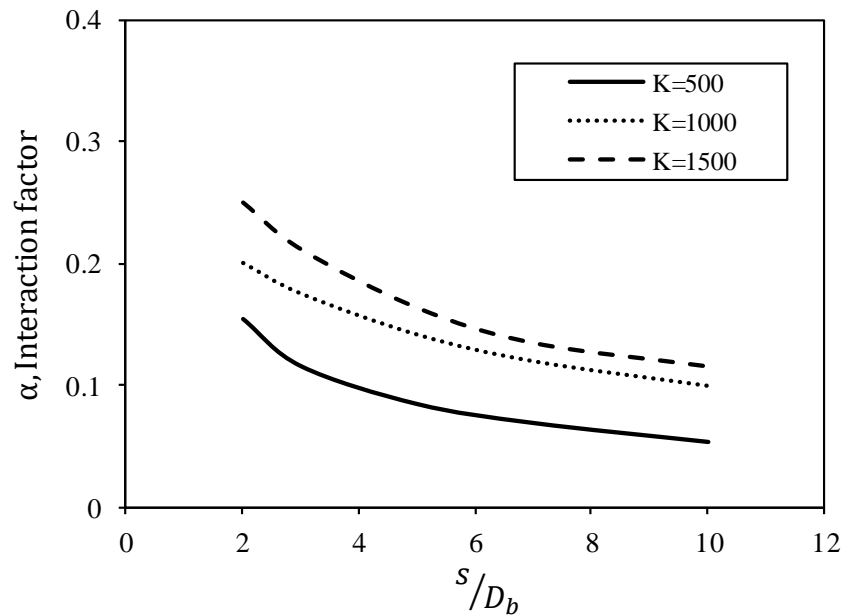
The interaction factor approach was first introduced by Poulos (1968) and Poulos and Mattes (1971). A group of two identical piles are loaded equally and the effect of adjacent pile is considered by means of interaction factor. The interaction factor was defined as the

ratio between the additional displacement due to adjacent pile to the displacement of pile under its own load. Poulos and Davis (1980) indicated that the interaction factor approach can be accurate for small pile groups. Mandolini et al. (2005) showed that the interaction factor approach can be used for large group with reasonable accuracy.

As the construction method of hollow bar micropiles is quite different from the conventional piles, the verified finite element model was used to provide a set of interaction factor curves considering the two main factors; pile stiffness factor and the slenderness ratio of the pile geometry. The pile stiffness factor is defined as the ratio between the micropile modulus of elasticity and the modulus of elasticity of the surrounding soil. Three different pile stiffness factors were considered; 500, 1000, 1500 which represents loose sand, medium dense sand and dense sand, respectively. Furthermore, to investigate the effect of the slenderness ratio of micropiles on the interaction between two micropiles, three slenderness ratios were considered; 25, 50 and 75. The interaction factor was considered at the design load which defined as the failure load divided by factor of 2. The outcome of the analysis is shown in Figures 7.27.

As it can be seen from Figure 7.27, the interaction between the micropiles decreases with the spacing between micropiles increases. The interaction between the two micropiles decreases as the micropile stiffness factor decreases which agrees with Abd Elaziz and El Naggar (2014) finding for micropiles installed in clay soil. Figure 7.27 can be used to obtain the interaction factor between micropiles group.

a)  $L/D = 25$ b)  $L/D = 50$



c)  $L/D = 75$

**Figure 7-27 Interaction factor for different slenderness ratio**

## 7.7 Summery and Main Findings

Finite element simulations were conducted using PLAXIS 3D software to investigate the effect of micropile installation in cohesionless soils. Two different mechanisms were used to simulate the effect of micropile installation: the increasing  $K_o$  method and the cavity expansion method. The Hardening Soil (HS) model was used in both methods to simulate the sandy soil around the micropiles while the micropiles were simulated using a linear elastic model. The finite element model was calibrated and verified using the load – settlement curves obtained from full-scale load tests. For the increasing  $K_o$  method, the coefficient of lateral earth pressure can be obtained from a load test and then applied to the

surrounding soil instead of  $K_0$  which increases the radial stresses around the pile resulting in increasing the micropiles capacity. In the cavity expansion method, the increase in radial stresses due to micropile installation is simulated by applying a prescribed displacement to the volume of soil that represents the micropile. The developed model was used to perform a parametric study to investigate the effect of several soil and micropile parameters on micropile performance. The main findings of this study are:

- Both methods seem to give good matching results to load – settlement curves obtained from full-scale load tests for single micropiles.
- The influence radius of the applied prescribed displacement is about 12 times the micropile diameter from the center of the micropile. Accordingly, placing the side boundaries of the finite element model at a distance of 15 times the micropile diameter should not affect the calculated response.
- The interface reduction factor plays an important role in defining the micropile behaviour under axial loading and should be selected carefully. The experimental results for HBMPs for the range of grouting pressure considered in this study showed that its value should be close to 0.90.
- The model confirms the micropiles group efficiency is equal to unity for micropile groups consisting of 2\*2 or 3\*3 micropiles in a square arrangement.
- The group settlement ratio increases as the total micropile group settlement increases at different rate based on the spacing between the micropiles in the group.
- The group settlement ratio decreases as the spacing to diameter ratio of the group increases from  $s/D = 2$  to  $s/D = 5$ .

- Set of interaction factor curves were proposed for two micropiles installed in different soils and with slenderness ratios.

## 7.8 References

- Abd Elaziz, A. Y., & El Naggar, M. H. (2014). Geotechnical Capacity of Hollow-Bar Micropiles in Cohesive Soils. *Canadian Geotechnical Journal*, 51(10), 1123-1138.
- Alnuaim, A., El Naggar, M.H. & El Naggar, M.H. (2016). Numerical Investigation of the Performance of Micropiled Rafts in Sand. *Computers and Geotechnics*, Vol. 77, pp. 91-105.
- Berezantsev, V. G., Khrisoforov, V. S., & Golubkov, V. N. (1961). Load Bearing Capacity and Deformation of Piled Foundations. *Proceedings. 5th Int. Conf. Soil Mech. and Found. Eng.*, Vol. 2, Paris, 11–15.
- Brinkgreve, R. B. J., Engin, E. & Swolfs, W. M. (2012). *Plaxis 3D 2011 Manual*, 2012.
- Bishop R. F., Hill R & Mott N. F (1945). Theory of Indentation and Hardness Tests. *Proceedings of Physical Society*. Volume 57, Issue 3, pp. 147-159.
- Briaud, J. L., Tucker, L. M., and Ng, E. (1989). Axially Loaded 5 Pile Group and Single Pile in Sand. *In Proceedings 12th Int. Conf. on Soil Mechanics and Foundations Engineering*, Vol. 2, Rio de Janeiro, 1121–1124
- Castro. J & Karstunen M. (2010). Numerical Simulations of Stone Column Installation. *Canadian Geotechnical Journal*. 47: 1127-1138.
- Elsherbiny, Z. & El Naggar, M.H. (2013). Axial Compressive Capacity of Helical Piles from Field Tests and Numerical Study. *Canadian Geotechnical Journal*, Vol. 50 (12), 1191-1203.
- Fahmy, A. and El Naggar, M.H. 2017. Cyclic lateral performance of helical tapered piles in silty sand. *The Journal of the Deep Foundations Institute*.

- FHWA. (2005). *Micropiles design and construction*. Federal Highway Administration (FHWA), U.S. Department of Transportation, Washington, D.C. Publication No. FHWA-NHI-05-039.
- Dijkstra J., Broere W. & Tol V., F. (2006). Numerical Investigation into Stress and Strain Development around a Displacement Pile in Sand. *Numerical Methods in Geotechnical Engineering*.
- Lancellotta, R. (1995). *Geotechnical Engineering*. A. A. Balkema, Rotterdam.
- Mandolini, A., Russo, G., & Viggiani, C. (2005). Pile Foundations: Experimental Investigation, Analysis and Design. *In Proceedings of the 16th International Conference on Soil Mechanics and Geotechnical Engineering*, Osaka 2005. Mill press Science Publishers, Rotterdam, the Netherlands. Vol. 1, pp. 177-213.
- Newson T., Hinchberger S. & Liang Y. (2009). The Mechanics of Inflatable Anchors in Cohesionless Soil. *Soils and Foundations*. Vol. 49, No. 3, pp. 409-420.
- Poulos, H.G. (1968). Analysis of settlement of pile groups. *Geotechnique*, 18(3): 449 – 471.
- Poulos, H.G., & Davis, E. H. 1980. *Pile Foundations Analysis and Design*. John Wiley and Sons.
- Poulos, H.G., & Mattes, N. S. (1971b). Settlement and Load Distribution Analysis of Pile Groups. *Aust. Geomechanics Journal*. Vol. G1. No. 1: 18-28.
- Randolph M. F, Carter J. P, Wrath C. P. (1979). Driven Piles in Clay– the Effects of Installation and Subsequent Consolidation. *Geotechnique* 29(4):361–393.
- Rose, A. V., Taylor, R. N. and El Naggar, M. (2013). Numerical Modelling of Perimeter Pile Groups in Clay. *Canadian Geotechnical Journal*, 50(3): 250-258.
- Sadek, M. & Shahrour, I. (2004). Three-Dimensional Finite Element Analysis of the



Seismic Behaviour of Inclined Micropiles. *Soil Dynamics and Earthquake Engineering*, 24(6):473-485.

- Said, I. (2006). *Comportement des Interfaces et Modelisation des Pieux Sous Charge Axiale*. PhD thesis, Ecole Nationale des Ponys et Chaussees.
- Satibi, M., Leoni S., Vermeer P., A. & Meij R., V., D. (2009). On the Numerical Analysis of Piled Embankments. *In Proceedings of the second International Workshop on Geotechnics of Soft Soils*. Glasgow. UK.
- Schanz T., Vermeer P., A. & Bonnier P., G. (1999). The Hardening Soil Model: Formulation and Verification. *Beyond 2000 in computational geotechnics*, 281-296.
- Shahrour, I. & Juran, I. (2004). Seismic Behaviour of Micropile Systems. *Ground Improvement*, 8(3): 109-120.
- Touma, F.T. & Reese, L.C. (1974). Behavior of Bored Piles in Sand. *Journal of the Geotechnical Engineering Division*, American Society of Civil Engineers, Vol.100, No. GT7, pp. 749-761.
- Vesić, A.S. (1963). Bearing Capacity of Deep Foundations in Sand. *Highway Research Record*, 39: 112–153.
- Wehnert, M. & Vermeer, P. A. (2004). Numerical Analysis of Load Tests on Bored Piles. *Proceedings of the 9th Symposium on Numerical Models in Geomechanics: NUMOG IX*, 25-27 August 2004, Ottawa, Canada
- Neely, J. W. (2008). Discussion of Settlement Ratio of Pile Groups in Sandy Soils from Field Load Tests by Y. Xu and L. M. Zhang. *Journal of Geotech. Geoenvironmental. Engineering.*, 2008, 134(9): 1419-1420.
- Yu HS, Houlsby GT (1991). Finite Cavity Expansion in Dilatant Soils: Loading Analysis. *Geotechnique* 41:173–183

**CHAPTER 8****8 Summary, Conclusions and Recommendations**

---

**8.1 Summary**

The main objectives of this research are to investigate the performance of single and micropiles group installed in cohesionless soil and study the effect of increasing the drill bit/ hollow bar ( $D_b/D_h$ ) ratio from 2.25 which presents the common practice to 3. The results should be of value for both practitioners and researchers. Furthermore, the mechanical properties of neat grout and various reinforced grouts were investigated to study the visibility of increasing the performance of micropile under lateral loading.

Twenty-two micropiles were installed in cohesionless soil, consists of six single micropiles and four micropiles groups. In the first stage, compression and tension loading tests were performed on six full-scale hollow bar micropiles to investigate the performance and capacity of hollow bar micropiles constructed with different diameter ratios of drill bit/hollow bar ( $D_b/D_h$ ). Two micropiles (MP2 and MP3) were instrumented with three vibrating wire strain gauges each to evaluate the distribution of load transfer along the micropile. The micropiles were constructed using hollow bars R51N along with tungsten carbide cross cut drill bits. The OD (Outer diameter) of the hollow bar is 51 mm and the ID (Inner diameter) is 33 mm. Three micropiles (MP2, MP5 and MP6) were installed with 152 mm drill bit (i.e.  $D_b/D_h=3$ ) and two (MP3 and MP4) with 115 mm drill bit (i.e.  $D_b/D_h=2.25$ ). The total length of each micropile was 6m with 5.75m embedded length.

In the second stage, six micropiles were tested under lateral loading. Fifteen full-scale loading tests were conducted on hollow bar micropiles to investigate the performance of micropiles under monotonic and cyclic lateral loads with different drill bit/ hollow bar diameter ratio of 2.25 and 3. One group of four micropiles with common spacing between the micropiles in groups,  $5D$  was tested under lateral monotonic loading. Furthermore, the mechanical properties of neat grout and various reinforced grouts were investigated in this study by performing several laboratory tests; compressive strength, tensile strength, modulus of elasticity, and flexural strength. Micropiles with 1000 mm length and 76 mm diameter were cast and subjected to pure bending moment tests in controlled environment to investigate in detail the effect of adding fibers on the bending moment capacity of micropiles. LPile model was developed utilizing the moment-curvature curves obtained from the pure bending moment tests and the results were reported. The optimum dosage of fibers based on the parametric study was selected and a full-scale micropile with 6 m length and 172 mm diameter was installed in cohesionless soil using reinforced grout.

In this stage, Full-scale loading tests were conducted on four groups of micropiles to investigate the performance of micropile groups with different drill bit/ hollow bar diameter ratio of 2.25 and 3 and two different common spacing between the micropiles in groups,  $s = 3D_b$  and  $5D_b$ . At least one micropile in each group was instrumented with three vibrating wire strain gauges to evaluate the force distribution along the micropile length.

In addition to the field load testing, a finite element analysis using PLAXIS 3D commercial software was conducted to complement the experimental results and further evaluate the micropile axial capacity when the ultimate load was not reached. Parametric study was

performed to investigate the effect of several parameters on the micropile performance and capacity.

## **8.2 Conclusions**

Based on the results of full-scale load tests, laboratory tests and numerical modeling, the main findings of this study are:

### **8.2.1 Single Micropiles**

Based on the actual measurements of exhumed micropiles diameters, the micropiles diameter increased by approximately 14% over the drill bit diameter.

#### **8.2.1.1 Monotonic compression performance**

- The load test results showed that as  $D_b/D_h$  increased from 2.25 to 3, the micropile stiffness increased by 38%.
- The compression capacity of the micropiles increased by about 17% as  $D_b/D_h$  increased from 2.25 to 3.
- Increasing the  $D_b/D_h$  ratio from 2.25 to 3 has a cost implication as the quantity of steel can be reduced by 50% by increasing the drill bit diameter to achieve  $D_b/D_h = 3.0$  comparing to the current practice.
- A new range of values for the ultimate bond resistance of grouted micropiles was suggested. The suggested values are between 150-250 kPa instead of the wide range

proposed by FHWA 120-360 kPa for micropiles installed in the same soil conditions.

### **8.2.1.2 Monotonic uplift performance**

- The load test results showed that as  $D_b/D_h$  increased from 2.25 to 3, the micropile stiffness increased by 32%.
- The tension capacity of the micropiles increased by about 22.5%, as  $D_b/D_h$  increased from 2.25 to 3.
- Increasing the  $D_b/D_h$  ratio from 2.25 to 3 has a cost implication as the quantity of steel can be reduced by 50% by increasing the drill bit diameter to achieve  $D_b/D_h = 3.0$  comparing to the current practice.
- The effect of preloading; compression and then tension has non-significant effect on the tension capacity of micropiles.

### **8.2.1.3 Monotonic lateral performance**

- The load - deflection response of single micropiles indicated a stiffer response for micropiles with drill bit/hollow bar diameter ratio equal to 3 than the response of ratio of 2.25 which presents the current practice.
- Increasing the drill bit/hollow bar diameter ratio from 2.25 to 3, improved the lateral capacity by about 32%.

- The first eight to nine micropile diameters depth have the major impact on the hollow bar micropiles performance under lateral loading.
- The maximum bending moments occurred at depth about 4.5 and 4.35 of micropiles diameters.
- It was demonstrated that the LPile software can be used to analysis the hollow bar micropiles under lateral loading following the procedure mention above.

#### **8.2.1.4 Cyclic axial performance**

- There was a variation in the axial head stiffness in the first five cycles as the axial stiffness varies between 330 kN/mm and 250 kN/mm, this variation may be attributed to the effect of cyclic tension test which was performed before the compression cyclic tests. However, the axial micropile stiffness stabilized at 330 kN/mm after the seven cycles.

#### **8.2.1.5 Cyclic lateral performance**

- The degradation parameter  $t$  varies from 0.084 to 0.033 and from 0.062 to 0.031 for micropiles with  $D_b/D_h = 3$  and  $D_b/D_h = 2.25$ , respectively. The degradation parameter  $t$  reaches the peak value at the first few cycles and then decreases with increasing the number of cycles and the load amplitude.

#### **8.2.1.6 Improving the lateral performance**

- Adding micro-steel fibers and steel fibers to the neat grout mix can enhance the tensile and flexural strengths with a slight increase in compressive strength.

- The bending moment capacity of micropiles increased and the post-cracking behaviour improved by adding micro-steel fibers and steel fibers to the grout mix.
- Micropiles cast with steel fibers showed larger lateral capacity and greatly increased ductility compared to micropiles constructed with neat grout, which failed in a brittle manner.
- The plastic hinge developed at a depth equal to 7.1 and 8.7 times the micropile diameter for micropiles constructed with no fibers and micropiles casted with steel fibers, respectively.
- The lateral capacity of micropile constructed with 1% of MSF grout increased by 10% compared to micropiles constructed with neat grout.

## **8.2.2 Micropiles Group**

### **8.2.2.1 Monotonic compression performance**

- The micropile groups constructed with drill bit/hollow bar diameter ratio,  $D_b/D_h = 3$  displayed 50% stiffer response than the groups constructed with  $D_b/D_h = 2.25$ . In addition, groups constructed with  $D_b/D_h = 3$  displayed 25% increase in capacity compared to groups constructed with  $D_b/D_h = 2.25$ . This demonstrates the benefit of using  $D_b/D_h = 3$  when larger capacity or stiffer response is required.
- The group efficiency at both working load and interpreted failure load are close to unity; between 0.97 and 1.06 for dense sand soils for both  $3D_b$  and  $5D_b$  center-to-center distance. This was confirmed by the results obtained from the finite element model.

- The average toe resistance accounted for about 12% of the total resistance of micropiles. Ignoring the toe resistance contribution to the total micropile resistance may be conservative.
- For hollow bar micropile groups constructed with spacing,  $s \geq 3D_b$ , the group efficiency ratio can be taken as 1.0.

### **8.2.2.2 Monotonic lateral performance**

- Considering the 25mm lateral deflection as a failure criterion for micropiles under lateral loads, the group efficiency of micropiles group with five diameters center-to-center distance is about 89%.

## **8.3 Recommendations for Future Research**

- Investigating the effect of grouting pressure for different soils on the micropile performance and capacity.
- Performing full-scale field tests for micropiles groups with different configuration installed in cohesive soil under axial and lateral loadings.
- Dynamic full-scale field testing of single and group of micropiles is suggested.
- Performing full-scale field testing on micropiles with steel fibers added to the grout mix to assess the effect of their addition on lateral performance.
- Investigating the effect of applying axial and lateral cyclic loading on micropile groups.



## Curriculum Vitae

**Name:** Maged A. Abdrahem

**Post -secondary Education and Degrees:** University of Benghazi, Benghazi Libya  
1995 - 1999 B.A.  
Glasgow University, Glasgow, UK  
2006 – 2007 MEdSc.  
Western University, London, Ontario, Canada  
2013 – 2018 PhD.

**Honours and Awards:** William and Lardner Award. GRC. UWO. London. 2015  
Lizzi Scholarship Award. (ISM). Vancouver, 2017  
Milos Novak Memorial Award. GRC. UWO. London. 2017

**Related Work and Experience**  
Teaching Assistant  
Western University  
2014 – 2017  
Geostructural Engineer  
Capita Symonds  
2010  
Geostructural Engineer  
ADPi  
2008 – 2009  
Civil Engineer  
General Working Authority  
1999 - 2005